INFORMATION TO USERS

This manuscript has been reproduced from the microfilm master. UMI films the text directly from the original or copy submitted. Thus, some thesis and dissertation copies are in typewriter face, while others may be from any type of computer printer.

The quality of this reproduction is dependent upon the quality of the copy submitted. Broken or indistinct print, colored or poor quality illustrations and photographs, print bleedthrough, substandard margins, and improper alignment can adversely affect reproduction.

In the unlikely event that the author did not send UMI a complete manuscript and there are missing pages, these will be noted. Also, if unauthorized copyright material had to be removed, a note will indicate the deletion.

Oversize materials (e.g., maps, drawings, charts) are reproduced by sectioning the original, beginning at the upper left-hand corner and continuing from left to right in equal sections with small overlaps.

Photographs included in the original manuscript have been reproduced xerographically in this copy. Higher quality 6" x 9" black and white photographic prints are available for any photographs or illustrations appearing in this copy for an additional charge. Contact UMI directly to order.

Bell & Howell Information and Learning
300 North Zeeb Road, Ann Arbor, MI 48106-1346 USA

UMI®
800-521-0600

MOLECULAR DYNAMICS AND REACTION KINETICS DURING POLYMERIZATION USING DIELECTRIC SPECTROSCOPY AND CALORIMETRY

By

DWAYNE ANDREW WASYLYSHYN, M.Eng.

A Thesis

Submitted to the School of Graduate Studies

in Partial Fulfilment of the Requirements

for the Degree

Doctor of Philosophy

McMaster University

MOLECULAR DYNAMICS AND REACTION KINETICS DURING POLYMERIZATION

DOCTOR OF PHILOSOPHY (1998)

(Materials Science and Engineering)

McMASTER UNIVERSITY

Hamilton, Ontario

TITLE: **Molecular Dynamics and Reaction Kinetics During Polymerization Using Dielectric Spectroscopy and Calorimetry**

AUTHOR: **Dwayne Andrew Wasylyshyn, M.Eng. (McMaster University)**

SUPERVISOR: **Professor G.P. Johari**

NUMBER OF PAGES: xx, 214

ABSTRACT

The evolution of molecular dynamics during the polymerization of linear-chain and network forming liquids was studied using dielectric spectroscopy and differential scanning calorimetry. Polymerization was carried out using step-addition reactions between epoxide and amine molecules, and by catalysis of epoxide molecules with tertiary amines. The former resulted in linear-chain or network structured polymers while the latter resulted in network polymers. The step-addition polymerizations resulted in linear-chain polymers by reacting stoichiometric quantities of diepoxide and monoamine molecules, and network structure polymers by reacting stoichiometric quantities of triepoxide and monoamine molecules, or diepoxide and diamine molecules.

The growth and extinction of localized (or secondary) relaxation processes during the polymerization were studied by measuring the changing dielectric properties using two techniques; fixed frequency dielectric measurements during heating of the partially polymerized samples, and isothermal dielectric measurements over the frequency range of 1 MHz to 20 GHz. The number of covalent bonds formed at any instant during the polymerization was determined by isothermal calorimetric measurements. Thus, the change in the dielectric properties during polymerization was associated with the increase in the number of covalent bonds. It was found that the localized relaxations evolve in a manner that is independent of the spontaneous increase in configurational entropy. The results also lend evidence towards the concept that these relaxations occur in regions of

relatively high energy, and the collapse of such regions led to the observed changes in the dielectric properties. As well, an analogy was made between the structural relaxation of a physically metastable glass and the polymerization of a chemically metastable liquid. This has lead to the concept of a chemical fictive temperature to describe the state of the polymerizing liquid.

The effects of pressure on the dielectric properties of the polymerizing liquids was studied using fixed frequency dielectric measurements. Pressure was step-increased, both at the beginning of the polymerization and at a time during the polymerization, then maintained. An increase in pressure increased the rate of polymerization, and thus the dielectric properties evolved more rapidly with time. The chemical effects of pressure during polymerization were examined using transition state theory and the concept of negative feed-back. The physical effects of pressure were investigated in terms of its effects on the equilibrium dielectric properties. It was shown that the polymerization kinetics are increased with increased pressure when the kinetics are in the mass-controlled regime, and decreased with increased pressure when the kinetics are in the diffusion-controlled regime. The transition from mass- to diffusion-controlled kinetics was investigated using the rate of change of the dielectric loss.

Finally, the chemical and physical effects of step-increased pressure upon the dielectric properties of polymerizing liquids in the mass-controlled regime were mathematically simulated using current concepts and formalisms. The simulated results were qualitatively similar to those obtained experimentally, demonstrating the adequacy of the understanding.

ACKNOWLEDGEMENTS

Firstly, I would like to thank Dr. G. P. Johari for his patient guidance and enthusiasm during the course of my graduate work. I learned much as a graduate student, not only from courses and lectures, but also from my many discussions with him on a wide range of topics. His many interests and unique point of view taught me that ideas must be constantly questioned, examined, and ultimately expressed in terms of the most fundamental concepts.

I would also like to thank my colleagues in the Department from whom I obtained advice and friendship during my research. The many research interests explored by graduate students, technicians and faculty within the Department of Materials Science and Engineering allowed me a diverse pool of knowledge to draw from. The years of friendship and misadventures made me realize that everything truly is more bearable when there are others in the same boat.

Finally, I would like to thank my family, who have supported me all the while (financially and morally). They have always done their best to ensure I had whatever resources were required in order to get me out into the real world faster.

TABLE OF CONTENTS

LIST OF FIGURES

LIST OF TABLES

CHAPTER I
INTRODUCTION

Over the last two decades, the use of thermosetting polymers has expanded into several technological sectors. They are used as structural materials in the automobile and aerospace industries, as encapsulating materials in the microelectronic and health science industries, and as general adhesives and protective coatings [Ellis (1993)]. This expansion of their applications requires that their processing aspects, particularly the transformation from a liquid to an elastic or brittle solid, be understood. The main focus of this thesis is on the evolution of physical properties during the process of this transformation.

The term 'thermoset polymer' refers to a group of polymers that are formed by step-addition reactions between dissimilar chemical species. Amongst them are a large number formed by using epoxy resins, which contain at least two reactive glycidyl ether, R-CH(O)-CH_2, (epoxide) groups [Horie *et al.* (1970)]. When an epoxy resin is completely polymerized, usually by reacting with an amine, the product is called an epoxy polymer. The ultimate structure of the polymer formed depends on the number of epoxide groups in the resin and the nature of the other reacting component, or curing agent, or hardener. Curing agents, or hardeners, generally contain a proton-donating group that reacts with the epoxide group by exchanging a proton for a covalent bond. Also, an amine or other

organic materials without a proton may act as a catalyst and produce a polymer structure from the resin alone by other mechanisms [Narcott (1953)]. The polymer formed in the former type of reaction can have either a linear-chain or a network structure. A linear structure is formed by the reaction of a stoichiometric mixture of epoxy resins and hardeners that have an average number of reactive sites per monomer equalling two, while the network structure is formed when this average exceeds two. Thus the final properties of a thermosetting polymer are determined by the chemical nature of the initial molecular species and their relative concentrations. They are also determined by the time, pressure, and temperature conditions of polymerization, which are generally considered as relaxational, dynamic, or time-dependent as they control both the short and long-time behaviour of the polymers [McCrum *et al.* (1967)].

The experimental work of this thesis was performed in order to study in detail; (i) the evolution of relaxation properties during the course of polymerization and relate it to the number of covalent bonds formed, and (ii) the change in the polymerization kinetics from that of mass-controlled to diffusion-controlled regime as the initially fluid state gradually becomes a brittle polymeric solid. For this purpose, dielectric and calorimetric measurements were performed to monitor the progress of polymerization with time and to develop formalisms based on the physico-chemical theories for relaxation phenomena. This leads to relations between the dielectric properties and the progress of polymerization.

Polymers of both linear and network-structures were prepared by reacting mono- and di-functional amines with di- and tri-functional epoxides, and their polymerization investigated under two conditions; (a) a constant pressure applied from the beginning of the polymerization, and (b) pressure step applied either at a relatively early stage of the polymerization and maintained thereafter, or at a relatively late stage of polymerization and maintained thereafter.

This thesis is divided into seven chapters. As a broader introduction to the subject, Chapter II provides a review of the literature as it pertains to the discussions, an introduction to the basic concepts of the polymerization process, descriptions of the chemicals used to facilitate the investigations, and a rigorous discussion of the theory of relaxation processes and their evolution during isothermal polymerization. Chapter III gives a detailed account of the measurement assemblies used and procedures followed during the course of this study. References to other experimental approaches are cited throughout this chapter to show the wide variety of measurement techniques that have been used to investigate the changing properties of liquids as they polymerize.

Chapter IV presents the results obtained during the polymerization of the molecular liquid mixtures using dielectric spectroscopy and calorimetric techniques, and the analysis of the results in terms of the relaxation time and the number of covalent bonds formed.

The results of the evolution of physical properties are discussed in Chapter V. The relaxation processes observed in the molecular liquid are compared with those of the

partially and completely polymerized states. This evolution is also examined using high-frequency time domain reflectometry.

In Chapter VI the dielectric properties measured during the polymerization of the thermosetting liquids under constant and a step-increased pressure are discussed in terms of the physical and chemical effects of pressure upon the reaction kinetics. These effects are examined with considerations to the transition state theory, diffusion-controlled kinetics, and Le Chatelier's principle, and conditions for the transition from mass-controlled to diffusion-controlled polymerization kinetics are deduced. The chemical and physical effects of pressure are mathematically simulated in order to demonstrate the correctness of our understanding of these effects upon the process of polymerization.

Finally, the conclusions of the thesis are given in Chapter VII. Throughout the thesis, references to the literature are given as required for discussion.

Due to the rapid progress of this field of research in relation to the concepts presented, it seemed necessary over the past three years to submit parts of this work for publication to scientific journals. These articles are listed in the Reference section, and are as follows;

1. Wasylyshyn, DA, and Johari, GP (1996), *Journal of Chemical Physics*, **104**, 5683.
2. Johari, GP, McAnanama, JG, and Wasylyshyn, DA (1996), *Journal of Chemical Physics*, **105**, 10621.
3. Wasylyshyn, DA, Johari, GP, Salvetti, G, and Tombari, E (1997), *Journal of Physics: Condensed Matter*, **9**, 10521.
4. Wasylyshyn, DA, and Johari, GP (1997), *Journal of the Chemical Society, Faraday Transactions*, **93**, 4025-4032 (1997).
5. Wasylyshyn, DA, Johari, GP, Tombari, E, and Salvetti, G (1997), *Chemical Physics*, **223**, 313.

6. Wasylyshyn, DA, and Johari, GP (1998), "Dielectric effects of step-increased pressure on the mass- and diffusion-controlled linear chain and network macromolecules growth", Accepted for publication by, *Chemical Physics*.
7. Wasylyshyn, DA, and Johari, GP (1998), "Steric hindrance effects on dielectric relaxation and polymerization kinetics of a monoamine-triepoxide mixture, thermochemistry and diffusion-control", Accepted for publication by, *Journal of Polymer Science, Part B: Polymer Physics*.

Part of the experimental work on the evolution of secondary relaxations was performed at Istituto di Fisica Atomica e Molecolare del CNR, Pisa, Italy. During the one month period spent there, two seminars based upon the work on the low temperature localized relaxations and on the general effects of pressure on the process of polymerization were presented by the Author.

CHAPTER II
BACKGROUND INFORMATION

2.1 LITERATURE REVIEW

The increasing interest in polymeric materials for specialized industries has resulted in an increased demand to understand the changes in their properties as polymerization progresses with a view to monitoring the process and the polymer's properties. As a consequence, there have been a large number of studies on them that utilize such methods as dielectric spectroscopy and calorimetry as techniques. While a review of the pertinent literature is provided in the text throughout the thesis when needed for discussions, a general review of the literature pertaining to studies on monitoring of polymerization by calorimetry and dielectric spectroscopy follows.

It is widely known that the dielectric properties of a polymer depend upon the average dipole moment of its repeat unit, their arrangement, the refractive index, the average diffusion time and its distribution [McCrum *et al.* (1967)]. But these properties also depend on the number density of cross-links, pressure [Chen *et al.* (1969)], temperature [McCrum *et al.* (1967)], and the ageing time of the solid polymer [Johari (1982)]. Therefore, dielectric methods are useful for measuring the irreversible change in the average dipole moment, refractive index, and average diffusion times and its distribution as macromolecules form and grow during step-addition reactions, and have been used

since the 1930's [Kienle and Race (1934), Aukward *et al.* (1958), Delmonte (1959)].

Amorphous polymers show at least two types of chain or segmented diffusion (or relaxation). The first is a cooperative, highly temperature-sensitive process known as the α-relaxation, usually observed above the glass-rubber (or liquid) transition temperature, T_g [McCrum *et al.* (1967)]. The second is an apparently non-cooperative, relatively temperature-insensitive process known as the β-relaxation, usually observed below T_g [Johari and Goldstein (1970)]. Both relaxations are also observable at temperatures above or below T_g, depending upon the frequency used for the measurements. Dielectric [McCrum *et al.* (1967), Karasz (1972), Charlesworth (1988a,b), Hofmann *et al.* (1994)] and mechanical studies [Fox and Loshaek (1955), DiMarzio(1955), Katz and Tobolsky (1962), McCrum *et al.* (1967), Matsuoka *et al.* (1987), Perez (1992)] provide information on the strength and characteristics of these relaxations and are therefore used for seeking structure-property relationships for amorphous and crystalline polymers.

Studies that relate the dielectric properties to the changing molecular structure of polymerizing liquids have increased more rapidly in recent years with advances in computer-assisted data acquisition. This has lead to new insights into the evolution of dielectric relaxation processes as the average dielectric relaxation time, $<\tau>$, of the liquid irreversibly increases when the polymerization reaches completion [Senturia and Sheppard (1986), Mangion and Johari (1991b), Parthun and Johari (1992), Johari (1993b), Cassettari *et al.* (1994), Deng and Martin (1994a), Williams *et al.*, (1995), Fournier *et al.* (1996)]. A comprehensive survey of the earlier studies are given by Senturia and Sheppard (1986) and

Johari (1993b). These insights have led to an understanding of the evolutions of the α- and β-relaxation processes with a spontaneous increase in the number of covalent bonds formed, the increase in the average relaxation time, $<\tau>$, and related properties [Johari (1994a), Parthun and Johari (1995a), Parthun *et al.* (1996), Wasylyshyn *et al.* (1996), Wasylyshyn and Johari (1997b)]. Empirical relations between $<\tau>$ and the extent of polymerization have also been sought, as by Tombari and Johari (1992) and more recently by Fournier *et al.* (1997).

Other relaxation methods have been used to investigate the progress of polymerization with the aim of developing monitoring procedures or understanding the molecular processes. These are; ultrasonic relaxation [Alig *et al.* (1992), Parthun and Johari (1992a,b), Younes *et al.* (1994),], mechanical relaxation [Enns and Gillham (1983), Wisanrakkit *et al.* (1987) and (1990)], infra-red absorption [Plazek and Frund (1990), Deng and Martin (1994b)], viscosity [Malkin and Kulichikhin (1991)], and most recently the dynamic heat capacity [Ferrari *et al.* (1996)]. Zhou and Johari (1997) have restudied several liquids that polymerize to form a cross-linked gel structure by using both dynamic mechanical relaxation [Zhou (1997)] and ultrasonic attenuation. The gelation time determined by using these two methods has been found to agree with that measured by dielectric spectroscopy [Parthun and Johari (1992a,b)], thus confirming the adequacy of the dielectric method.

The rate at which polymerization proceeds towards the ultimate extent of reaction depends upon whether the polymerization is in the mass- or diffusion controlled regime

[Hamman (1957), Isaacs (1981)]. When a chemical reaction is in the mass-controlled regime, the reaction rate can be expressed in the general form,

$$\left(\frac{\partial\alpha}{\partial t}\right)_T = K(1-\alpha)^{\bar{N}} \tag{2.1}$$

where $(\partial\alpha/\partial t)_T$ is the slope of the isothermal plot of the extent of reaction, α, against the polymerization time, t, K is the reaction rate constant, and $\bar{N}$ is the order of the reaction. For polymerization reactions, Equation (2.1) is not expected to be valid, because the product further reacts and the types of reacting species increases rapidly. For diepoxides-diamines reactions, Horie *et al.* (1970) have re-expressed Equation (2.1) in the semi-empirical form,

$$\left(\frac{\partial\alpha}{\partial t}\right)_T = (k_1 - k_2\alpha^{\bar{m}})(1-\alpha)^{\bar{n}} \tag{2.2}$$

where k_1 and k_2 are rate constants for both the primary and secondary amine reactions, assuming that the two reactions occur at a similar rate [Horie *et al.* (1970), Riccardi *et al.* (1984), Barton (1985), Carrozzino *et al.* (1990) and references therein], and $\bar{m}$ and $\bar{n}$ are empirical parameters. Equation (2.2) has been used to fit the calorimetric data for polymerization in the mass-controlled regime [Horie *et al.* (1970), Riccardi *et al.* (1984), Barton (1985), Riccardi and Williams (1986), Carrozzino *et al.* (1990), Wasserman and Johari (1993) and (1994)], and it is found that in a narrow range, k_1 and k_2 have an Arrhenius dependence with temperature.

The effect of pressure on k_1 and k_2 is not well understood, but its effect on polymerization has been discussed generally in terms of the transition state theory [Evans

and Polanyi (1935)]. In this theory, the reactants are considered to form a metastable state before irreversibly transforming into the products of reaction [Evans and Polanyi (1935)]. A general reaction process can be written as, $A+B \leftrightarrow X^{\neq} \rightarrow C$, where A and B are the reactants, $X^{\neq}$ is the transition state in equilibrium with A and B, and C is the product of the reaction. The equilibrium constant, $K^{\neq}$ is expressed as [Glasstone *et al.* (1941)],

$$\frac{k^{\neq}h}{k_B T} = \exp\left(\frac{-\Delta G^{\neq}}{RT}\right) = K^{\neq} \tag{2.3}$$

where $k^{\neq}$ is the rate constant for the formation of the product, h is Planck's constant, k_B is Boltzmann's constant, and $\Delta G^{\neq}$ is the free energy of activation. Thus, the pressure dependence of $k^{\neq}$ is expressed as,

$$\frac{\partial \ln k^{\neq}}{\partial P} = -\frac{\Delta V^{\neq}}{RT} \tag{2.4}$$

where $\Delta V^{\neq}$ is the volume of activation. From Equation (2.4), it is seen that for $\Delta V^{\neq} < 0$, an increase in pressure increases $k^{\neq}$, and thus accelerates the reaction. For $\Delta V^{\neq} > 0$, a similar increase in pressure decreases $k^{\neq}$, thus slowing the reaction. Hamman (1957) showed that for a non-ionic bimolecular reaction, $\Delta V^{\neq}$ is negative. From transition state theory, this implies that $\ln k^{\neq}$ (and thus the reaction rate) increases as the pressure is increased, which is observed experimentally [Hamman (1957), Isaacs (1981)], and has been attributed to an increased number density of reacting species, and therefore in the frequency of their collisions. This ignores any interaction between the reacting species and the medium in general, and thus, by definition, is only applicable in the mass-controlled regime where only the quantity of the reactants present affects the rate of reaction.

A rapid decrease in the rate of reaction is observed when the viscosity reaches a high value and diffusion-control of the kinetics has set in, typically when polymerization approaches completion. This has been discussed in terms of a 'negative feed-back' mechanism [Johari and Mangion (1991)] according to which the result of a reaction is a decrease in the diffusion coefficient, which in turn slows the reaction. Thus, a state is ultimately reached such that further reactions are possible only after a prohibitively long period. As a consequence, isothermal polymerization rarely reaches completion unless the polymerization temperature is such that the polymer product remains fluid or does not vitrify.

Once diffusion-control has set in, an increase in viscosity upon an increase in pressure will slow the reaction. This conflicts with the transition state theory's predictions that pressure would increase the reaction rate. That the reaction kinetics move from a mass-controlled regime to a diffusion-controlled regime if the viscosity becomes sufficiently high has been considered by Isaacs (1981). The effects of P on the polymerization rate therefore depends upon the nature of the kinetics for the two time regimes, *i.e.*, an increase in P increases the polymerization rate in the mass-controlled regime but decreases it in the diffusion-control regime.

Waite (1960) described conditions for the mass-controlled and diffusion-controlled regimes in terms of a parameter, $s \approx \exp[(E_D^* - E_R^*)/RT]$, where R is the gas constant, T the temperature, E_R^* the activation energy for the chemical reaction and E_D^* that for the diffusion of the reacting species towards one another. He showed that the

absolute magnitude was not as important, only that the difference, $(E_D^* - E_R^*)$, changes from negative to positive at certain value of α, or t. Thus, he showed that for diffusion-controlled kinetics, $s >> 1$ but for mass-controlled kinetics $s << 1$. The conditions for the transition from mass-controlled to diffusion-controlled, however, was not developed. In the empirical approach by Fournier *et al.* (1996), diffusion-control kinetic data that was obtained using calorimetry was also used to describe the behaviour of the dielectric relaxation rate, or equivalently, τ, during polymerization. They stated that in the mass-controlled regime, $\log\tau$ decreases linearly with t, but after the onset of diffusion-control, it decreases more rapidly with t. This qualitative behaviour of $\log\tau$ with t was not substantiated by the data [Fournier *et al.* (1996)].

In addition to the effect that pressure has on the chemical aspects of polymerization, there is also an effect on the physical aspects. An increase in pressure is found to affect the dielectric properties of liquids [Johari and Dannhauser (1969a), Chen *et al.* (1969), Johari and Whalley (1972)]. The dielectric relaxation time, τ, and the low- and high -frequency limiting permittivities, ε_∞ and ε_s, measured under various conditions of P and T for different alcohols in their studies showed that the magnitude of each of these equilibrium properties increased with an increase in P, and that the increase itself was greater at low T than at high. The increase in ε_∞ with P was attributed to the decrease in the vibrational frequencies, and the increase in the refractive index. The increase in ε_s with P was attributed to the increase in the number density of dipoles, and the orientational correlations of the molecules [Chen *et al.* (1969)].

2.2 POLYMERIZATION OF A THERMOSETTING MIXTURE

As mentioned earlier, thermoset polymers form by chemical reactions between two (or more) types of low molecular weight monomeric species, each of which must have two or more functional groups (reactive sites). Polymerization proceeds as a functional group of one type of monomer reacts with that of the other to form a covalent bond between them. For a linear-chain forming thermoset, the reacting functional groups on the monomers combine to form a linear chain by step-addition. For network forming thermosets, the functional groups combine to form a junction point, which produces a cross-link. This results in the continuous growth of a 3-dimensional macromolecule.

When polymerization leads to a network structure, after growing for a certain period of time, the molecular network extends continuously over the volume of the liquid, thus transforming the viscous liquid to a gel-like solid, a phenomenon known as gelation that usually occurs prior to vitrification. The unreacted molecules or molecular segments in the material remain mobile and diffuse although the material becomes a highly elastic solid after gelation. This diffusivity allows further polymerization over an experimental time scale. Gelation has been found to occur at 55% - 80% consumption of diepoxide groups during the reaction of diepoxides with diamines in stoichiometric amounts [Flory (1941) and (1953), Stockmayer (1943), DeGennes (1979), Adolf *et al.* (1990), Parthun and Johari (1993), Wasylyshyn and Johari (1997)]. As the chemical reaction progresses in the gelled state, the microscopic viscosity and T_g of the gelled state increases. When T_g has increased

to the temperature of the isothermal cure, the state of the polymer changes from that of a mechanically low modulus gel (about 1 MPa) to a high modulus, vitreous solid (about 1 GPa). Associated with this state is an extremely low diffusivity that slows the rate of chemical reactions until they become unobservable. In summary, when a multifunctional epoxide and amine molecules chemically react, and the reaction approaches completion, the shear modulus increases from virtually zero of a liquid to about 1 MPa of a gel and finally to about 1 GPa of a brittle, glassy polymer.

The step addition reaction between a multifunctional epoxide molecule and a multifunctional amine molecule is illustrated in Figure 2.1 for a single amine group reacting with two epoxide groups of two separate epoxide molecules. In the first reaction step, the primary amine of the $-NH_2$ functional group chemically reacts with the epoxide group of the multifunctional epoxide molecule, breaks the ring open to form a hydroxyl -OH group, and its nitrogen atom covalently bonds with the terminal atom of the epoxide molecule. Thus, the primary amine becomes a secondary amine, with a functionality of one.

In the second reaction step, the secondary amine reacts with one epoxide group of another multifunctional epoxide molecule resulting in a branched tertiary amine, which now serves as a link between the two epoxide molecules. The degree of molecular branching in the polymer also depends upon the polymerization temperature, since the rates of reaction of the primary and secondary amines are found not to be equal [Horie *et al.* (1970), Ryan and Dutta (1979), Mijovic *et al.* (1984), Riccardi *et al.* (1984), Dušek (1985), Riccardi and Williams (1986), Grenier-Loustalot *et al.* (1987) and (1988), Kim and Kim (1987),

(1)

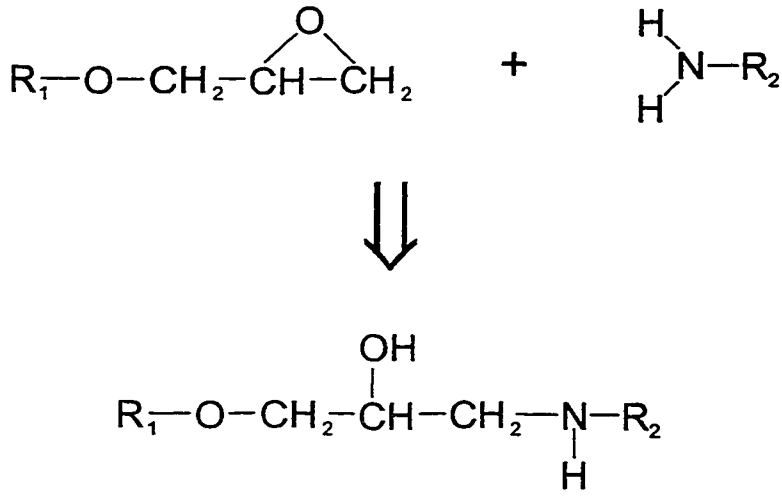

(2)

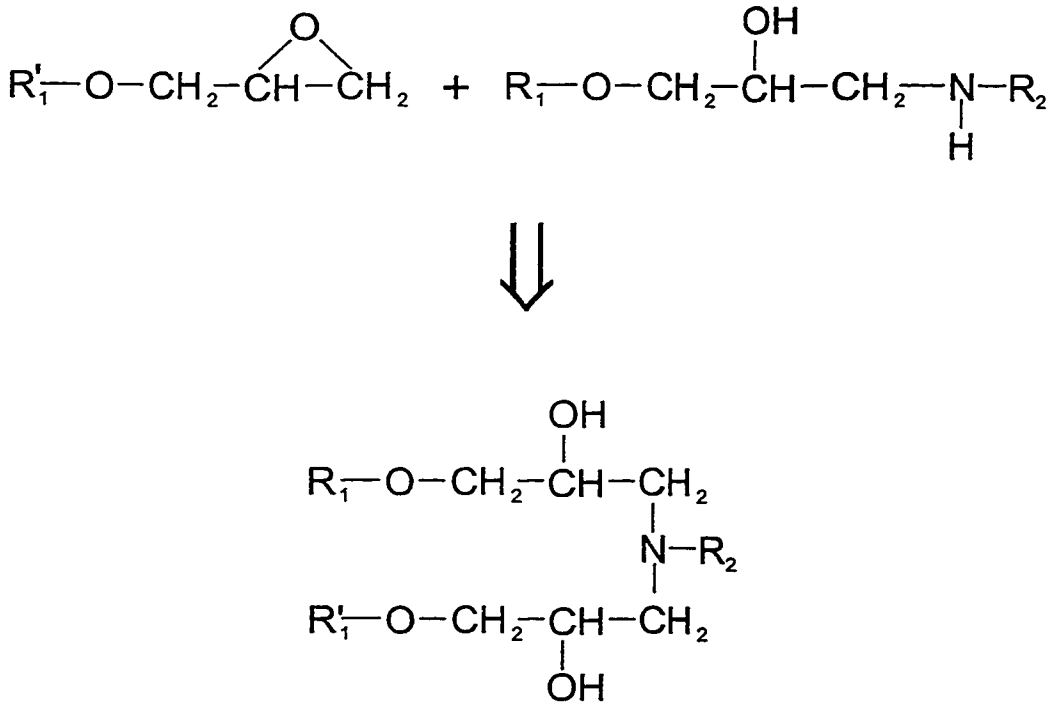

Figure 2.1: The reaction steps which occur for the reaction between an epoxide group and an amine group.

Carrozzino *et al.* (1990)]. Thus, polymerization occurs until the reactions have either reached completion or have become imperceptibly slow. Ultimately, the initial liquid becomes a dense polymeric solid under isothermal conditions.

The mechanism of the catalytic polymerization of a difunctional epoxide molecule by the catalyst N, N-dimethylbenzylamine and the sequence of polymerization reaction at temperatures below 363 K is illustrated in Figure 2.2 [Narracott (1953), Tanaka *et al.* (1967), Fedtke *et al.* (1987), Alig and Johari (1993)]. The first step in the sequence is an addition reaction between $C_6H_5CH_2N(CH_3)_2$ and one epoxide group of the diepoxide molecule, which has separated charges, forming a zwitterion. In the second step, the zwitterion reacts with one epoxide group of another diepoxide molecule. This increases the chain length and further separates the negatively and positively charged atoms of the zwitterion along the chain. In the third reaction, the zwitterion dissociates into a chain with a $CH_2=C(R_1)$-O- group (R_1 being the first reacting epoxide molecule lacking one epoxide group) at one end and -$CH(R_1')$-OH at the other end (R_1' being the second reacting epoxide molecule lacking one epoxide group). This double-bonded group further reacts to produce a cross-linked network and the original amount of the tertiary amine catalyst remains in the molecular network. A fraction of this amine may remain H-bonded to the protons of the -OH groups in the polymerized epoxy network structure in which the distance between two cross-links is on the average the same as the length of the cross-link itself, after complete polymerization.

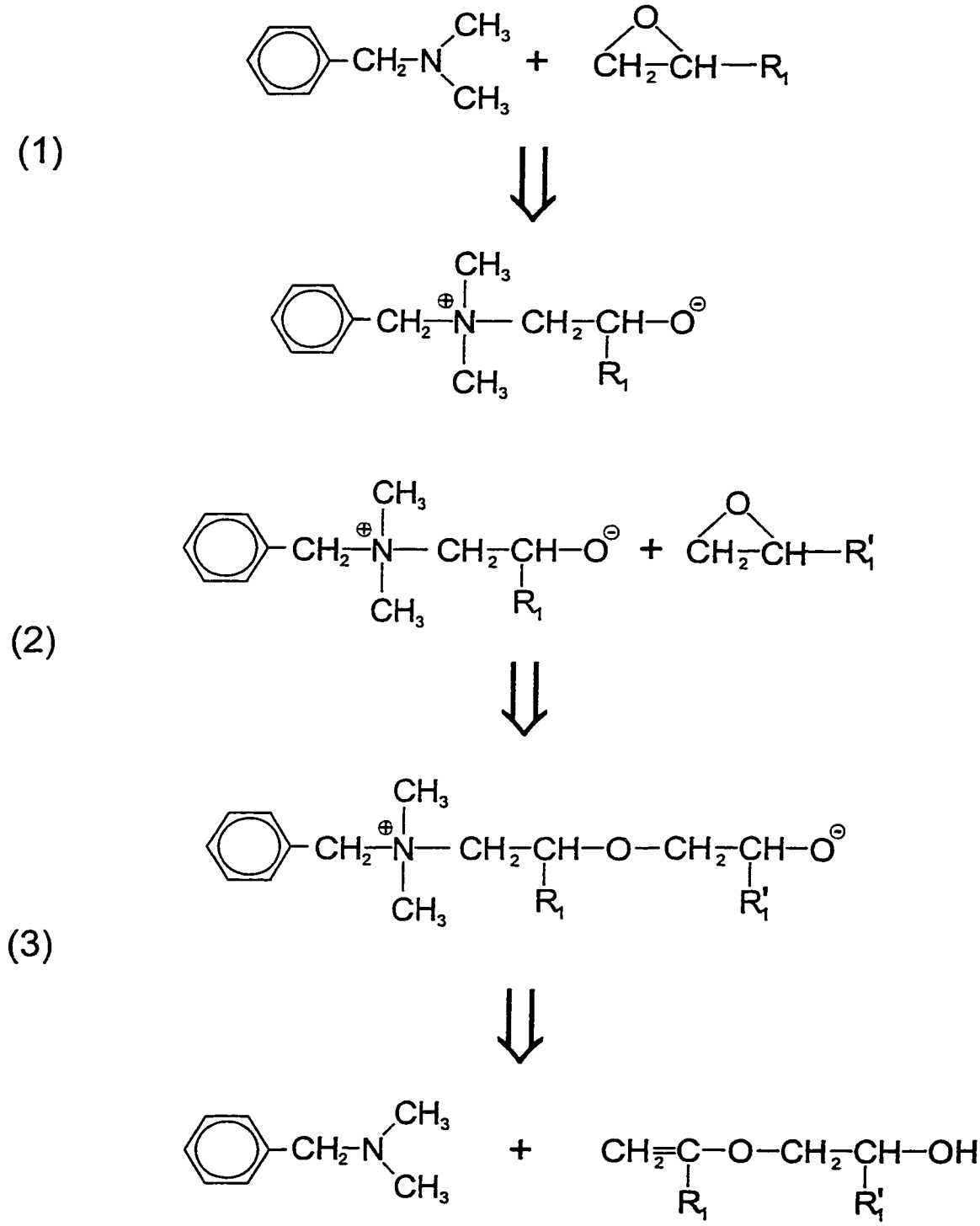

Figure 2.2: The reaction steps that occur for the catalysis of diepoxide molecules with N, N dimethylbenzylamine present in small quantities (5 or 10 mole percent).

As the macromolecule grows during the polymerization the volume decreases as the non-directional Van der Waals interactions are replaced by stronger and directional covalent bonds, and the configurational entropy decreases. The decrease in the diffusivity, volume, and configurational entropy cause T_g of the isothermally polymerizing liquid to increase to a value corresponding to the polymerization temperature.

2.3 CHEMICAL STRUCTURES

The molecular structures of the epoxide molecules used for preparing the thermoset polymers are shown in Figure 2.3, where the diglycidyl ether of bisphenol-A (DGEBA) is a di-functional epoxide resin, and the Tactix-742 (Tactix) is a tri-functional epoxide resin. The various formulae and structures of the amines, or curing agents, used to react with these epoxide resins are shown in Figure 2.4. According to the IUPAC nomenclature, these are; 1,2-diaminoethane (EDA), 1,6-diaminohexane (HDA), aniline (AN), *n*-hexylamine (HA), and cyclo-hexylamine (CHA). For the catalytic polymerization of DGEBA, the catalyst used was dimethylbenzylamine (DMBA), whose formula is also shown in Figure 2.4. Reactions of DGEBA with EDA and HDA, and catalysis by DMBA, result in cross-linked structures, while reactions between DGEBA and AN, HA, and CHA result in linear-chain structures. The reaction mechanism for DGEBA with an amine-based curing agent was described in the previous section, as was the reaction mechanism for the catalysis of DGEBA by DMBA.

diglycidyl ether of bishenol-A (DGEBA)

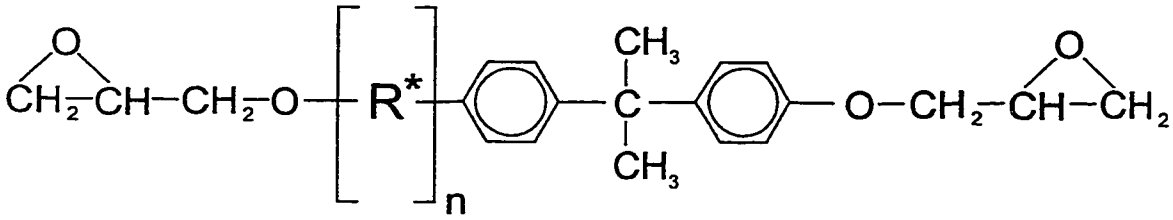

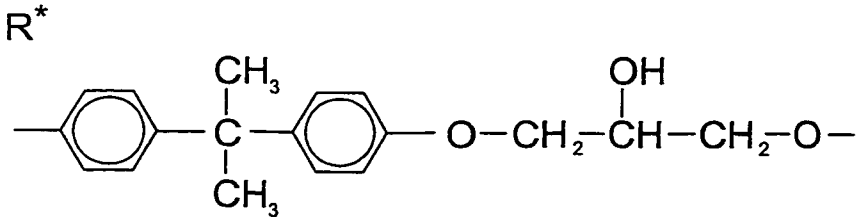

Tactix-742 (Tactix)

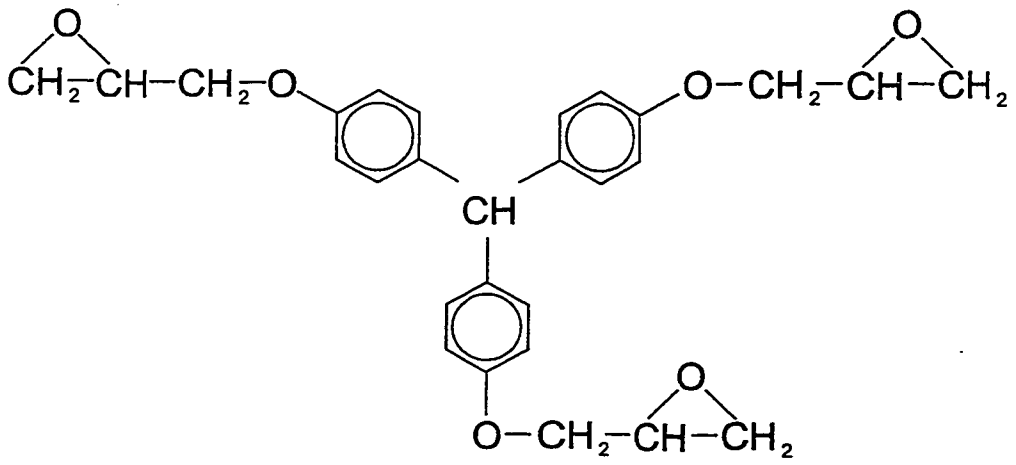

Figure 2.3: The chemical structures of the two types of epoxy molecules used in this study; diglycidyl ether of bishenol A (DGEBA), and Tactix-742 (Tactix).

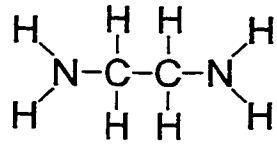

ethane 1,2 diamine (EDA)

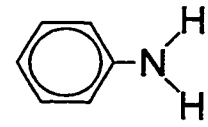

aniline (AN)

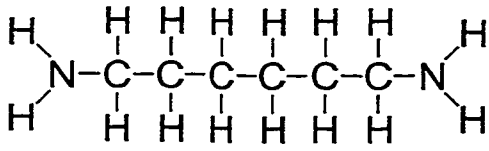

hexane 1,6 diamine (HDA)

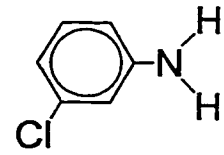

3-chloroaniline (3CA)

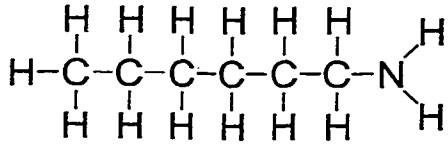

hexylamine (HA)

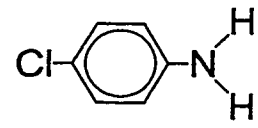

4-chloroaniline (4CA)

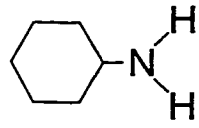

cyclo-hexylamine (CHA)

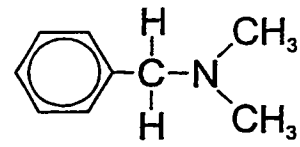

dimethylbenzylamine (DMBA)

Figure 2.4: The chemical structures of aniline (AN), 3-chloroaniline (3CA), 4-chloroaniline (4CA), 1,2-diaminoethane (EDA), 1,6-diaminohexane (HDA), *n*-hexylamine (HA), cyclohexylamine (CHA), and dimethylbenzylamine (DMBA).

2.4 THEORY OF DIELECTRIC RELAXATION

Generally, dielectric measurements are made by placing a sample between two capacitor plates to which a fixed (or sinusoidal) electric field is applied. The dielectric sample, devoid of free electrons, undergoes preferential alignment of molecular and ionic dipoles within its bulk, causing both instantaneous and time-dependent charge build-up on the capacitor plates. The build-up of surface charge per unit surface area is called the polarization of a dielectric material. The time-dependent electrical polarization (charge per unit area), $P(t)$, of the dielectric sample can therefore be expressed as,

$$P(t) = P_\infty + P_o\left(1 - \phi(t)\right) \tag{2.5}$$

where P_∞ is the instantaneous polarization associated with the electronic transitions and atomic vibrations, and P_o is the time-dependent dipolar polarization. $\phi(t)$ is a relaxation function that describes the time-dependent approach of the polarization from P_∞ to $(P_\infty + P_o)$, its equilibrium value. The polarization and charge displacement, $D(t)$, for a constant electric field, $E(t) = E_o$, are related through the expression;

$$D(t) = \varepsilon_o E(t) + P(t) = \varepsilon_o \varepsilon\,(t) E(t) \tag{2.6}$$

where ε_o is the permittivity of vacuum (= 8.854 pF/m). Since $D(t)$ and $P(t)$ are time-dependent, $\varepsilon(t)$ is the time-dependent permittivity of the sample under the boundary conditions $\varepsilon(t \rightarrow 0) = \varepsilon_\infty$ (or $\omega \rightarrow \infty$) and $\varepsilon(t \rightarrow \infty) = \varepsilon_s$ (or $\omega \rightarrow 0$), where ω is the angular frequency ($=2\pi f$), and ε_∞ and ε_s are the limiting high frequency and static (low frequency) permittivities respectively. In a manner similar to Equation (2.6), $\varepsilon\,(t)$ can be related to $\phi\,(t)$ through the equation,

$$\varepsilon(t) = \varepsilon_\infty + (\varepsilon_s - \varepsilon_\infty)(1 - \phi(t)) \tag{2.7}$$

When the electric field is not constant, but applied by incremental amounts, the Boltzmann superposition principle [Boltzmann (1877), Hopkinson (1877), Curie (1888)] is applied. The charge displacement, $D(t)$, at any time, t, due to an electric field, $E(t)$, applied in steps, becomes the sum of displacements, $dD(t)$, arising from the incremental field, $dE(t)$, of each step applied at previous times, μ, when $\mu \leq t$. This is expressed as,

$$\frac{D(t)}{\varepsilon_o} = \int_{-\infty}^{t} \frac{\partial E(\mu)}{\partial \mu} \varepsilon(t - \mu) d\mu \tag{2.8}$$

By substituting $a = t - \mu$ and integrating Equation (2.8) by parts, one obtains,

$$\frac{D(t)}{\varepsilon_o} = \varepsilon_\infty E(t) + \int_0^\infty E(t-a) \frac{\partial \varepsilon(a)}{\partial a} da \tag{2.9}$$

Substituting Equation (2.7) into Equation (2.9) gives,

$$\frac{D(t)}{\varepsilon_o} = \varepsilon_\infty E(t) + (\varepsilon_s - \varepsilon_\infty) \int_0^\infty E(t-a) \left(-\frac{\partial \phi(a)}{\partial a} \right) da \tag{2.10}$$

The relationship between a sinusoidal electric field, $E^*(t) = E_o \exp(i\omega t)$, and the resulting charge displacement, $D^*(t) = D_o \exp[i(\omega t - \delta)]$, where t is the time of the measurement, E_o is the electric field amplitude, D_o is the charge displacement amplitude, δ is the dielectric loss angle and $i = (-1)^{1/2}$, is expressed as;

$$D^*(t) = \varepsilon_o \varepsilon^* E^*(t) \tag{2.11}$$

ε^* in Equation (2.11) is the complex dielectric permittivity. $E^*(t)$ and $D^*(t)$ are denoted by E^* and D^* from here on. Combining Equation (2.11) with $E^* = E_o\exp(i\omega t)$ and $D^* = D_o\exp[i(\omega t - \delta)]$ leads to the equations;

$$\varepsilon^* = \frac{D^*}{\varepsilon_o E^*} = \frac{D_o}{\varepsilon_o E_o}(\cos\delta - i\sin\delta) = \varepsilon' - i\varepsilon'' \tag{2.12}$$

$$\varepsilon' = |\varepsilon_o|\cos\delta \tag{2.13}$$

$$\varepsilon'' = |\varepsilon_o|\sin\delta \tag{2.14}$$

$$\tan\delta = \varepsilon''/\varepsilon' \tag{2.15}$$

Here, ε', ε'', and $\tan\delta$ are referred to as the dielectric permittivity, dielectric loss and loss factor, respectively, and $|\varepsilon| = D_o/\varepsilon_o E_o$.

By treating the superposition principle in the dynamic manner, one obtains,

$$\frac{D^*}{\varepsilon_o} = \varepsilon_\infty E^* + (\varepsilon_s - \varepsilon_\infty)\int_0^\infty E_o \exp(i\omega(t-a))\frac{\partial\phi(a)}{\partial a}\,da \tag{2.16}$$

Equation (2.16) is further simplified, and a is replaced by t, to express ε^* in the equation,

$$\varepsilon^* = \varepsilon_\infty + (\varepsilon_s - \varepsilon_\infty)\int_0^\infty \exp(-i\omega t)\left(-\frac{\partial\phi(t)}{\partial t}\right)dt \tag{2.17}$$

The integral term on the right hand side of Equation (2.17) is recognized as a Laplace transform, therefore this equation can be expressed as,

$$N_\varepsilon^* = \frac{(\varepsilon^* - \varepsilon_\infty)}{(\varepsilon_s - \varepsilon_\infty)} = \mathcal{L}\left(-\frac{\partial\phi(t)}{\partial t}\right) \tag{2.18}$$

where $\mathcal{L}(y)$ is the one-sided Laplace transform of y, and N_ε^* is the normalized complex dielectric permittivity.

2.5 RELAXATION SPECTRA

2.5.1 The Single Relaxation Time

To describe the rate at which a time-dependent property, such as polarization, reaches its equilibrium value, a relaxation function $\phi(t)$ must be defined. If the rate at which the property changes toward equilibrium, or 'relaxes', is proportional to the property's deviation from its equilibrium value at a constant characteristic relaxation time, τ_o, the relaxation function corresponds to exponential decay [Debye (1929), Fröhlich (1949)], given by,

$$\phi(t) = \exp\left(-\frac{t}{\tau_o}\right) \tag{2.19}$$

Substitution of Equation (2.19) into Equation (2.18) leads to,

$$N^* = \frac{1}{1 + i\omega\tau_o} \tag{2.20}$$

Expressions for the normalized permittivity, N', and loss, N'', components are given by;

$$N' = \frac{1}{1 + \omega^2\tau_o^2} \tag{2.21}$$

and

$$N'' = \frac{\omega\tau_o}{1 + \omega^2\tau_o^2} \tag{2.22}$$

where τ_o is the single relaxation time and represents the time required for the total dipolar polarization of a dielectric to decrease by a factor of e after the removal of the electric field. The corresponding behaviour when observed in the frequency domain is a spectrum with a half-width of 1.141 decades. This behaviour is known as Debye behaviour and is only

observed for dilute solutions of polar molecules in non-polar solvents and for substances at high temperatures. This behaviour is not observed for amorphous solids or highly viscous liquids [Davidson and Cole (1951), Smyth (1955), Davidson (1961), Davies (1965), McCrum *et al.* (1967), Johari (1973)].

2.5.2 Distribution of Relaxation Times

The relaxation behaviour observed for all amorphous materials is often considered as a superposition of exponential relaxation functions of the form [Fröhlich (1949)],

$$\phi(t) = \int_0^\infty \exp\left(\frac{-t}{\tau}\right) g(\tau)\, d\tau \qquad (2.23)$$

where,

$$\int_0^\infty g(\tau)\, d\tau = 1 \qquad (2.24)$$

Here, $g(\tau)$ is the normal relaxation time distribution function.

Much work has been done on empirical representations of $g(\tau)$ [Wagner (1913), Whitehead and Banos (1932), Yeager (1936), Fuoss and Kirkwood (1941), Cole and Cole (1941), Davidson and Cole (1950) and (1951), Hamon (1952), Havriliak and Negami (1966), Williams and Watts (1970)] that best describe the ε' and ε'' data of dielectric materials. The most widely used empirical formula, first used by Kohlrausch (1847) for time-domain creep measurements, then by Douglas (1963), (1966) for stress relaxation measurements, and later adapted by Williams and Watts (1970) for dielectric studies, is expressed as,

$$\phi(t) = \exp\left(-\left(\frac{t}{\tau_o}\right)^{\beta}\right) \qquad (2.25)$$

This is known as the stretched exponential function, where β, the stretch parameter, describes the non-exponentiality of the decay for values $0 < \beta < 1$. In the frequency domain it is observed as an asymmetric broadening of the ε' and ε'' spectra with a half-width greater than 1.141 decades. The stretched exponential becomes the exponential decay function (Debye behaviour) for $\beta = 1$.

The differences between the Debye and stretched exponential behaviours are also illustrated by the complex plane plots of ε'' versus ε', which are known as Cole-Cole plots [Cole and Cole (1941)] and are shown in Figure 2.5. The curves in the figure represent $\beta = 1$ (Debye) and $\beta = 0.5$ (stretched exponential). The Debye behaviour shown in Figure 2.5 is represented as a semi-circle in the complex plane plot with radius $(\varepsilon_s - \varepsilon_\infty)/2$ and centre at $(\varepsilon_s - \varepsilon_\infty)/2$ on the ε' axis. Since it is a semi-circle, the plots are symmetrical about $\omega\tau_o = 1$, therefore τ_o is equal to the average relaxation time, $\langle\tau\rangle$. Most materials however, display a behaviour where the low frequency side of the complex-plane plots remains semi-circular but the high frequency side is drawn out, which is illustrated in Figure 1.5 for $\beta = 0.5$. This 'skewed arc' is typical of most dynamic dielectric, ultrasonic, and mechanical studies [McCrum, *et al.* (1967)]. The characteristic relaxation time, τ_o, for the stretched exponential is related to the average relaxation time, $\langle\tau\rangle$, by [Moynihan *et al.* (1973)],

$$\langle\tau\rangle = \frac{\tau_o}{\beta}\Gamma\left(\frac{1}{\beta}\right) \qquad (2.26)$$

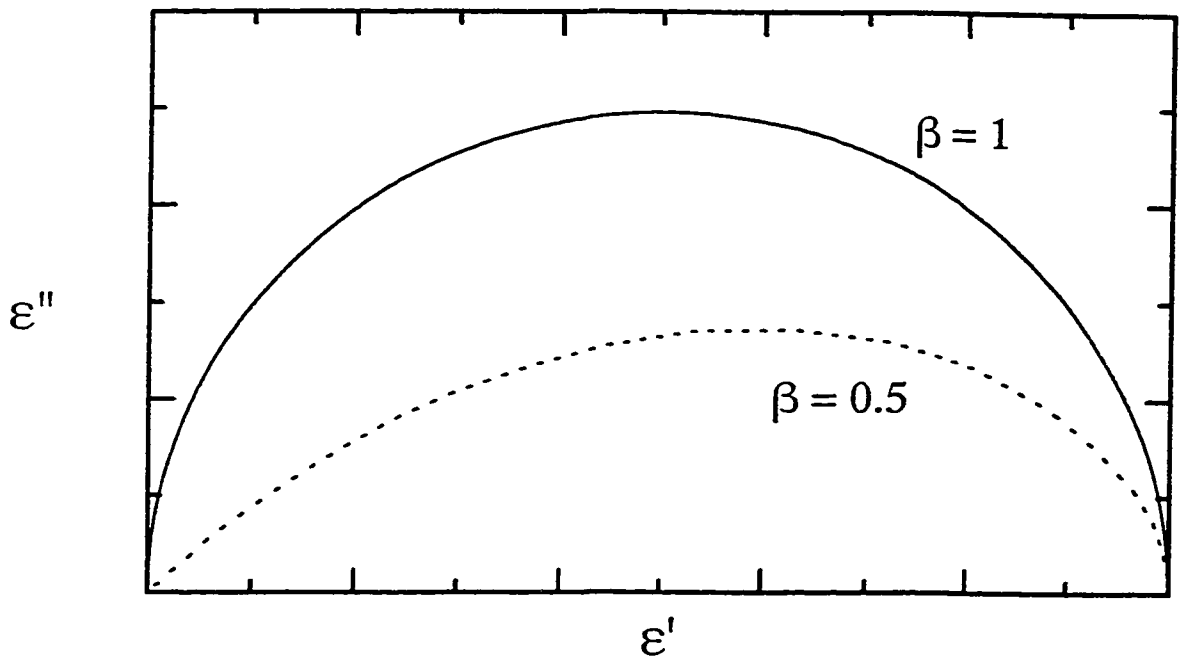

Figure 2.5: A plot of ε'' against ε' corresponding to $\beta = 1$ (solid line) and $\beta = 0.5$ (dashed line) from Equation (2.25).

where $\Gamma(y)$ represents the gamma function of y.

The substitution of Equation (2.25) into Equation (2.18) and performing the Laplace transform and substituting $z = \omega\tau_o$, leads to the result,

$$N' = \pi z V_\beta(z) - 1 \tag{2.27}$$

and

$$N'' = \pi z Q_\beta(z) \tag{2.28}$$

N' and N'' are the real and imaginary components of the normalized complex permittivity described earlier and V_β and Q_β are integrals defined by,

$$V_\beta = \frac{1}{\pi}\int_o^\infty \exp(-u^\beta)\sin(zu)du \tag{2.29}$$

$$Q_\beta = \frac{1}{\pi}\int_0^\infty \exp(-u^\beta)\cos(zu)du \qquad (2.30)$$

The evaluation of Equations (2.29) and (2.30) has been done [Moynihan *et al.* (1973), Lindsey and Patterson (1980), Dishon *et al.* (1985), Muzeau *et al.* (1991)] for $0.1 < \beta < 0.7$ and for $10^{-3} < \omega\tau_o < 10^4$. The values of V_β and Q_β for different values of β and $\omega\tau_o$ have been organized into tables from which the normalized quantities, N' and N'', have been obtained.

2.6 RELAXATION BEHAVIOUR AND THE EVOLUTION OF MOLECULAR DYNAMICS

The above discussion is usually applied to chemically stable materials maintained isothermally. In this 'time-invariant' case, τ_o of the material is constant, but the magnitudes of ε' and ε'' are frequency-dependent. During a macromolecule's growth upon polymerization, τ_o is not constant, but changes from ~1 ns to ~10^4 s [Johari (1994a)]. Hence, the magnitudes of ε' and ε'' depend upon both ω and τ_o, the latter increasing with the polymerization time, t. (Note that when calorimetric data is available, the state of the reaction can be expressed in terms the number of bonds formed instead of t. This will be discussed in Section 4.1).

First we discuss how the relaxation theory developed for the time-invariant case is applicable to the time-variant case. There are two procedures for calculating τ_o and β of Equation (2.25) as in recent studies [Tombari and Johari (1992), Cassettari *et al.* (1994), Deng and Martin (1994a), Parthun and Johari (1995c), Parthun *et al.* (1996), Wasylyshyn *et*

al. (1996), Wasylyshyn and Johari (1997b)]. In the first, multifrequency measurements were used and the relaxation spectra of both ε' and ε'' were interpolated from the data at a fixed polymerization time, or for a fixed number of covalent bonds [Tombari and Johari (1992), Cassettari *et al.* (1994), Deng and Martin (1994a), Parthun and Johari (1995c), Parthun *et al.* (1996), Wasylyshyn *et al.* (1996), Wasylyshyn and Johari (1997b)]. Equation (2.25) was then fitted to the spectra and the values of τ_o and β were obtained. In the second procedure [Mangion and Johari (1990) and (1991b), Johari *et al.* (1996), Wasylyshyn and Johari (1997b)], ε' and ε'' were measured for a single fixed frequency as the reaction progressed and the number of covalent bonds formed increased spontaneously at a constant temperature. From this single frequency measurement, τ_o and β were calculated by writing Equation (2.25) in the approximate form:

$$[\phi(t')] = \exp\left(-\left(\frac{t'}{\tau_o(t)}\right)^{\beta(t)}\right) \qquad (2.31)$$

where $\beta(t)$, taken as independent of the polymerization time or the number of covalent bonds formed in the limited range of polymerization time, was written as γ, the reaction parameter, and t' represented the duration of the relaxation. Thus, τ_o could be obtained as a function of t or the number of covalent bonds formed by a procedure simpler than, and with an accuracy comparable to, that obtained from the interpolated spectra in the first procedure [Tombari and Johari (1992), Cassettari *et al.* (1994), Deng and Martin (1994a), Parthun and Johari (1995c), Parthun *et al.* (1996), Wasylyshyn *et al.* (1996), Tombari *et al.* (1997), Wasylyshyn and Johari (1997b)]. Equation (2.31) is useful only for measurements at

frequencies high enough that during the time of measurement at that frequency, the effects due to the chemical reactions (increase in the number of bonds formed) are negligible, or the parameters of Equation (2.17) other than the relaxation time change negligibly.

Since a Laplace transformation of Equation (2.31) does not seem meaningful, as stated before [Mangion and Johari, (1990) and (1991b), Tombari and Johari (1992), Johari (1994a) and (1994b)] and Equations (2.25) and (2.31) do not commute, it must be stressed that the use of Equation (2.31) be made only on the approximation that $(\partial\phi(t')/\partial t)$, β, ε_s and ε_∞ do not change with t during polymerization, so that $\beta(t)$ could be replaced by the reaction parameter, γ, for the time-variant chemical and physical states of a polymerizing liquid. So, two aspects need to be stressed here: (i) the use of γ is mathematically rigorous when ϕ, ε_s, ε_∞ and β do not change with t, and is approximate when they do, and,(ii) in the present approximate form, the Fourier transform of Equation (2.31) will not lead to the same equation as in the time-domain. Nevertheless, the procedure using single-frequency data, although less precise, is experimentally simpler and mathematically less complex, and when multi-frequency data are not available and the number of independently adjustable parameters needs to be minimized, the dynamics of polymerization or other reactions can be adequately understood by a single, fixed frequency measurement of the dielectric, dynamic mechanical and ultrasonic properties. It should also be stressed that data simulation, double blind analysis of data on other polymerizing systems [Parthun *et al.* (1996)], as well as a variety of experiments on different materials [Tombari and Johari (1992), Cassettari *et al.* (1994), Deng and Martin (1994a), Johari and Pascheto (1995), Parthun and Johari (1995c),

Wasylyshyn *et al.* (1996), Tombari *et al.* (1997), Wasylyshyn and Johari (1997b)] during their polymerization have amply confirmed that τ_o and β calculated from the multi-frequency data are in satisfactory agreement with the τ_o and γ calculated from the single frequency data. The latter method should be considered as a mathematically non-rigorous procedure, as originally proposed [Mangion and Johari, (1990) and (1991b)], and inconsistent with the Fourier transform procedures used for the time-domain, only in as much as ϕ, ε_s, ε_∞ and β are invariant of t. It should also be stressed that single frequency data and the relevant analysis *not* be used with temperature or pressure as a continuous variable in measurements of chemically and physically stable systems because in such a case the change in τ_o does not dominate the change in ε' and ε'', since ε_s and β also change by relatively large amounts [Johari and Dannhauser (1969a), Chen *et al.* (1969), Johari and Whalley (1972)]. Nevertheless, it is worth pointing out that two mathematical equations that themselves do not commute, as Equations (2.25) and (2.31) do not, can yield the same answer. Here, of course, the approximation that the effect of increase in τ_o on ε' and ε'' is many orders of magnitude greater than the effects of changes in ε_s and β have made that more probable.

CHAPTER III

MEASUREMENT ASSEMBLIES AND EXPERIMENTAL PROCEDURES

3.1 MEASUREMENT EQUIPMENT

3.1.1 Differential Scanning Calorimetry

The principle of differential scanning calorimetry requires that a sample material and a reference material be maintained at an identical, predetermined, temperature. This is achieved by containing the sample and reference materials within identical metal pans in separate compartments, each with its own heater and thermometer. A schematic diagram of this assembly is shown in Figure 3.1. The measurable quantity is the power added to or withdrawn from the sample and reference compartments in order to maintain the zero temperature differential.

When a chemical reaction or phase transformation occurs within a sample material, heat is released or absorbed. This heat is determined and then balanced by the differential scanning calorimeter (DSC) in the form of electrical current to maintain an identical temperature between the sample and reference materials. This power difference can be measured under the conditions of a constant heating rate, q, such that plots of $(dH/dt)_q$ against T are obtained, or by maintaining the sample isothermally, such that plots of $(dH/dt)_T$ against t are obtained. Enthalpy changes due to chemical reactions, phase

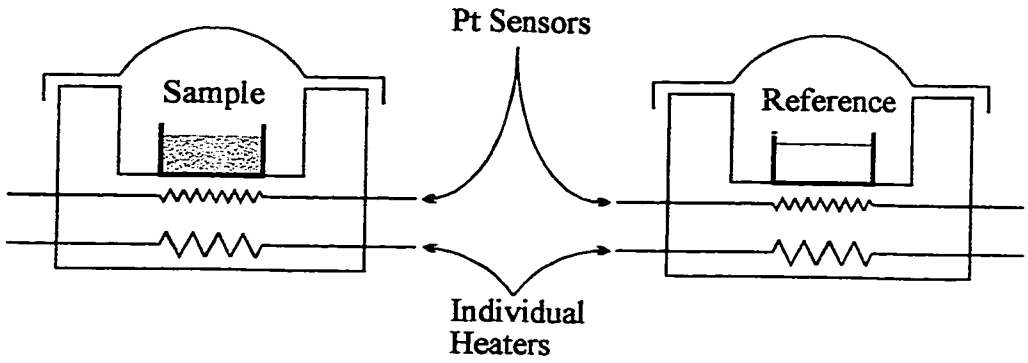

Figure 3.1: A schematic diagram of the DSC assembly.

transformations, or physical interactions within the sample material produce peaks in the plots of $(dH/dt)_q$ against T whose area are proportional to the enthalpy change in the sample material. For isothermal measurements of $(dH/dt)_T$ as a function of time, the DSC's operation is similar to that described above.

The Calorimeter Assembly

A Perkin Elmer DSC-4 Differential Scanning Calorimeter (DSC) was used for measurements of the extent of reaction and number of covalent bonds formed during polymerization. It was used for both the constant heating rate and the constant temperature modes in this study. The pans used to contain the sample and reference were aluminum pans of approximately 5 mm diameter, 2 mm height, 0.1 mm thickness and 21 mg nominal mass. The sample and reference pans were placed in separate compartments (or cells) mounted on identical, isolated bases with separate heaters and thermometers. An empty aluminum pan was placed in the reference compartment to balance the thermal

mass with that of the sample compartment. A typical sample mass was 25-30 mg with a volume slightly less than that contained within the aluminum pan. This mass was small enough to prevent thermal gradients across the sample material. This also minimized the thermal lag between the sample and the temperature sensors. An aluminum lid was sealed onto the sample pan by crimping when evolution of volatiles or the spilling of the liquids was a concern. The reference pan in this case was also sealed with a lid to maintain a similar thermal mass. Both open and sealed sample pans were used in this study. The sample and reference pans were closed into their respective compartments of the assembly and a ~0.75 ml/min continuous flow of either dry nitrogen or argon gas was attained by applying approximately 25 psi pressure. This maintained an inert environment, and no particular choice of the purge gas seemed necessary. Interfaced with the DSC assembly was a standard IBM personal computer that allowed one to automate the data acquisition and measurement variables. All data was stored on computer diskettes. The control and analysis program was written in Turbo Pascal by Dr. Günter Sartor [Sartor *et al.* (1994)]. This improved the speed and convenience of the data acquisition compared with the computer station and software originally supplied by Perkin Elmer Corporation. It also provided the data in a final format compatible with most standard analytical software.

The DSC equipment was calibrated periodically using indium as a sample, such that the measured latent heat and melting temperature were within 5.0% and 0.2 K, respectively, of literature values. During measurements over a wide temperature range,

the power difference may not remain zero even with empty sample and reference cells. This reproducible deviation was due to the power requirements of the electronics and the thermal properties of the physical construction of the cells and heaters. By measuring this background signal (with empty sample and reference pans) beforehand, the data obtained for the sample was corrected for by subtracting the two measurements. All measurements performed over a temperature range were corrected in this manner.

In the temperature scanning mode, a linear heating rate, q, of 10 K/min was used for all cases, covering temperature ranges of 228 K to 273 K and 323 K to 563 K. $(dH/dt)_T$ measurements as a function of reaction time and of temperature were made with a full scale range of 10 mcal/s with an accuracy of 5%. For isothermal studies, the samples were stabilized at 30 K below the desired measurement temperature before heating it to the predetermined temperature at 50 K/min. Since a typical time span for an isothermal experiment in this study was 60 ks, any errors due to the time taken to increase the temperature from the initial to the ultimate temperature were insignificant.

3.1.2 Dielectric Spectroscopy

For a parallel plate capacitor, with plate area, A, and separation, l, the capacitance in vacuum is given by,

$$C_o = A\varepsilon_o / l \tag{3.1}$$

where ε_o = 8.854 pF/m. If a dielectric material is placed between the two plates in full contact with them, the new capacitance is $C = \varepsilon C_o$, where ε is the dielectric permittivity of the material. When a sinusoidal voltage of the form,

$$V^* = V_o \exp(i\omega t) \tag{3.2}$$

is applied across these parallel plates, the capacitance becomes complex such that $C^* = \varepsilon^* C_o$. The resulting current is also a complex quantity and is expressed as,

$$I^* = A\left(\frac{\partial D^*}{\partial t}\right) \tag{3.3}$$

Equation (3.3) can be rewritten as,

$$I^* = \left(\frac{\partial (C^* V^*)}{\partial t}\right) \tag{3.4}$$

It can be shown that the expansion of Equation (3.4) leads to the relation,

$$I^* = \omega C_o V^* (\varepsilon'' + i\varepsilon') \tag{3.5}$$

The resulting complex admittance, Y^* ($=I^*/V^*$), can be expressed as

$$Y^* = \omega C_o (\varepsilon'' + i\varepsilon') \tag{3.6}$$

A dielectric material can be represented as a resistance in parallel, R_{par}, with a capacitance, C_{par} whose admittance,

$$Y^* = 1/R_{par} + i\omega C_{par} \tag{3.7}$$

leads to the current, $I^* = Y^* V^*$. From this, the following relations are found;

$$\varepsilon' = C_{par}/C_o \tag{3.8}$$

$$\varepsilon'' = 1/R_{par}\omega C_o \tag{3.9}$$

$$\tan\delta = 1/R_{par}C_{par}\omega \tag{3.10}$$

The dielectric material can also be represented as a resistance in series, R_{ser}, with a capacitance, C_{ser}. By the same treatment as above, the impedance, Z^* (= $1/Y^*$) = $R_{ser}+1/i\omega C_{ser}$, results in the following equations;

$$\varepsilon' = C_{ser}/C_o\left(1+\tan^2\delta\right) \tag{3.11}$$

$$\varepsilon'' = R_{ser}C_{ser}^2\omega/C_o\left(1+\tan^2\delta\right) \tag{3.12}$$

$$\tan\delta = R_{ser}C_{ser}\omega \tag{3.13}$$

For the dielectric studies done here, the parallel circuit representation was used.

The Dielectric Measurement Assembly

Except for the dielectric studies on the DMBA-catalyzed polymerization of DGEBA, all dielectric measurements were made using a microprocessor-controlled GenRad, Inc. Digibridge GR 1689 automatic RLC meter. The RLC meter (Digibridge) calculates the desired parameters from a series of 8 voltage measurements that include both quadrature ($\pi/2$) and inverse (π) vector components of the voltages across the material under test, Z_x, and across a standard resistor, R_s, both of which carry the same current. Each set of voltage measurements is made in rapid sequence with the same phase-sensitive detector and analogue-to-digital converter. In this way, properly chosen differences between those measurements cancel out the fixed offset errors, and the ratios

between these measurements subtract out the common current and scale factor effects of the detector-converter.

Figure 3.2 shows a schematic block diagram of the Digibridge. I_x is the current provided by the sine-wave generator across the known internal resistance standard, R_s, and the unknown impedance, Z_x, in series. Two voltages, e_1 and e_2 are produced across the impedance sample and resistor standard respectively from individual differential amplifiers with the same gain, K. The voltages produced are,

$$e_1 = KZ_xI_x \tag{3.14}$$

$$e_2 = KR_sI_x \tag{3.15}$$

From Equations (3.14) and (3.15) the unknown complex quantity, $Z_x = Z^*$, can be calculated from,

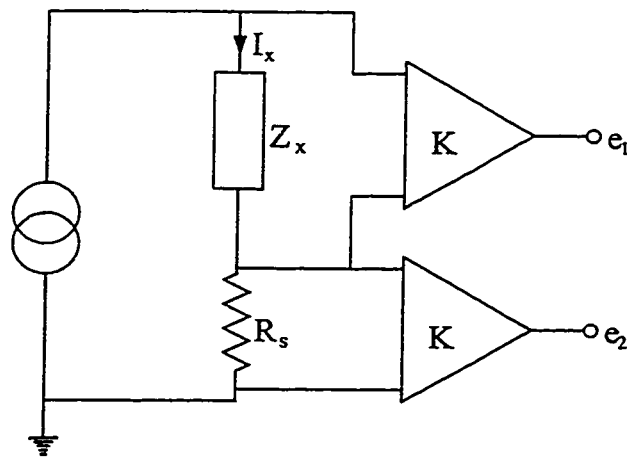

Figure 3.2: A schematic diagram of the GenRad 1689 Digibridge.

$$Z^* = R_s(e_1/e_2) \tag{3.16}$$

Z^* values are then used to calculate the capacitance, C_{par} (or C_{ser}), and the loss, tanδ, by the built-in microprocessor. The calculated value of C_{par} and tanδ are accurate to within 1% and 0.1% respectively.

The Digibridge was connected, via an IEEE-488 interface, to an IBM portable computer with a BASIC program written by myself for this purpose. (This program was adapted and modified from the original program written by J.Y. Cavaille of this group in 1986.) This increased the automation of the Digibridge's data acquisition. With this assembly, measurements can be made under both isothermal (variable frequency) and isochronal (fixed frequency, variable temperature) modes.

The Standard Dielectric Cell

A disposable dielectric cell was used for the dielectric studies of the sub-T_g relaxations during polymerization, and of the molecular dynamics during the polymerization of the DGEBA-amine mixtures. The cell was composed of a variable capacitor consisting of 18 rigid steel plates with an approximate diameter of 7 mm and a length of 15 mm. The capacitance could be varied by rotating 9 of the plates about a common axis relative to the other 9 plates by means of a turn-screw. The model 0109 variable PC mount capacitors used in the study were manufactured by Johnson Trimmer Capacitors. Their nominal air capacitance was approximately 16.5 pF, which was measured prior to each dielectric experiment.

The capacitor was connected to the Digibridge as follows; The two capacitor leads were soldered to the ends of two shielded RG-174/U coaxial cables, with the other ends of the cables spliced and soldered to the respective RG-59/U coaxial cables with standard BNC plugs on the opposite ends, and connected to the Digibridge assembly. All spliced and exposed wiring was electrically insulated with poly-tetrafluoroethylene (PTFE) and electrical tape. The capacitor was then immersed into the liquid sample, contained in a glass vial 35 mm long and 10 mm in diameter. A cork stopper was fitted into the open end to secure the coaxial leads and thermocouple. Entrapment of air bubbles between the plates was carefully avoided by rotating the cork and capacitor within the liquid to displace any air. A schematic diagram of the dielectric cell is shown in Figure 3.3. The problem of changing cell geometry during polymerization is eliminated here, since the parallel plates are rigidly and completely surrounded by the liquid. The temperature of the sample mixture was monitored by means of a copper-constantan (T-type) thermocouple. Its one end was immersed into the sample ~2 mm above the ceramic collar of the capacitor and the other end in an ice-bath stabilized at 273.2 K. The EMF produced by the thermocouple was measured with a Hewlett Packard HP 3478A multimeter that was interfaced with the computer for automatic data storage with the respective dielectric data at that instant of time. The glass vial containing the capacitor immersed in the liquid was wrapped with sufficient aluminum foil to provide electrical shielding and adequate thermal contact with the block. This assembly is referred to as the 'standard dielectric cell'. Finally, the whole assembly was grounded

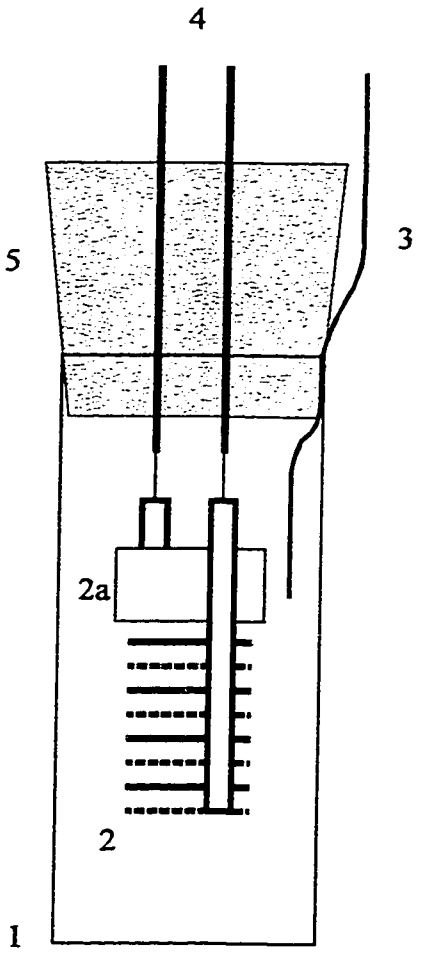

1. Glass Vial
2. Capacitor
2a. Ceramic Collar
3. Thermocouple
4. Co-axial Leads
5. Cork

Figure 3.3: A schematic diagram of the standard dielectric cell used for measuring dielectric properties at ambient pressures.

with a wire from the Digibridge to the aluminum block maintained at the desired temperature.

The High Pressure Assembly

For studying the dielectric properties of polymerizing mixtures at high pressures, it was necessary to construct an assembly that could apply and maintain high pressures to a vessel containing a dielectric cell for the period of 15-40 ks required for an experiment to reach completion. Such an apparatus was initially constructed by J.G. McAnanama of this group under my supervision, which I later modified further. Figure 3.4 shows the schematic diagram of the pressure assembly. It consisted of a Enerpac P228 hydraulic pump (1) connected to HIP 60-13HF4 three-way and two-way valves (V1 and V2, respectively), then to a 10 ksi calibrated Heiss gauge (2) (based upon a Bourdon tube mechanism) and ultimately to the stainless steel pressure vessel (3). Connections were made with HIP 304 stainless steel tubes (1/4 in. outer diameter, 1/16 in. inner diameter) rated for 5 kbar, and 1/2 inch stainless steel cone-and-socket compression fittings were used to connect the tube segments to one another, the valves, the vessel, and the pressure gauge. These fittings are designed such that, when sufficiently tightened, the ends of the tubes formed metal to metal seals with the component they were attached to. All threaded components were wrapped in PTFE tape before connecting and tightening. The hydraulic fluid used was ISO-VG-32 Hydraulic Jack Oil, purchased from Canadian Tire Corporation. With this set-up, the hydraulic fluid itself transmitted the pressure to the dielectric cell contained within the pressure vessel.

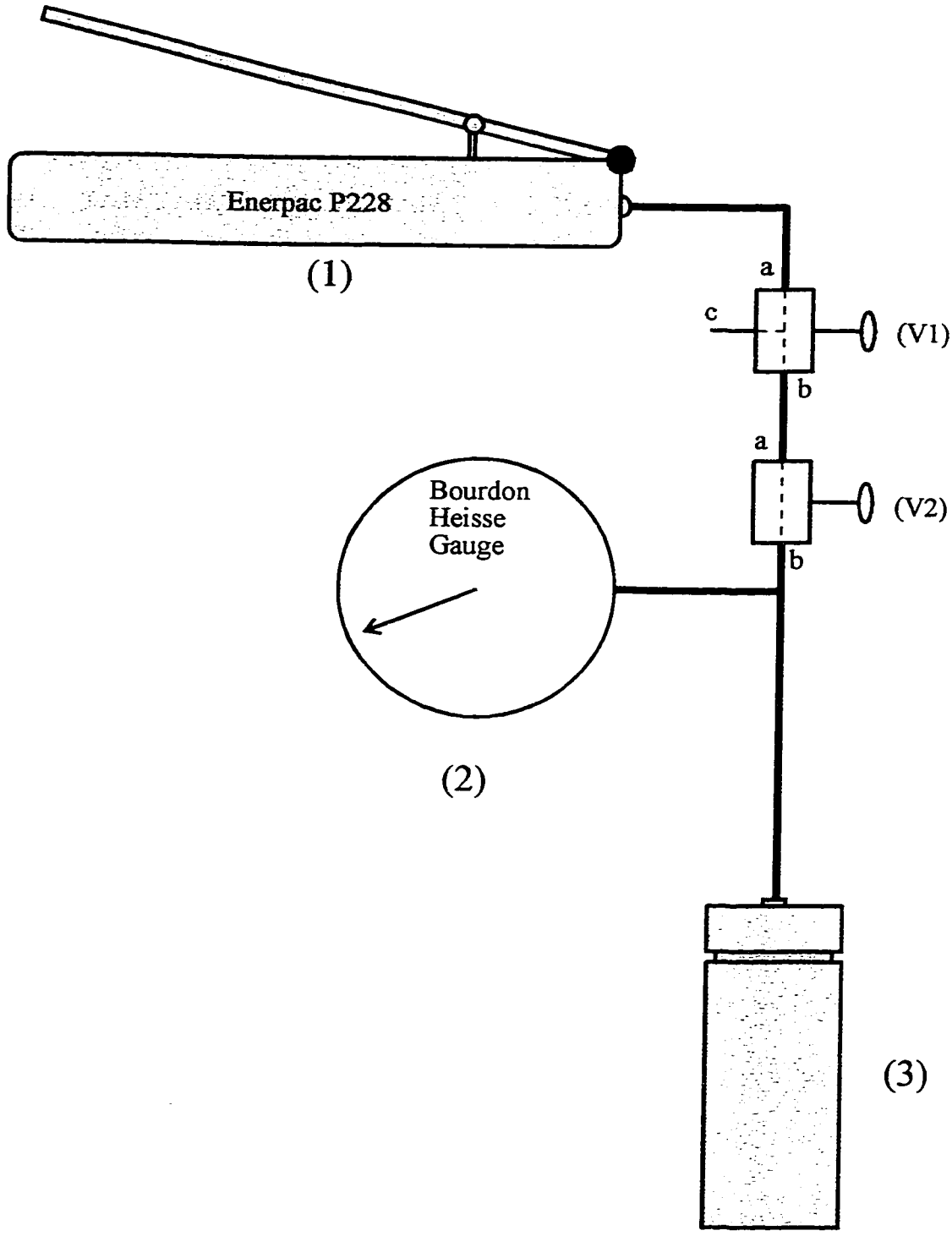

Figure 3.4: A schematic diagram illustrating the connections between the various components of the high-pressure assembly, including; a manual hydraulic pump (1), Heiss gauge (2), pressure vessel (3), and precision valves (V1 and V2).

The pressure vessel was constructed of austinetic stainless steel for high strength and corrosion resistance. It consisted of a threaded cylindrical base and a matching threaded top as shown in Figure 3.5. The base had a height of 140 mm and an outside diameter of 50.8 mm. Concentric to its cylindrical axis was drilled a 110 mm deep bore with a diameter of 25 mm. The threaded top was ~42.5 mm high and the diameter of the threaded portion was 41.2 mm

The threaded top had four axially symmetric and equidistant bore-holes drilled through it. Two of the diametrically opposite bore-holes at 22 mm distance were threaded, and the pressure tube from the hydraulic pump was connected to it. This allowed the hydraulic fluid to be pumped into the pressure vessel to a desired pressure. A stainless steel sheathed copper-constantan thermocouple that protruded 29 mm from the bottom surface of the threaded top was inserted through the second hole. A threaded fitting was used to seal the thermocouple inlet in the same manner as with the pressure inlet. The other two bore-holes had a stainless steel sheathed coaxial wire inserted into each of them, each protruding 30 mm from the bottom surface of the threaded top. These two coaxial wires were held in place and permanently sealed to the threaded top with a silver brazing alloy. Thus, of the four bore-holes, only the pressure-line and thermocouple could be detached from the threaded top when required.

The two coaxial leads protruding from the pressure vessel were connected to the Digibridge assembly in a manner similar to that of the standard dielectric cell, in that two RG-174/U coaxial cables were spliced and solder-connected to each of the sheathed

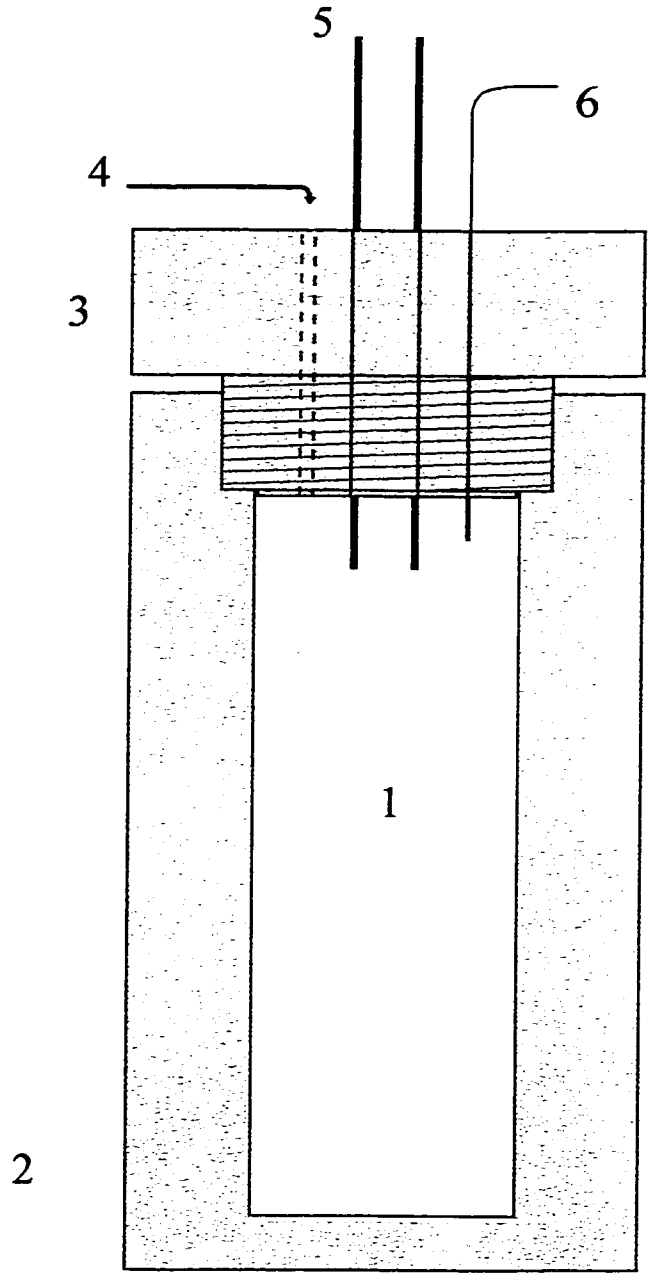

1. Inner Volume
2. Threaded Base
3. Threaded Cap
4. Pressure Fluid Inlet
5. Co-axial Leads
6. Thermocouple

Figure 3.5: A schematic diagram of the pressure vessel used to contain the high-pressure dielectric cell.

coaxial leads, with the opposite ends of the two cables attached to standard BNC plugs, which were in turn connected to the Digibridge assembly. All spliced and exposed wiring was electrically shielded with aluminum foil and wrapped with PTFE and electrical tape.

The copper and constantan wires of the stainless steel sheathed thermocouple protruding out of the bottom of the threaded cap were tightly twisted together then sealed with a drop of commercial epoxy glue, thus sealing and electrically insulating it. To the other end of this thermocouple was attached the same type of PTFE-insulated flexible T-type thermocouple as was used with the standard dielectric cell. It was attached to the sheathed wires such that the two copper and the two constantan wires were connected. The other end of this flexible thermocouple wire was tightly twisted together and inserted into a dewar flask containing ice-water stabilized at 273.2 K. The EMF produced by the temperature difference of the two ends was measured and recorded in the same manner as with the standard dielectric cell.

When tightly sealed together, the threaded top and base combined to form the pressure vessel. To ensure that an adequate seal was made between the top and base of the pressure vessel upon tightly screwing them together, both PTFE and copper-beryllium gaskets were used, as well, PTFE tape was wrapped around the threads of the top before they were connected together and tightened. Hydrostatic pressure was applied to the fluid in the vessel in the following manner; initially, valve V1, shown in Figure 3.4, was set such that channel c was closed and a and b were open, allowing hydraulic fluid to flow

into the vessel. Valve V2 was set such that channels a and b were open. The pressure was increased to the desired level using the manual Enerpac pump. Once the desired pressure was reached, valve V2 was closed, thus isolating the pressure vessel from the pump, allowing constant pressures to be maintained for the duration of a dielectric experiment. The decrease in pressure due to the sample's volume contraction during polymerization was compensated by increasing the pressure in the line leading up to the vessel, then carefully opening valve V2 to allow this fluid into the vessel. This was necessary since the sample's volume is known to contract by up to ~10% as it polymerizes [Choy and Plazek (1986)]. The pressure vessel was originally rated for a maximum *gas* pressure of 250 bar. However, experiments with the vessel's capabilities using hydraulic fluid showed that it could maintain pressures up to ~625 bar for up to 70 hours. The pressure read from the gauge was accurate to ~4 bar.

The High-Pressure Dielectric Cell

Because the hydraulic fluid itself transmitted the pressure to the sample within the pressure vessel, a cell was designed such that it could be isolated from the fluid during the dielectric measurements. It was also necessary that each sample be easily removed after an experiment and a new cell re-connected prior to the next experiment. Such a cell was designed, and is illustrated in Figure 3.6. This cell was an improvement over an earlier design described by Johari *et al.* (1996) and Wasylyshyn and Johari (1997a). The main component of the current cell consisted of a solid PTFE cylinder 20 mm long and 16 mm in diameter. A 2.3 mm diameter shaft was drilled through this cylinder, 4.8 mm

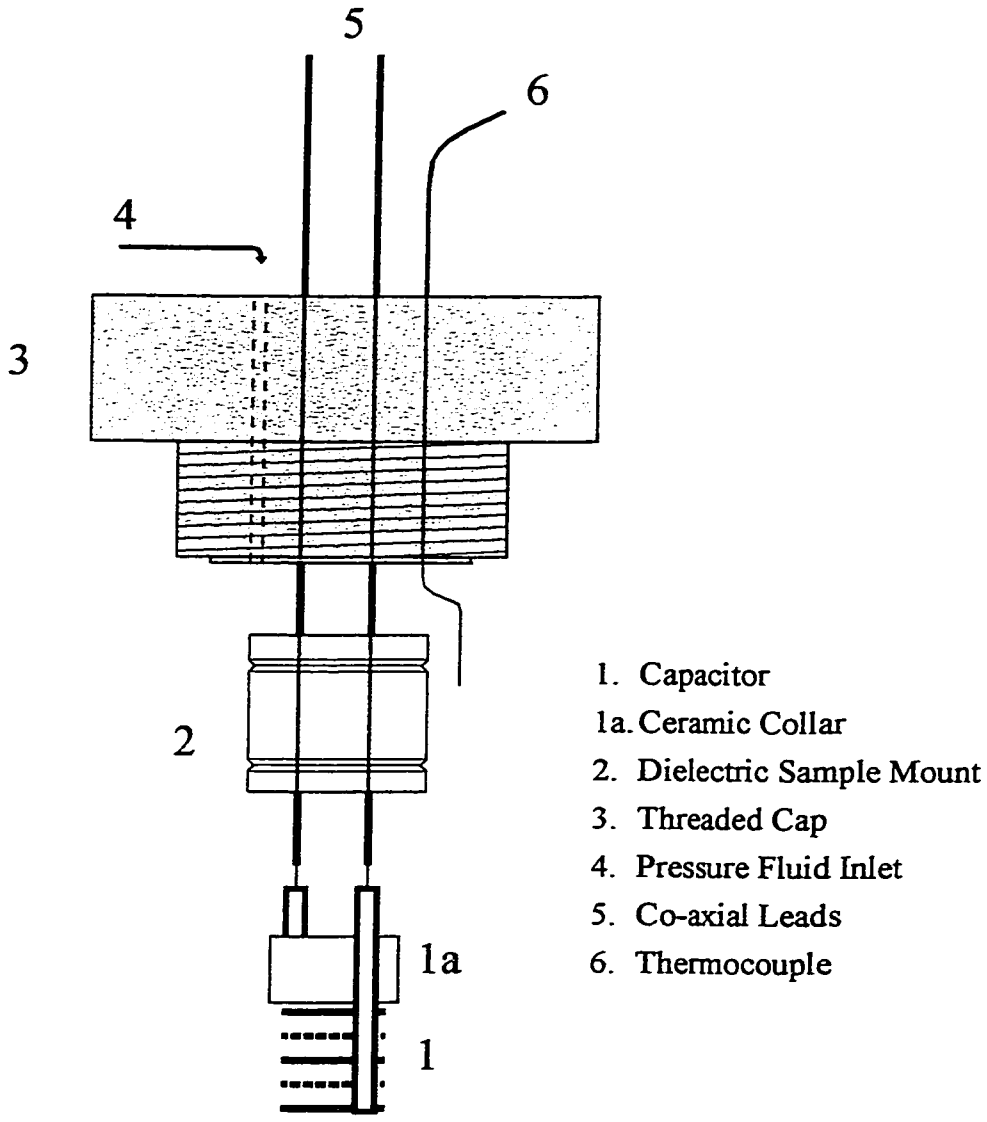

Figure 3.6: A schematic diagram of the high-pressure dielectric cell used with the pressure vessel for high-pressure dielectric measurements.

from and parallel to, its cylindrical axis. On its diametrically opposite side, a second identical shaft was drilled. Two 25 mm long steel rods, 2.3 mm in diameter were inserted into these shafts such that one end of the PTFE cylinder had both rods protruding 5 mm from its surface, and the other end such that the ends of the rods were flush with it. These are referred to as the top and bottom, respectively, of the PTFE cylinder. Two ~0.5 mm deep grooves were machined around the circumference of the PTFE cylinder 4 mm from its top and 3 mm from its bottom. The bottom of the cylinder was polished until the surface was smooth and reflective. This PTFE cylinder, with its embedded steel rods, is referred to as the 'dielectric sample mount'.

Each of the two rods protruding out the top of the dielectric sample mount were spot -welded to separate stainless steel sheathed coaxial leads protruding from the bottom of the threaded top described in the last section. Epoxy glue was then liberally applied to the welded area up to and including the bottom 2 - 4 mm of the coaxial wires. This was done both to isolate the inner wire from the outer sheath and to provide strength to the wire-to-rod weld, which was prone to bumping and jarring during sample removal after a dielectric experiment was completed. For some of the earlier measurements, a slot was machined into the top of the dielectric sample mount in between the two rods, into which was placed a grounded metal foil. This was done to decrease the errors due to the capacitor formed by the two rods within the PTFE cylinder. This mount was later replaced with an identical one but without the metal, as errors in the electrical properties due to the aforementioned effect were negligible.

Two 10 mm long, 22 AWG insulated wires were soldered to the two connections of the tunable air capacitor, described earlier in this section. The free ends of these wires were then each soldered onto each of the two smoothed faces of the rods on the bottom of the sample mount. Thus, the soldered capacitor extended ~11 mm from the bottom of the sample mount. The nominal capacitance of the assembly in air was 16.5 - 17 pF, and the capacitance of the dielectric sample mount alone (*i.e.*, no capacitor connected to it) was 0.3 - 0.4 pF, and was considered insignificant in comparison with the values of 100 pF or more measured.

The liquid sample to be studied was transferred to a 60 mm long, 20 mm diameter, and 0.1 mm thick, flexible rubber bag. Inserted into the liquid-containing bag was a 10 mm diameter, 30 - 40 mm long, and 0.7 mm thick glass tube liner, open at both ends. It was placed such that the glass liner remained upright within the rubber bag. The rubber bag was then placed onto the end of the dielectric sample mount such that the capacitor was inserted into the upright glass liner filled with liquid and the mouth of the rubber bag surrounded the PTFE cylinder. A wire was wrapped around the mouth of the rubber bag such that it was tightened against the lower groove on the circumference of the PTFE cylinder. The entire sample was covered by a second rubber bag of slightly larger diameter than the first, and similarly tightened by a wire to the upper groove on the PTFE cylinder. To summarize, the assembly consisted of the dielectric sample mount with the miniature capacitor soldered to it, immersed in 5 - 7 g of liquid mixture contained in a doubled-up rubber bag, but isolated from the inner rubber bag by the glass tube.

Precautions were taken to ensure that no air bubbles were entrapped between the parallel plates of the capacitor.

The double-bagged assembly was immersed into the hydraulic fluid contained within the base of the pressure vessel, which was already brought to a constant, desired temperature by keeping it inside a large thermostatically controlled aluminum block for several hours, and then the threaded top was screwed on and tightened. The entire operation, from the mixing of monomers to tightening the vessel took ~11 min. The hydrostatic pressure could then be raised to the desired level with the manual pump, as described in the preceding section.

The volume of hydraulic fluid within the vessel, being ~5 times that of the liquid sample, itself acted as a thermostat, and the temperature of the fluid was indistinguishably close to that of the monomeric liquid sample. The pressure vessel was kept inside the large thermostatically controlled aluminum block for the duration of the experiment, and its temperature was controlled to ±0.2 K, which is also the uncertainty of the temperature measurements.

The Thermostat Assembly and Temperature Control

A metal cylinder (steel or aluminum) nominally 6 cm in diameter and 16 cm long with a concentric 0.5 cm diameter, 5 cm deep bore was used as a thermostat assembly for the dielectric experiments using the standard dielectric cell. For experiments with the high-pressure cell and vessel, a 9 cm diameter and 25 cm long cylinder with a 16 mm deep, concentric 53 mm diameter bore was used. Both thermostats were constructed by

wrapping a woven glass fibre cloth around the block to electrically insulate the cylinder. High resistance nichrome wire was wound around the block to provide 600 W of heating power. The windings were then coated with plaster of paris to protect them and keep them in position. The unit was placed axially inside a slightly larger aluminum can to allow an annular space of approximately 2 - 4 cm from the wall of the can to the edge of the coated block. While keeping the bore-holed end flush with the top of the can, sand and silica fibres were packed into the airspace around the block for further insulation. Finally, with the leads of the electrical heating wire insulated with glass cloth and protruding out of the top of the can, plaster of paris was poured into the annular space in order to seal in the exposed sand/silica fibre mix. For dielectric measurements well above the room temperature, the thermostat assembly was allowed to remain in the ambient air. For colder temperatures, it was placed in yet another larger aluminum can with a diameter approximately 4 cm larger than the thermostat to allow the loose packing of silica fibres in the annular space. This whole assembly was then placed in a larger dewar flask containing liquid nitrogen. The temperature of the furnace was controlled by one of two temperature control units; A Eurotherm 808 temperature control unit manufactured by the Eurotherm Company was used for isothermal temperature control and for a linear heating rate starting above the room temperature. A Valley-Forge Instrument Company PC60105 was used to provide a linear heating rate starting from 100 K. Compared with the sample placed within it, the block was massive, and acted as an efficient heat sink such that the temperature, as limited by the temperature controllers,

could be controlled to less than ±0.5 K for over a day, and ±0.1 K for several hours during the course of isothermal measurements, providing that no extreme exotherms resulted from chemical reactions of the sample under study.

3.1.3 Time Domain Reflectometry

Time domain reflectometry (TDR), can be performed using a variety of different experimental configurations [Cole (1983)], the method used here involved total reflection of the incident wave. In general, this requires that the sample cell be placed as the termination of a coaxial transmission line. A schematic diagram of the experimental assembly is illustrated in Figure 3.7.

From transmission line theory [Johnson (1950), Bertolini *et al.* (1990)], the cell is considered to be an ideal section of an open circuit terminated coaxial line filled with a sample of dielectric constant, ε_x. In this case, the input admittance, y_x, can be expressed as,

$$y_x = iG_o\sqrt{\varepsilon_x}\tan(z_x) \tag{3.17}$$

where $z_x = (\omega d / c)\sqrt{\varepsilon_x}$, ω is the angular frequency, c is the speed of light, d is the coaxial line length and G_o is the characteristic admittance of the cell. y_x can also be expressed as a function of the Laplace transforms, $v_o(\omega)$ and $r_x(\omega)$, of the incident and reflected pulses, $V_o(t)$ and $R_x(t)$, respectively, at the separation plane between the cell and the coaxial line through the relation,

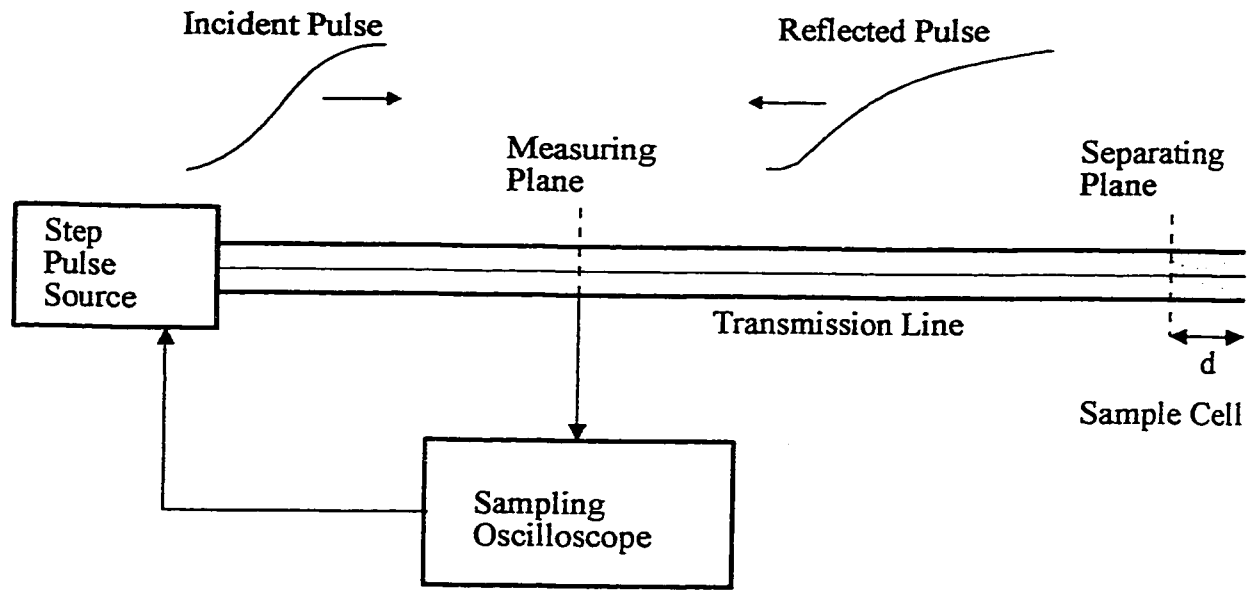

Figure 3.7: A schematic diagram of the method in which TDR generates incident pulses and measures the reflected pulses to determine the dielectric properties of materials.

$$y_x = iG_o\sqrt{\varepsilon_x}\tan(z_x) \tag{3.18}$$

where G_c is the characteristic admittance of the line connecting the pulse generator to the cell, which is typically ~0.02 S.

Instead of measuring $V_o(t)$ on a plane within the cell, better results are obtained when the reflected pulses are instead measured on a plane along the coaxial line between the cell and the pulse source, provided $V_o(t)$ does not change. With this set-up, two pulses are monitored; the reflected pulse, $R_x(t)$, from the cell containing the sample with unknown dielectric properties, and the reflected pulse, $R_s(t)$, from the cell with the reference sample of known dielectric properties. The reference material used during the experiments was air, thus, $R_s(t)$ is not time-dependent. The sample and reference were placed into identical cells that were mounted on the termination ends of identical coaxial lines to ensure that any differences arising between their properties was due to the

differing dielectric properties of the sample and reference materials, and not an artefact of the experimental set up.

If Equation (3.18) is written for each of the two samples (known and unknown), and then combined to eliminate $v_o(\omega)$, one obtains,

$$\frac{r_r(\omega)-r_x(\omega)}{r_r(\omega)+r_x(\omega)}=\frac{y_x(\omega)/G_c-y_r(\omega)/G_c}{1-y_x(\omega)y_r(\omega)/G_c^2} \tag{3.19}$$

If a reflection function is defined such that,

$$\varrho_{xr}(\omega)=\frac{c}{i\omega d\gamma}\frac{r_r(\omega)-r_x(\omega)}{r_r(\omega)+r_x(\omega)} \tag{3.20}$$

where $\gamma = G_o/G_c$, $r_r(\omega)$ is the Laplace transform of $R_r(t)$, and Equations (3.17) and (3.19) are combined, the following working equation is obtained,

$$\frac{\varepsilon_x z_r \cot(z_r)-\varepsilon_r z_x \cot(z_x)}{z_x z_r \cot(z_x)\cot(z_r)-\gamma^2\varepsilon_{xr}\varepsilon_r(\omega d/c)^2}-\varrho_{xr}(\omega)=0 \tag{3.21}$$

Assuming ε_r, d, and γ are known, Equation (3.21) can be solved numerically for ε_x at any value of the angular frequency, ω. The only approximation in this equation is that the cell is represented as an ideal section of the coaxial line.

The reflection function, $\varrho_{xr}(\omega)$ is calculated from the Laplace transform of the pulses, $R_x(t)$ and $R_r(t)$, which have step-like shapes. This implies that truncation errors will exist if the direct Laplace transform is calculated for any single pulse owing to the finite width of the experimental time window, t_w, chosen. These errors can be avoided if the reflection function is written in the equivalent form,

$$\varrho_{xr}(\omega) = \frac{c}{d\gamma} \frac{\mathcal{L}\left[R_r(t) - R_x(t)\right]}{\mathcal{L}\left[\mathrm{d}\left(R_r(t) + R_x(t)\right)/\mathrm{d}t\right]} \tag{3.22}$$

where $\mathcal{L}[x]$ denotes the Laplace transform operator applied to x [Cole *et al.* (1980)]. The functions transformed in Equation (3.22) assume zero values when $t > t_w$ for a suitable choice of t_w. This procedure can also be used in the presence of dc conductivity, when the difference $[R_r(t) - R_x(t)]$ assumes a constant value for $t > t_w$. In this case, Equation (3.22) can be re-expressed as,

$$\varrho_{xr}(\omega) = \frac{c}{i\omega d\gamma} \frac{\mathcal{L}\left[\mathrm{d}\left(R_r(t) - R_x(t)\right)/\mathrm{d}t\right]}{\mathcal{L}\left[\mathrm{d}\left(R_r(t) + R_x(t)\right)/\mathrm{d}t\right]} \tag{3.23}$$

In general, the characteristic impedance of the transmission line connecting the measuring plane to the dielectric cell is not uniform along the propagation axis. This introduces spurious reflections of the traveling pulses superimposed on the reflections from the sample cell. The effect of these reflections are corrected by using linear circuit analysis [Cole (1983)] to derive a relationship between the admittance measured at the measuring plane, $\bar{y}_x(\omega)$, and the desired property, $y_x(\omega)$, the input admittance at the separating plane. $y_x(\omega)$ of the cell containing the sample of dielectric constant, $\varepsilon_x(\omega)$, can be related to $\bar{y}_x(\omega)$ through the bilinear transformation,

$$\bar{y}_x = \frac{a(\omega) + b(\omega) y_x(\omega)}{1 + c(\omega) y_x(\omega)} \tag{3.24}$$

where $a(\omega)$, $b(\omega)$ and $c(\omega)$ are complex quantities characterizing the measuring system. For any two samples having dielectric constants $\varepsilon_x(\omega)$ and $\varepsilon_r(\omega)$, the Laplace transforms

$\bar{r}_x(\omega)$ and $\bar{r}_r(\omega)$ of the respective reflected signals monitored at the measuring plane are related to $\bar{y}_x(\omega)$ and $\bar{y}_r(\omega)$ by an analogous form of Equation (3.19) except that the admittances, y, and reflections, r, are replaced by $\bar{y}$ and $\bar{r}$, respectively.

A reflection function, $\bar{\varrho}_{xr}(\omega)$ can be defined using $\bar{\varrho}_x(\omega)$ and $\bar{\varrho}_r(\omega)$ in place of $r_x(\omega)$ and $r_r(\omega)$, respectively, in Equation (3.20), such that through this new reflection function, Equations (3.19) and (3.24), it follows that,

$$\varrho_{xr}(\omega) = \frac{A^*(\omega)\bar{\varrho}_{xr}(\omega)}{1+B^*(\omega)\bar{\varrho}_{xr}(\omega)} \tag{3.25}$$

where A^* and B^* are complex quantities independent of y_x.

Equation (3.25) thus gives the reflection function corrected for the spurious reflections caused by the admittance effects of the coaxial line used to transmit the pulse signal to the sample cell. The parameters A^* and B^* are determined by measuring the dielectric properties of two different liquid samples (in addition to the reference sample) in the frequency range of interest prior to an experiment. These measured values are then compared to the actual known values. This procedure of calculating A^* and B^* from Equations (3.21) and (3.25) through the measurement of several standard materials is henceforth referred to as the bilinear calibration procedure (BCP).

The sample cell used for the TDR measurements consisted of a shielded coaxial open circuit, as illustrated in Figure 3.8(a). In this case, the input admittance can be approximated by Equation (3.17), provided that one substitutes the actual length, d_m, of the inner conductor pin, with an equivalent electrical length, d, which takes into account the contribution of the fringing field. This additional length is usually on the order of $(r_1 - r_2)/2$, where r_1 and r_2 are the inner and outer radii of the annular space within the cell, respectively [Somlo (1967), Cole *et al.* (1989), Bertolini *et al.* (1990)]. For samples of high dielectric permittivity at high frequencies, it is necessary to minimize the quantity z_x $(= (\omega d/c)(\varepsilon_x)^{1/2})$ by reducing the length, d, of the pin. Unfortunately, to adequately

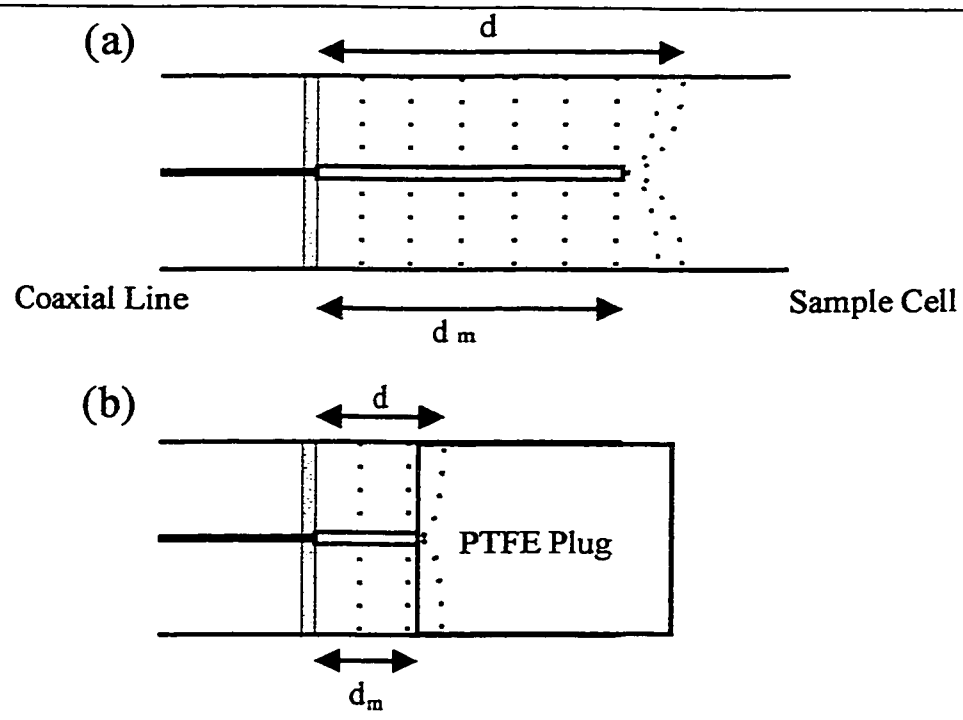

Figure 3.8:(a) A schematic diagram of the coaxial sample cell terminated by a shielded open circuit; **(b)** cell with PTFE plug substituting the liquid in the fringing field volume. The dashed lines denote electric field lines.

minimize z_x, the value of d that must be used is on the order of the extra length representing the fringing field. The presence of the fringing field makes the use of Equation (3.17) inappropriate. To solve this problem, the cell represented in Figure 3.8(b) was used such that the sample was confined by a plug of low dielectric permittivity (ε ~2), which was inserted into the cell up to the top of the inner conducting pin [Mashimo *et al.* (1987), Bertolini *et al.* (1990)]. The use of a PTFE plug allowed the equivalent length, d, to coincide with the mechanical length, d_m, and the input admittance of the cell filled to the top of the conducting pin with a liquid of dielectric permittivity, ε_x, is correctly represented by,

$$\tilde{y}_x = (y_x + y_p)/(1 + z_{sc} y_p) \qquad \textbf{(3.26)}$$

where y_p is the input admittance of the section of the cell containing the plug, y_x and z_{sc} are the open circuit admittance and the short circuit impedance of the section of the cell containing the sample [Johnson (1950)]. In most cases, the product $z_{sc} y_p << 1$, thus, Equation (3.26) can be approximated by, $\tilde{y}_x = y_x + y_p$, meaning that the dielectric plug can be mathematically treated as a discontinuity in the transmission line. Because the consecutive application of two or more bilinear transformations results in a bilinear transformation, it follows that a single BCP, via Equation (3.25), takes into account both the mismatches along the transmission line and the effect of the dielectric plug terminating the cell.

Time Domain Reflectometry Assembly

A dual channel experimental assembly was used for the TDR measurements [Cole *et al.* (1980), Bertolini *et al.* (1990)] at Istituto Fisica e Molecolare del CNR, Pisa, Italy. The main components of the assembly are comprised of a Tektronix 7854 waveform processing oscilloscope (WPO), a 7S12 TDR/sampler, a 7S11 sampling unit, a S52 pulse generator, and two S6 feed-through sampling heads. A schematic illustration of this setup is shown in Figure 3.9.

The step-like pulse (rise time ~20 ps, amplitude ~250 mV) from the pulse generator passes through a sampling head and is reflected from the discontinuities created by the sample cell at the opposite end of the coaxial line. The combination of the S52 pulser and the S6 sampler increases the actual rise time to about 35 ps. A small, high-frequency component of the signal, extracted by a directional coupler (Narda DCS-110, 10 dB, 7-12.4 GHz), passes through the second sampling head and is reflected at the opposite end of the open terminated coaxial line. This signal has an impulsive shape, an amplitude of ~20mV, and full duration, half maximum (FDHM) of ~50 ps.

The choice of time window, t_w, through which the reflected signals are observed, determines the frequency range that is attainable with this assembly. The minimum frequency possible is related by $f_{min} \approx 1/t_w$, while the maximum frequency by $f_{max} \approx N/2t_w$, where N is number of sampled and digitized points used. In order to attain the desired frequency range used here, and to account for sample cell "charging time" [Cole *et al.* (1980)], t_w was chosen to be 5 ns.

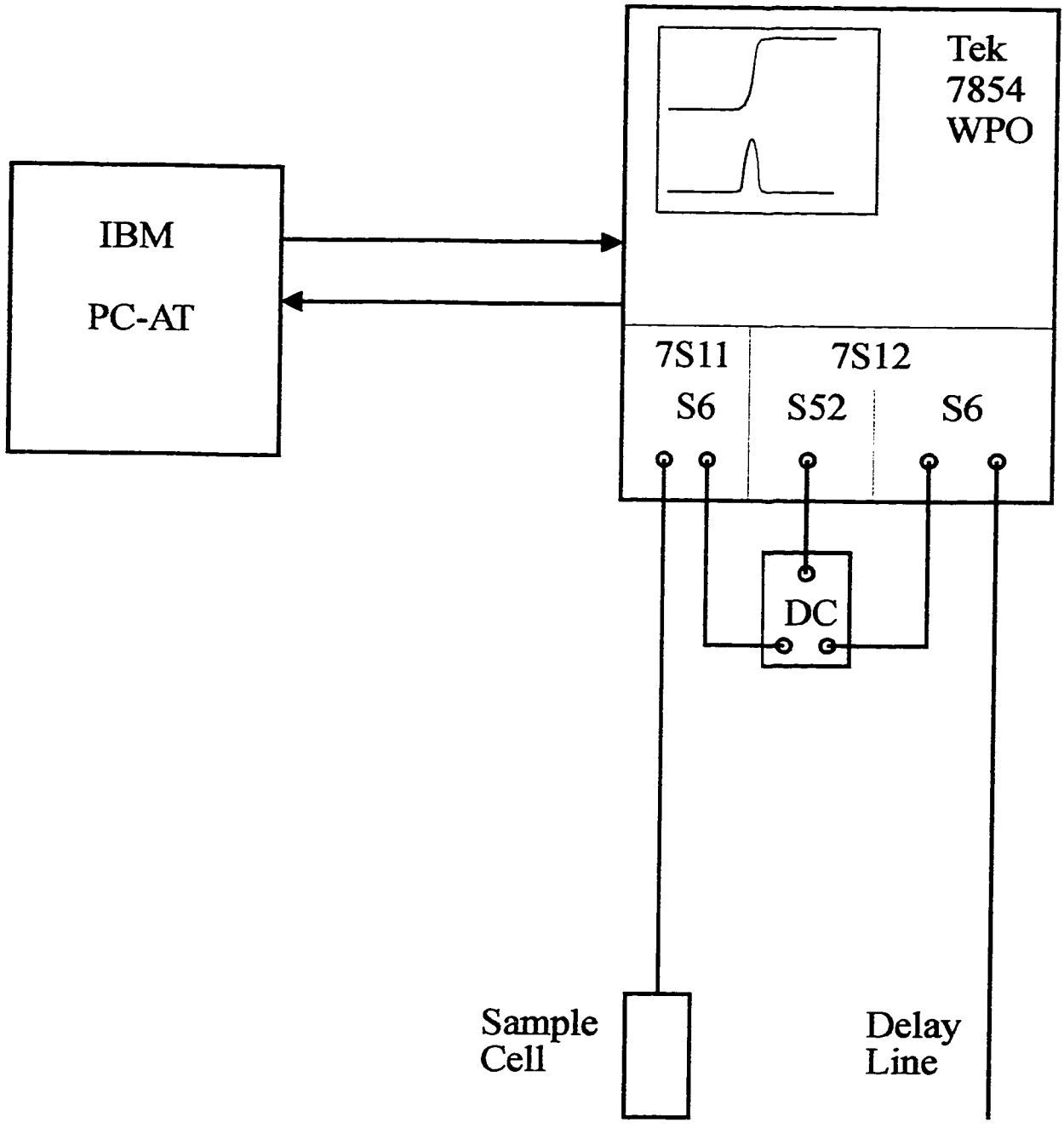

Figure 3.9: An illustration of a the TDR experimental assembly. Abbreviations are described in the text.

The transmission lines used were low-loss, semi-rigid coaxial cables equipped with standard SMA connectors. The cells that contained the liquid sample of unknown dielectric permittivity were made by assembling parts of commercially available SMA connectors or SMA/APC-7 adapters. Cells of internal diameter 3.65 mm and depth of 5.05 mm were used. The liquid sample was injected into the cell using a syringe, to the height of the inner conducting pin, d_m = 2.5 mm. The temperature of the cell was controlled by placing it between two commercially available heater/cooler platens, based upon the principle of a Peltier cell, where one face of a platen was the hot junction and the opposite face the cold junction. The sample cell was sandwiched between the two platens such that the hot surface of each platen was in contact with the sample cell but the cold surfaces were isolated from it and regulated with circulating water at ~300 K. The Peltier cells were controlled with an electronic PID controller built in-house for the purpose. The temperature of the Peltier cells was monitored by the PID controller using a T-type thermocouple built into the platens. Because the sample cell was significantly smaller than the platens, and the volume of liquid sample was ~0.05 ml, the sample temperature was assumed to be equal to the temperature of the platens. Thus, the temperature of the sample cell could be controlled to ± 0.1 K in the range 230 to 350 K (Temperatures less than ambient could be attained by reversing the dc current to the Peltier cells).

The signal, $R_x(t)$, reflected from the sample cell and its associated referencing pulse, $P(t)$ from the second transmission line, were sampled and digitized alternately in

512 equal time intervals with an average of 60 acquisitions performed in order to minimize the noise. The acquisition procedure was automated by interfacing the apparatus to a standard PC-AT computer via an IEEE-488 interface port, thereby also allowing the results of the reflected and reference waveforms to be stored in ASCII-type files. The mathematical treatment of the 'raw' data acquired using the above mentioned equations and procedures was performed after the experiment was complete, and was automated with the use of mathematical computer algorithms prepared for the task. A detailed description of the use of such programs as well as the mathematical operators used in each have been given by Cole *et al.* (1989), and Bertolini *et al.* (1990).

Frequency Domain Spectrometry (FDS) was used to measure the dielectric properties of polymerizing liquids in the frequency range 1 MHz to 70 MHz in order to extend the frequency range measured by the TDR method. Measurements were made using an assembly built around a capacitance bridge. The conductance and capacitance were determined from the phase shift, $\tan\delta$, and the relative amplitude of the sinusoidal voltages measured on the sample and reference arm [Tombari and Johari (1992)]. The FDS assembly consisted of a radio frequency circuit, a Tektronix AFG 2020 sinusoidal signal generator, and a Tektronix TDS420 Oscilloscope for digitizing the waveforms. These instruments were interfaced to a standard PC-AT computer via an IEEE GPIB 488 interface for automatic data acquisition and storage.

The FDS sample cell acting as a capacitor was a coaxial design with an outer cylinder of external diameter of 14 mm, internal diameter of 7 mm and a height of 38

mm. The inner pin was 3 mm in diameter and 32 mm in length. Both the outer cylinder and the conducting pin were machined from stainless steel and were gold plated. Temperature control of the sample cell was attained using a digital PID controller built in-house for the purpose and a dual Peltier cell arrangement similar to that for the TDR assembly.

3.2 EXPERIMENTAL PROCEDURES

3.2.1 Preparation of the Thermosetting Polymers

Several different types of epoxide-based polymers were prepared depending upon the particular study. For studying the evolution of secondary (or local) relaxations at a constant frequency, polymerization was carried out by reacting either a diepoxide with monoamines, or by reacting a triepoxide with monoamines. The product of the former is a linear chain polymer while that of the latter is a network-structure (cross-linked) polymer. The liquid mixtures were obtained by mixing stoichiometric amounts of one of the monoamines; aniline (AN), 3-chloroaniline (3CA), 4-chloroaniline (4CA), and cyclohexylamine (CHA), purchased from Aldrich Chemical Co., with one of the two epoxide molecules; diglycidyl ether of bisphenol A (DGEBA), a diepoxide, and Tactix 742 (Tactix), a triepoxide, donated by Shell Petroleum as Epon 828 and Dow Chemical Co., respectively. These substances will be referred to by their abbreviations in parentheses. For stoichiometric compositions, 1 mol of monoamine needed to be mixed

with 1 mol of DGEBA and 3 mol of monoamine needed to be mixed with 2 mol of Tactix.

Accurately weighed amounts of the two components were then mechanically mixed in a 3 ml glass vial for approximately 2 min at 298 K for the DGEBA mixtures and for approximately 10 min at 308 K for the more viscous Tactix mixtures. Approximately 2 ml of a homogenous, transparent liquid was obtained in each case. This liquid was then transferred to either a standard dielectric cell or aluminum DSC sample pan, both described in Sections 2.1.2 and 2.1.1, respectively.

For the study of the evolution of secondary, or β-, relaxations over a spectrum of frequencies at several stages of the reaction, catalytically polymerizing mixtures, consisting of DGEBA mixed with either 5 or 10 mole% dimethylbenzylamine (henceforth DMBA5 and DMBA10, respectively) were used. DMBA was purchased from Aldrich Chemical Co. and was used as received. These mixtures were prepared by weighing amounts of approximately 5 g and mechanically mixing the components for 1 - 2 min at 298 K. A portion of the ultimately transparent, colourless and homogenous liquid was then transferred to either an aluminum DSC sample pan (5 - 10 mg) or to a TDR sample cell (.03 - .05 ml) within 2 - 3 min of mixing.

For studying the effects of pressure on the evolution of molecular dynamics during polymerization, mixtures of DGEBA were prepared using a stoichiometric amount of each of the following amines; 1,2-diamino ethane (EDA), 1,6-diamino hexane (HDA), hexylamine (HA), and aniline (AN). All amines were purchased from Aldrich Chemical

Co., and used as received. For the studies under pressure only, the DGEBA was degassed in an evacuated desiccator for 7 - 10 min immediately prior to mixing with each amine. Each mixture was prepared by weighing in amounts of 8 - 10 g, and mixing for approximately 5 min. Once a homogenous liquid mixture was obtained, it was transferred to the rubber bag of the high-pressure dielectric cell and affixed to the dielectric sample mount as described in Section 3.1.2.

3.2.2 Calorimetric and Dielectric Measurement Procedures

The $(dH/dt)_T$ data measured by DSC was used to determine the number of covalent bonds formed during the course of polymerization for the two studies on the evolution of the localized relaxation process. For this purpose, 10 - 20 mg of each liquid mixture contained in an aluminum sample pan was allowed to react isothermally for a period of 40 - 70 ks at preselected temperatures, and $(dH/dt)_T$ was measured. To completely react the mixtures, the sample was thereafter heated at 10 K/min and $(dH/dt)_q$. measured. The total heat evolved during the ramp-heating plus the heat evolved during the isothermal polymerization was equal to the total heat of reaction.

Dielectric measurements at a constant frequency were performed with the GenRad GR1689 Digibridge described in Section 3.1.2 for both: (i) the evolution of localized relaxations and (ii) the effects of pressure on the molecular dynamics. For studying the evolution of localized relaxations, the freshly mixed liquid sample was transferred to the standard dielectric cell, then ε' and ε'' were measured at a fixed frequency of 1 kHz from

77 K to a temperature ~20 K below the preselected isothermal reaction temperature, T_r, at a heating rate of 1K/min. Thereafter, the mixture was transferred to a second thermostat block previously equilibrated at T_r and the sample isothermally reacted for a predetermined length of time. The dielectric cell containing the partially polymerized mixture was then cooled to 77 K and ε' and ε'' again measured over the same range and at the same rate as initially. This step was repeated several times until the mixture had completely polymerized. The interval of time during which isothermal polymerization at T_r occurred was increased such that the data were collected after near-equal increases in the number of covalent bonds formed, as determined from calorimetry. The last set of ε' and ε'' measurements during heating were made after almost completely polymerizing the mixture by maintaining it at 30 - 50 K above its ultimate glass transition temperature, T_g, for almost 16 hours. This procedure was used to study the evolution of localized relaxations for the polymerization of; i) DGEBA with AN, and CHA, ii) Tactix with AN, 3CA, and 4CA, and, iii) DGEBA catalyzed with 5 mol% DMBA, each at preselected temperatures and times.

For the studies at high pressures, four different types of experiments were performed as follows; In the first experiment, ε' and ε'' were measured continuously at a frequency of 1 kHz during the isothermal polymerizations of DGEBA in stoichiometric mixtures with CHA and with EDA at three different temperatures and at pressures of 1, 103, and 206 bar. In the second experiment, ε' and ε'' were measured continuously at 1 kHz frequency while the pressure was instantaneously increased from 1 to 200 bar at an

early stage of the isothermal polymerization of DGEBA mixed with EDA, HDA, AN, or HA. In the third experiment, ε' and ε'' were measured continuously while the pressure was instantaneously increased from 1 to 200 bar at a later stage of the isothermal polymerization of the same mixtures at the same temperatures as the second experiment above. Finally, in the fourth experiment using pressure, ε' and ε'' were measured continuously while the pressure was instantaneously increased to 200 bar then decreased to 1 bar several times at a predetermined time interval during the isothermal polymerization of the same mixtures at the same temperatures as the second experiment above.

The net errors in the dielectric data are likely combination of the errors in the weighing and mixing of the reactants, the elapsed time between mixing and beginning the measurements, and the uncertainties in the temperature and pressure. In addition, the reported uncertainty of the capacitance and loss measured by the Digibridge are 0.1% and 1%, respectively. The data reported here are therefore uncertain by no more than 1% in ε' and 2% in ε''. This was confirmed by repeat measurements of some of the mixtures.

For studying the evolution of secondary relaxations over a spectrum of frequencies while polymerization progressed, the TDR and FDS assemblies were used. For the mathematical treatment of the TDR data, it was necessary to calibrate the assembly using air, chloroform, heptane and methylene chloride as dielectric standards at 298 K [Bertolini *et al.* (1990)]. For the experiments, the reflectivity was measured over a range of frequencies from 100 MHz to 25 GHz at several stages of the catalytic

polymerization of DGEBA with DMBA5 and with DMBA10 at 335.4 K. Using the mathematical procedures described in Section 3.1.3 and by Bertolini *et al.* (1990), the complex permittivity (ε' and ε'') was calculated from the reflectivity.

The FDS assembly also required calibration, which was performed using air, CCl_4, CH_2Cl_2, and $CHCl_3$ in a manner similar to that for the TDR assembly. The sample under study was prepared such that the polymerizing mixture that was poured into the FDS sample cell was taken from the same supply mixture prepared for the TDR assembly in order to ensure the two assemblies measured their respective dielectric properties for mixtures of identical chemical compositions. Measurements were taken such that a single program triggered first the FDS data acquisition, then the TDR data acquisition. In this manner, two data files were obtained for each spectrum at the same time of polymerization; one contained the FDS dielectric data from 1 MHz to 70 MHz, and the other contained TDR dielectric data from 100 MHz to 25 GHz. To summarize, the freshly prepared liquid sample was divided between the TDR and the FDS sample cells, and the computer program started thereafter such that at regular time intervals, spectra were obtained from 1 MHz to 70 MHz by the FDS assembly and 100 MHz to 25 GHz by the TDR assembly.

The total number of bonds formed at the time each spectrum was determined by calculated using calorimetry in separate experiments at the same polymerization temperatures. Thus, the change in the dielectric properties measured as a function of time was related to the number of covalent bonds formed during polymerization.

CHAPTER IV

RESULTS AND DATA ANALYSIS

4.1 CALORIMETRIC STUDIES AND THE NUMBER OF COVALENT BONDS FORMED

Polymerization of DGEBA-CHA, DGEBA-AN, Tactix-AN, Tactix-3CA, Tactix-4CA, DGEBA-DMBA5 and DGEBA-DMBA10 was studied isothermally at temperatures of 313.4, 343.0, 332.0, 360.6, 349.5, 335.4 and 335.4 K, respectively. The plots of $(dH/dt)_T$ against the polymerization time, t, for the seven mixtures, are shown in Figure 4.1. $(dH/dt)_T$ initially decreases steadily to a minimum value, and then increases towards a plateau value at long polymerization times. At this time the sample is close to vitrification and further polymerization can be observed only after an extremely long period of time elapses at that temperature. Depending upon the mixture and the isothermal temperature used, the duration over which $(dH/dt)_T$ was measured varied between 30 to 60 ks. The plot for Tactix-3CA shows $(dH/dt)_T$ against t with a final plateau value that is less than its initial value. This feature is unique to this mixture and will be discussed later in this section.

The total heat of reaction was then determined by heating the partially polymerized sample at a constant rate, q, of 10 K/min from ~320 to ~550 K. The upper limit of the temperature differed for different mixtures, but was achieved when $(dH/dt)_q$ reached a plateau-like value as the temperature increased. Plots of $(dH/dt)_q$ against the

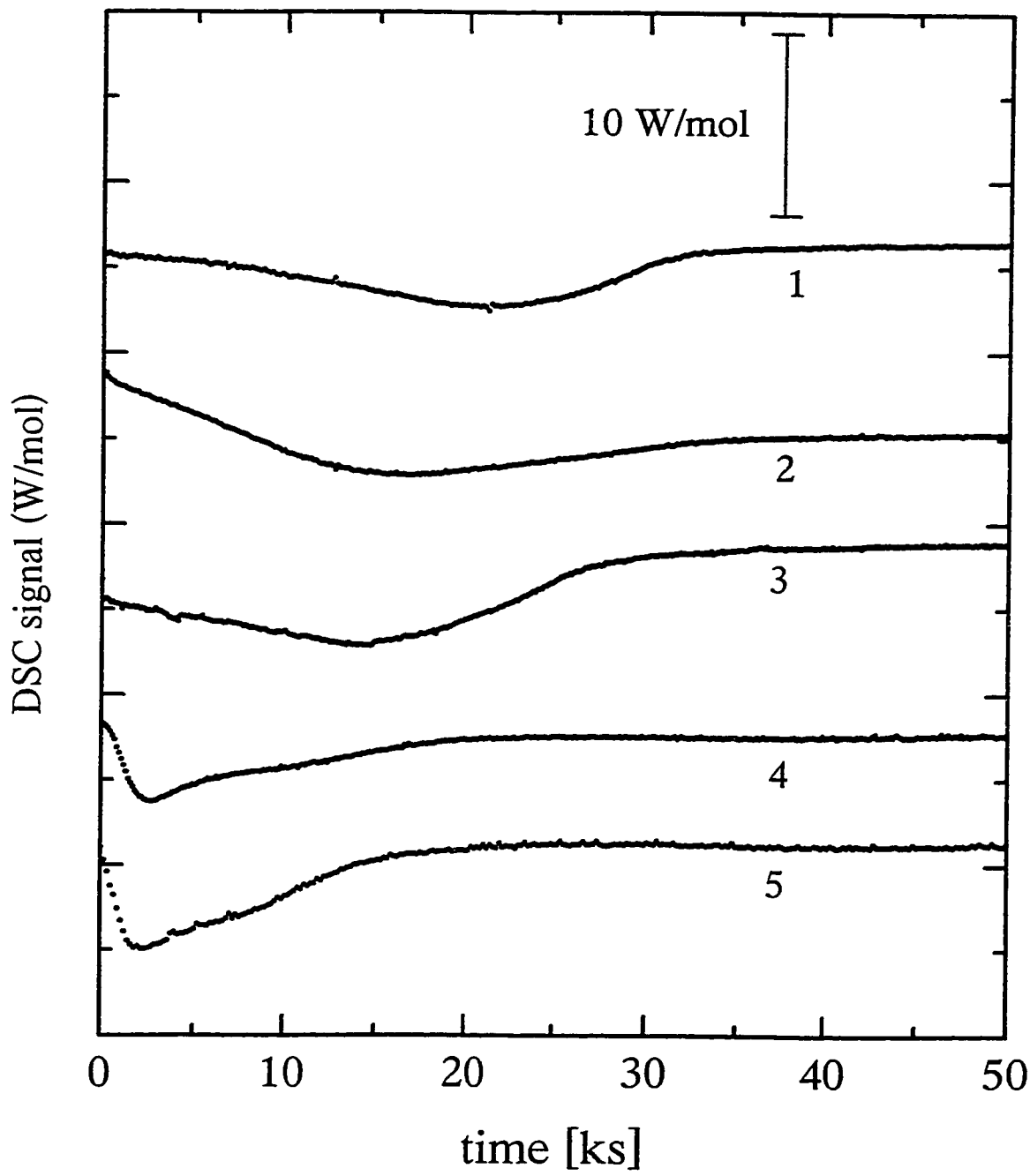

Figure 4.1: The measured DSC output plotted against the reaction time for the isothermal polymerizations of the following molecular liquids; (1), Tactix-AN at 332.0 K, (2) Tactix-3CA at 360.6 K, (3) Tactix-4CA at 349.5 K, (4) DGEBA-DMBA5 at 335.4 K, and (5) DGEBA-DMBA10 at 335.4 K.

temperature for the seven mixtures are shown in Figure 4.2. The shape of the curves is qualitatively similar to that of Figure 4.1, except that the exotherm is preceded by a sharp endothermic peak. This peak is partly due to, i) the enthalpy recovery overshoot after the glass → rubber (or liquid) transition of the partially polymerized mixture that had physically aged, as observed by Plazek and Frund (1990), Wisanrakkit and Gillham (1990), and Wasserman and Johari (1993, 1994), and, ii) the sharp exotherm from the polymerization process. The heats of reaction for each of the mixtures were less than those determined from the area of the $(dH/dt)_T$ curves of Figure 4.1, indicating that most of the polymerization had already occurred during the isothermal measurements.

The total heats of reaction for the polymerization of each of the seven mixtures was obtained by integrating the sample's isothermal plot from $t = 0$ to a time, t_{max} at which the evolution of heat due to polymerization was unobservable, typically 30 - 60 ks, and adding to this the integrated area under the plot obtained upon further heating of the sample from temperature, T_1, below T_g, to a final temperature, T_2, at 10 K/min. The total heat of reaction is expressed by,

$$\Delta H^{o}_{total} = \int_{0}^{t_{max}} \left(\frac{\partial H}{\partial t}\right)_T dt + \frac{1}{q}\int_{T_1}^{T_2} \left(\frac{\partial H}{\partial t}\right)_q dT \qquad (4.1)$$

ΔH^{o}_{total} was found to be 54.8, 79.2, 77.8, 68.5, 69.6, 56.5, and 47.7 kJ per mole of epoxide group initially present for DGEBA-CHA, DGEBA-AN, Tactix-AN, Tactix-3CA, Tactix-4CA, DGEBA-DMBA10 and DGEBA-DMBA5, respectively. Data for DGEBA-CHA and DGEBA-AN were taken from Parthun and Johari (1995) and Parthun *et al.* (1996),

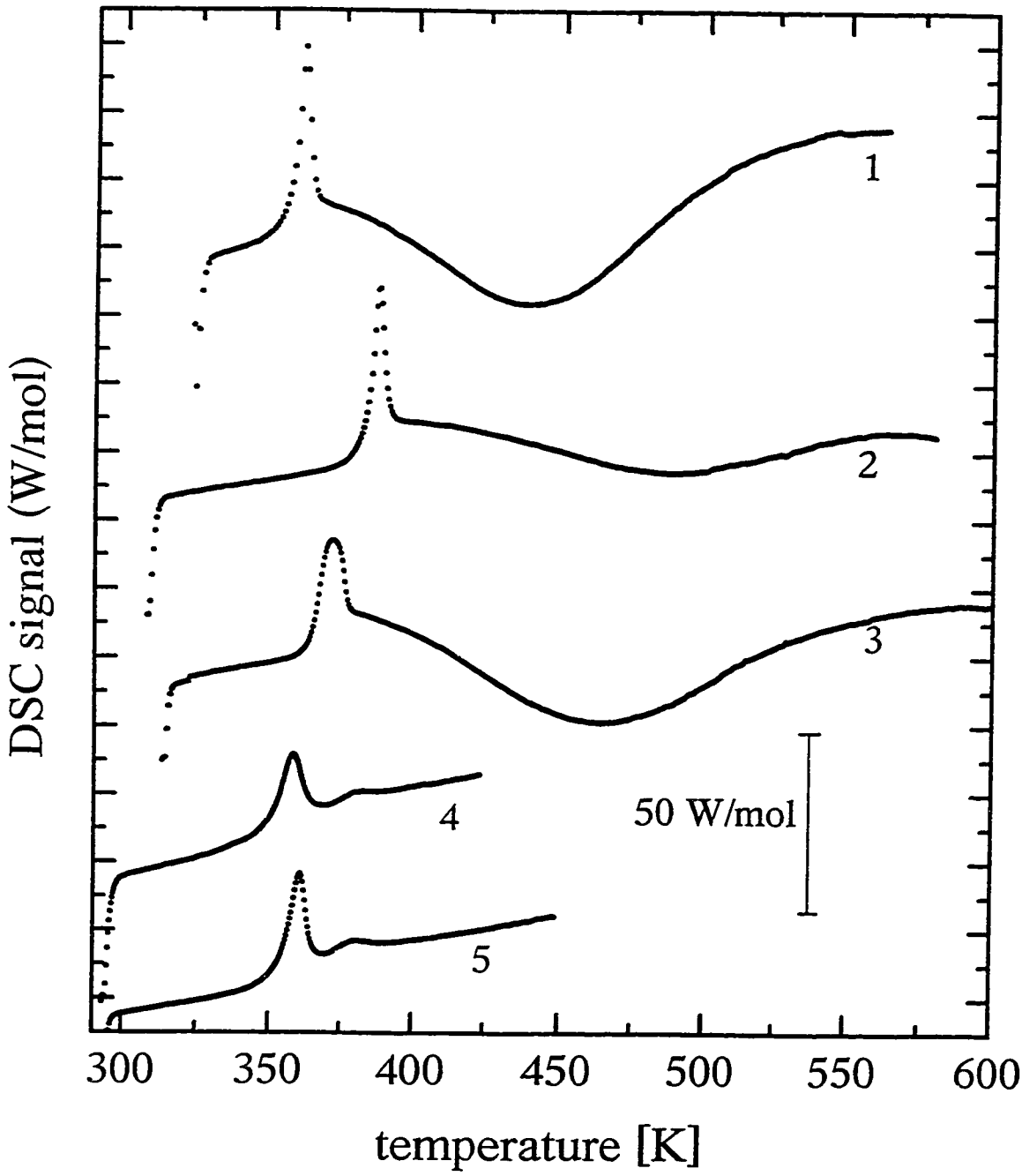

Figure 4.2: The measured DSC output plotted against the temperature at a heating rate of 10 K/min following the isothermal polymerization shown in Figure 4.1 for the following molecular liquids; (1), Tactix-AN, (2) Tactix-3CA, (3) Tactix-4CA, (4) DGEBA-DMBA5, and (5) DGEBA-DMBA10.

respectively. In order for Equation (4.1) to be valid, the contribution to ΔH^{o}_{total} from the second integral on the RHS must vary negligibly with the temperature. As reported above, the total heat released per mole of bonds formed was typically 70 kJ, and this is relatively large in comparison with the expected contributions from $(\partial \Delta H^{o}_{total}/\partial t)$ over a temperature range of ~ 200 K. For this reason, the errors introduced by this approximation are not considered significant.

A baseline must be defined for the plots in Figures 4.1 and 4.2 in order to calculate the enclosed area according to Equation (4.1). For all the liquids except for Tactix polymerizing with 3CA, this baseline was a straight line connecting the first measured data point to the data where $(dH/dt)_T$ reaches a plateau-like value. The curves in Figure 4.1 for Tactix reacting with 3CA show that the magnitude of the plateau in $(dH/dt)_T$ is significantly less than the initial value, which leads to errors when a straight line is used to enclose the area. Barton (1985) has described a reiterative calculation to obtain a non-linear baseline based on the extent of reaction, $\alpha(t)$. This method requires, however, that an initial plateau value precedes the decrease to the minimum value in $(dH/dt)_T$, which is usually not the case in isothermal measurements of polymerization. In the absence of another method for determining the area enclosed by this curve, a straight-line baseline was used. α, at an instance of polymerization, t, is then calculated from,

$$\alpha(t) = \frac{\Delta H^{o}(t)}{\Delta H^{o}_{total}} \tag{4.2}$$

where $\Delta H^{\circ}(t)$ is the amount of heat evolved up to the time, t. Since the heat evolved is due to the formation of covalent bonds during polymerization, the number of bonds, $N(t)$, is calculated from,

$$N(t) = bN_A\alpha(t) \tag{4.3}$$

where N_A is Avogadro's number and b the number of bonds formed in one mole of the stoichiometric mixture. $b = u/(v+w)$ when u bonds form between v molecules of epoxide and w molecules of amine. For polymerization of DGEBA and monoamine (CHA or AN), $b = 1$. For Tactix and monoamine (AN, 3CA, or 4CA), $b = 6/5$, and for the catalytic polymerization of DGEBA by DMBA, $b = 2$. Therefore, the ultimate value of N attained, $N(\infty)$, is $6.022\text{x}10^{23}$ for DGEBA reacting with monoamines, $7.23\text{x}10^{23}$ for Tactix reacting with monoamines, and $12.04\text{x}10^{23}$ for DGEBA catalyzed with DMBA. Equations (4.2) and (4.3) assume that the heat released per covalent bond is the same during the entire polymerization. Since the heat evolved per mole of bonds is small in comparison with the total heat released during polymerization, the errors associated with this approximation are not considered significant. Thus, the polymerization time becomes equivalent to the number of covalent bonds formed through Equations (4.2) and (4.3) and the measured properties may be written as a function of a molecular structure-oriented property, namely $N(t)$ or $\alpha(t)$. For Tactix polymerizing with AN, 3CA and 4CA, and for DGEBA catalytically polymerizing with 5 and 10 mol% DMBA, the plots of $\alpha(t)$ against t are given in Figure 4.3 to facilitate direct comparison.

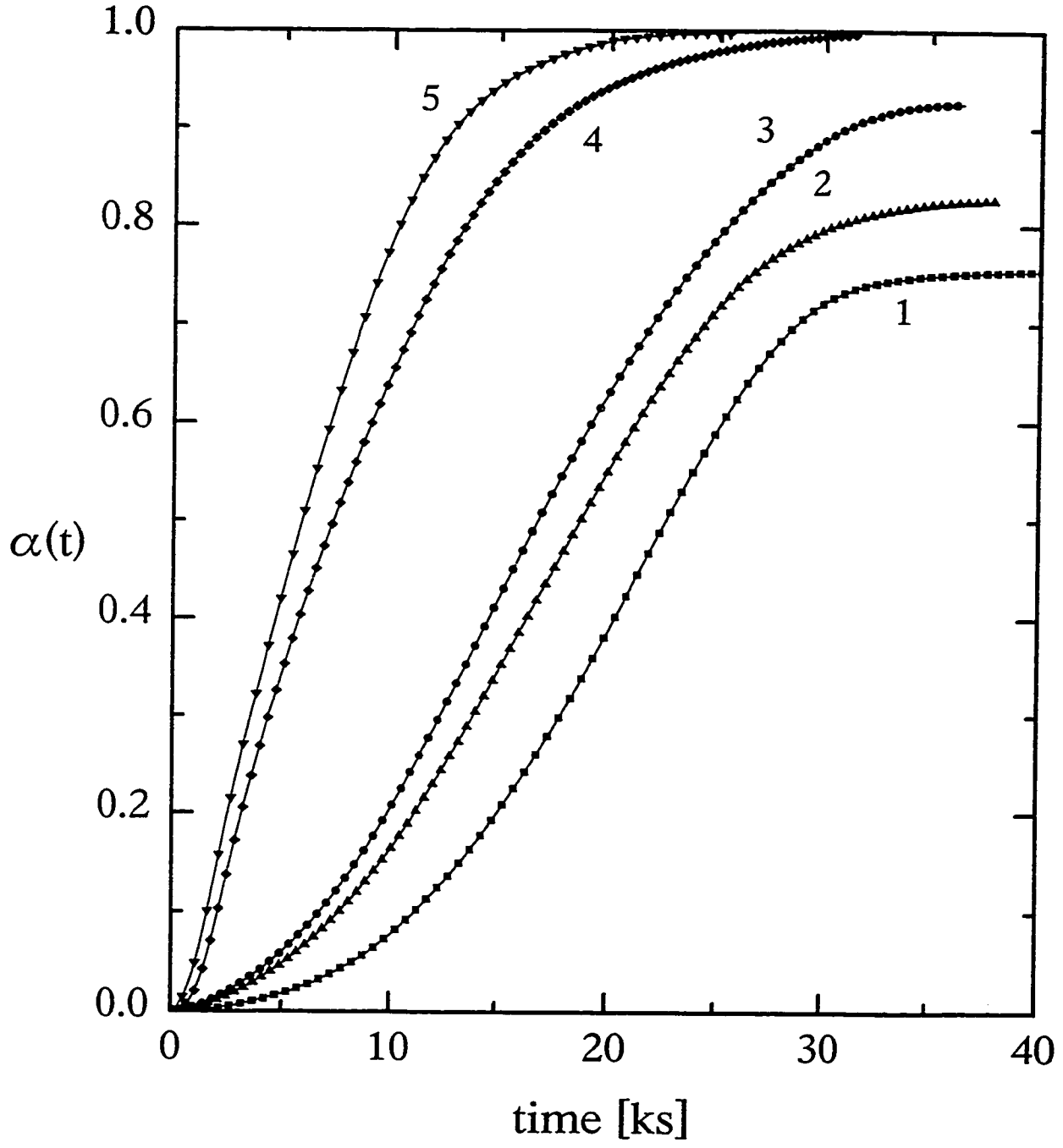

Figure 4.3: $\alpha(t)$ plotted against the isothermal polymerization time for the following molecular liquids; (1), Tactix-AN at 332.0 K, (2) Tactix-3CA at 360.6 K, (3) Tactix-4CA at 349.5 K, (4) DGEBA-DMBA5 at 335.4 K, and (5) DGEBA-DMBA10 at 335.4 K.

4.2 DIELECTRIC STUDIES OF LOCALIZED RELAXATIONS

4.2.1 The Fixed Frequency Measurements

The procedure described in Section 3.1.2 was used to measure $\varepsilon^*(N,\omega,T)$ at a fixed frequency, f, of 1 kHz ($\omega = 2\pi f$) and for a fixed $N(t)$, as a function of temperature, which was increased at 1 K/min. Plots of ε' and ε'' against the temperature are shown in Figures 4.4 to 4.9 for DGEBA-CHA, DGEBA-AN, Tactix-AN, Tactix-3CA, Tactix-4CA and DGEBA-DMBA5, respectively. In Figure 4.9, the results for DGEBA-DMBA10 at $N = 0$ and $N = N(\infty)$ are included for comparison. Each plot in these figures represents ε' or ε'' measured for several constant values of $N(t)$, as indicated by the associated numbers in each figure. For these figures, Curve 1 corresponds to the dielectric loss measured for $N(t) = 0$, while the final measurement in each figure is taken for $N(t) = N(\infty)$, as described in Section 3.2.2. The polymerization temperatures for each mixture are 313.4, 343.0, 332.0, 360.6, 349.5, and 335.4 K, for DGEBA-CHA, DGEBA-AN, Tactix-AN, Tactix-3CA, Tactix-4CA, and DGEBA-DMBA5, respectively.

The plots of ε'' against temperature in Figures 4.4 to 4.9 are all qualitatively similar. In general, for $N(t) = 0$, two peaks are observed in ε'',one in the temperature range 135 - 150 K, and the second in the range 250 - 265 K. As $N(t)$ increases, both the low- and high-temperature peaks decrease in height, and while the position of the former remains relatively unchanged, that of the latter shifts to higher temperatures. Also, for $N(t) > 0$, a third peak appears and evolves in the temperature range of 200 to 250 K. In Figures 4.7

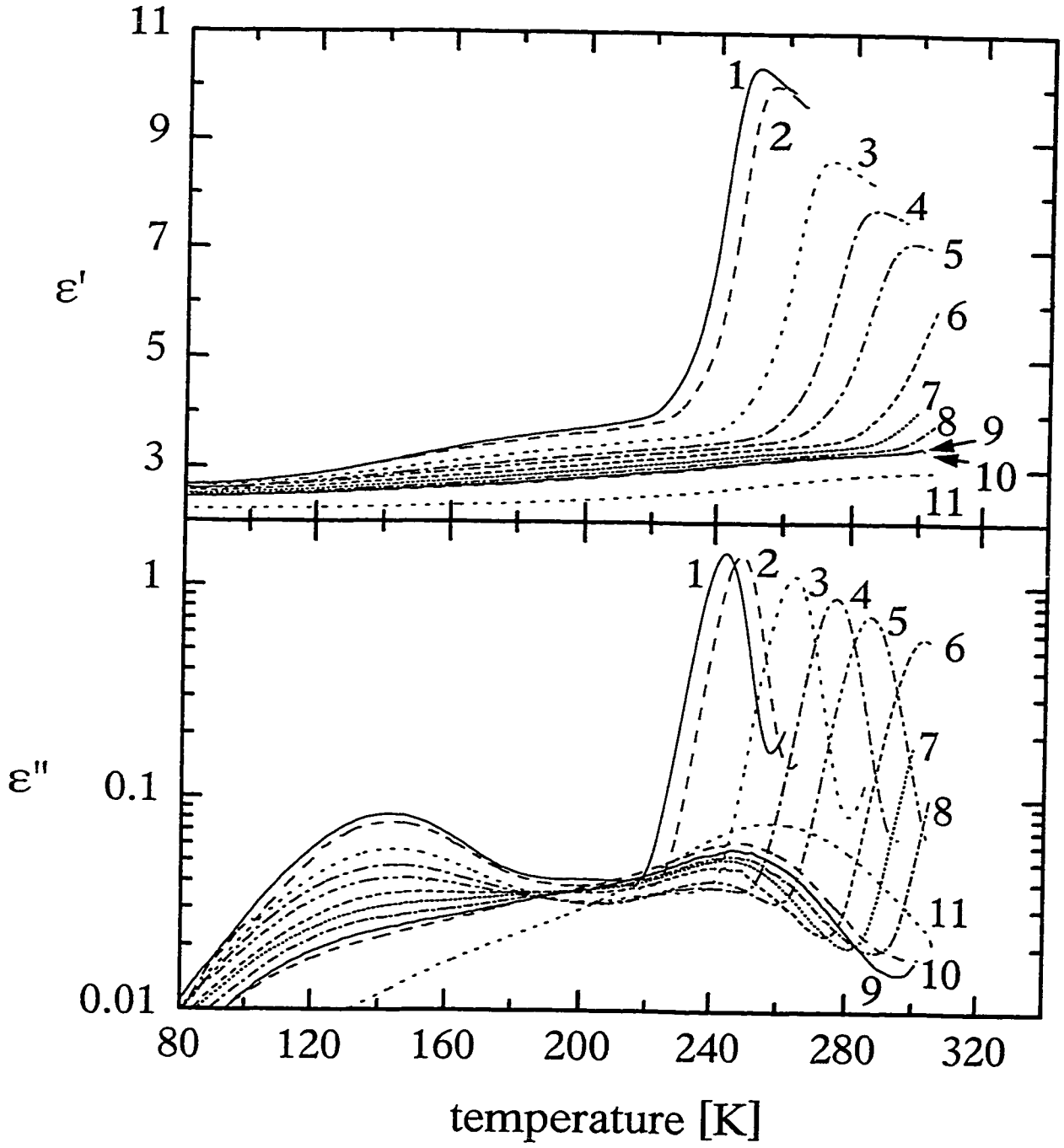

Figure 4.4: ε′ and ε″ for 1 kHz frequency of the DGEBA-CHA mixture polymerizing at 313.4 K is plotted against the temperature. Each curve is labelled according to the number of covalent bonds formed, $N(t)$, as follows (to be multiplied by 10^{23}); (1) 0, (2) 0.34, (3) 0.91, (4) 1.48, (5) 2.06, (6) 2.63, (7) 3.20, (8) 3.77, (9) 4.34, (10) 4.91, (11) 6.02.

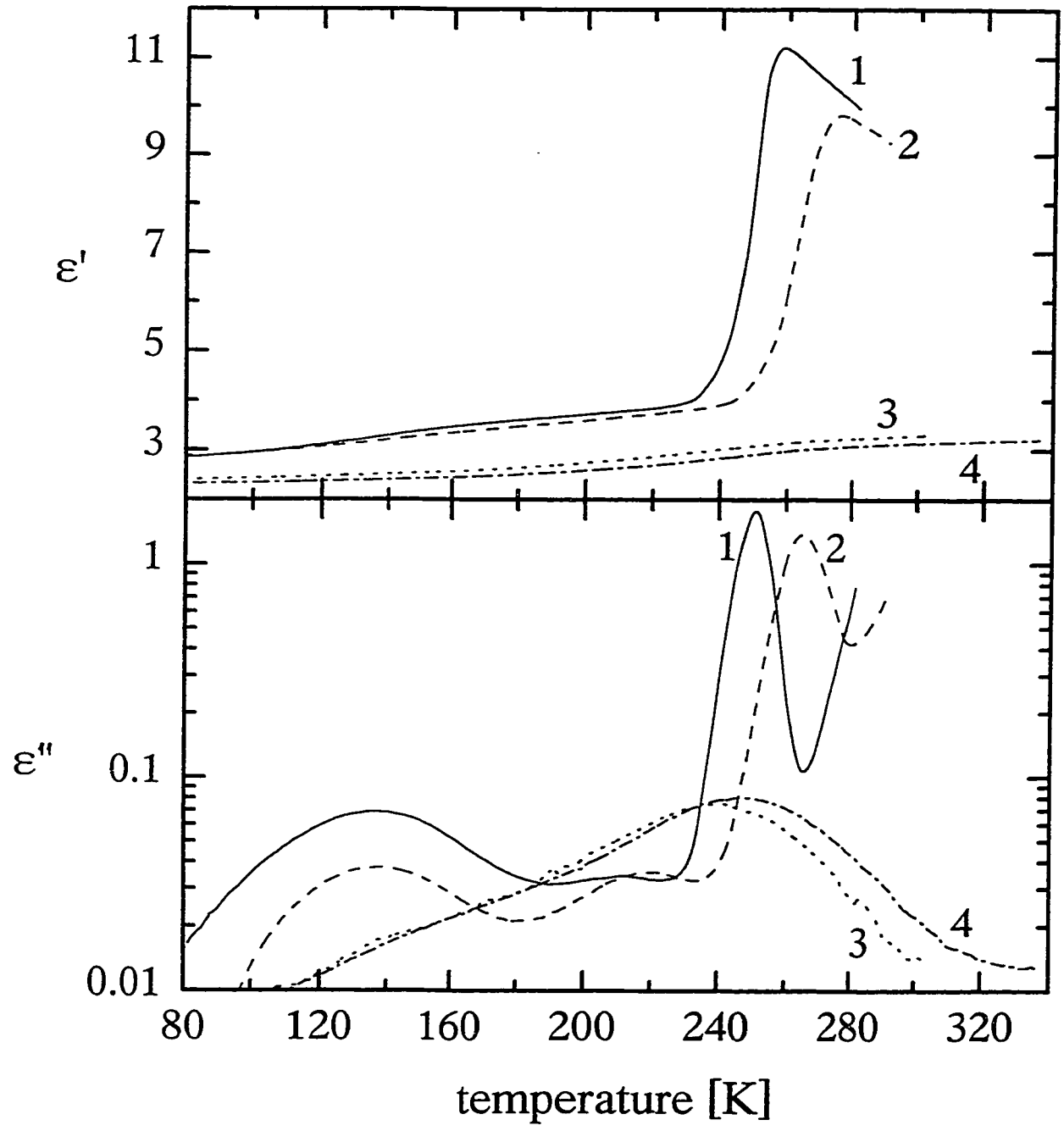

Figure 4.5: ε′ and ε″ for 1 kHz frequency of the DGEBA-AN mixture polymerizing at 343.0 K is plotted against the temperature. Each curve is labelled according to the number of covalent bonds formed, $N(t)$, as follows (to be multiplied by 10^{23}); (1) 0, (2) 0.34, (3) 4.34, (4) 6.02.

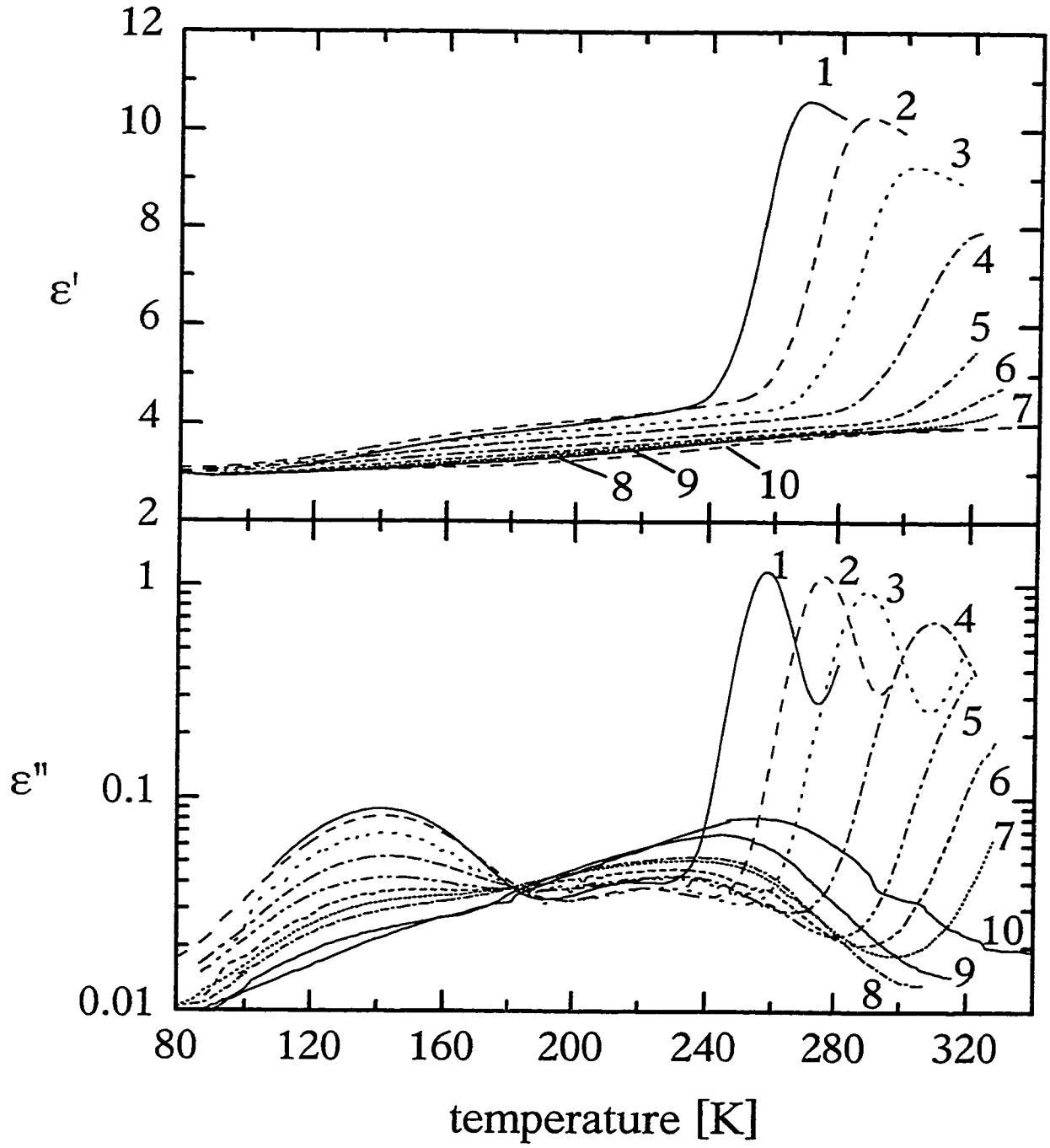

Figure 4.6: ε' and ε'' for 1 kHz frequency of the Tactix-AN mixture polymerizing at 332.0 K is plotted against the temperature. Each plot is labelled according to the number of covalent bonds formed, $N(t)$, as follows (to be multiplied by 10^{23}); (1) 0, (2) 0.34, (3) 0.91, (4) 1.48, (5) 2.06, (6) 2.63, (7) 3.20, (8) 4.32, (9) 5.48, (10) 7.23.

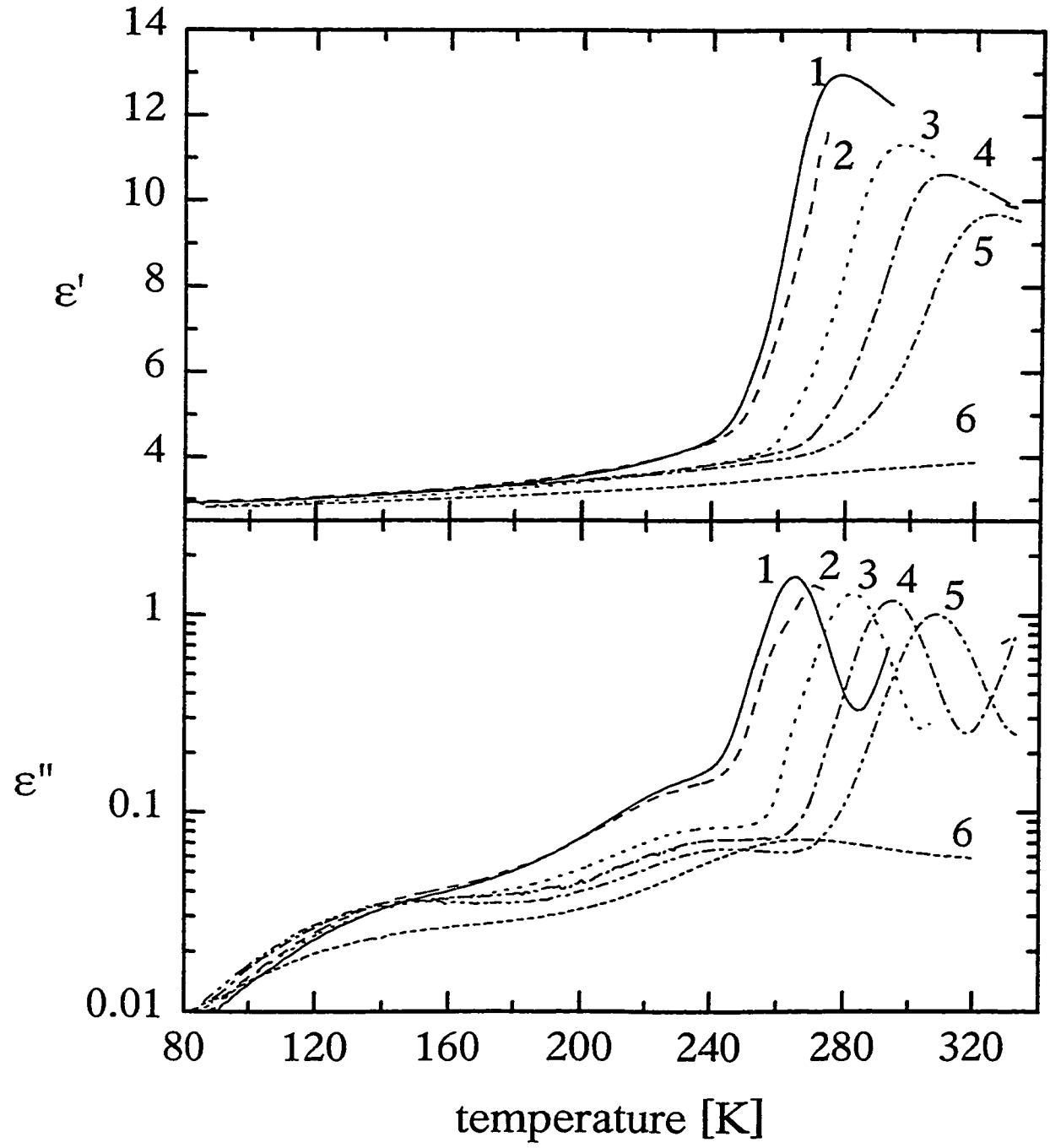

Figure 4.7: ε′ and ε″ for 1 kHz frequency of the Tactix-3CA mixture polymerizing at 360.6 K is plotted against the temperature. Each plot is labelled according to the number of covalent bonds formed, $N(t)$, as follows (to be multiplied by 10^{23}); (1) 0, (2) 0.10, (3) 0.70, (4) 1.40, (5) 2.17, (6) 7.23.

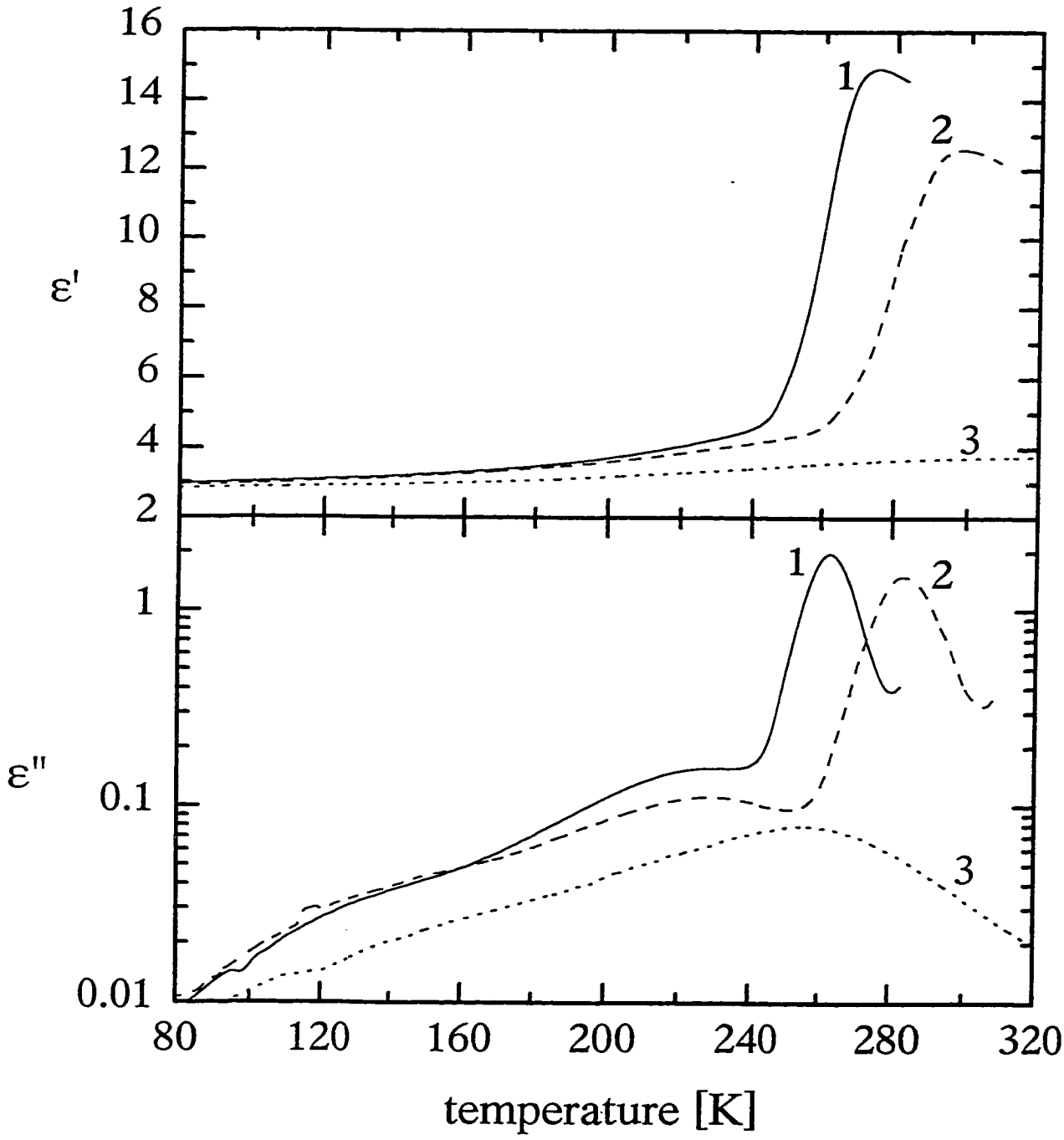

Figure 4.8: ε′ and ε″ for 1 kHz frequency of the Tactix-4CA mixture polymerizing at 349.5 K is plotted against the temperature. Each plot is labelled according to the number of covalent bonds formed, $N(t)$, as follows (to be multiplied by 10^{23}); (1) 0, (2) 0.73, (3) 7.23.

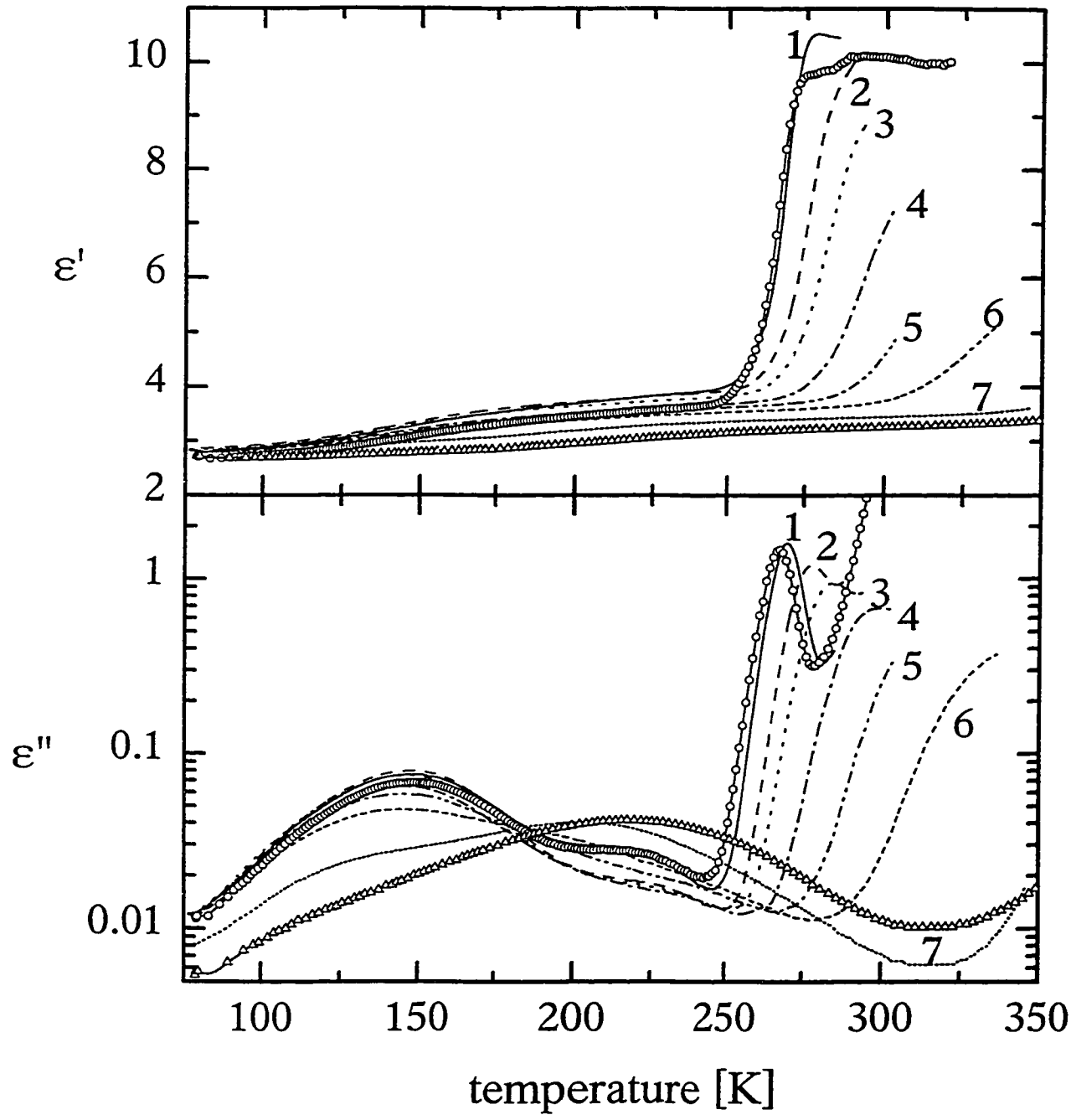

Figure 4.9: ε′ and ε″ for 1 kHz frequency of the DGEBA-DMBA5 mixture polymerizing by catalysis at 335.4 K is plotted against the temperature. Each curve is labelled according to the number of covalent bonds formed, $N(t)$, as follows (to be multiplied by 10^{23}); (1) 0, (2) 1.2, (3) 2.4, (4) 4.8, (5) 7.2, (6) 9.6, (7) 12.04. Circles and triangles respectively represent unreacted and fully reacted DGEBA-DMBA10.

and 4.8 for Tactix-3CA and Tactix 4CA, the low temperature peak in ε'' is not well resolved for any value of $N(t)$.

4.2.2 Time Domain Reflectometry Measurements

To further investigate the evolution of localized relaxation processes, the dielectric properties of the DGEBA-DMBA5 and DGEBA-DMBA10 mixtures were measured over the frequency range 100 MHz to 25 GHz during polymerization. Figures 4.10 and 4.11 show selected ε' and ε'' spectra out of the more than 130 measured for the mixtures at 335.4 K using the TDR measurement assembly. Each curve in these figures represents a dielectric spectrum at a specific value of $N(t)$ during the catalytic polymerization of DGEBA with DMBA. The two figures are qualitatively similar in that ε'' for both shows a single broad peak at ~0.8 GHz whose height decreases from ~1.4 to 0.1 as $N(t)$ increases from 0 to $N(\infty)$ during polymerization. For $N(t) = 0$, ε' in these two figures decreases in a broad step-like manner from a plateau value of ~8.5 to a constant value of ~3.5, as frequency increases. As $N(t)$ increases towards $N(\infty)$, the low-frequency plateau value of ε' decreases towards ~3.5 and the step-like feature vanishes, thus, for $N(\infty)$, ε' remains nearly constant with varying frequency.

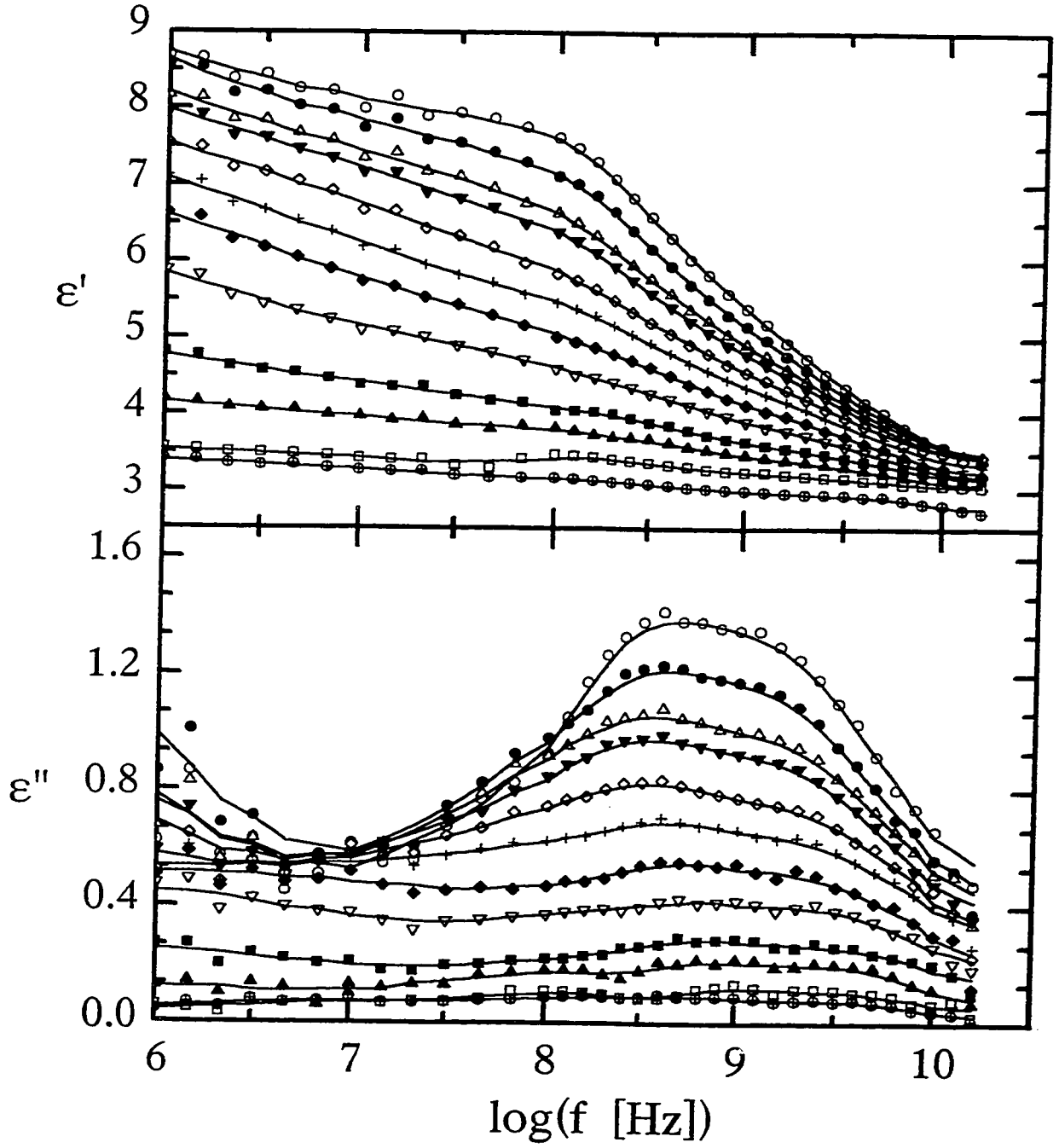

Figure 4.10: Selected TDR spectra of ε′ and ε″ plotted against the frequency for the isothermal polymerization at 335.4 K of DGEBA-DMBA5. The symbols correspond to $N(t)$ values of ($x10^{23}$);(○) 0.03, (●) 0.33, (Δ) 1.11, (▼) 1.67, (◇) 2.41, (+) 3.16, (◆) 3.89, (▽) 4.95, (■) 6.56, (▲) 7.93, (□) 12.02, (⊕) 12.04.

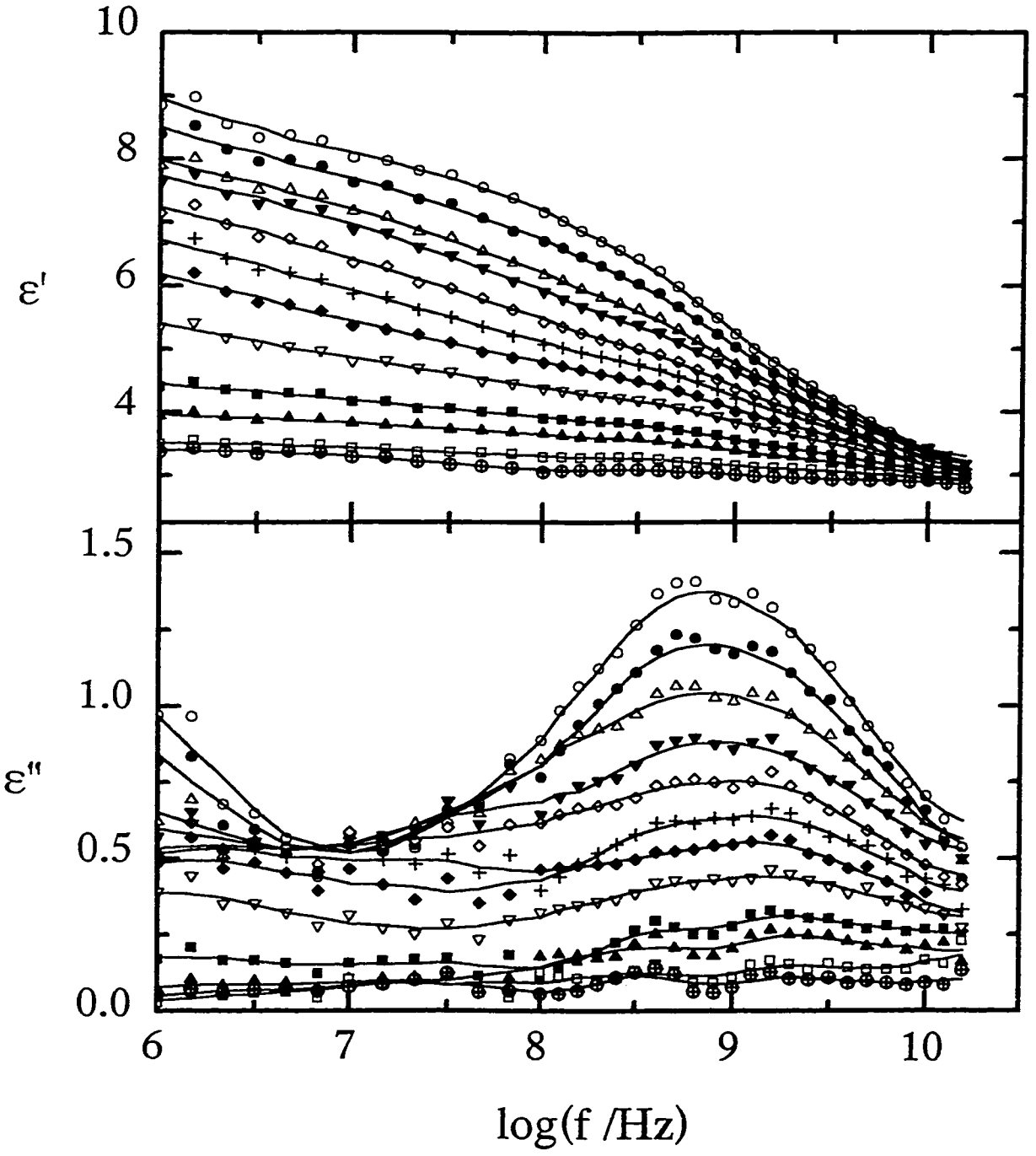

Figure 4.11: Selected TDR spectra of ε′ and ε″ plotted against the frequency for the isothermal polymerization at 335.4 K of DGEBA-DMBA10. The symbols correspond to $N(t)$ values of ($x10^{23}$);(○) 0.09, (●) 0.89, (△) 1.75, (▼) 2.19, (◇) 3.09, (+) 4.01, (◆) 4.91, (▽) 6.21, (■) 8.07, (▲) 9.49, (□) 12.01, (⊕) 12.04.

4.3 DIELECTRIC MEASUREMENTS OF POLYMERIZATION UNDER HYDROSTATIC PRESSURES

4.3.1 Isobaric Polymerization

For the DGEBA-CHA mixture, which formed a linear-chain structure, the dielectric properties were measured at pressures of 1, 103, and 206 bar, and at temperatures of 300.2, 307.5, and 313.8 K during the course of polymerization. (Measurements at 103 bar for polymerization at 300.2 K seemed unnecessary). For the DGEBA-EDA mixture, which formed a network structure, measurements were made at the same pressures but at 296.6, 306.1, and 314.0 K. The ε' and ε'' data for a fixed frequency of 1 kHz at ~60 s intervals are shown in Figures 4.12 to 4.14 for DGEBA-CHA at 300.2, 307.5, and 313.8 K, respectively, and those of DGEBA-EDA at 296.6, 306.1, and 314.0 K, respectively, are shown in Figures 4.15 to 4.17.

Isobaric experiments at 1 bar and 200 bar were further performed on each of the DGEBA-AN, DGEBA-HA, DGEBA-EDA, and DGEBA-HDA mixtures at 351.5 K, 303.7 K, 307.2 K, and 303.4 K, respectively. The products of the first two polymerizations were linear-chain polymers, and those of the last two were cross-linked network polymers. The plots of the measured ε' and ε'' against the polymerization time are shown in Figures 4.18 to 4.21.

In Figures 4.12 to 4.21, ε' is seen to decrease from an initial plateau value towards a long-time limiting value as the polymerization continued. The rate at which ε' decreased with time not only depended upon the range of polymerization time considered, but also on the temperature and pressure of the reacting mixture. As

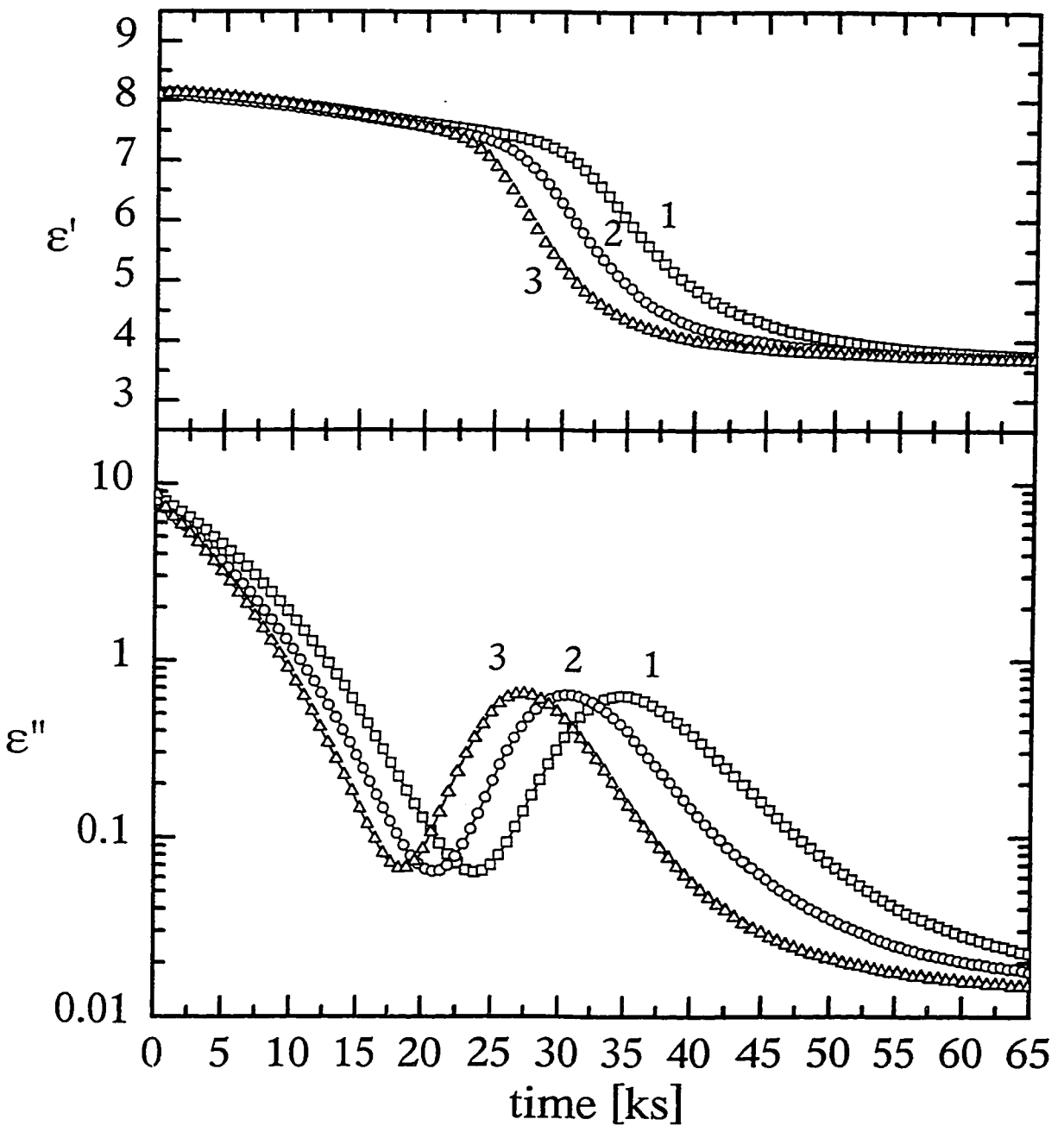

Figure 4.12: ε′ and ε″ measured for 1 kHz frequency is plotted against the reaction time for the isothermal polymerization of DGEBA-CHA at 300.2 K. The curves labelled 1, 2, and 3 refer to measurements taken at isobaric pressures of 1, 103, and 206 bar, respectively.

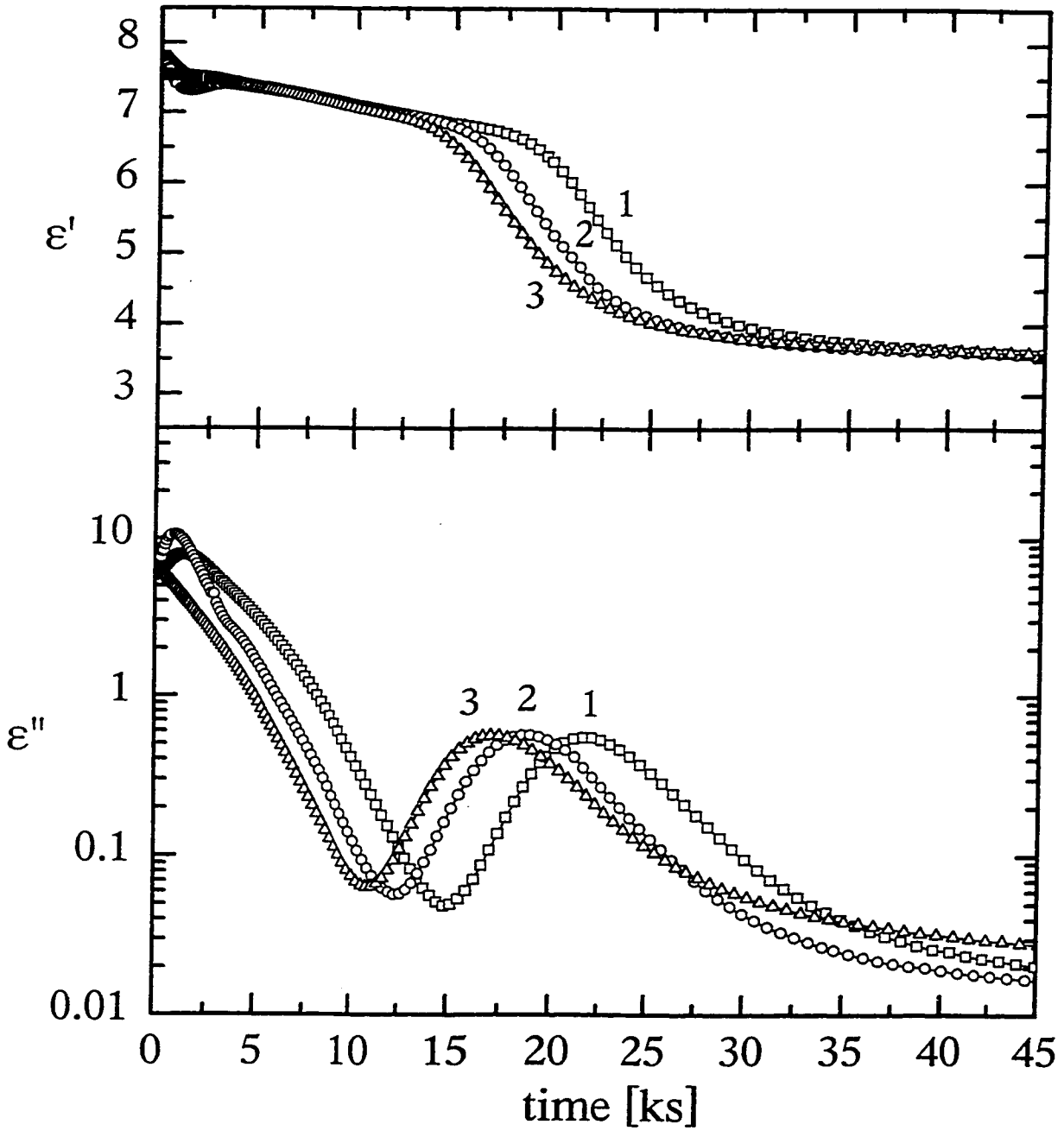

Figure 4.13: ε′ and ε″ measured for 1 kHz frequency is plotted against the reaction time for the isothermal polymerization of DGEBA-CHA at 307.5 K. The curves labelled 1, 2, and 3 refer to measurements taken at isobaric pressures of 1, 103, and 206 bar, respectively.

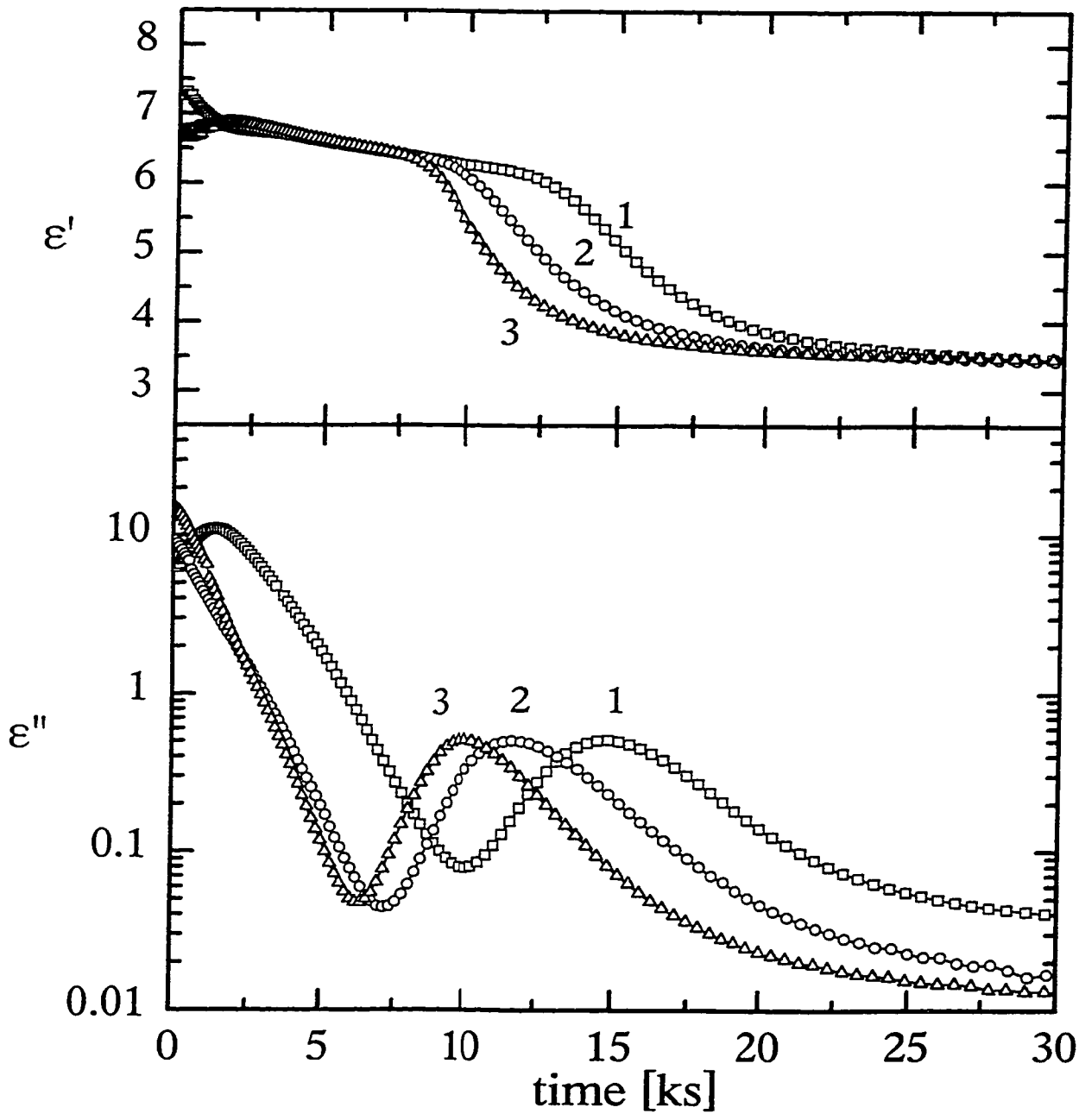

Figure 4.14: ε′ and ε″ measured for 1 kHz frequency is plotted against the reaction time for the isothermal polymerization of DGEBA-CHA at 313.8 K. The curves labelled 1, 2, and 3 refer to measurements taken at isobaric pressures of 1, 103, and 206 bar, respectively.

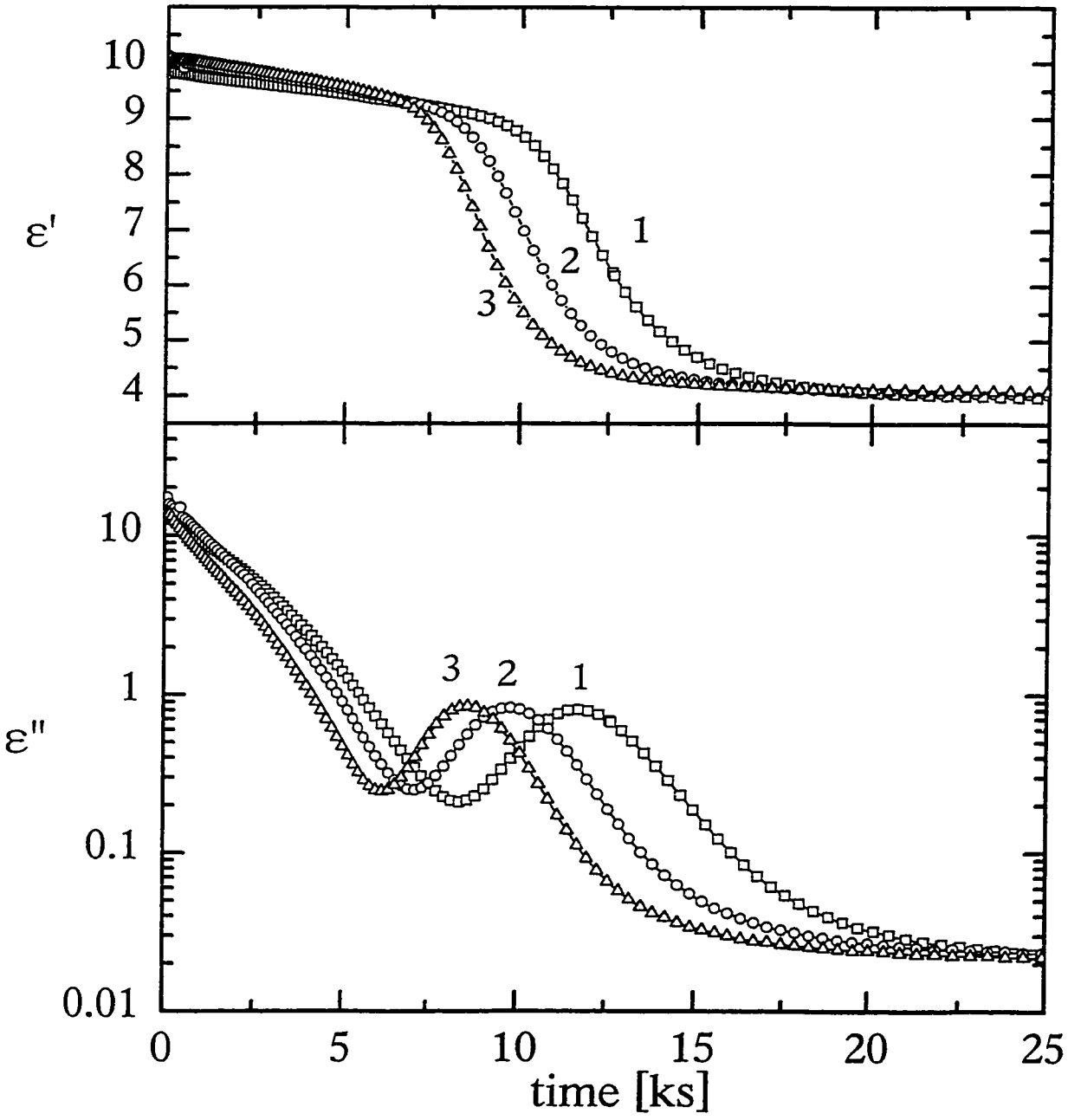

Figure 4.15: ε′ and ε″ measured for 1 kHz frequency is plotted against the reaction time for the isothermal polymerization of DGEBA-EDA at 296.6 K. The curves labelled 1, 2, and 3 refer to measurements taken at isobaric pressures of 1, 103, and 206 bar, respectively.

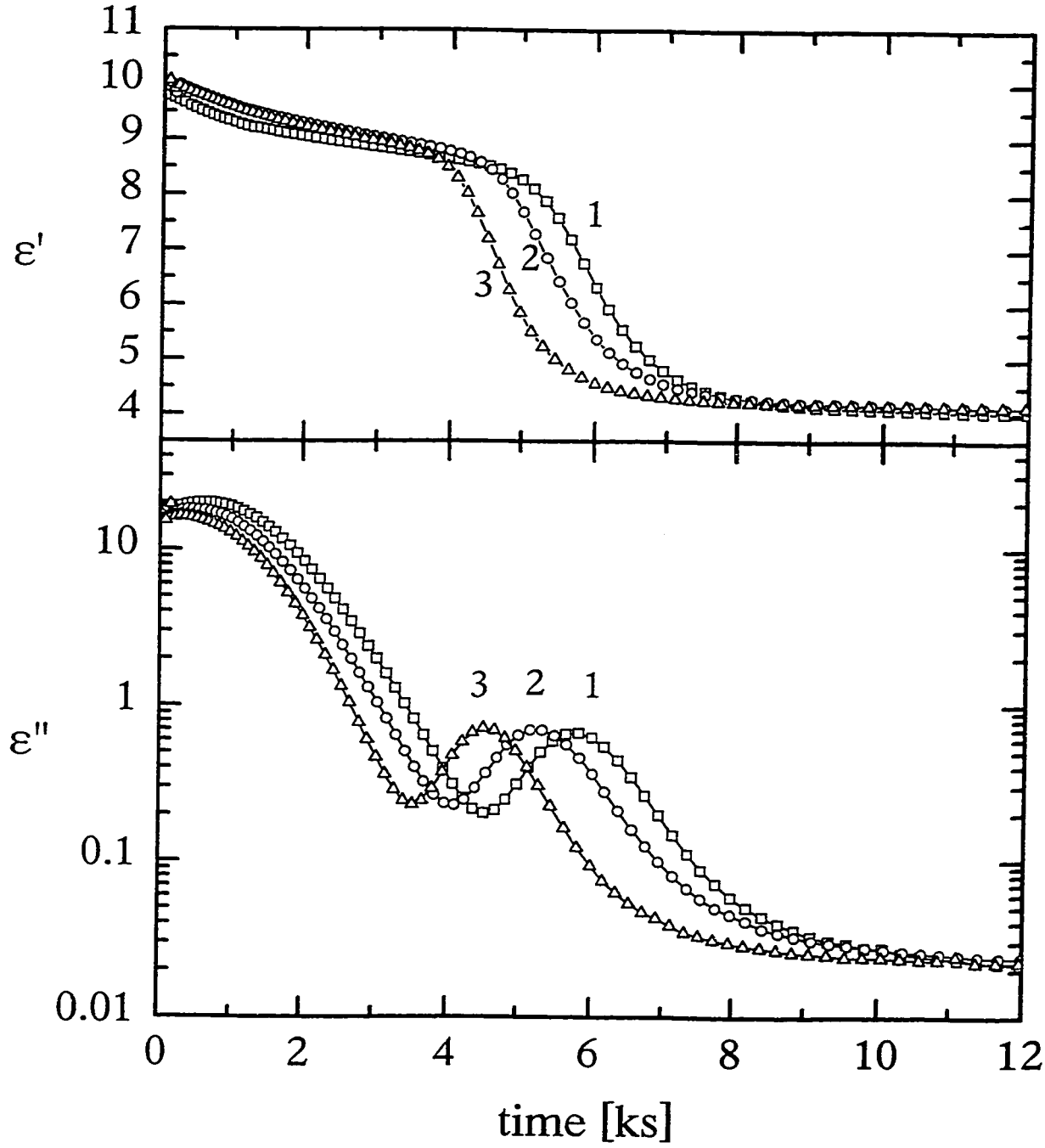

Figure 4.16: ε′ and ε″ measured for 1 kHz frequency is plotted against the reaction time for the isothermal polymerization of DGEBA-EDA at 306.1 K. The curves labelled 1, 2, and 3 refer to measurements taken at isobaric pressures of 1, 103, and 206 bar, respectively.

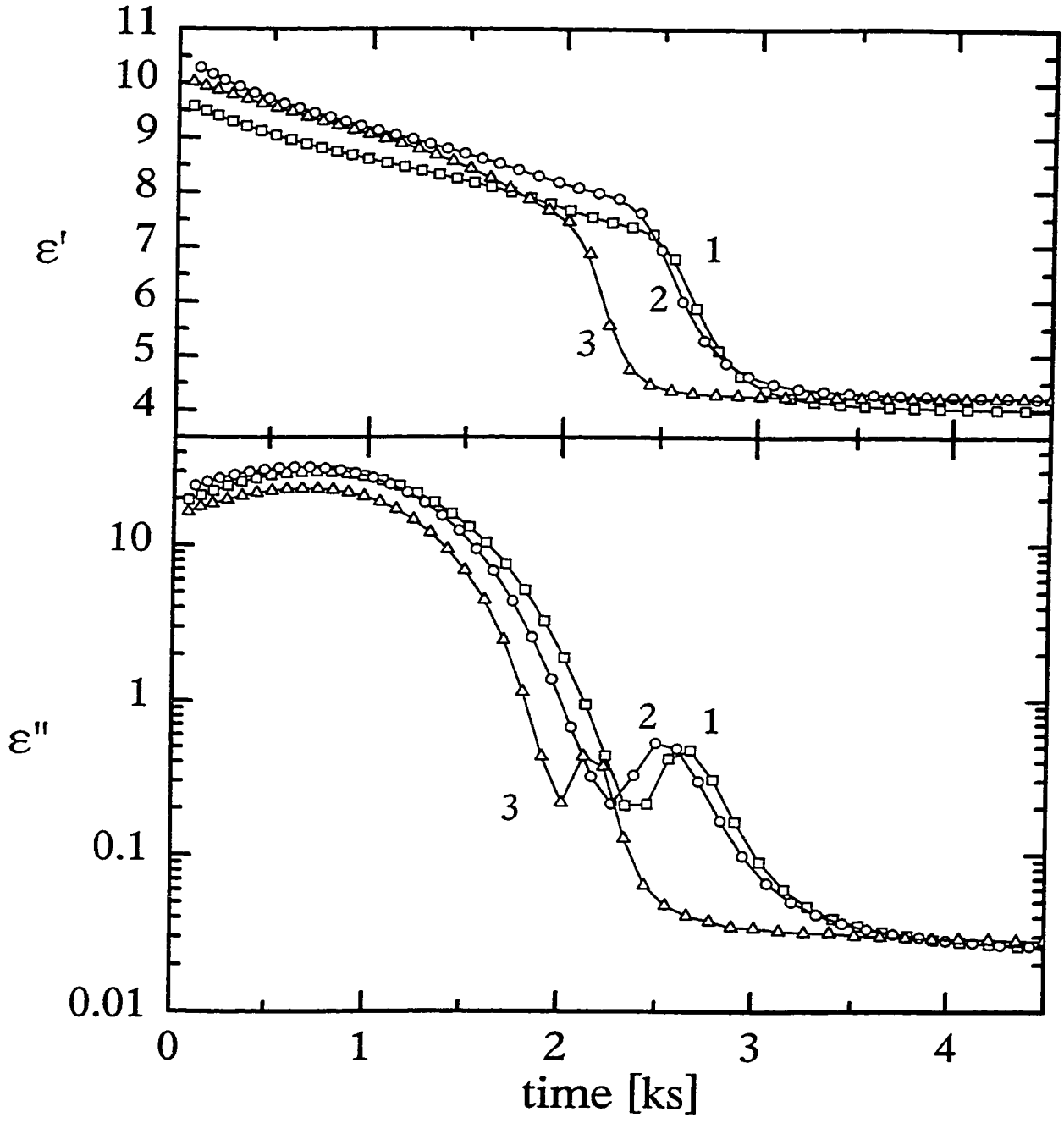

Figure 4.17: ε′ and ε″ measured for 1 kHz frequency is plotted against the reaction time for the isothermal polymerization of DGEBA-EDA at 314.0 K. The curves labelled 1, 2, and 3 refer to measurements taken at isobaric pressures of 1, 103, and 206 bar, respectively.

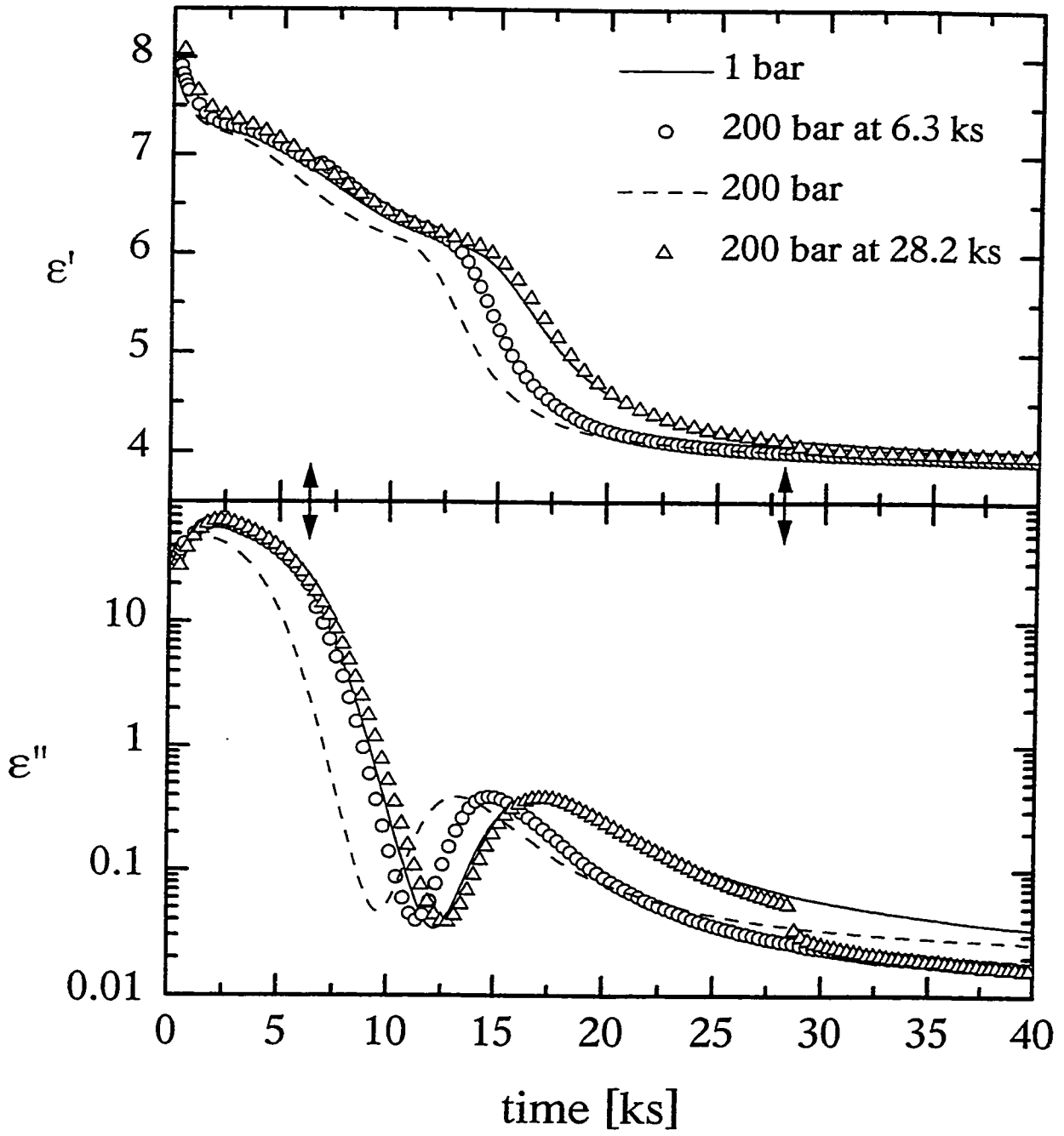

Figure 4.18: ε′ and ε″ measured for 1 kHz frequency plotted against the reaction time for the isothermal polymerization of DGEBA-AN at 351.5 K under the indicated conditions of pressure. The arrows denote times of 6.3 and 28.2 ks.

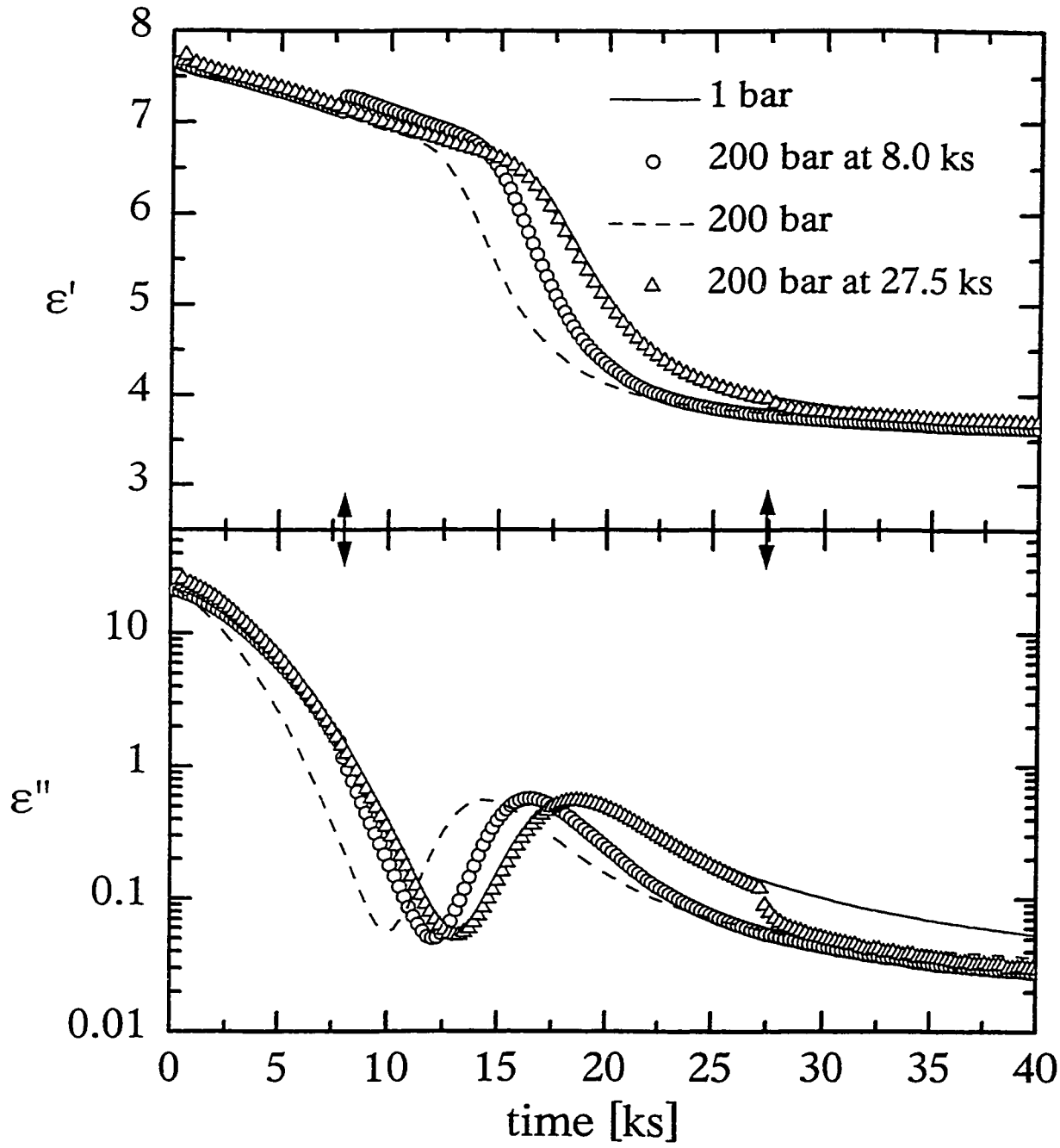

Figure 4.19: ε′ and ε″ measured for 1 kHz frequency plotted against the reaction time for the isothermal polymerization of DGEBA-HA at 303.7 K under the indicated conditions of pressure. The arrows denote times of 8.0 and 27.5 ks.

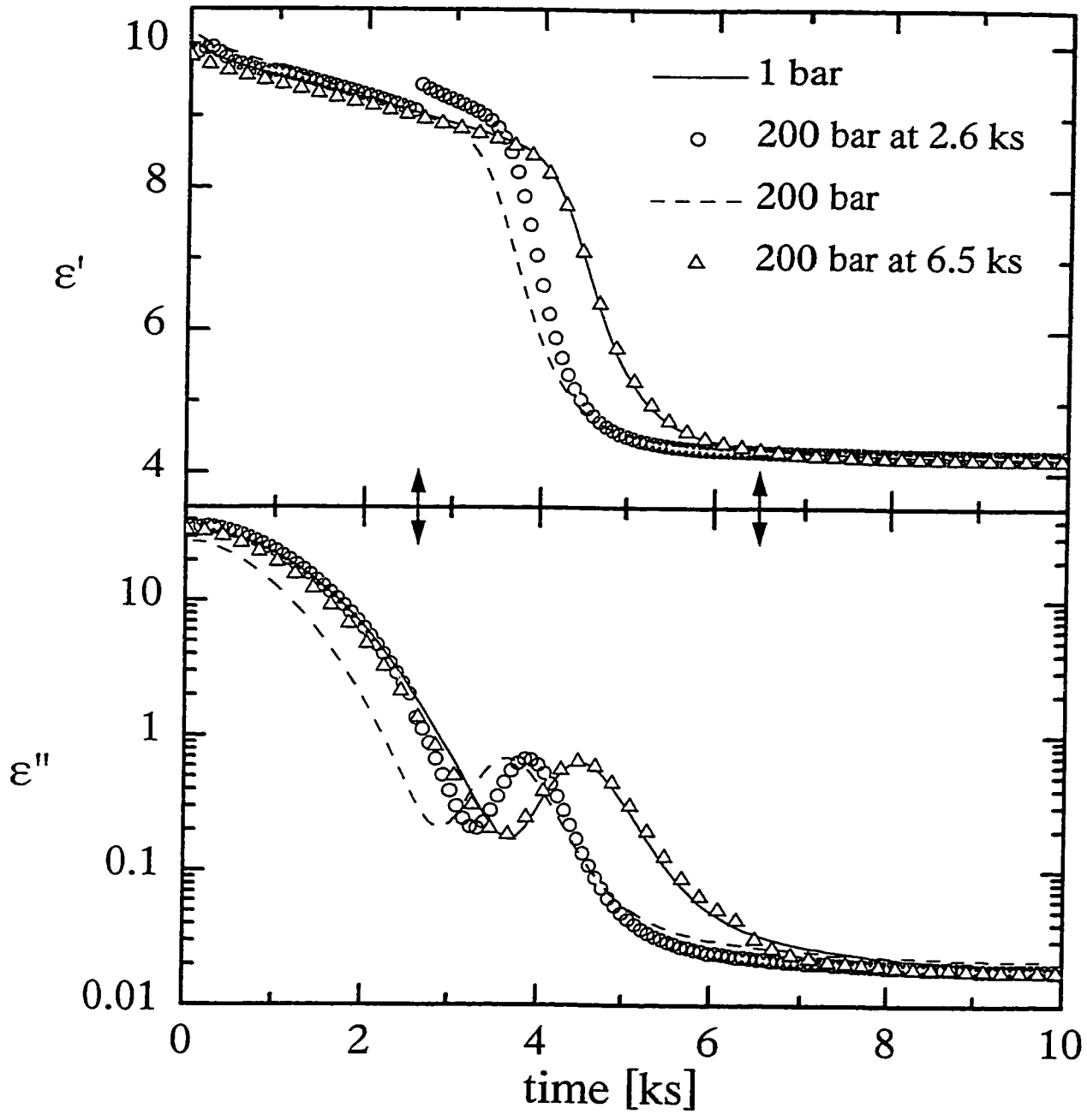

Figure 4.20: ε′ and ε″ measured for 1 kHz frequency plotted against the reaction time for the isothermal polymerization of DGEBA-EDA at 307.2 K under the indicated conditions of pressure. The arrows denote times of 2.6 and 6.6 ks.

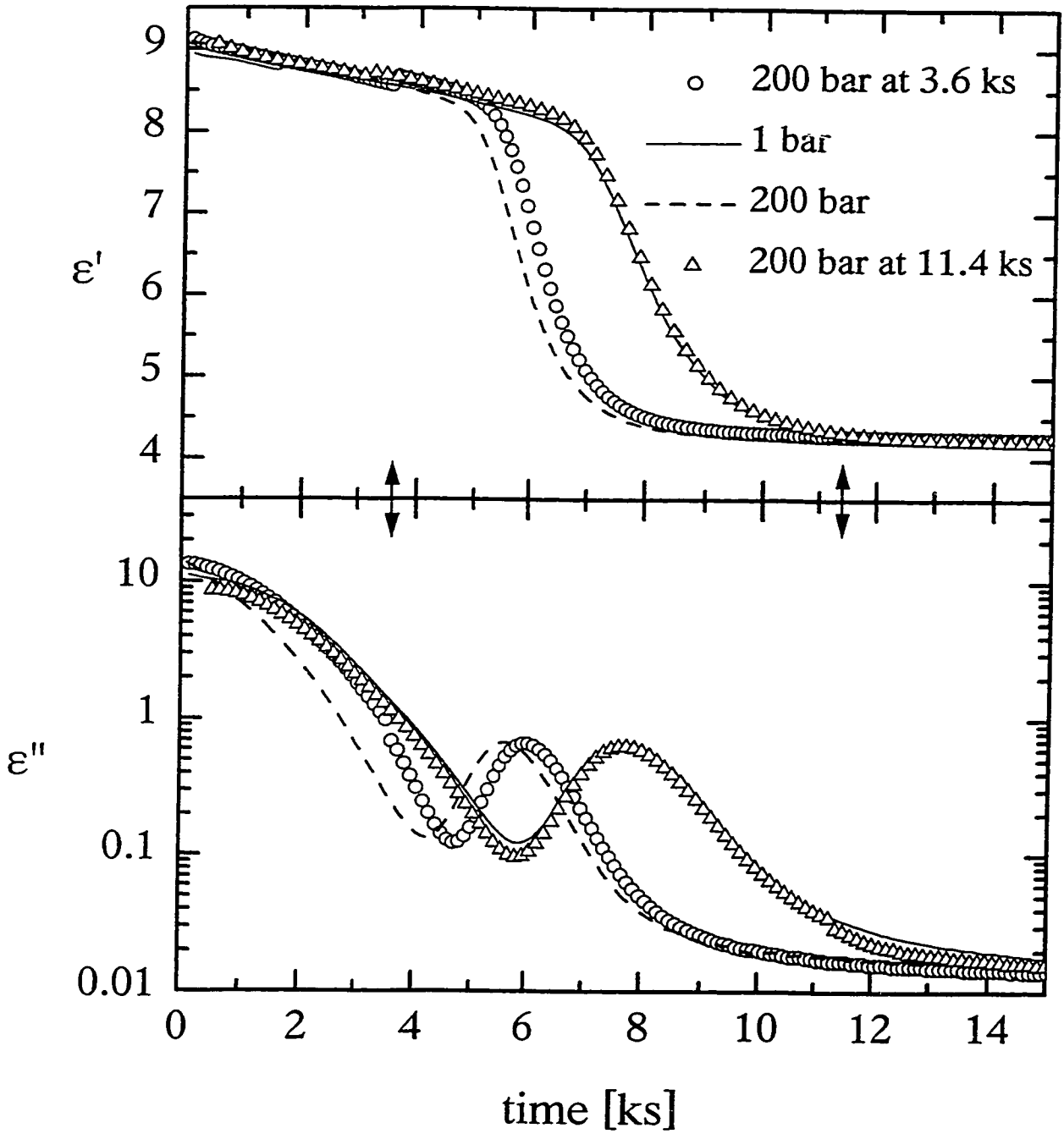

Figure 4.21: ε' and ε'' measured for 1 kHz frequency plotted against the reaction time for the isothermal polymerization of DGEBA-HDA at 303.4 K under the indicated conditions of pressure. The arrows denote times of 3.6 and 10.9 ks.

polymerization progressed and new covalent bonds formed, ε'' initially decreased to a local minimum, then increased to a peak value and finally decreased towards a limiting low value. These figures show that, for both mixtures, an increase in either the pressure at constant temperature, or the temperature at constant pressure, shifts the features of the ε' and ε'' plots towards shorter polymerization times.

To determine the relaxation time, $<\tau>$, as a function of t, the ε' and ε'' data were analyzed in terms of the theories described in Section 2.6. Briefly, the mathematical treatment used is as follows; Each data point (N' and N'') calculated from the procedure of Section 2.6 corresponds to a unique value of the normalized complex permittivity, $N^*(\omega\tau_o)$, which in turn corresponds to a unique set of ε' and ε'' values from Equations (2.14), (2.23), and (2.24). Thus, N^* becomes a unique function of τ_o alone, since ω is fixed. Therefore, each theoretical ε' and ε'' data point corresponds to a particular value of τ_o. By matching each theoretical pair of ε' and ε'' with the measured pair, a value of τ_o could be associated with each instance of the reaction time of the measurement. For the case where the measured point did not match with the calculated one, a value for τ_o was linearly interpolated from the two adjacent calculated ones. Thus, ε' and ε'' data for 1 kHz measurements at three temperatures and three pressures for the DGEBA-CHA and DGEBA-EDA mixtures were matched against the values calculated from Equations (2.23) and (2.24) to obtain approximately 20 values of $\tau_o(t)$ at different polymerization times. These τ_o values were converted to $<\tau>$ by rewriting Equation (2.26) as $<\tau> = (\tau_o/\gamma)\Gamma(1/\gamma)$ for the chemically variant case here.

To summarize, the time-variant calculation procedure was used to determine τ_o and γ because: (i) Accurate multi-frequency measurements could not be obtained due to relatively short polymerization times, ~2 ks, (in comparison, ~1 ks is needed to collect a 25 frequency spectrum), (ii) single-frequency measurements allow determination of τ_o over a greater range of polymerization time than the multi-frequency measurements, and (iii) the τ_o values obtained from the single-frequency procedure have been found to agree well with those obtained from the multi-frequency spectrum method within experimental errors [Tombari and Johari (1992), Deng and Martin (1994a), Parthun *et al.* (1996), Wasylyshyn and Johari (1997b)].

Nevertheless, multi-frequency measurements of ε' and ε'' were performed on the DGEBA-HA mixture at 303.7 K and isobaric pressures of 1 and 200 bar. In these experiments, a pair of ε' and ε'' data were collected as functions of the polymerization time at 28 frequencies from 12 Hz to 100 kHz during the course of polymerization. The results are shown in Figures 4.22 and 4.23 for polymerization of DGEBA-HA at 1 bar and 200 bar, respectively. These 28 frequencies are; 0.012, 0.017, 0.025 0.033, 0.050, 0.067, 0.1, 0.12, 0.167, 0.25, 0.333, 0.5, 0.67, 1.0, 1.2, 1.67, 2.5, 3.33, 5.0, 6.67, 10.0, 12.0, 16.67, 25.0, 33.33, 50.0, 66.67, and 100.0 kHz. (For clarity, Figures 4.22 and 4.23 do not contain the results for frequencies less than 0.1 kHz, although these results are described later in this section). Measurements at 1 bar were begun 5.8 ks after the DGEBA-HA mixture was stabilized at the desired polymerization temperature of 303.7 K, while the measurements at 200 bar were begun 2.1 ks after the mixture was stabilized.

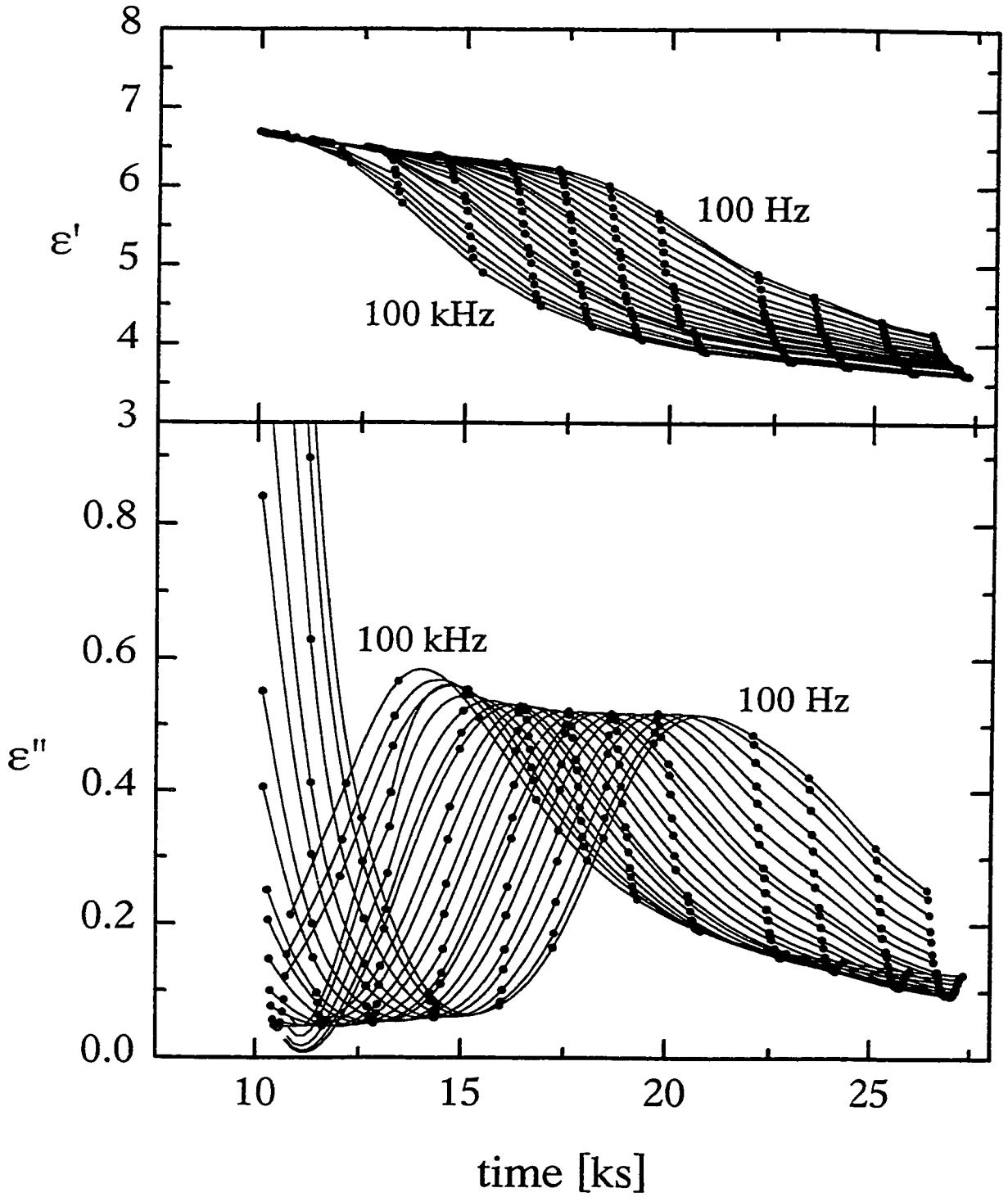

Figure 4.22: ε′ and ε″ measured for the polymerization of DGEBA-HA at 303.7 K and 1 bar pressure is plotted against the reaction time for the following frequencies; 0.1, 0.12, 0.167, 0.25, 0.333, 0.5, 0.67, 1.0, 1.2, 1.67, 2.5, 3.33, 5.0, 6.67, 10.0, 12.0, 16.67, 25.0, 33.33, 50.0, 66.67, and 100.0 kHz. Measurements less than 0.1 kHz have been omitted for clarity.

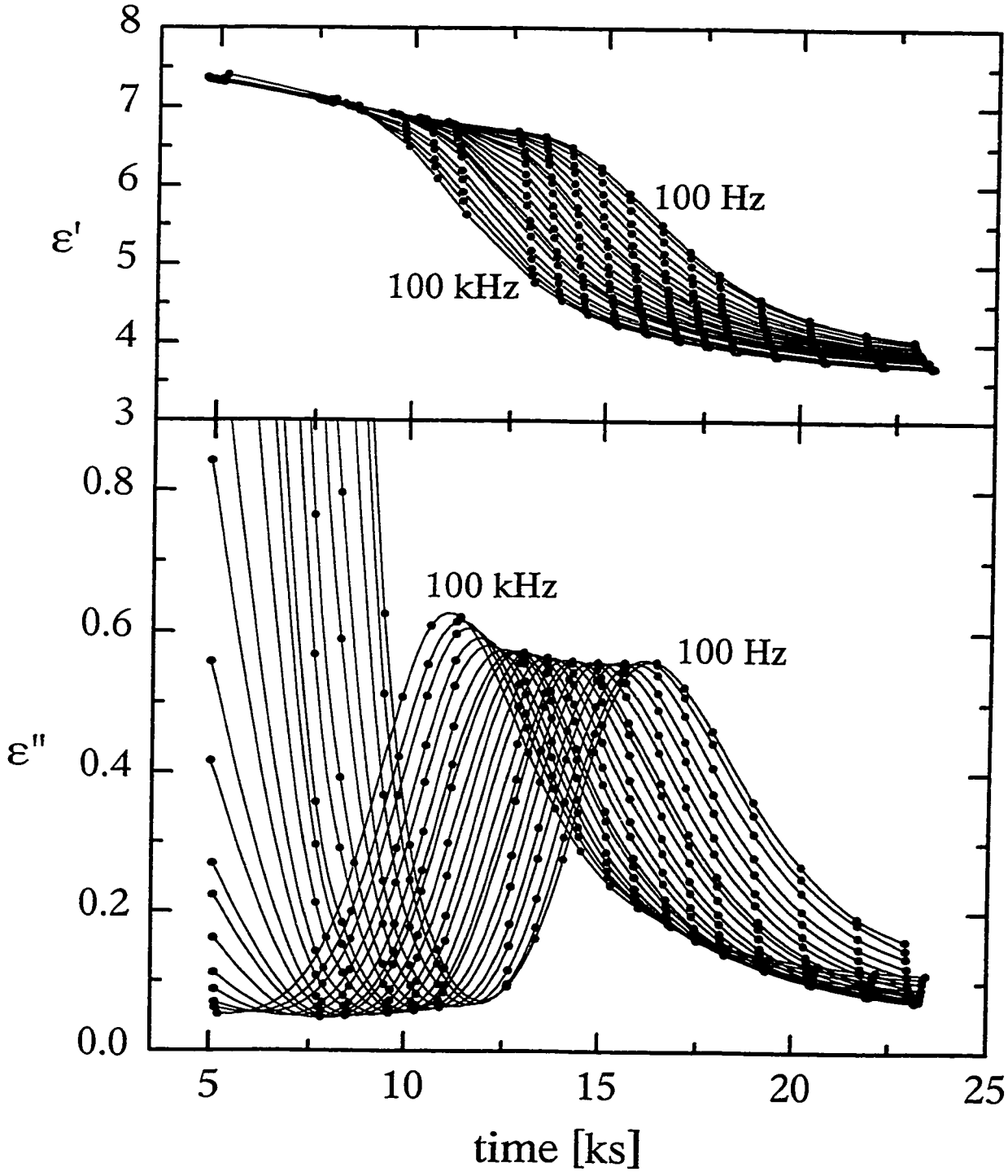

Figure 4.23: ε′ and ε″ measured for the polymerization of DGEBA-HA at 303.7 K and 200 bar pressure is plotted against the reaction time for the following frequencies; 0.1, 0.12, 0.167, 0.25, 0.333, 0.5, 0.67, 1.0, 1.2, 1.67, 2.5, 3.33, 5.0, 6.67, 10.0, 12.0, 16.67, 25.0, 33.33, 50.0, 66.67, and 100.0 kHz. Measurements less than 0.1 kHz have been omitted for clarity.

As seen in Figures 4.22 and 4.23, the initial value of ε' remains relatively constant as t increases. From this plateau value, ε' decreases slowly with increasing t, goes through an inflection point, then decreases slowly towards a limiting value as $t \rightarrow \infty$. For increasing values of the measurement frequencies, the curves shift bodily towards earlier times. The initial plateau value of ε' at $t \rightarrow 0$ remains at a constant value with an increase in the measurement frequency. All the curves for the various measurement frequencies approach a single, limiting value, $\varepsilon'(t \rightarrow \infty)$, as t approaches infinity. The values of $\varepsilon'(t \rightarrow \infty)$ are 3.6 and 3.7 for polymerization at 1 and 200 bar, respectively, of DGEBA-HA at 303.7 K. The limiting values for ε' as $t \rightarrow 0$, $\varepsilon'(t \rightarrow 0)$ are 6.8 and 7.5 for polymerization at 1 and 200 bar, respectively, of DGEBA-HA at 303.7 K.

ε'' shown in Figures 4.22 and 4.23 decrease to a local minimum, increase to a maximum, then ultimately decreases towards a limiting value with increasing t. The positions of the minimum and maximum in ε'' shift to earlier times with an increase in the measurement frequency.

To obtain the relaxation spectrum from the plots in Figures 4.22 and 4.23 at a certain t, ε' and ε'' were determined for several fixed instants of time as a function of frequency. This was done by using ε' and ε'' data at adjacent times to linearly interpolate for values at specific values of constant time, t. Since the number of measured ε' and ε'' values was large and interpolation done from close intervals of data points, the errors associated with this method were negligible in comparison with the measurement uncertainties [Parthun *et al.* (1996), Wasylyshyn *et al.* (1996)]. Figures 4.24 and 4.25

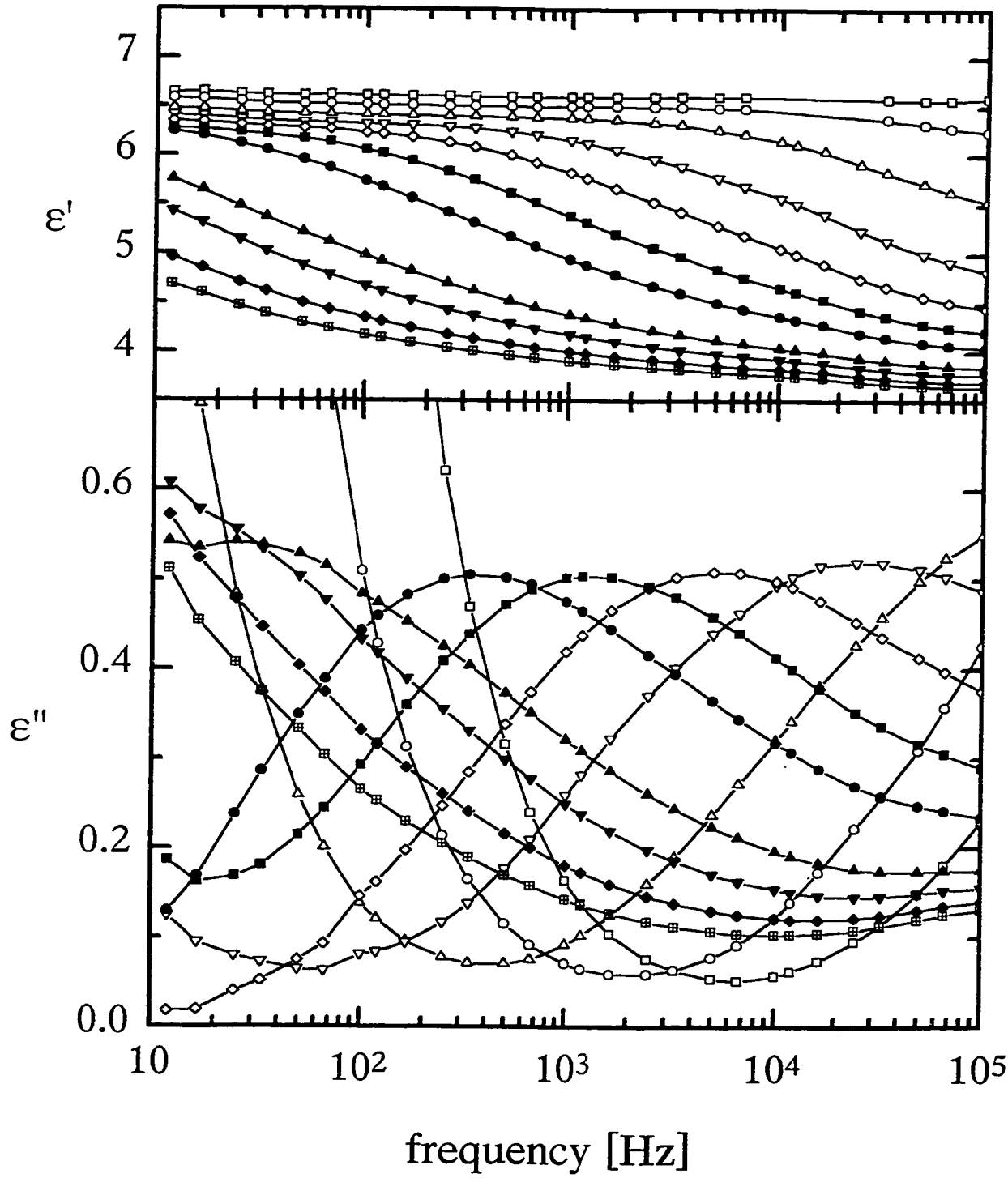

Figure 4.24: ε′ and ε″ spectra obtained from the interpolation of the data from Figure 4.22 as described in the text. The curves represent spectra obtained for 1 bar pressure at times of reaction corresponding to; (□) 11.0, (○) 12.3, (△) 14.0, (▽) 15.7, (◇) 17.0, (■) 18.2, (●)19.4, (▲) 21.8, (▼) 23.2, (◆) 24.9, and (⊞) 26.2 ks.

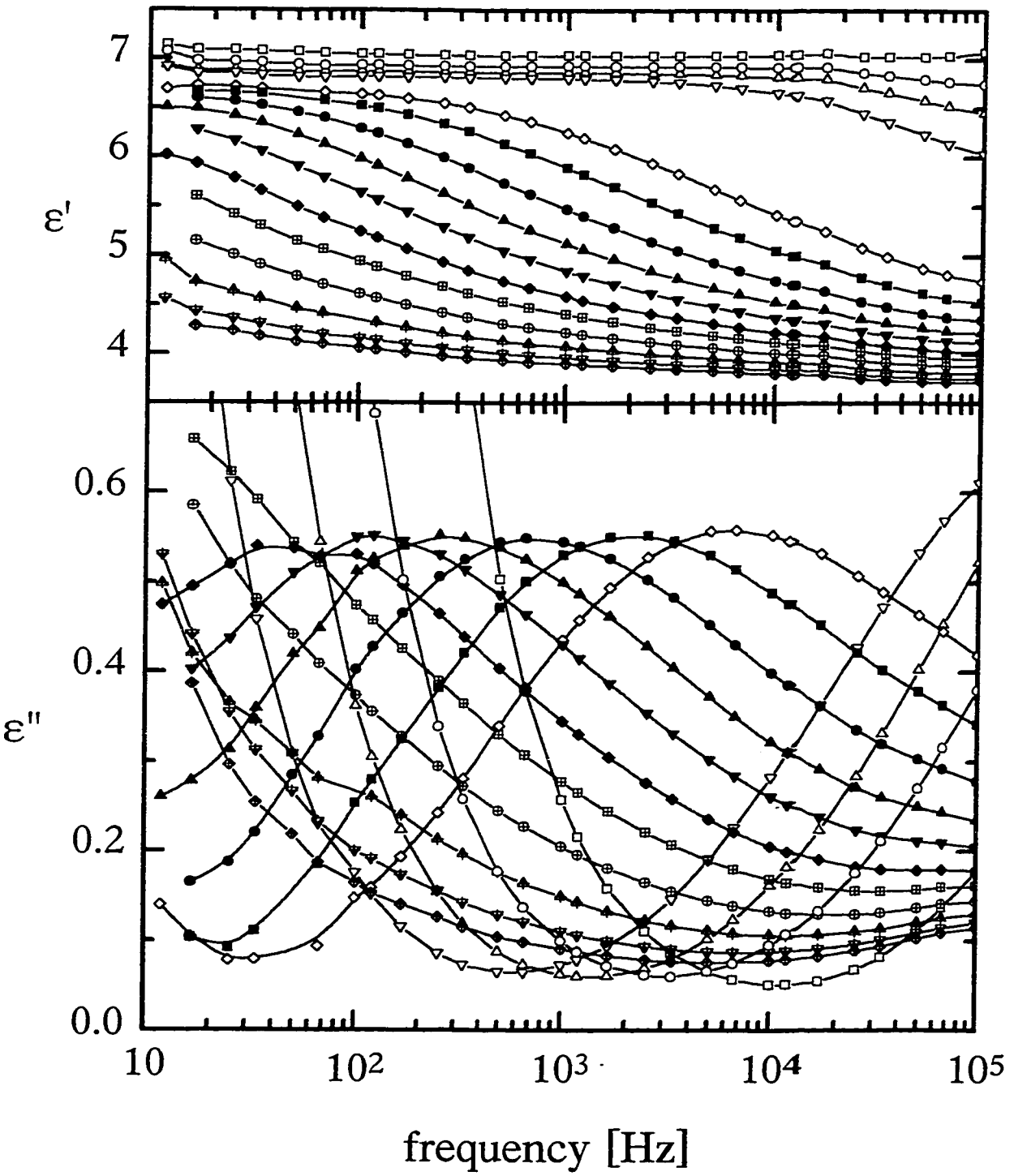

Figure 4.25: ε′ and ε″ spectra obtained from the interpolation of the data from Figure 4.23 as described in the text. The curves represent spectra obtained for 200 bar pressure at times of reaction corresponding to; (□) 8.0, (○) 9.2, (△) 10.0, (▽) 10.7, (◇) 13.2, (■)13.9, (●) 14.7, (▲) 15.4, (▼) 16.1, (◆) 16.9, (⊞) 17.7, (⊕) 18.8, (◬) 20.1, (⧨) 21.6, and (⧩) 22.7 ks.

show the ε' and ε'' spectra at different instants of time during the polymerization of DGEBA-HA at 303.7 K, and 1 and 200 bar, respectively. The polymerization time for the spectra in Figure 4.24, from right to left, are; 11.0, 12.3, 14.0, 15.7, 17.0, 18.2, 19.4, 21.8, 23.2, 24.9, and 26.2 ks. Those of Figure 4.25, from right to left, are; 8.0, 9.2, 10.0, 10.7, 13.2, 13.9, 14.7, 15.4, 16.1, 16.9, 17.7, 18.8, 20.1, 21.6, and 22.7 ks.

4.3.2 Isobaric Polymerization After a Step-Increase in Pressure During The Macromolecule's Growth

In the experiment described above, polymerization was performed at several pressures and temperatures from its very beginning to the virtual end of polymerization. To investigate the instantaneous effect of hydrostatic pressure applied during the course of polymerization in one set of experiments, pressure was step-increased from 1 bar to 200 bar in the early stages of the polymerization and then maintained constant for the entire duration of polymerization. In the second set, the pressure was similarly increased, but in the later stages of polymerization, and then maintained constant for the remaining duration. Figures 4.18 to 4.21 show the resulting measured ε' and ε'' for a constant frequency of 1 kHz for each of the four mixtures, DGEBA-AN, DGEBA-HA, DGEBA-EDA, and DGEBA-HDA, at 351.5, 303.7, 307.2, and 303.4 K, respectively. In each of these four figures there are four plots each for ε' and ε''; (i) for polymerization at 1 bar for the entire duration, (ii) similar to (i), but at 200 bar, (iii) for polymerization initially at 1 bar but step-increased to 200 bar at a time shown by an arrow at an early stage of polymerization, and (iv) similar to (iii), but the pressure step-increased to 200 bar at a

later stage of polymerization. The early and late stages at which pressure was increased to 200 bar, respectively, are; for DGEBA-AN at 6.3 and 28.2 ks; for DGEBA-HA at 8.0 and 27.4 ks; for DGEBA-EDA at 2.6 and 6.6 ks; and for DGEBA-HDA at 3.6 and 10.9 ks.

Figures 4.18 to 4.21 show that when pressure was step-increased by 200 bars at an early stage of the polymerization, ε' increased by 1% and ε'' decreased by 30% for DGEBA-HDA. For DGEBA-EDA, DGEBA-AN, and DGEBA-HA, ε' increased by 3.8%, 0.6% and 2.2%, respectively, and ε'' decreased by 34%, 22%, and 25%, respectively. For these same liquid mixtures, a pressure step-increase from 1 bar to 200 bar in the later stages of the polymerization decreased ε'' by 14%, 7.7%, 26%, and 25%, respectively. No change in ε' was detected after a pressure was step-increased and then step-decreased during the late stages of polymerization of the four liquids.

In addition to the above-described experiments, further experiments were performed when pressure was step-increased and then step-decreased at regular intervals during the course of the polymerization of DGEBA-AN, DGEBA-HA, DGEBA-EDA, and DGEBA-HDA at the same temperatures as in the preceding experiments. In the new experiments, polymerization of each liquid was begun at 1 bar. After a duration of 500 - 1000 s, the pressure was step-increased to 200 bar. After an equal duration of time, the pressure was step-decreased back to 1 bar. This procedure was repeated five to six times during the course of the polymerization. The effects on ε' and ε'' for each of the mixtures are shown in Figures 4.26 to 4.29 for DGEBA-AN, DGEBA-HA, DGEBA-EDA, and

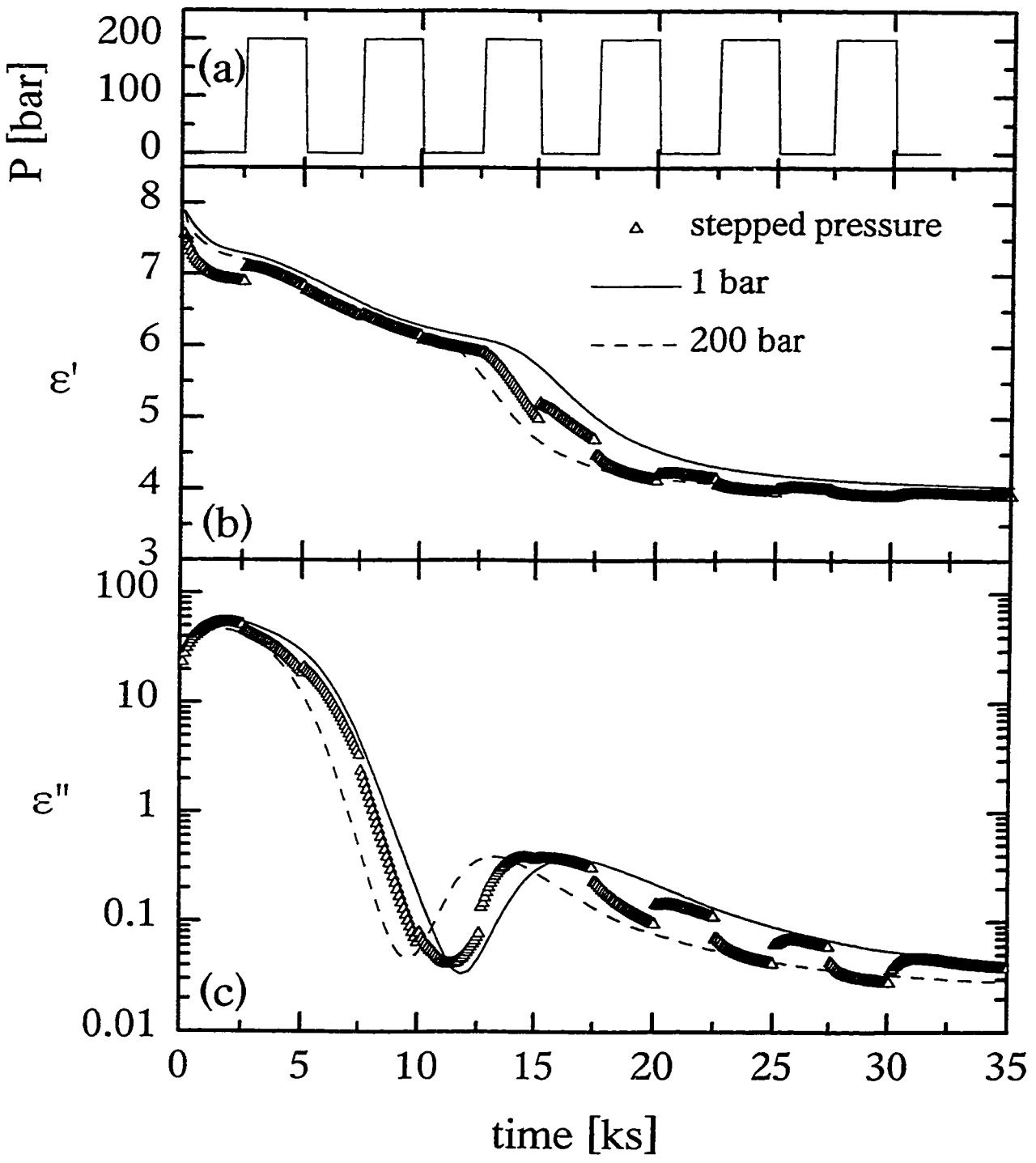

Figure 4.26: **(a)** The stepped-pressure profile applied during the isothermal polymerization of DGEBA-AN at 351.5 K, **(b)** ε' and, **(c)** ε'' measured for 1 kHz frequency plotted against the reaction time during polymerization with the stepped-pressure profile indicated in (a).

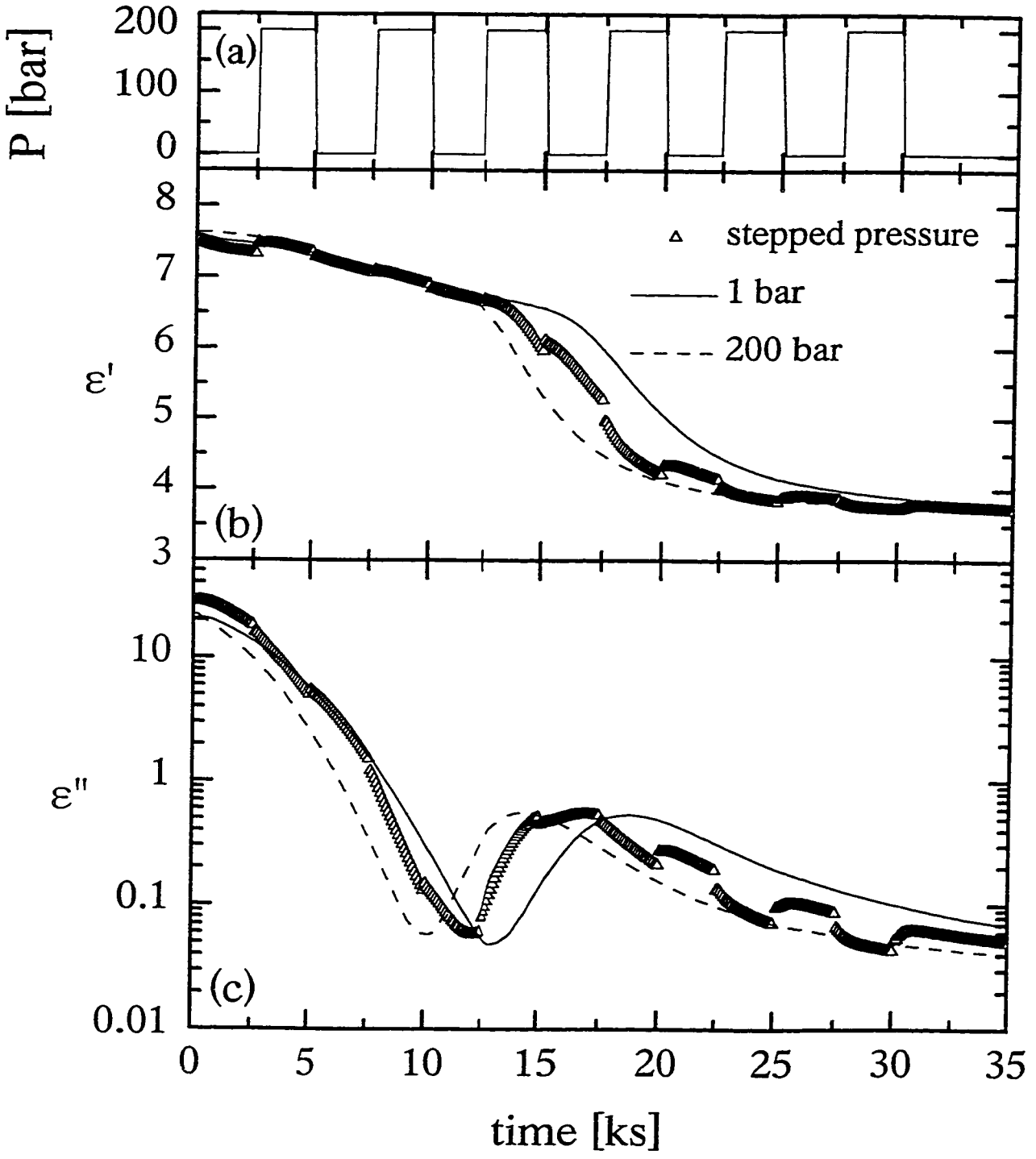

Figure 4.27: **(a)** The stepped-pressure profile applied during the isothermal polymerization of DGEBA-HA at 303.7 K, **(b)** ε′ and, **(c)** ε″ measured for 1 kHz frequency plotted against the reaction time during polymerization with the stepped-pressure profile indicated in (a).

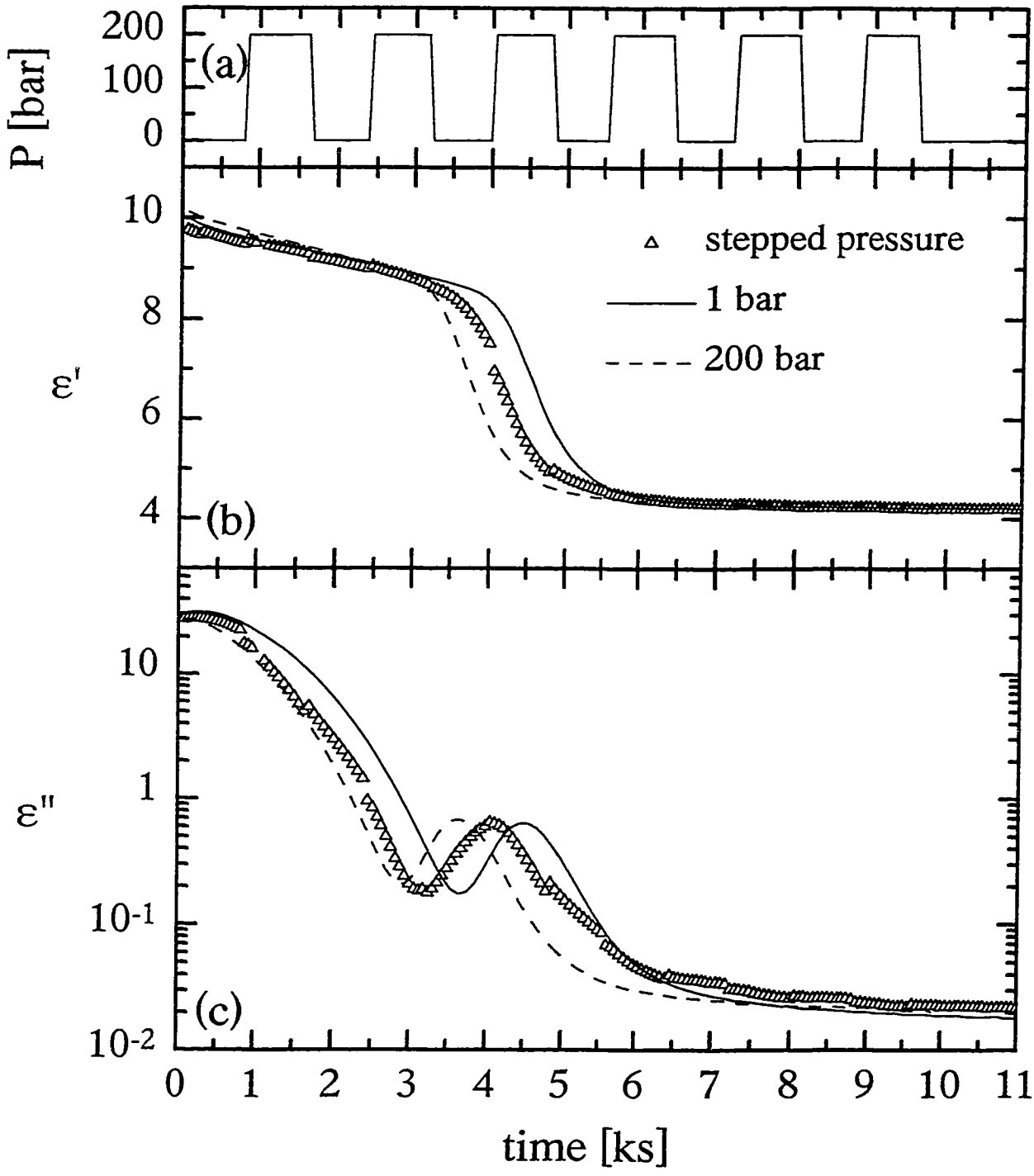

Figure 4.28: **(a)** The stepped-pressure profile applied during the isothermal polymerization of DGEBA-EDA at 307.2 K, **(b)** ε′ and, **(c)** ε″ measured for 1 kHz frequency plotted against the reaction time during polymerization with the stepped-pressure profile indicated in (a).

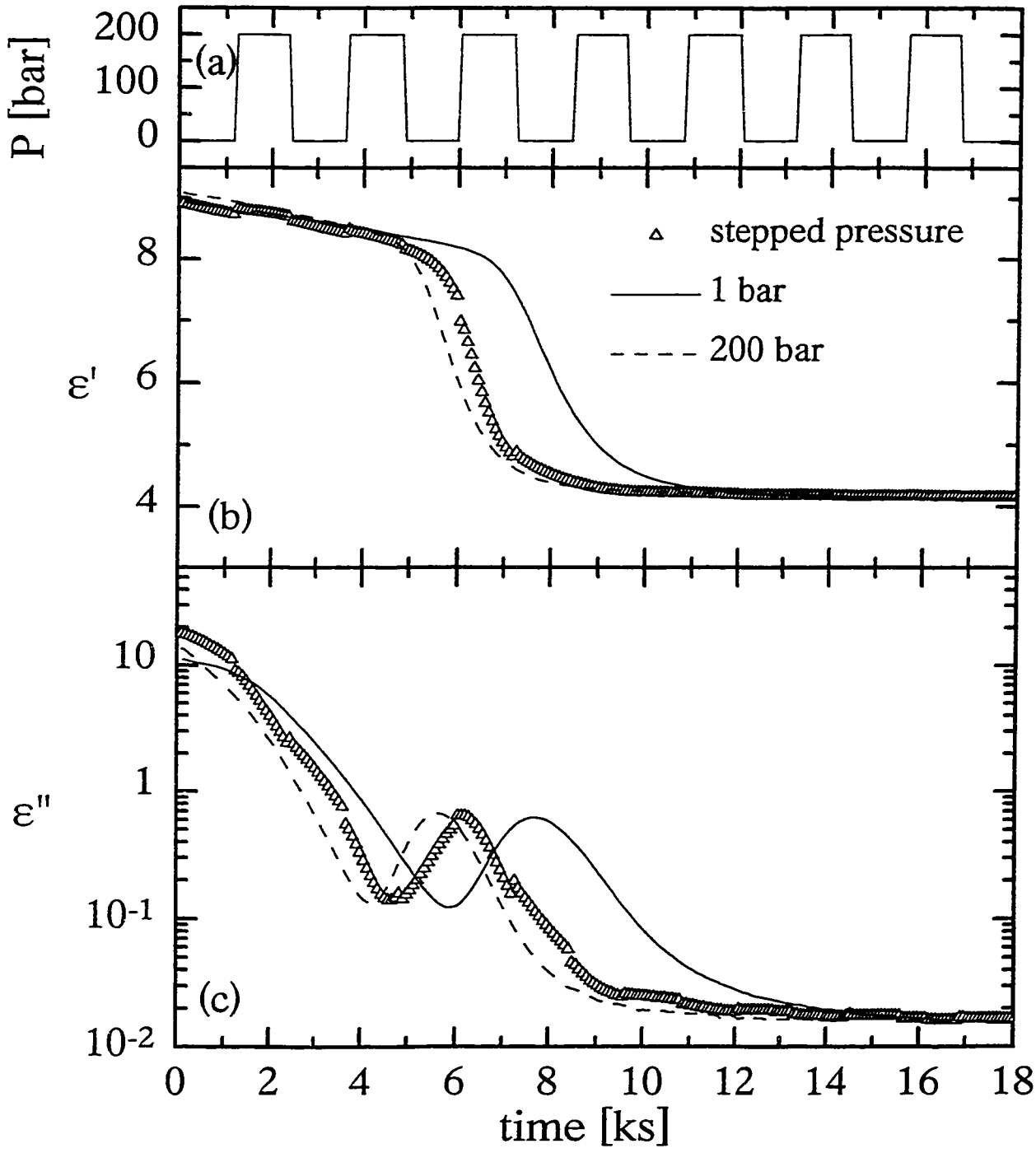

Figure 4.29: **(a)** The stepped-pressure profile applied during the isothermal polymerization of DGEBA-HDA at 303.4 K, **(b)** ε' and, **(c)** ε'' measured for 1 kHz frequency plotted against the reaction time during polymerization with the stepped-pressure profile indicated in (a).

DGEBA-HDA, respectively. These show that ε' and ε'' vary with polymerization time in a qualitatively similar manner as for the polymerizations where the pressure is maintained constant during the polymerization. However, an increase of pressure affects ε' and ε'' for each of the four mixtures such as to produce a discontinuity, or 'jog', in the ε' and ε'' data. The magnitude and sign of the 'jog' for the four mixtures, which seems to depend upon the range of polymerization time, will be considered in Section 6.3.

CHAPTER V

EVOLUTION OF LOCALIZED RELAXATION PROCESSES DURING POLYMERIZATION

5.1 DIELECTRIC RELAXATION AND LOCALIZED DIFFUSION

Localized translational and rotational diffusions in an otherwise rigid structure of a glass have been observed as a dielectric loss peak or relaxation below T_g when measurements at a fixed frequency are made as a function of temperature [McCrum *et al.* (1967), Johari and Goldstein (1970)]. The rate of these relaxations is found to increase on heating according to the Arrhenius equations, and decrease with an increase in the molecular weight of the polymer [McCrum *et al.* (1967)].

As polymerization occurs, and weak Van der Waals interactions are replaced by directional covalent bonds, the density of the liquid and the configurational restrictions to molecular diffusion within its structure increases, and permanent changes occur in the net molecular dipole moment and in the mechanism of Brownian diffusion. In general, the optical refractive index, the viscosity [Malkin and Kulichikhin (1991)], the velocity of sound [Aronhime and Gillham (1987), Alig *et al.* (1992), Younes *et al.* (1994), Parthun and Johari (1995a)], the mechanical modulus [Aronhime and Gillham (1987)], and the intermolecular vibrational frequencies [Aronhime and Gillham (1987), Plazek and Frund (1990), Younes *et al.* (1994), Parthun and Johari (1995a)] all increase irreversibly. Each of these properties reach their respective maximum values as the total number of bonds

formed reaches its maximum value under isothermal conditions. In a study aimed at understanding the evolution of the localized modes of motion in the glassy states of chemically similar but structurally different materials obtained after a partial polymerization, it is necessary to first use the results of Section 4.2 to determine the relaxation features of the (unpolymerized) molecular liquids as follows.

5.1.1 The Molecular Relaxations in the Unpolymerized Liquids

Figures 4.4 - 4.9 show that there are two relaxation peaks corresponding to two processes; one appears as a prominent sub-T_g (localized, or secondary) relaxation peak in the temperature range 135 - 150 K, and the other a main, or α-relaxation peak in the temperature range 245 - 265 K for the various mixtures before any detectable polymerization has occurred as denoted in the figures by curves labeled 1. For the compositions of Tactix and 3CA and Tactix and 4CA, the sub-T_g relaxation process cannot be resolved at these temperatures for 1 kHz measurements, but ε'' at these temperatures remains high, thus indicating a significant contribution from a sub-T_g relaxation process. For comparison of the DGEBA-DMBA5 and DGEBA-DMBA10 mixtures, the ε' and ε'' data for their unpolymerized and fully polymerized states are distinguished in Figure 4.9.

For the unpolymerized state of Tactix-3CA and Tactix-4CA, a slight plateau-like feature for ε'' in the temperature range between the two peaks appears, as is seen in Figures 4.7 and 4.8. It is possible that this feature is a reflection of the broad distribution of relaxation times for the α-relaxation process, as Muzeau *et al.* (1992) have concluded from

similar findings in the mechanical relaxation measurements of polymers made for a fixed frequency. It should not be seen, however, as a new relaxation process [Parthun and Johari (1995b), Muzeau *et al.* (1994)], because this plateau-like, and in some cases peak-like, feature does not appear in chemically-stable liquids slow-cooled to the glassy state [Muzeau *et al.* (1992) and (1994)], or in glassy materials that have been annealed for a significant period of time [Muzeau *et al.* (1992) and (1994)]. It has been shown analytically that in the dielectric data, this plateau-like feature may also appear when the dc conductivity of the material is relatively high and has a particular variation with temperature [Parthun and Johari (1995b)]. Thus, this feature may not vanish entirely on slow cooling or annealing. Parthun and Johari (1995b) demonstrated that it is possible to separate the dc conductivity contributions from the dielectric relaxation features of such materials. In either case, the plateau-like feature is not seen as indicative of a molecular or dipolar relaxation and it is concluded that, as for other molecular glasses [Johari and Goldstein (1970)], the molecular glasses studied here show only one relaxation peak that can be attributed to the localized motions in the otherwise rigid matrix of a glass. Although the sub-T_g ε''-peak is not observable for two of the cases here (Tactix-3CA and Tactix-4CA), the occurrence of the localized dipolar diffusion that produced it could be revealed by multifrequency dielectric measurements [Johari and Pathmanathan (1986), Johari and Pascheto (1994), Wasylyshyn *et al.* (1996)] or by measurements under a high hydrostatic pressure [Johari and Whalley (1972)]. For the cases in which it is clearly observed, the height of the sub-T_g peak remains in the ε'' range of 0.07 - 0.09, as shown in Table 5.1 and Figures 4.4 to 4.9. It is within the

Table 5.1: The temperature of polymerization (T_r), the height and temperature of the ε″ peak (ε''_{peak}, T_{max}) for the unreacted ($N = 0$), half polymerized ($N = N(\infty)/2$) and completely polymerized states ($N = N(\infty)$) for the systems studied.

Mixture	T_r [K]	ΔH^o_{tot} kJ/mol epoxide	$N(0)$-state ε''_{max} (T_{max})		$N(t)=N(\infty)/2$-state ε''_{max} (T_{max})		$N(\infty)$-state ε''_{max} (T_{max})
			sub-T_g process	α-process	sub-T_g process (1)	sub-T_g process (2)	sub-T_g process
DGEBA-CHA	313.4	54.8	0.0828 (143.5 K)	1.45 (243.2 K)	0.0302 (152.6 K)	0.0484 (244.9 K)	0.0771 (257.6 K)
DGEBA-AN	343.0	79.2	0.0688 (136.6 K)	1.79 (251.3 K)	0.0329 (153.3 K)	0.0551 (231.3 K)	0.0345 (252.3 K)
DGEBA-DMBA5	335.4	47.7	0.0758 (147.0 K)	1.618 (269.7 K)	Unclear	Unclear	0.0405 (204.2 K)
DGEBA-DMBA10	335.4	56.5	0.068 (147.9 K)	1.469 (267.6 K)	Unclear	Unclear	0.0416 (217.4 K)
Tactix-AN	332.0	77.8	0.0899 (140.5 K)	1.171 (257.9 K)	0.0254 (153.9 K)	0.0523 (237.0 K)	0.0812 (256.5 K)
Tactix-3CA	360.6	68.5	Unclear	1.56 (265.1 K)	Unclear	Unclear	0.0726 (267.5 K)
Tactix-4CA	349.5	69.6	Unclear	1.97 (262.3 K)	Unclear	Unclear	0.085 (256.1 K)

range 0.03 to 0.09 for similar mixtures from an earlier study by Parthun and Johari (1995b). The temperature of the relaxation peaks, their ε'' heights determined from Figures 4.4 to 4.9, the polymerization temperature, T_r, and the total heat of polymerization, ΔH°_{total}, are listed in Table 5.1.

5.1.2 The Effects of Covalent Bonds on Localized Relaxations

Figures 4.4 to 4.9 show that features of the ε'' curves obtained change in several ways as the number of covalent bonds formed, $N(t)$, increases during polymerization of each of the six mixtures; DGEBA-AN, DGEBA-CHA, Tactix-AN, Tactix-3CA, Tactix-4CA, and DGEBA-DMBA5. The prominent peak in ε'' that occurs in the 135-150 K range, and which is characteristic of the monomeric state, decreases in height and gradually becomes extinct. A new sub-T_g relaxation process emerges, which is characteristic of the polymerized state, whose peak appears in a higher temperature range. Concurrently, the height of the peak associated with this process increases and shifts to a slightly higher temperature as $N(t)$ increases.

The heights of the low-temperature, sub-T_g relaxation peak of the unpolymerized mixture, $\varepsilon''_{peak,1}$, and of the high-temperature, sub-T_g relaxation peak of the polymerized mixture, $\varepsilon''_{peak,2}$, are plotted against the extent of polymerization, $\alpha(t)$ in Figure 5.1. In this figure, the results for all the seven mixtures have been combined, with the corresponding values for DGEBA-DMBA10 in its initial and final state also shown. The clustering of the ε''_{peak} data for the Tactix-AN, Tactix-3CA, Tactix-4CA, DGEBA-CHA, and DGEBA-AN

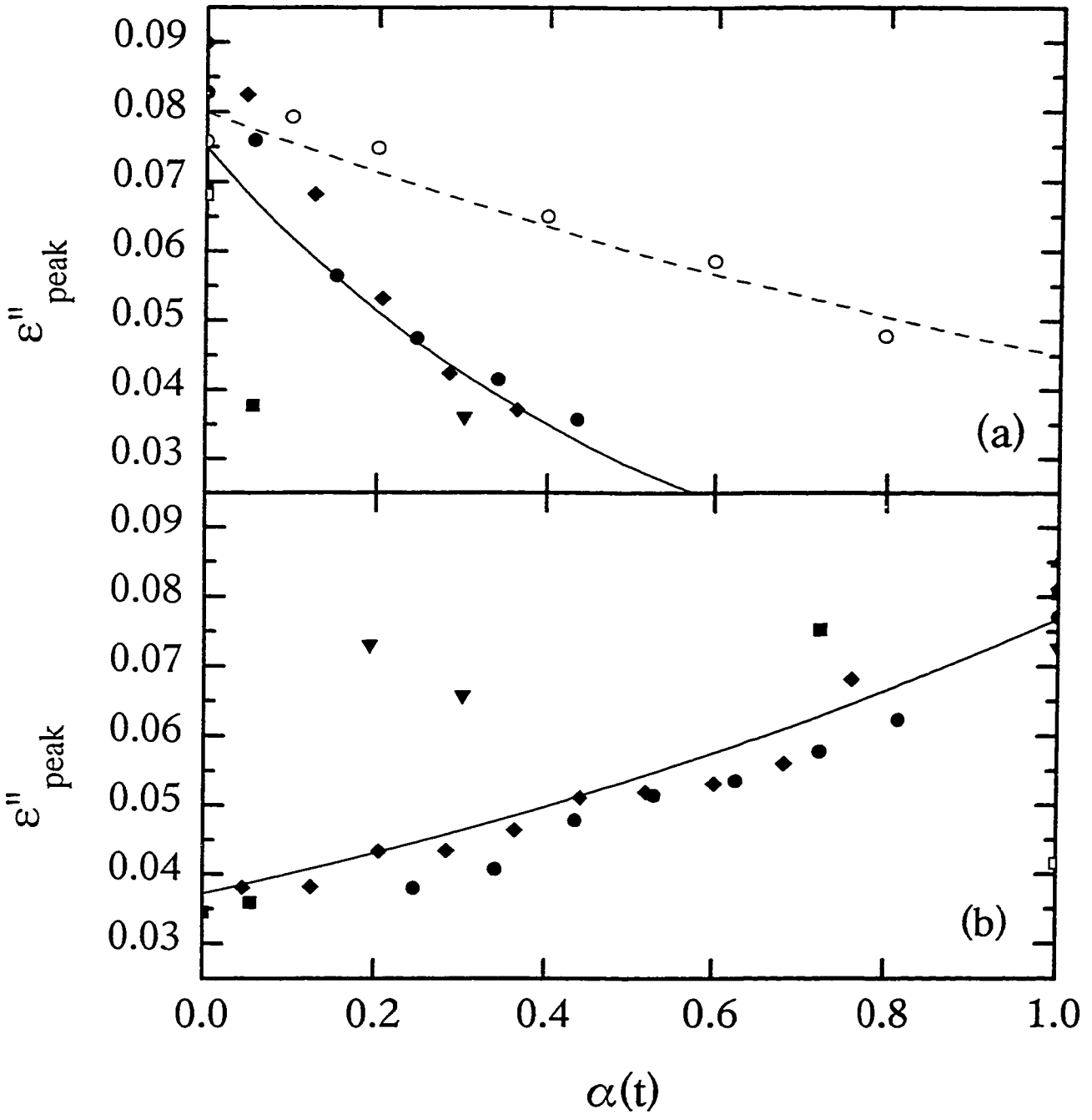

Figure 5.1: **(a)** The height of the ε″ peak for the lowest temperature sub-T_g relaxation process measured for 1 kHz frequency plotted against $\alpha(t)$. The solid and dashed lines were calculated using Equations (5.1) and (5.4), respectively. **(b)** The height of the ε″ peak for the highest temperature sub-T_g relaxation process measured for 1 kHz frequency plotted against $\alpha(t)$. The solid line was calculated using Equation (5.2). The closed symbols are for the reaction of epoxides with amines, and the open symbols are for the catalysis of DGEBA with DMBA.

mixtures into a narrow region clearly shows that the effects observed transcend the details of the molecular nature of the liquid for addition polymerization. Since the former three of these macromolecules form network structures and the latter two form linear-chain structures, as described in Section 2.2, it is also evident from Figure 5.1 that the effects do not depend upon the topology of the disordered structure formed. Instead, the effects depend only on $N(t)$ and the resulting configurational restriction that increases the glass transition temperature, T_g, of the mixture.

The data for the DGEBA-DMBA5 and DGEBA-DMBA10 mixtures in Figure 5.1 are similar to each other, but do not superpose with the data for the other five mixtures described above, which is a reflection of the difference between catalyzed polymerization mechanisms and the uncatalyzed, whose details have been given in Section 2.2. The linear chains formed by addition polymerization are composed of alternating DGEBA and amine molecules. For the network structures formed, each N-atom links two diepoxide molecules with the hydrocarbon group of the amine acting as a cross-link. This network structure differs from that formed on the DMBA-catatalyzed DGEBA, where each DGEBA molecule is bonded to four other DGEBA molecules, the length of the cross-link is the same as that of the repeat unit, and the DMBA molecules remain unbonded to the growing macromolecule. These differences in macromolecular structures contribute to the differing evolution of $\varepsilon''_{peak,1}$ and $\varepsilon''_{peak,2}$ for the two types of polymerizations in addition to that from differing bond properties, cross-link densities, and the dipole moment of the diffusing segments.

The decrease of $\varepsilon''_{peak,1}$, with $\alpha(t)$ for the polymerization of the DGEBA-CHA, DGEBA-AN, Tactix-AN, Tactix-3CA, and Tactix-4CA mixtures observed here (Figure 5.1(a)) is expressed as,

$$\varepsilon''_{peak,1}(\alpha) = 0.075\exp\left[-1.905\alpha(t)\right] \tag{5.1}$$

The increase of $\varepsilon''_{peak,2}$, with $\alpha(t)$ for the polymerization of the same mixtures observed here follows,

$$\varepsilon''_{peak,2}(\alpha) = 0.03725\exp\left[0.725\alpha(t)\right] \tag{5.2}$$

These empirical relations may be useful for the theoretical developments by others in the future.

The data in Table 5.1 also confirms the earlier observations [Wasylyshyn and Johari (1996)] that the temperature of the α-relaxation peak of the unpolymerized molecular liquid is significantly different from the temperature of the sub-T_g relaxation peak of the polymerized state ($\varepsilon''_{peak,2}$) for $N(t \rightarrow \infty)$ in three cases. This observation, along with that in an earlier study by Parthun and Johari (1995b), is evidence against the view [Williams *et al.* (1995)] that long-range diffusion modes of the supercooled molecular liquid, which show up as the α-relaxation peak at temperatures above T_g, become the localized relaxation modes at temperatures below the T_g of the macromolecule formed by polymerization. Parthun and Johari [(1995b)] have discussed the conditions for which the α-relaxation peak of the monomeric liquid measured for a certain fixed frequency may appear at the same temperature as the sub-T_g relaxation peak of the polymer of the same chemical constituents. Therefore, for a fixed frequency measurement, when the temperature of the α-relaxation

peak of the monomeric liquid and the temperature of the sub-T_g relaxation peak of the polymeric glass formed after polymerization are similar, it appears to be coincidental.

This is also evident from the manner by which $\varepsilon''_{peak,2}$ changes with an increase in $N(t)$. If the high-temperature, sub-T_g relaxation peak, *i.e.* $\varepsilon''_{peak,2}$, was the remnants of the α-relaxation peak observed for the monomeric liquid, its height would be expected to decrease with increase in $N(t)$. The data in Table 5.1 and Figures 4.4 to 4.9 show that this is not the case. Thus, Williams *et al.*'s (1995) conjecture on the origin of the sub-T_g relaxation peak is not supported by experiments.

Considering that the relaxation time, τ, of the sub-T_g relaxation process is given by,

$$\tau = \left[\left(h/k_B T\right)\exp\left(-\Delta S^*/R\right)\right]\exp\left(\Delta H^*/RT\right) \qquad (5.3)$$

where k_B is the Boltzmann constant, h the Planck constant, R the gas constant, ΔS^* the entropy of activation, and ΔH^* the enthalpy of activation, it is evident that a constant ΔS^* indicates that ΔH^* for the sub-T_g relaxation process of the polymeric glass, $\varepsilon''_{peak,2}$ would be higher than that of the sub-T_g relaxation process of the monomeric glass, $\varepsilon''_{peak,1}$. Alternatively, on the assumption that ΔH^* does not change, this means that $(-\Delta S^*)$ increases as the number of covalent bonds formed increases.

The molecular kinetics of the sub-T_g relaxation process for monomeric and polymeric glasses has been found to be of the Arrhenius type [McCrum, *et. al* (1967), Johari (1973)], and it seems likely that monomeric and polymeric states of the same substance would have similar Arrhenius kinetics for localized diffusion. ΔH^* and ΔS^* could not be determined here, however, in an earlier study [Johari (1986), Pathmanathan and

Johari (1988)] of polypropylene glycol of different chain lengths, it was shown that the kinetics remain of the Arrhenius type with an increase in the molecular weight, but both ΔH^* and ΔS^* change with $N(t)$. For example, ΔH^* = 28.7 kJ/mole when the molecular weight of the polymer was 425 [Pathmanathan and Johari (1988)] and 19.4 kJ/mole when the molecular weight was 4000 [Johari (1986)]. The corresponding pre-exponential factors contained within the square parentheses of Equation (5.3) were 0.0252 ps [Pathmanathan and Johari (1988)] and 17.9 ps [Johari (1986)], respectively. Thus, it appears that both ΔH^* and ΔS^* in Equation (5.3) would increase as $N(t)$ increases.

5.2 THE EVOLUTION OF LOCALIZED RELAXATIONS BY MICROWAVE SPECTROSCOPY

As described in the preceding section, spectra in the gigahertz (GHz) frequency range for the liquid state at $T >> T_g$ also show the evolution of relaxation processes, which is related to the sub-T_g relaxation by an Arrhenius equation [Johari (1973)]. These GHz range spectra were studied for the DGEBA-DMBA5 and DGEBA-DMBA10 mixtures during polymerization from a molecular liquid state to a cross-linked polymeric solid. Since DMBA acted as a catalyst the significance of its contributions to the measured dielectric properties needs to be examined. This is done by plotting in Figure 5.2 the ε' and ε'' spectra of their (unpolymerized) molecular liquid states. Although the ε''-peak in this figure appears at a slightly higher frequency for the 10% DMBA liquid mixture, which is due to the lower viscosity of the mixture with a lesser amount of DGEBA, the height of the ε''-peak and the ε' values differ only marginally between the

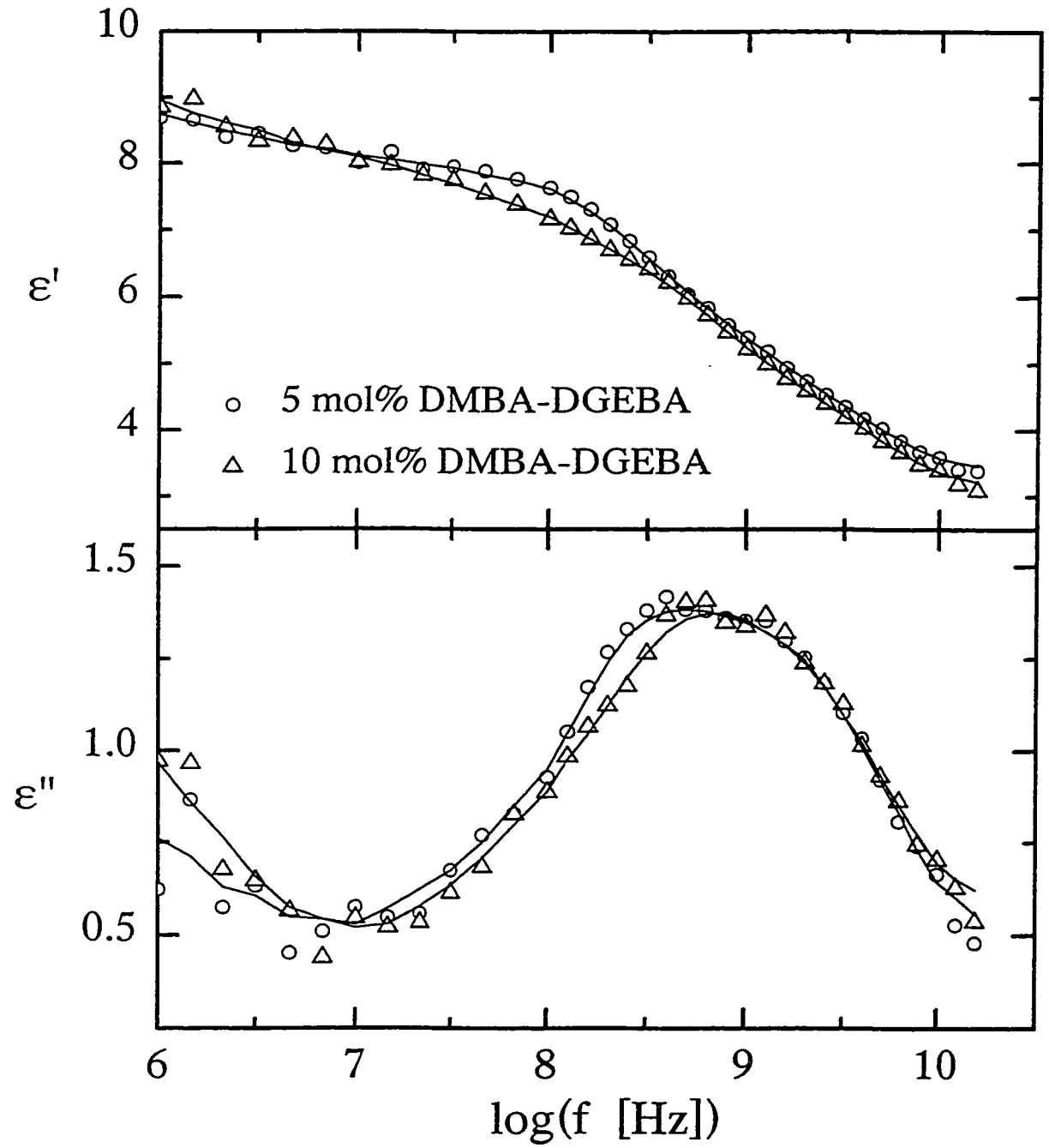

Figure 5.2: The ε′ and ε″ spectra of the unreacted DGEBA-DMBA5 and DGEBA-DMBA10 mixtures at 335.4 K.

two mixtures. As well, ε' and ε'' are higher at the lowest frequency for the 10 mol% mixture than for the 5 mol% mixture. This seems to be due to an increase in the dc conductivity and the consequent increase in the interfacial polarization. Thus, most of the dielectric polarization is due to the orientational diffusion of the dipoles associated with the DGEBA molecules in the mixture, and that doubling the amount of DMBA from 5 mol% to 10 mol% does not change ε_s or the half-width of the spectrum significantly. A similar conclusion is reached by comparing the fixed frequency data for the two compositions plotted in Figure 4.9. After vitrification of the mixture, the DMBA molecules remain in the polymer matrix in both cases and may contribute to dielectric polarization, but the magnitude or relevance of their contribution is not clearly known.

5.2.1 The Extinction of the GHz Relaxation Process During Polymerization

The spectra in Figures 4.10 and 4.11 show that there is only one relaxation peak at ~0.65 GHz, with a spectral half-width of 2.4 decades for the (unpolymerized) liquid states of DGEBA reacted with either DMBA5 or DMBA10. The peak in ε'' does not change its position in the frequency plane with an increase in $N(t)$ within the experimental error, but its height decreases to near-zero as $N \rightarrow N(\infty)$. The relaxation time for this GHz relaxation process is 0.24 ns ($\tau = 1/2\pi f$), which corresponds well to a Maxwellian viscosity, η_M, of a few Poise, deduced from $\eta_M = \tau G_\infty$, where G_∞ is the limiting high-frequency shear modulus, typically 1 GPa. A value of 8.2 ± 0.3 for ε_s of both molecular liquids at 335.4 K deduced from Figures 4.10 and 4.11 are consistent with the increased

value of 10.5 at 275 K for 5 mol% and 10.0 at 280 K for 10 mol% deduced from the 1 kHz measurements in Figure 4.9. Since no other relaxation is observable at lower frequencies, it follows that all polarization in the two liquids relaxes by this dynamics.

Earlier studies [Cassettari *et al.* (1994)] have shown that two new relaxation processes evolve on isothermal polymerization, the rate of one, the Johari-Goldstein relaxation [Angel (1995), Frick and Richter (1995)], remains relatively unchanged, while the rate of the other, the α-relaxation, rapidly decreases until its ε'' peak moves out of the low frequency end of the experimental spectral window before isothermal vitrification has occurred. These changes in the high-frequency dielectric spectrum as $N(t)$ increases spontaneously during polymerization are similar to the phenomenon observed when a molecular or low-viscosity polymer liquid is cooled from a high temperature where its viscosity is only a few Poise and its relaxation time only a few nanoseconds. As the liquid is cooled, its total orientational polarization, denoted by $\Delta\varepsilon$ (ε_s - ε_∞), increases according to the Curie-Weiss law ($\varepsilon_s \propto 1/(T-T_o)$), and a new relaxation process, the α-relaxation, evolves. The rate of the α-relaxation continues to slow more rapidly as the liquid is cooled, and as it does, its behaviour deviates progressively more from Arrhenius behaviour until its ε'' peak moves out of the low-frequency side of the experimental spectral window before the liquid vitrifies.

Once the α-relaxation process has evolved from the Johari-Goldstein relaxation in a liquid, $\Delta\varepsilon$ relaxes by two relaxation dynamics. The α-process relaxes with a progressively larger fraction of $\Delta\varepsilon$ as the liquid is cooled [Cassettari *et al.* (1994)], and

the fraction relaxing by the Johari-Goldstein process decreases. Thus, in the glassy state, only a small magnitude of the latter is observed. But, as the molecular liquid polymerizes, the consequences for the net orientation polymerization differ from those of cooling, because $\Delta\varepsilon$ *decreases* during polymerization as a result of the reduction of the net dipole moment and a decrease in the orientational correlation factor, even when the density increases on polymerization [Pathmanathan and Johari (1988), Johari (1994a), Parthun and Johari (1995a,c), Wasylyshyn and Johari (1997b)], and $\Delta\varepsilon$ *increases* during cooling, according to the Curie-Weiss law.

5.2.2 The GHz Frequency Relaxation and the Sub-T_g Relaxation

To investigate the changes in the low-temperature peak and its relation to the changes in the peak observed in Figures 4.10 and 4.11, ε''_{peak}, at GHz frequencies, and that in the 145 - 150 K range for the 1 kHz frequency was determined from the DGEBA-DMBA5 data in Figure 4.9, and is plotted against $N(t)$ in Figure 5.3(a) and (b). (The decrease of the ε'' peak height for the 5 mol% mixture is similar to that for the 10 mol% mixture, which further confirms that DMBA's contribution to the dielectric behaviour is not significantly increased by doubling its amount, as discussed earlier in this section.)

It is evident that both the ε'' peak height and its rate of decrease for the fixed 1 kHz frequency differs from that observed in the MHz - GHz spectral range. The data for the decrease in ε''_{peak} in the 145- 150 K range for the 5 mol% mixture, as seen in Figure 5.3(a), is empirically described by:

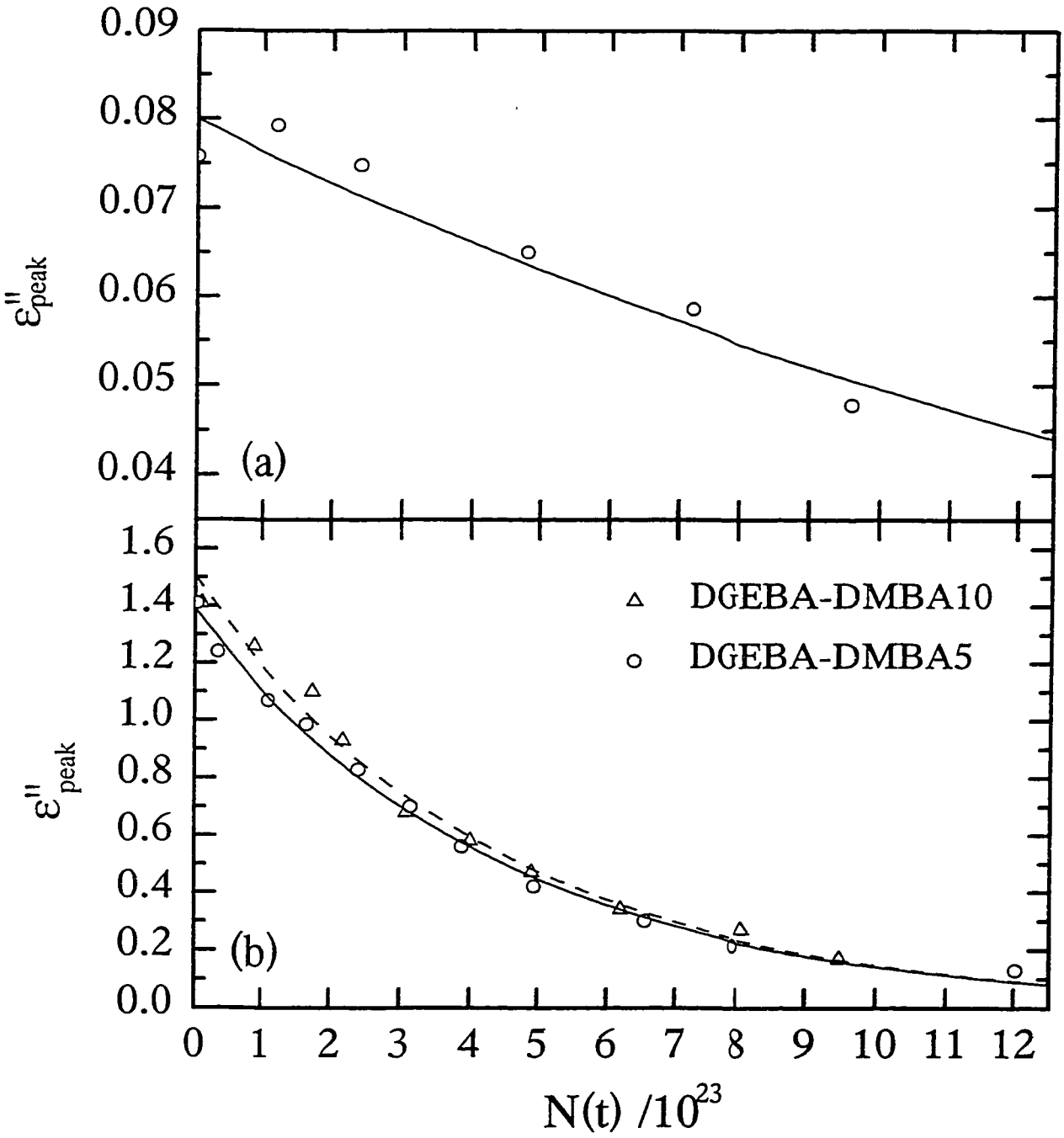

Figure 5.3: **(a)** The height of the ε″ peak measured for 1 kHz frequency is plotted against $\alpha(t)$ for the polymerization of the DGEBA-DMBA5 mixture at 335.4 K. The solid line is calculated with Equation (5.4). **(b)** The corresponding plot of the height of the ε″ peak in the GHz frequency range for the DGEBA-DMBA5 and DGEBA10 mixtures polymerizing at 335.4 K. The solid line is the fit of Equation (5.5) to the DGEBA-DMBA5 mixture and the dashed line is that of Equation (5.6) to the DGEBA-DMBA10 mixture.

$$\varepsilon''_{peak} = 0.08\exp(-0.576\alpha(t)) \quad \textbf{(5.4)}$$

The decrease in ε''_{peak} in the GHz frequency region for the 5 mol% mixture, as seen in Figure 5.3(b), is described by,

$$\varepsilon''_{peak} = 1.39\exp(-2.739\alpha(t)) \quad \textbf{(5.5)}$$

and that for the GHz frequency region for the 10 mol% mixture, as seen in Figure 5.3(b) is described by,

$$\varepsilon''_{peak} = 1.51\exp(-2.794\alpha(t)) \quad \textbf{(5.6)}$$

$\alpha(t)$ in Equations (5.4) to (5.6) is equal to $N(t)/(12.044\text{x}10^{23})$. The form of Equations (5.5) and (5.6) and the parameters are similar within the experimental errors. This shows that the fastest relaxation would not completely disappear when $N(t)$ reaches its limiting value (Note that, $\alpha(t) = N(t)/N(t = \infty)$), although it may become undetectable due to the instrumental limitations.

5.2.3 Relaxation Dynamics and Configurational Entropy

As discussed in Section 5.1, the weak Van der Waals' interactions are replaced with stronger directional covalent bonds upon polymerization. Accordingly, an increase in $N(t)$ is expected to decrease the configurational entropy, S_{conf}, as molecular reorientation is further hindered upon covalent bonding. The latter is manifested as an increase in the macroscopic viscosity and the dielectric relaxation time. But, since the position of the ε'' peaks, (τ = 0.24 ns) seen in Figures 4.10 and 4.11 do not change as $N(t)$ increases or S_{conf} decreases, its relaxation mechanism should be independent of S_{conf}. Only

the α-relaxation, which is associated with the glass-transition of the liquid, is sensitive to the decrease in S_{conf} as $N(t)$ increases under isothermal conditions. Similarly, as the temperature of the relaxation peaks for 1 kHz frequency (τ = 0.159 ms), $\varepsilon''_{peak,1}$, seen in Figures 4.4 to 4.9 do not change with increase in $N(t)$, it follows that this relaxation mechanism is also independent of S_{conf}.

According to the configurational entropy theory [Adam and Gibbs (1965)], the characteristic relaxation time associated with a molecular diffusion process,

$$\tau = \tau^{(\infty)} \exp\left(c/k_B T S_{conf}\right) \tag{5.7}$$

where $c = \Delta\mu s_c^*/k_B$ and $\Delta\mu$ is the potential energy hindering the cooperative rearrangement per monomer segment of the molecule, s_c^* is the critical entropy of the smallest volume of relaxing molecules, k_B is the Boltzmann constant, and $\tau^{(\infty)}$ is the average relaxation time at $T \rightarrow \infty$, *i.e.* $\tau(T \rightarrow \infty)$. Since s_c^* represents the general topological condition for a cooperative transition, it does not change with the molecular weight of a polymer [Adam and Gibbs (1965)], and $\Delta\mu$ is independent of the length of a chain or the size of the network. Thus, the magnitude of c in Equation (5.7) does not change on polymerization as originally discussed [Adam and Gibbs (1965)] and $\tau^{(\infty)}$ is equal to ~10^{-13} s, the vibrational time scale. In the original description [Adam and Gibbs (1965)], S_{conf} becomes zero at a temperature about 0.7-0.8T_g, however, recent arguments based on the defect theory for the glass structure [Johari and Perez (1994)], point out that S_{conf} should become zero only at 0 K and not above it. Despite that, the irreversible change with the polymerization time can be discussed in

terms of the configurational entropy theory because the α-relaxation has not been studied at $T < T_g$ as follows.

At a constant temperature, $\ln\tau$ is proportional to the inverse of S_{conf}, and if S_{conf} were to remain constant, τ would vary with the temperature in an Arrhenius manner. The absence of any significant positional change in ε''_{peak}, for the GHz frequency relaxation of Figures 4.10 and 4.11, and in the 145 - 150 K sub-T_g relaxation process, $\varepsilon''_{peak,1}$ in Figure 4.9 for the 5 mol% mixture, shows that τ of these two, fast relaxation processes does not change significantly. This implies that the exponential term in Equation (5.7) for these processes remains constant with an increase in $N(t)$. Since S_{conf} does decrease on polymerization, this process can only be independent if the ratio, c/S_{conf}, in Equation (5.7) were to remain constant during polymerization. From the discussions of Section 5.1.2 and Figures 4.4 to 4.8 for the other polymerizing liquids of DGEBA-AN, DGEBA-CHA, Tactix-AN, Tactix-3CA and Tactix-4CA, not only does the height of the peak, $\varepsilon''_{peak,1}$, decrease on polymerization, but the temperature of the peak also remains nearly constant at 148 K, within the experimental errors. It seems unlikely that the ratio, c/S_{conf}, would be independent of the chemical constitution of the monomeric liquid mixture and of the polymeric structure ultimately formed. Alternatively, it is also conceivable that Equation (5.7) does not apply to localized relaxation processes whose occurrence requires no cooperativite diffusion. In this respect, τ of the Johari-Goldstein relaxations in the glassy state as well as in the liquid state (the latter in the GHz frequency range when the α-relaxation process has not yet developed) is determined entirely by the thermal energy,

k_BT. The characteristic τ of the α-relaxation is determined both by the thermal energy and S_{conf}, since the temperature of its peak shifts with the measurement frequency and its frequency in the GHz spectra with temperature. These observations provide evidence in favour of the theory [Cavaille *et al.* (1989)] that localized, hindered reorientation of molecules is at the origin of the α-relaxation process dynamics, and the continued slowing of the α-relaxation process upon cooling causes the freezing-in of the structure on the observer's time scale, *i.e.* the liquid to glass transition. In other words, molecular motions in a vitrified state begin at particular sites in its disordered structure, and evolve with time. The α-relaxation dynamics is a consequence of this evolution [Cavaille *et al.* (1989)]. The dynamics of the hindered reorientation itself is only insignificantly affected by the development and separation of the long range motions of the α-relaxation dynamics.

5.3 CHEMICAL AND PHYSICAL METASTABILITIES AND THE MOLECULAR DYNAMICS

Generally speaking, covalent bonds differ from Van der Waals' and dipolar interactions only in as much as they are directional and fixed-distance interactions. In this view, the physical consequences of a macromolecule's growth by chemical reactions are manifestly analogous to the physical consequences of spontaneous structural relaxation, or physical ageing, of the glassy state of a material, both occurring under isothermal conditions. For this purpose the chemically unstable state of the monomeric liquid obtained by mixing the two components may be seen as phenomenologically equivalent to the "zero-

time", kinetically metastable, but chemically stable glassy state of a material. Since $\varepsilon''_{peak,1}$ does decrease on structural relaxation, of both molecular and polymeric glasses [Johari (1973), (1976) and (1982), Parthun and Johari (1995b)], as it does with an increase in $N(t)$, this analogy seems to have experimental support. In this case, if covalent bonds are seen merely as a special case of intermolecular interactions, the loss of chemical metastability on polymerization and the ultimate approach to a chemically stable state are phenomenologically similar to the loss of kinetic metastability and the approach to a physically stable state.

With regard to the similarities between chemical and physical metastability as described above, differences do occur in the two cases that must be addressed. In particular, once a macromolecule has formed by polymerization, it cannot be restored to its original molecular (monomeric) state merely by heating it above its T_g and thereafter cooling it. (Theoretically, however, a macromolecule's degradation by photodissociation can restore it to the original molecular state virtually isothermally.) Contrary to this, once physical ageing has occurred, the original "zero-time", kinetically unstable state can be restored by heating the glass to a temperature above its T_g and thereafter cooling the liquid at the same rate as used previously for obtaining the original "zero-time" state.

Another difference between the consequences of polymerization and of spontaneous structural relaxation is that an increase in $N(t)$ during polymerization increases both the density and T_g, however, on spontaneous structural relaxation or physical ageing, T_g has not been found to increase [Johari (1976) and (1982), Parthun and Johari (1995b)]. But, when

one considers that the relaxation time of a structurally relaxed high-density glass would be higher than that of a structurally less relaxed, low-density glass, we deduce that the temperature at which the relaxation time of the densified glass will reach a certain value, provided the density of the glass did not decrease as a result of an increase in configurational or non-vibrational contributions to its volume, will be higher than the temperature at which the relaxation time of the less dense glass will reach the same value under the same conditions. As is well recognized now, the equilibrium state of a structurally relaxed glass is reached when the glass is heated to its fictive temperature [Winter-Klein (1939), Tool (1946), Narayanaswamy (1971), Moynihan *et al.* (1973)], and that thereafter, the equilibrium state is maintained on further heating as the configurational contribution to volume continues to increase. However, when a structurally relaxed glass is heated rapidly enough such that its structure cannot reach its configurational equilibrium, the "observed T_g" will be higher than for a structurally less-relaxed glass. In this regard, there is an analogy with the results of the increase in the number of covalent bonds. The similarities between a macromolecule's growth and its structural relaxation, both isothermally, thus appear more significant than initially expected.

The above-given information can be used to develop a picture for the evolution of the relaxation behaviour of liquids as they polymerize. With the premise that a chemically reacting liquid mixture at "zero time" is kinetically and thermodynamically metastable in the same sense as the glassy state obtained by cooling a chemically inert liquid is kinetically and thermodynamically metastable, it is possible to envisage that a

decrease in the volume, V, enthalpy, H, and entropy, S, as a result of polymerization, is analogous to the decrease in the same quantities during the annealing of a glass. In the case of structural relaxation, the glassy state is obtained by hyperquenching a liquid, such as water [Johari *et al.* (1987) and (1990)] and aqueous solutions [Hofer *et al.* (1989)], resulting in fictive temperatures that are extremely high. Consequently, the liquid's structure is frozen-in at a high temperature and V, H and S of the glassy state are also extremely high. This structure is expected to have a low density and to show only one fast relaxation process, the Johari-Goldstein relaxation, because at the temperature of structural freezing on hyperquenching, the α-relaxation process dynamics has not evolved. Annealing of this structure isothermally would, according to the above discussion, decrease V, H and S, which would lead to the development of the α-relaxation process, thereby producing two relaxation peaks in the ε'' frequency spectrum.

The dielectric study here also shows that the loss of chemical metastability of a liquid of nanosecond relaxation time causes a redistribution of the total orientation polarization into two or more relaxations, the kinetics of the faster relaxation (the GHz-frequency process) remains unchanged, but the new dynamics of the α-relaxation evolves. It continuously shifts to a lower frequency until the shift becomes imperceptible at the vitrification time. The loss of physical metastability is generally discussed in terms of a continuous decrease in T_f, the structural fictive temperature of a glass [Tool (1946), Narayanaswamy (1971)]. One may define an analogous chemical fictive temperature, $T_{f,chem}$ [Wasylyshyn *et al.* (1997a,b)] for polymers in which polymerization rarely reaches

completion before it vitrifies. This is illustrated in Figure 5.4, where the fictive temperatures of both the physically metastable (a) and chemically metastable (b) cases are marked on the equilibrium line. This was done by horizontally extending to the equilibrium line the points from their position on the vertical dashed line. Figures 5.4(a) and (b) illustrate how polymerization in one case and structural relaxation in the other decrease the fictive temperatures from the initial $T_{f,chem,1}$ to $T_{f,chem,5}$ or $T_{f,1}$ to $T_{f,5}$ when the samples are kept isothermally at T_5.

With the analogy of structural relaxation in mind, the conclusion thus reached in the case of isothermal polymerization is that the localized relaxation in a monomeric glass occurs in regions where molecular segments exist in a higher energy state than in the other regions [Cavaille *et al.* (1989), Johari (1993a), Johari and Perez (1994)]. It is thus anticipated that an increase in the size of a macromolecule, or $N(t)$, causes a collapse of the high-energy regions in a manner similar to that of isothermal structural relaxation or physical ageing. Concomitantly, the strength of the sub-T_g relaxation process decreases, as reflected by the decrease in $\varepsilon''_{peak,1}$. The random packing of the newly formed polymeric structure creates within the disordered glassy matrix new high-energy states, where the increased configurational restrictions require a higher thermal energy for local diffusion, hence the temperature of the new sub-T_g relaxation peak, $\varepsilon''_{peak,2}$, is increased compared with that of $\varepsilon''_{peak,1}$, the monomeric sub-T_g peak.

The studies described in this chapter lead to the conclusions that the extinction of the monomeric sub-T_g relaxation peak and the subsequent growth of the polymeric sub-T_g

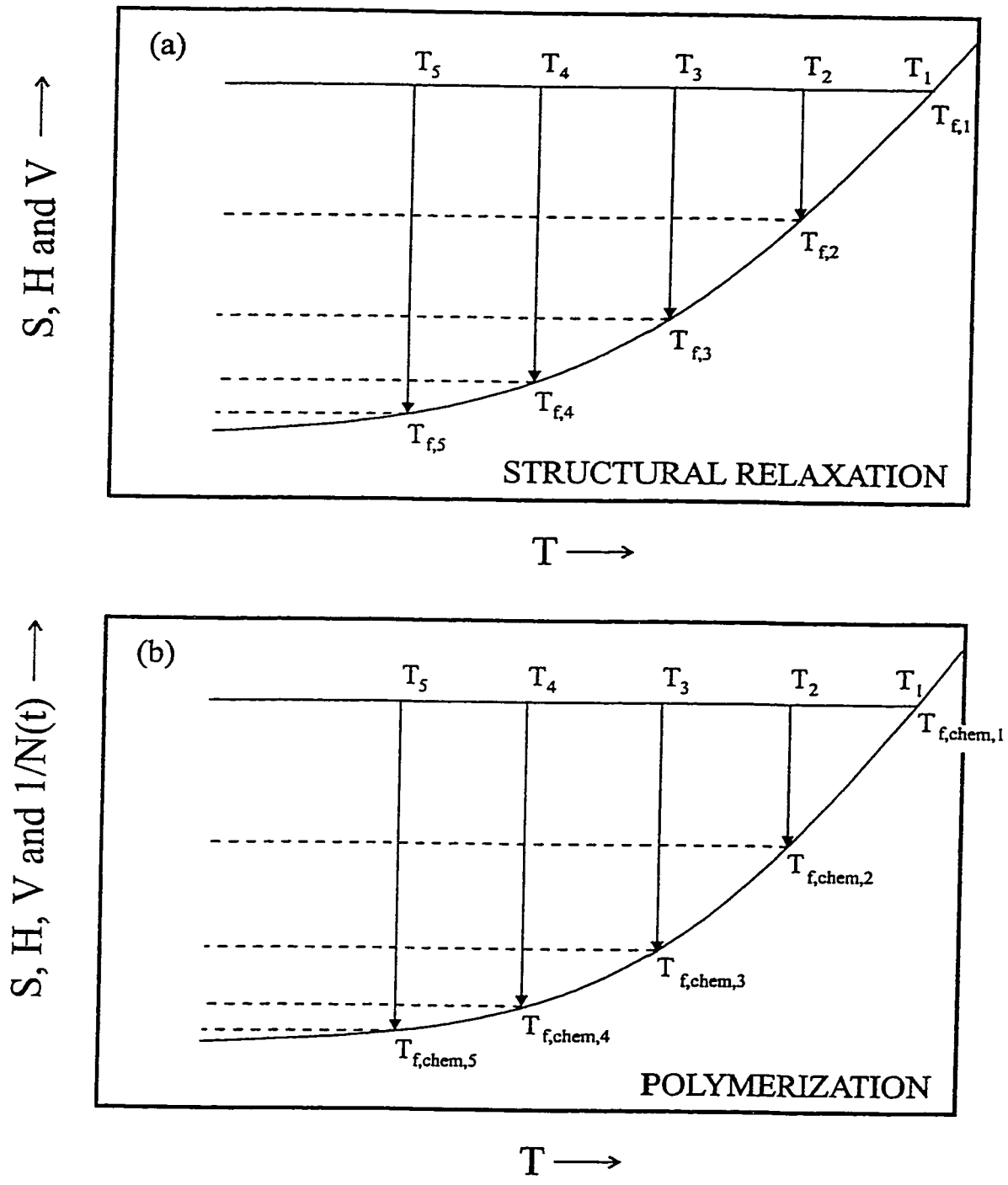

Figure 5.4: An illustrative analogy between **(a)** a physically metastable state, and **(b)** a chemically metastable state. Both undergo irreversible changes with time, and both are seen to approach the equilibrium state as discussed in the text.

relaxation peak during polymerization occur in a manner that is independent of the spontaneous change in configurational entropy. Additionally, the results lend evidence towards the concept that the localized relaxations occur in the monomeric glass in regions of higher energy than in other regions. Polymerization destroys these regions, thus causing the extinction of the monomeric sub-T_g relaxation peak. However, new higher energy states form in the polymer, thus the polymeric sub-T_g peak grows during the course of polymerization.

CHAPTER VI

THE EFFECTS OF PRESSURE ON THE MOLECULAR DYNAMICS AND THE REACTION KINETICS OF POLYMERIZATION

6.1 THE EFFECTS OF ISOBARIC PRESSURE ON POLYMERIZATION

Hydrostatic pressure alters the chemical physics of a time-dependent, chemically-*invariant* process in a manner that excludes the entropy change resulting from the occurrence of that process. Instead, the change in volume on compression predominates the effects [Johari and Dannhauser (1969a), Chen *et al.* (1969), Johari and Whalley (1972)]. In general, pressure reduces the diffusion coefficient, or the structural relaxation rate, and increases the number density of the molecules. Therefore, one expects that for a polymerization process, which is both time-dependent and chemically *variant*, an increase in pressure would decrease the diffusion rate (or increase the viscosity) of the polymerizing liquid, thus slowing the chemical reactions. However, the increase in pressure is also expected to increase the number density of reacting molecules in the liquid, thus increasing the probability of their mutual approach, which is expected to increase the reaction rate. The former would occur only after the polymerization reactions have become diffusion-controlled, *i.e.* when the diffusion time of one reacting species towards another is the rate-limiting step. The latter occurs in most cases of chemical reactions that are entirely mass-controlled, *i.e.* when the amount of reactants remaining is the rate-limiting step. In an

intermediate situation, when an increase in pressure causes the reaction kinetics to change from the mass-controlled to the diffusion-controlled regime under isothermal conditions, the effects of the increase in the reaction rate by increase in density can be partly compensated for by the decrease in the reaction rate on increase in the viscosity of the liquid. In such a situation, hydrostatic pressure is expected to have little effect on the polymerization reaction.

Pressure also changes the equilibrium constant, K, of a reaction according to the equation, $(d\ln K/dP) = -(\Delta V/RT)$, where ΔV is the volume change of reaction, R the gas constant and P and T are the pressure and temperature, respectively. For polymerization, ΔV is negative since the product is denser than the reactants, hence K increases on increasing the pressure. Thus, a reaction may be brought to near-completion, if the kinetics are fast enough to allow it, by increasing the pressure on a polymerizing liquid. Two effects of hydrostatic pressure can therefore be identified: (i) a change in the reaction rate; an increase when the reaction is mass-controlled, and a decrease when it is diffusion-controlled, and (ii) a change in the extent of reaction according to Le Chatelier's principle.

In addition, there is a third effect, which is related to the viscosity and the average dielectric relaxation time, $\langle\tau\rangle$, of the polymerizing liquid, and is considered in terms of the configurational entropy, which decreases as (a) polymerization occurs [Johari *et al.* (1996)] and (b) as the hydrostatic pressure is increased. All the three effects of pressure, (i) a change in the polymerization rate, (ii) an increase in the extent of polymerization, and (iii) a decrease in the configurational entropy of the polymerizing liquid, are therefore inter-

related, and can be studied by a technique that allows one to determine the molecular diffusion time or structural relaxation time. Although any of the dynamic structural properties, *i.e.* viscosity [Malkin and Kulichikhin (1991)], ultrasonic attenuation [Aronhime and Gillham (1987), Alig *et al.* (1992), Younes *et al.* (1994), Parthun and Johari (1992a) and (1992b)], Brouillon light scattering [Mangion and Johari (1991)], dynamic mechanical spectroscopy [Aronhime and Gillham (1987)], dynamic heat capacity [Ferrari *et al.* (1996)], calorimetry [Barton (1985), Cassettari *et al.* (1993a,b)] can be used for such studies, experience has shown that dielectric measurements are the most convenient of these techniques [Mangion and Johari (1990), Johari (1990b) and (1994), Tombari and Johari (1992), Cassettari *et al.* (1994), Deng and Martin (1994a), Parthun and Johari (1995b), Parthun *et al.* (1996), Wasylyshyn *et al.* (1996), Wasylyshyn and Johari (1997b)], particularly at high pressures [Johari *et al.* (1996)].

The ε' and ε'' plotted against the polymerization time, t, shown in Figures 4.12 to 4.14 for DGEBA-CHA at 300.2, 307.5, and 313.8 K, respectively, Figures 4.15 to 4.17 for DGEBA-EDA at 296.6, 306.1, and 314.0 K, respectively, and Figures 4.18 to 4.21 for DGEBA-AN, DGEBA-HA, DGEBA-EDA, and DGEBA-HDA at 351.5, 304.0, 307.2, and 303.4 K, respectively, were analyzed by the procedure described in Section 2.6. The values of the parameters, γ, $\varepsilon'(t \rightarrow 0)$, $\varepsilon'(t \rightarrow \infty)$ and $t(\varepsilon''_{max})$ thus obtained from the time-variant ε' and ε'' measured for 1 kHz frequency for polymerization at various isothermal and isobaric conditions are listed in Table 6.1 for DGEBA-CHA at 300.2, 307.5, and 313.8 K, and 1, 103, and 206 bar, and for DGEBA-EDA at 296.6, 306.1, and 314.0 K, at

Table 6.1: The parameters obtained using Equations 2.17 and 2.18 to analyze the dielectric data from the DGEBA-CHA and DGEBA-EDA polymerizations under the isothermal temperatures and isobaric pressures indicated.

T /K	P /bar	$\varepsilon'(t \rightarrow 0)$	$\varepsilon'(t \rightarrow \infty)$	$t(\varepsilon''_{max})$ /ks	γ
DGEBA-CHA					
300.2	1	6.63	3.67	34.2	0.34
300.2	103	7.32	4.05	30.7	0.35
300.2	206	7.41	4.12	27.6	0.35
307.5	1	6.71	3.90	21.6	0.35
307.5	103	6.82	3.92	19.6	0.35
307.5	206	6.86	3.98	17.0	0.35
313.8	1	6.32	3.77	14.8	0.35
313.8	103	6.31	3.74	11.7	0.35
313.8	206	6.40	3.80	10.1	0.35
DGEBA-EDA					
296.6	1	9.04	4.42	11.7	0.31
296.6	103	9.20	4.58	9.8	0.32
296.6	206	9.32	4.58	8.6	0.32
306.1	1	8.47	4.40	5.8	0.29
306.1	103	8.75	4.47	5.2	0.29
306.1	206	8.81	4.47	4.5	0.29
314.0	1	7.37	4.32	2.8	0.29
314.0	103	7.91	4.56	2.5	0.29
314.0	206	7.55	4.50	2.1	0.28

1, 103, and 206 bar. Corresponding values of these parameters for DGEBA-AN, DGEBA-HA, DGEBA-EDA, and DGEBA-HDA at 351.5, 304.0, 307.2, and 303.4 K, respectively, are given in Table 6.2. For comparison with the measured data, ε' and ε'' calculated back from these parameters are plotted with the measured data of ε' and ε'' in Figure 6.1 for the DGEBA-CHA mixture at 307.5 K and 1, 103 and 206 bar, and Figure 6.2 for the DGEBA-EDA mixture at 296.6 K and 1, 103 and 206 bar. The close agreement between the calculated and measured values in these figures demonstrates the adequacy of the single-frequency measurement procedure. The fits to the rest of the measured data discussed above were similarly satisfactory, and have been excluded for brevity. From the values of τ_o and γ in Table 6.1, the variation of $\langle\tau\rangle$ with the polymerization time, t, was calculated, and is shown in Figure 6.3 for the DGEBA-CHA mixture at 300.2, 307.5 and 313.8 K and 1, 103 (excluded at 300.2 K) and 206 bar, and Figure 6.4 for the DGEBA-EDA mixture at 296.6, 306.1 and 314.0 K and 1, 103 and 206 bar. Similarly, Figure 6.5 shows $\log\langle\tau\rangle$ against t, for DGEBA-AN and DGEBA-HA at 351.5 and 304.0 K, respectively, and Figure 6.6 shows that for DGEBA-EDA and DGEBA-HDA at 307.2 and 303.4 K, respectively.

As discussed in Sections 2.6 and 4.3.1, the difficulty in measuring ε' and ε'' spectra at different instants of the polymerization time when the polymerization reached completion in less than 3 ks made it necessary to determine τ from fixed frequency measurements. Nevertheless, to further demonstrate that the fixed frequency measurements also yield satisfactory values of τ at high-pressures, and that the pressure

Table 6.2: The parameters obtained using Equations 2.17 and 2.18 to analyze the dielectric data from the isothermal polymerizations of DGEBA with AN, HA, EDA, and HDA under the various conditions of pressure as indicated.

Mixture (T_r /K)	P /bar	$\varepsilon'(t \rightarrow 0)$	$\varepsilon'(t \rightarrow \infty)$	γ
DGEBA-AN (351.5 K)	1	6.04	4.08	0.34
	200	6.08	4.10	0.35
	200 at 6.6 ks	6.12	4.13	0.35
DGEBA-HA (304.0 K)	1	6.58	3.85	0.35
	200	6.76	3.92	0.35
	200 at 8.0 ks	6.71	3.89	0.36
DGEBA-EDA (307.2 K)	1	8.54	4.61	0.29
	200	8.83	4.66	0.29
	200 at 2.6 ks	9.05	4.65	0.27
DGEBA-HDA (303.4 K)	1	8.10	4.52	0.31
	200	8.32	4.67	0.33
	200 at 3.6 ks	8.37	4.69	0.32

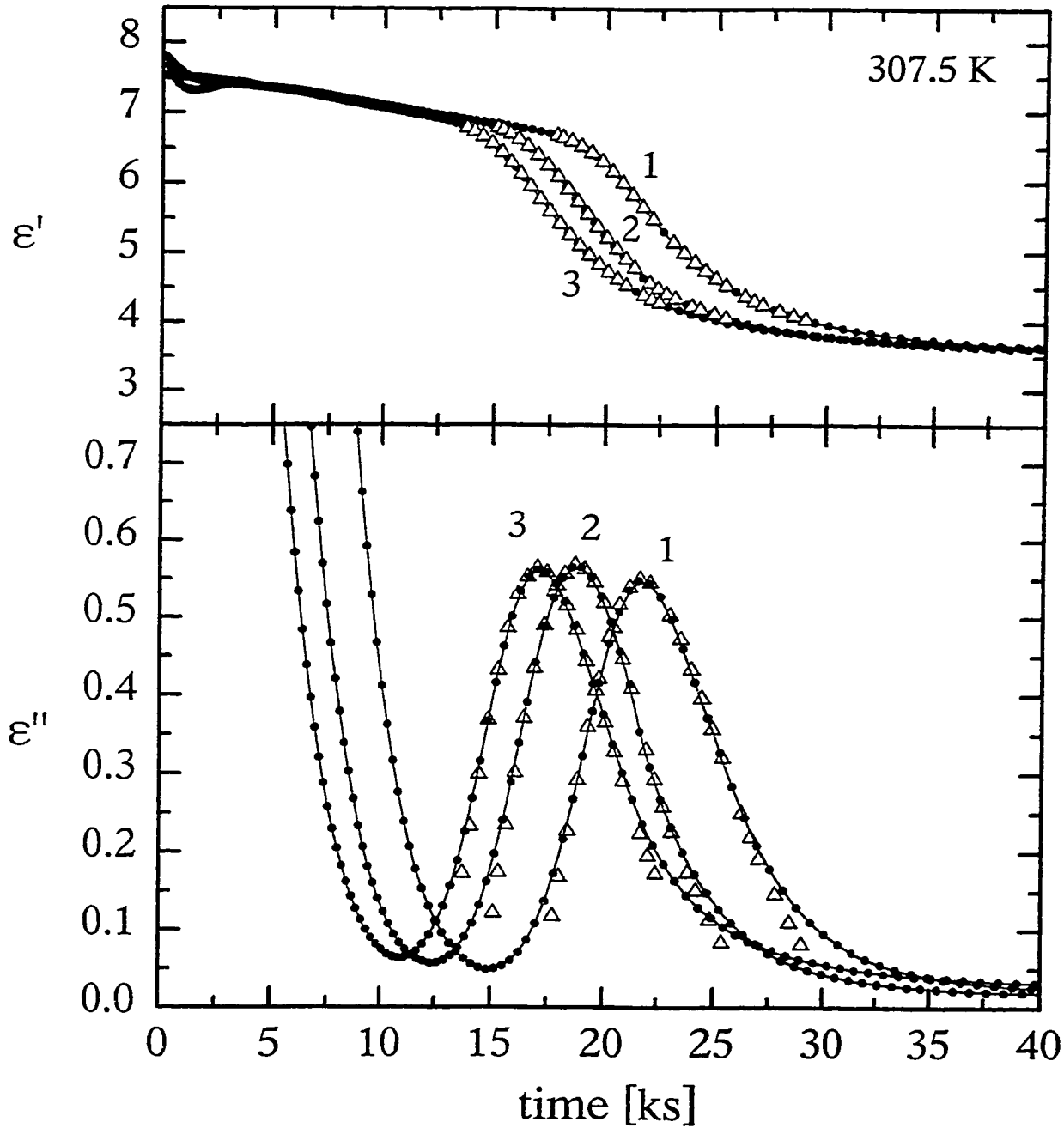

Figure 6.1: The calculated values (△) and measured values (●) of ε′ and ε″ are plotted against the reaction time for DGEBA-CHA at 307.5 K at a fixed measurement frequency of 1 kHz. Curves 1, 2, and 3 refer to measurements taken at 1, 103, and 206 bar, respectively. The parameters used for the calculated curves are reported in Table 6.1.

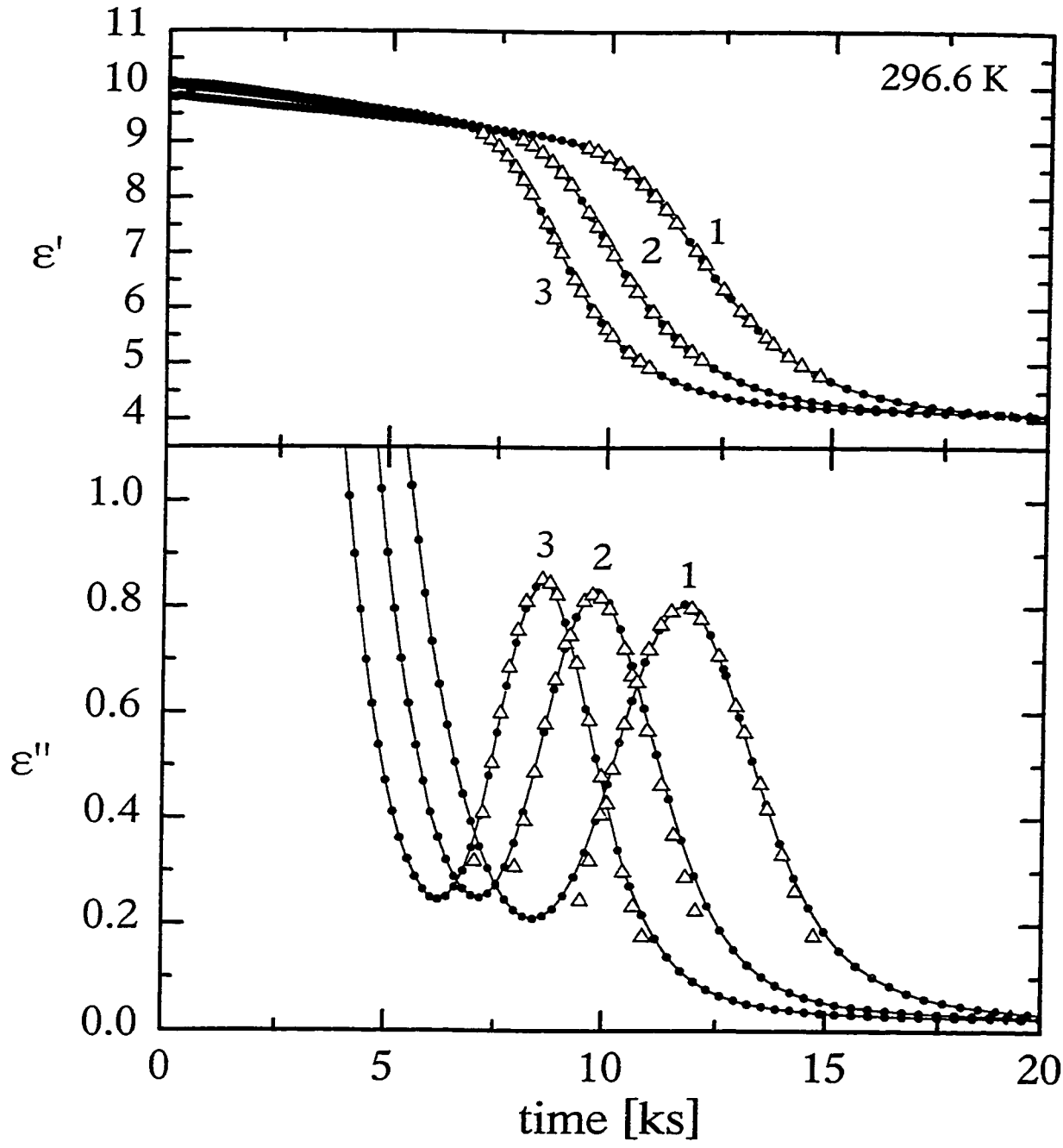

Figure 6.2: The calculated values (△) and measured values (●) of ε′ and ε″ are plotted against the reaction time for DGEBA-EDA at 296.6 K at a fixed measurement frequency of 1 kHz. Curves 1, 2, and 3 refer to measurements taken at 1, 103, and 206 bar, respectively. The parameters used for the calculated curves are reported in Table 6.1.

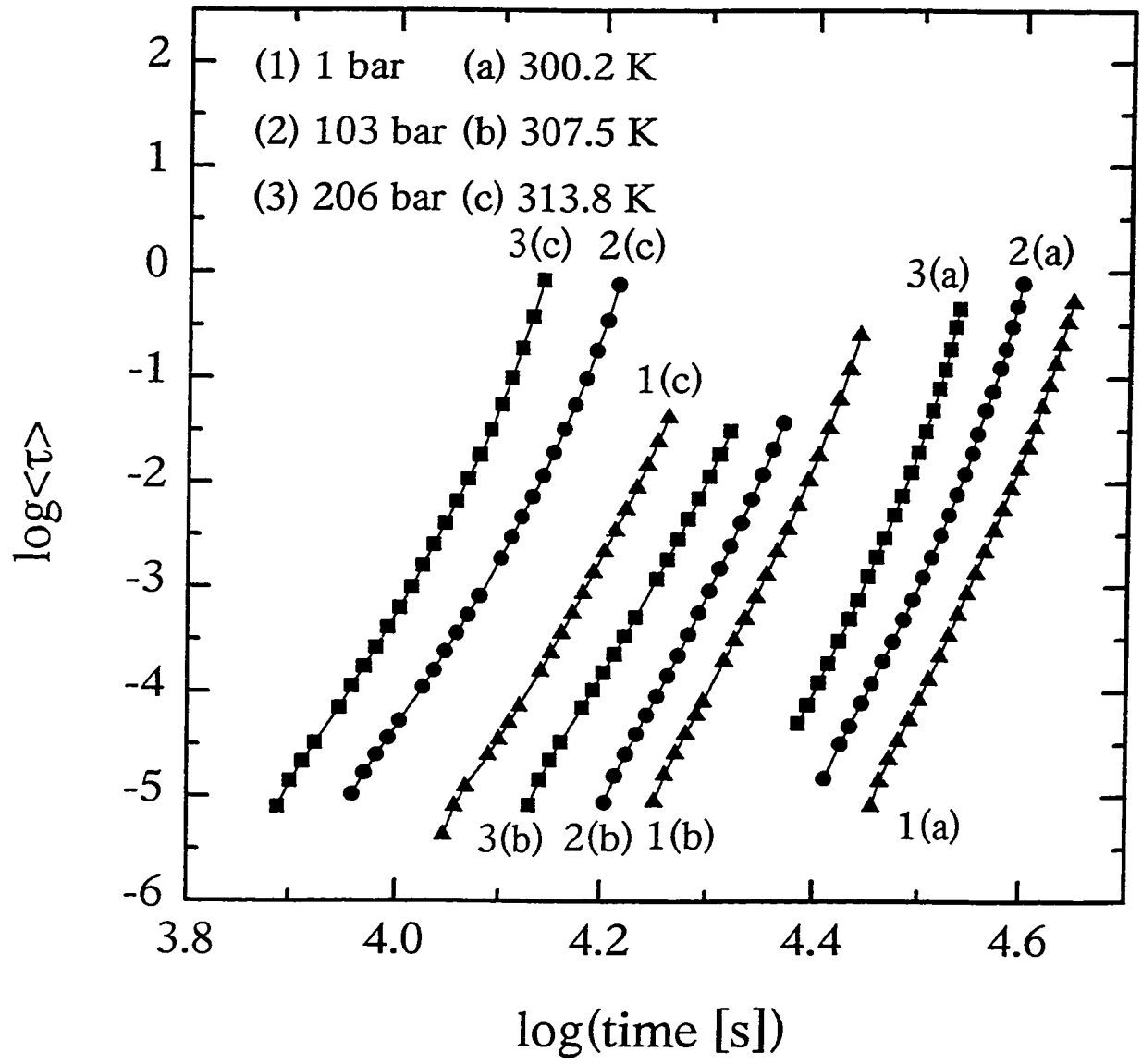

Figure 6.3: The average relaxation time, $\langle\tau\rangle$, is plotted against the reaction time for the polymerization of DGEBA-CHA at the pressures and temperatures indicated. Notations (1), (2), and (3) refer to pressures of 1, 103, and 206 bar, respectively, and (a), (b), (c) refer to temperatures of 300.2, 307.5, 313.8 K, respectively.

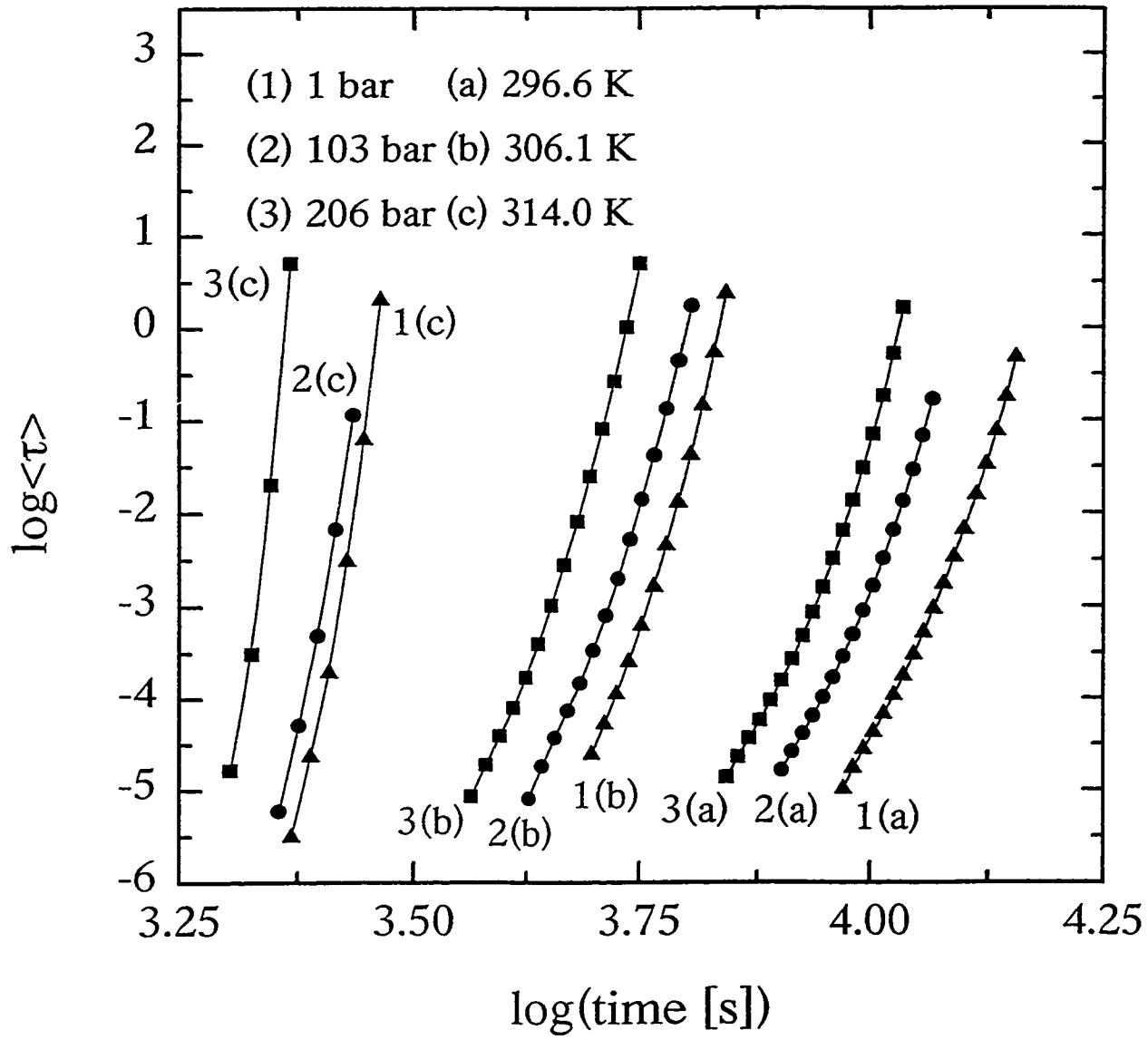

Figure 6.4: The average relaxation time, $<\tau>$, is plotted against the reaction time for the polymerization of DGEBA-EDA at the pressures and temperatures indicated. Notations (1), (2), and (3) refer to pressures of 1, 103, and 206 bar, respectively, and (a), (b), (c) refer to temperatures of 296.6, 306.1, 314.0 K, respectively.

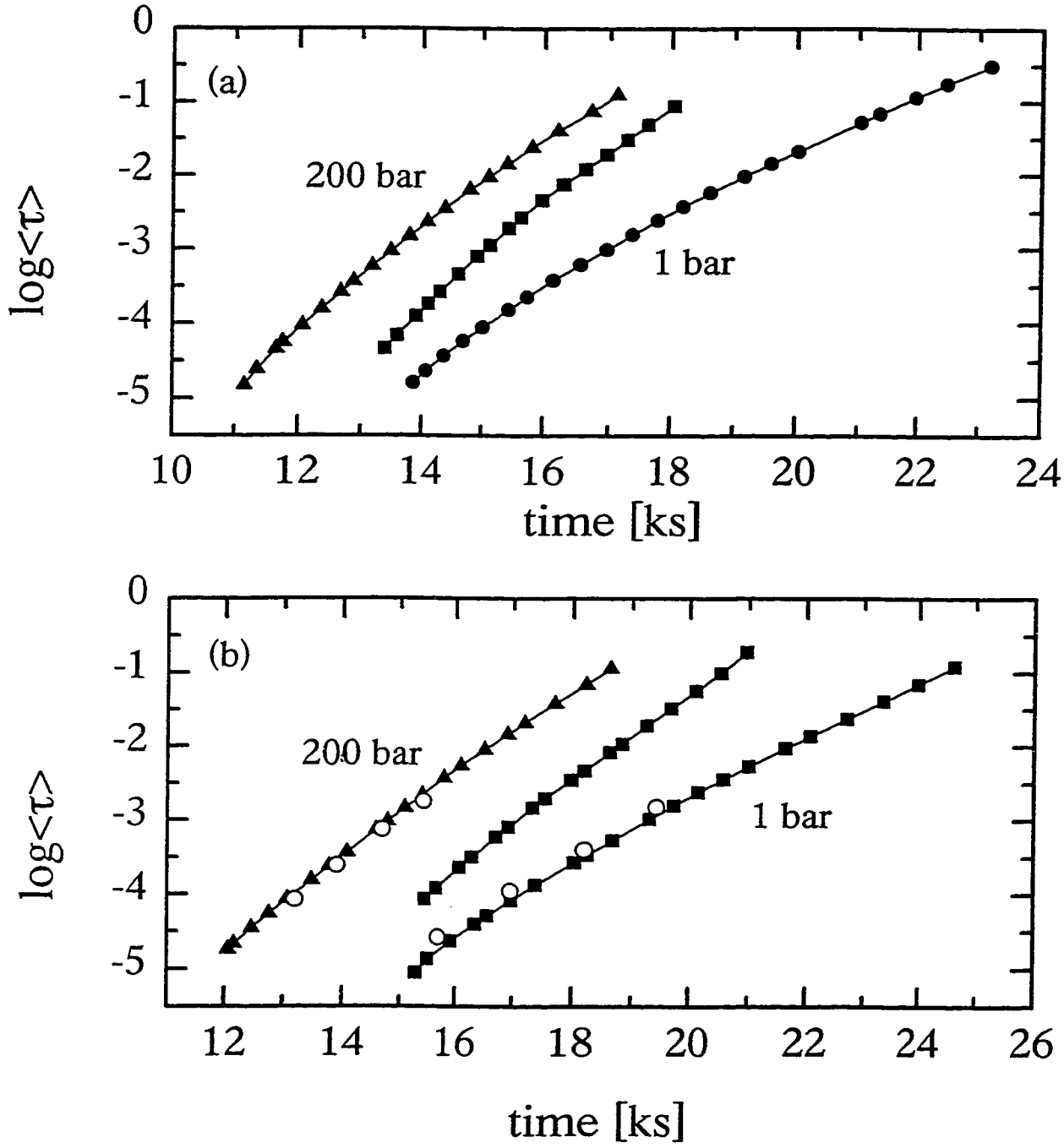

Figure 6.5: The average dielectric relaxation time, $\langle\tau\rangle$, is plotted logarithmically against the polymerization time, t, for; **(a)** the DGEBA-AN mixture at 351.5 K. The dots are for 1 bar, triangles for 200 bar, and squares after raising the pressure to 200 bar at 6.6 ks; **(b)** the DGEBA-HA mixture at 304.0 K. The dots are for 1 bar, triangles for 200 bar, and squares after raising the pressure to 200 bar at 8.0 ks. The open circles are calculated from the dielectric spectra as described in Section 2.6.

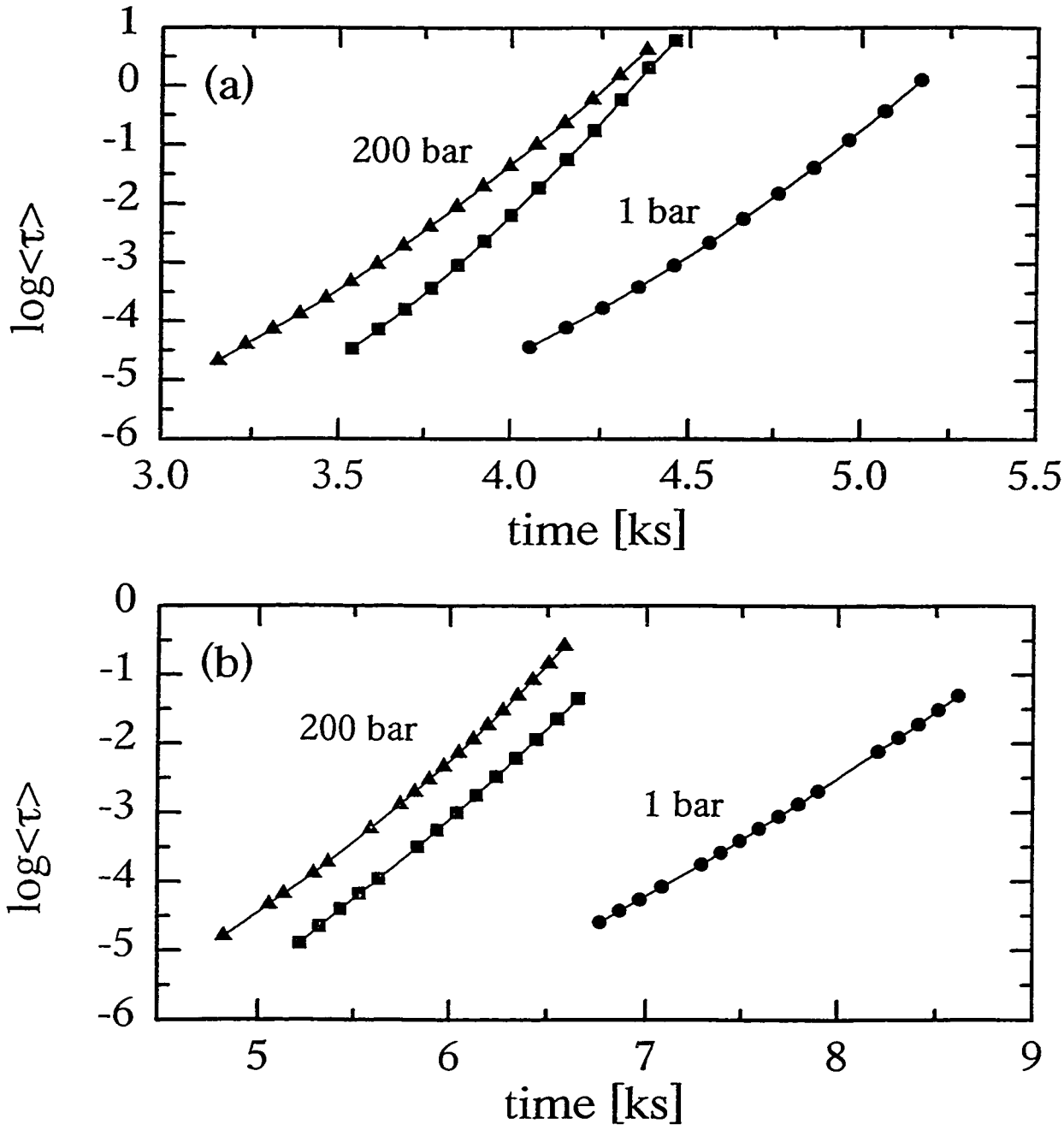

Figure 6.6: The average dielectric relaxation time, $\langle\tau\rangle$, is plotted logarithmically against the polymerization time, *t*, for; **(a)** the DGEBA-EDA mixture at 307.2 K. The dots are for 1 bar, triangles for 200 bar, and squares after raising the pressure to 200 bar at 2.6 ks; **(b)** the DGEBA-HDA mixture at 303.4 K. The dots are for 1 bar, triangles for 200 bar, and squares after raising the pressure to 200 bar at 3.6 ks.

did not affect the approximations made in the analysis of the fixed-frequency data, the ε' and ε'' spectra were obtained at fixed intervals during the polymerization of DGEBA-HA by the procedure described in Section 2.6, and are shown in Figure 4.24 for 1 bar and in Figure 4.25 for 200 bar pressure. Values of $\log\langle\tau\rangle$ determined from the spectra are included in Figure 6.5(b) for the polymerization of DGEBA-HA at 304.0 K and at 1 and 200 bar. The agreement between the two sets of τ values confirms, as before [Parthun and Johari (1995c), Mangion and Johari (1991b), Wasylyshyn and Johari (1997b)] that the chemical entities formed during polymerization at different temperatures and pressures, and their concentrations, which are expected to differ considerably, have the same macroscopic relaxation time within experimental errors. The distribution parameter, β, from Equation (2.21), for the spectra is 0.35±0.01 at 1 and 200 bar, as calculated from Figures 4.24 and 4.25.

6.1.1 The Effects of Pressure on Molecular Dynamics

The peaks in the plots of ε'' against t in Figures 4.12 to 4.21 and 6.1 and 6.2 occur during polymerization when a structure is produced within the liquid that has an average relaxation time equal to is the inverse of the angular frequency used for the dielectric measurement (6.28 krads/s, here). As these peaks shift towards a shorter polymerization time on increasing the pressure, the structure whose relaxation time is 159 μs (1/6.28 krads/s) is formed sooner at higher pressures than at lower, or that pressure has raised the polymerization rate. This effect is qualitatively similar to that of an increase in the

polymerization temperature, which also raises the polymerization rate and shifts the features of the ε' and ε'' plots to shorter times [Mangion and Johari (1990) and (1991b), Parthun and Johari (1992a) and (1992b), Johari (1994a), Johari and Pascheto (1995)]. Figures 6.3 and 6.4 quantitatively show this apparent equivalence between the temperature and pressure effects on the molecular dynamics in the plots of $\log\langle\tau\rangle$ against $\log(t)$, where the curves shift bodily towards shorter times when the temperature is increased at constant pressure, or when the pressure is increased at constant temperature. This response of the rate of polymerization to the temperature and pressure is expected, since at a higher temperature the viscosity of the mixture is low, the reaction is mass-controlled and the molecular diffusion time is short. The polymerization rate would be accelerated also by increasing the temperature once the reaction has become diffusion-controlled, as increasing the temperature reduces the viscosity. Consequently, an entity of certain $\langle\tau\rangle$ in the liquid's polymeric structure will be formed after a shorter time of reaction, even as an increase in the temperature reduces the relaxation time in general for all entities formed on polymerization.

The effect of pressure on the reaction kinetics is not obvious, and appears counterintuitive. It requires two considerations, namely, (i) the viscosity of the liquid increases on increasing the pressure, and (ii) a higher probability of reaction among the species present when the density increases. An increase in viscosity alone would increase the diffusion time of the reacting species according to the Stokes-Einstein equation, thereby slowing the reaction kinetics and consequently the rate of increase in $\langle\tau\rangle$ with t. An increase in the density brings the reactive sites in closer proximity and thus increases the

probability of reaction, or accelerates the reaction. The thermodynamic driving force increases because the volume change on polymerization is negative as the low density reactants convert into a high density product, *i.e.*, pressure should favour polymerization according to Le Chatelier's principle, and thus the extent of reaction at equilibrium is more at high pressures than at low pressures. The relative contributions of the thermodynamic and the diffusional processes of polymerization under pressure may be examined in terms of formalisms incorporating both the kinetic and the thermodynamic effects.

The irreversible increase in $\langle\tau\rangle$ with the polymerization time at different T, P and t may be written as,

$$d\ln\langle\tau\rangle = \left(\frac{\partial \ln\langle\tau\rangle}{\partial T}\right)_{P,t} dT + \left(\frac{\partial \ln\langle\tau\rangle}{\partial P}\right)_{T,t} dP + \left(\frac{\partial \ln\langle\tau\rangle}{\partial t}\right)_{T,P} dt \qquad \textbf{(6.1)}$$

where the first coefficient refers to the change in $\langle\tau\rangle$ with change in temperature, T, the second to that with change in pressure, P, and the third term to that with change in polymerization time, t. Equation (6.1) describes how $\langle\tau\rangle$ will change when, for example, both T and P fluctuate during polymerization. The first coefficient is usually found to be negative for $t \rightarrow 0$ and $t \rightarrow \infty$, *i.e.*, when the liquid's state is time-invariant [Johari (1994a)]. Studies from dielectric [Parthun and Johari (1992a)] and ultrasonic [Parthun and Johari (1995a)] measurements have shown that this coefficient is positive during the course of polymerization, *i.e.*, when $0 < t < \infty$, which is also seen in Figures 6.3 and 6.4. These data also show that $(\partial \ln\langle\tau\rangle/\partial P)_{T,t}$ which will be discussed in terms of the polymerization kinetics, is also positive. The coefficient, $(\partial \ln\langle\tau\rangle/\partial t)_{T,P}$, in Equation (6.1) remains positive

as long as the polymerization occurs, and becomes zero when the polymerization has stopped. The positive value for each term in Equation (6.1) means that a certain state of the liquid during the course of its polymerization, as characterized by its $\langle\tau\rangle$, can be attained by using any number of combinations of T, P and t.

In earlier studies [Mangion and Johari (1990) and (1991b), Tombari and Johari (1992), Johari (1994a)], it was shown that the average relaxation time increases with an increase in the number of covalent bonds according to the equation,

$$\ln\langle\tau\rangle = \ln\langle\tau\rangle_o + S\alpha^p \qquad (6.2)$$

where α is the extent of polymerization, $\langle\tau\rangle_o$ is the average relaxation time of the unpolymerized mixture, *i.e.* $\langle\tau\ (t = 0)\rangle$ or $\langle\tau\ (\alpha = 0)\rangle$, p is an empirical parameter that is characteristic of polymerization and S is numerically equal to the normalized value of $\langle\tau\rangle$ at the polymerization temperature, *i.e.*, $S = \ln(\langle\tau\rangle_\infty/\langle\tau\rangle_o)$. Here, $\langle\tau\rangle_\infty$ is the value of $\langle\tau\rangle$ when polymerization has reached completion, *i.e.* $\langle\tau\ (\tau = \infty)\rangle$ or $\langle\tau\ (\alpha = 1)\rangle$. The value of p varies with both temperature and pressure [Mangion and Johari (1990) and (1991b), Tombari and Johari (1992), Johari (1994a)], and α can be expressed also as the number of covalent bonds formed [Wasylyshyn and Johari (1997b)]. The value of S increases as temperature decreases and/or pressure increases because $\langle\tau\rangle_\infty$ increases more rapidly than $\langle\tau\rangle_o$, since, for the same temperature and pressure, the fully reacted polymer is nearer to its vitreous state than the unpolymerized liquid is to its vitreous state. So, for a low polymerization temperature, the increase in $\langle\tau\rangle_o$ on increase in pressure is much less than

the increase in $\langle\tau\rangle_\infty$ and the magnitude of S is relatively high. By differentiating Equation (6.2) with respect to t,

$$\left(\frac{\partial \ln\langle\tau\rangle}{\partial t}\right)_{P,T} = \alpha^p\left(\frac{\partial S}{\partial t}\right)_{P,T} + Sp\alpha^{p-1}\left(\frac{\partial \alpha}{\partial t}\right)_{P,T} \qquad \textbf{(6.3)}$$

Since S is independent of t, the first term on the right-hand-side of Equation (6.3) is zero, and,

$$\left(\frac{\partial \ln\langle\tau\rangle}{\partial t}\right)_{P,T} \propto \left(\frac{\partial \alpha}{\partial t}\right)_{P,T} \alpha^{p-1} \qquad \textbf{(6.4)}$$

with S and p as constants of proportionality. By substituting Equation (6.4) into Equation (6.1), we obtain,

$$d\ln\langle\tau\rangle = \left(\frac{\partial \ln\langle\tau\rangle}{\partial T}\right)_{P,t} dT + \left(\frac{\partial \ln\langle\tau\rangle}{\partial P}\right)_{T,t} dP + Sp\alpha^{p-1}\left(\frac{\partial \alpha}{\partial t}\right)_{T,P} dt \qquad \textbf{(6.5)}$$

Each of the first two terms on the right-hand-side of Equation (6.5) contains the combined effect of the increase in $\ln\langle\tau\rangle$ with increase in α and the change in α with change in temperature and pressure. Thus, $\partial\ln\langle\tau\rangle$ itself contains contributions from two processes:

(i) irreversible chemical reactions that increase the number of covalent bonds spontaneously and thereby raise $\langle\tau\rangle$, and

(ii) reversible physical processes of compression or decompression, and heating, or cooling, that raise $\langle\tau\rangle$ on compression or cooling and lower $\langle\tau\rangle$ on decompression or heating for a structure containing a fixed number of covalent bonds.

Equation (6.1) may thus be written as:

$$d\ln\langle\tau\rangle = \left[\left(\frac{\partial \ln\langle\tau\rangle}{\partial\alpha}\right)_{T,P}\left(\frac{\partial\alpha}{\partial T}\right)_{P,t} dT + \left(\frac{\partial \ln\langle\tau\rangle}{\partial\alpha}\right)_{T,P}\left(\frac{\partial\alpha}{\partial P}\right)_{T,t} dP + S\alpha^{p-1}\left(\frac{\partial\alpha}{\partial t}\right)_{T,P}\right] + \left[\left(\frac{\partial \ln\langle\tau\rangle}{\partial T}\right)_{\alpha,P} dT + \left(\frac{\partial \ln\langle\tau\rangle}{\partial P}\right)_{\alpha,T} dP\right] \tag{6.6}$$

where the three terms in the first square brackets on the right-hand-side refer to the effects of irreversible chemical changes and the two terms in the second square brackets refer to the effects of reversible physical changes. (Note that the fixed t for the pressure and temperature coefficients of α means that they are obtained from the fixed t cuts of the plots of α against t for different P or T conditions.) A simpler way to express Equation (6.6) in order to differentiate the chemical and physical contributions is to eliminate t as the parameter and use α or $N(t)$ as an indication of the progress of polymerization. As was done in the analyses of Chapter 4 and in recent work [Tombari and Johari (1992), Cassettari *et al.* (1994), Parthun and Johari (1995c), Parthun *et al.* (1996), Wasylyshyn and Johari (1997b)], α may instead be used to represent the state of the system, and Equation (6.6) can be expressed more simply as,

$$d\ln\langle\tau\rangle = \left(\frac{\partial \ln\langle\tau\rangle}{\partial T}\right)_{P,\alpha} dT + \left(\frac{\partial \ln\langle\tau\rangle}{\partial P}\right)_{T,\alpha} dP + \left(\frac{\partial \ln\langle\tau\rangle}{\partial\alpha}\right)_{P,T} d\alpha \tag{6.7}$$

By combining with Equation (6.2), Equation (6.7) can by re-expressed in the form,

$$d\ln\langle\tau\rangle = \left(\frac{\partial \ln\langle\tau\rangle}{\partial T}\right)_{P,\alpha} dT + \left(\frac{\partial \ln\langle\tau\rangle}{\partial P}\right)_{T,\alpha} dP + Sp\alpha^{p-1} d\alpha \tag{6.8}$$

where the first and second terms on the right-hand-side of Equation (6.8) represent the purely physical effects of temperature and pressure on $\langle\tau\rangle$ and the third term the chemical effect at constant T and P.

Although it is appropriate to express the state of the system in terms of a material's intrinsic variable, α, as in the other work presented here, the lack of facilities for calorimetry at high pressures prevented conversion of t to α. This is also true for Equation (6.6), where the term, $(\partial\alpha/\partial t)$, appears. To circumvent the issue of α, Equations (6.6) and (6.8) may be re-written in a more general form in terms of the chemical and physical contributions,

$$d\ln\langle\tau\rangle = \left[d\ln\langle\tau\rangle\right]_{chem} + \left[d\ln\langle\tau\rangle\right]_{phys} \qquad \textbf{(6.9)}$$

where the subscript *chem* refers to the chemical, and hence irreversible, process when the polymerization continuously progresses towards the equilibrium, and the subscript *phys* refers to the physical process when no structural change occurs as a result of chemical reaction.

All coefficients in the first square brackets of Equation (6.6) are positive, *i.e.*, $\langle\tau\rangle$ increases as α increases, and α itself increases when T is increased at a constant P or when P is increased at a constant T. α also increases as t increases until the polymerization has reached completion, and thereafter α becomes constant with t. Once the polymerization has reached its limiting α value for a given T and P, these three terms become zero ($[d\ln\langle\tau\rangle]_{chem} = 0$) and the last two terms in the square brackets in Equation (6.6) become important. Under the latter conditions, the two terms in the second set of brackets in Equation (6.6),

namely $(d\ln\langle\tau\rangle/dT)_{\alpha,P}$ and $(d\ln\langle\tau\rangle/dP)_{\alpha,T}$, are negative and positive, respectively. It may be noted that $(d\ln\langle\tau\rangle/dT)_{\alpha,P}$ is positive for constant α when $0 < \alpha < 1$, as seen in Figures 6.3 and 6.4.

As stated above, the data available here are insufficient for resolving the various contributions to $\langle\tau\rangle$ from chemical and physical effects in Equations (6.6) or (6.8). It is hoped that these equations will be useful when more extensive data become available, as discussed before [Wasylyshyn and Johari (1997a)].

A Comparison of the Dynamics During Linear Chain and Network Polymerization

One of the temperatures for the linear chain polymerization of DGEBA-CHA, 313.8 K, is sufficiently similar to the temperature, 314.0 K, for the network polymerization of DGEBA-EDA to allow comparisons between the two types, although the size, nature and shape of the amine molecule used in the two cases differ. For a comparison of their molecular dynamics, $\log\langle\tau\rangle$ is plotted against $\log t$ for DGEBA-EDA at 314.0 K and 1, 103 and 206 bar, and DGEBA-CHA at 313.8 K at those same pressures in Figure 6.7. This figure and Figures 4.14 and 4.17 show that the relaxation features during polymerization of the DGEBA-EDA mixture appears at shorter times than those of the polymerization of the DGEBA-CHA mixture, or that to produce entities in the structure whose relaxation time is 1 ms at 313.9 ± 0.1 K and 206 bar, the polymerization time is 10.2 ks for the DGEBA-CHA mixture and 2.1 ks for the DGEBA-EDA mixture. The nearly five times more rapid increase in $\langle\tau\rangle$ for the DGEBA-EDA mixture is partly attributable to its faster polymerization kinetics and partly to the more rapid increase in the steric hindrance to

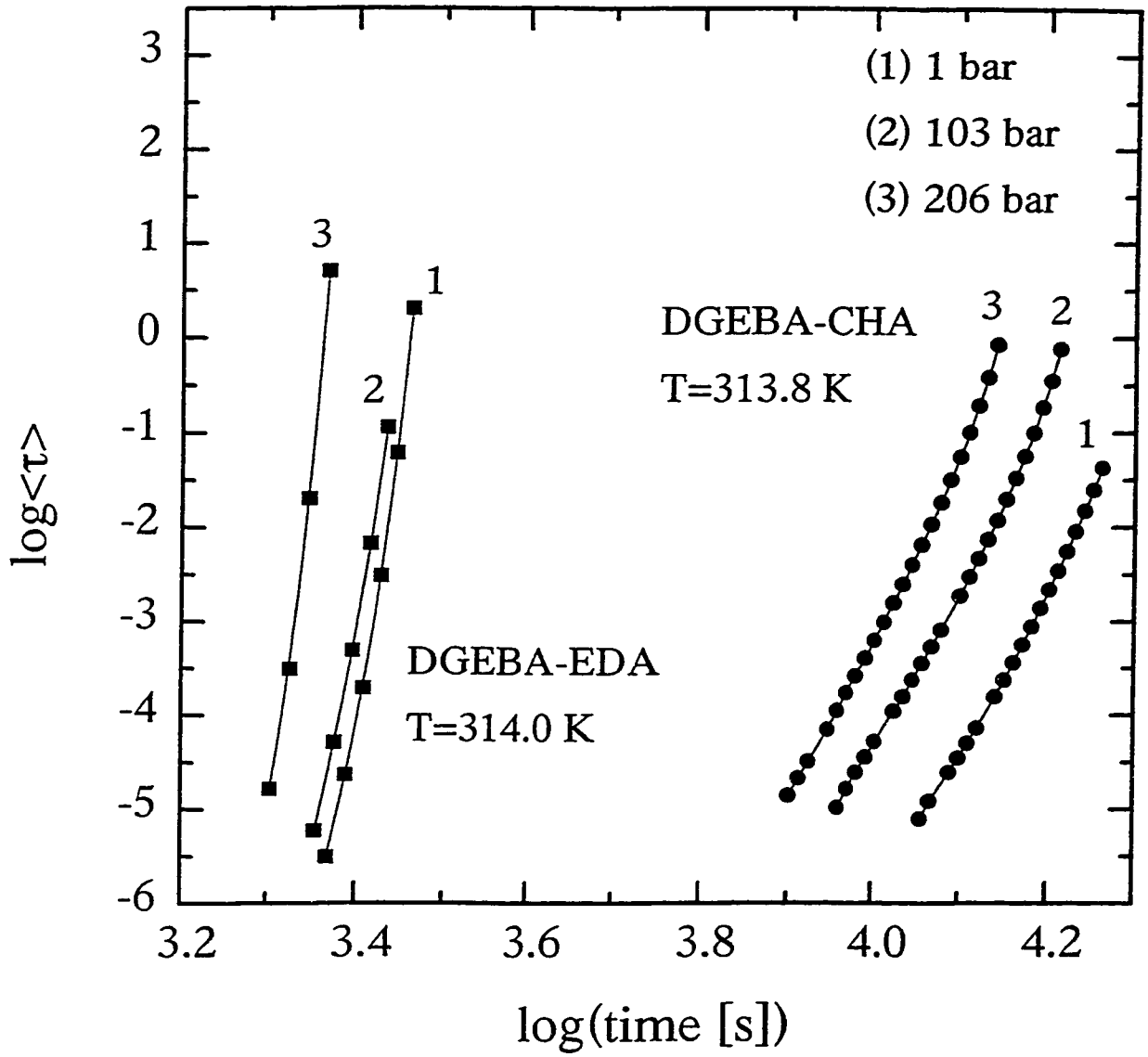

Figure 6.7: For comparison, the average relaxation time, $\langle\tau\rangle$, is plotted against the reaction time for the polymerization of DGEBA-CHA and DGEBA-EDA at pressures of 1, 103, and 206 bar, and an average temperature of 313.9 K.

dipolar reorientation in the network structure formed on polymerization in comparison with the linear-chain structure formed for the DGEBA-CHA mixture. In terms of viscosity, the longer relaxation time after a shorter polymerization period is interpreted as a more rapid rise in viscosity, resulting from the formation of a network polymer, than that resulting from the formation of a linear-chain polymer, even if the number of covalent bonds formed at their respective times in the two cases were the same.

6.1.2 The Equivalence Between the Temperature and Pressure

As mentioned in the previous section, the effects of pressure on the rate of change of $\langle\tau\rangle$ with the polymerization time is qualitatively similar to that of temperature, which implies an equivalence between the temperature and the pressure when reaching a certain state of polymerization, as defined by its $\langle\tau\rangle$. The equivalence may be represented by a perfect differential for an imposed constant value of $\langle\tau\rangle$;

$$\left(\frac{\partial P}{\partial T}\right)_{t,\langle\tau\rangle} = -\left(\frac{\partial P}{\partial t}\right)_{T,\langle\tau\rangle}\left(\frac{\partial t}{\partial T}\right)_{P,\langle\tau\rangle} \qquad \textbf{(6.10)}$$

The magnitude of these terms varies with $\langle\tau\rangle$, T, P and t, as is evident from the data plotted in Figures 6.3 and 6.4, which lie on curved lines with slopes changing with t, T and P. This means that the magnitude of each of the three coefficients in Equation (6.10) depends upon $\langle\tau\rangle$. Since the two coefficients on the right-hand-side of Equation (6.10) are positive, $(\partial P/\partial T)_{t,\langle\tau\rangle}$ should be negative. These coefficients were determined by cross plots of the data in Figure 6.3, and are listed in Table 6.3.

Table 6.3: The values of $(\partial P/\partial T)_{t,<\tau>}$ in bar/K for the polymerization of DGEBA-CHA and DGEBA-EDA obtained from the cross-plots of Figures 6.3 and 6.4 at the constant values of $<\tau>$ and T_r shown.

Mixture	T_r	$<\tau>$				
		31.6 μs	100 μs	1 ms	31.6 ms	100 ms
DGEBA-CHA	300.2 K	-49	-49	-	-49	-
	307.5 K	-53	-54	-	-58	-
	313.8 K	-55	-55	-	-54	-
DGEBA-EDA	296.6 K	-	-18	-50	-	-18
	306.1 K	-	-85	-76	-	-49
	314.0 K	-	-184	-159	-	-15

To demonstrate the T and P equivalence for the DGEBA-CHA mixture, Figure 6.8 shows the construction of isobaric surfaces in polymerization temperature, relaxation time and polymerization time space. The corresponding plot for the polymerization of the DGEBA-EDA mixture is shown in Figure 6.9. In these figures a certain value of $<\tau>$ may be reached by a variety of different paths involving temperature, pressure and the polymerization time. Thus, in terms of processing, the pressure, temperature and polymerization time become parameters that can be used to attain a desired value of $<\tau>$. Since the mixture's viscosity, η, can be related to $<\tau>$ through $\eta = <\tau>G_\infty$, the physical state of the polymerizing mixture can be obtained through one's choice of P, T or t. As stated earlier, α or $N(t)$, are more appropriate measures of the system's structure and would allow one to compare all types of polymerizing mixtures since α and $N(t)$ are intrinsic material variables describing an element of the structure formed. Other material variables such as the molecular weight or number weight distributions could also be used.

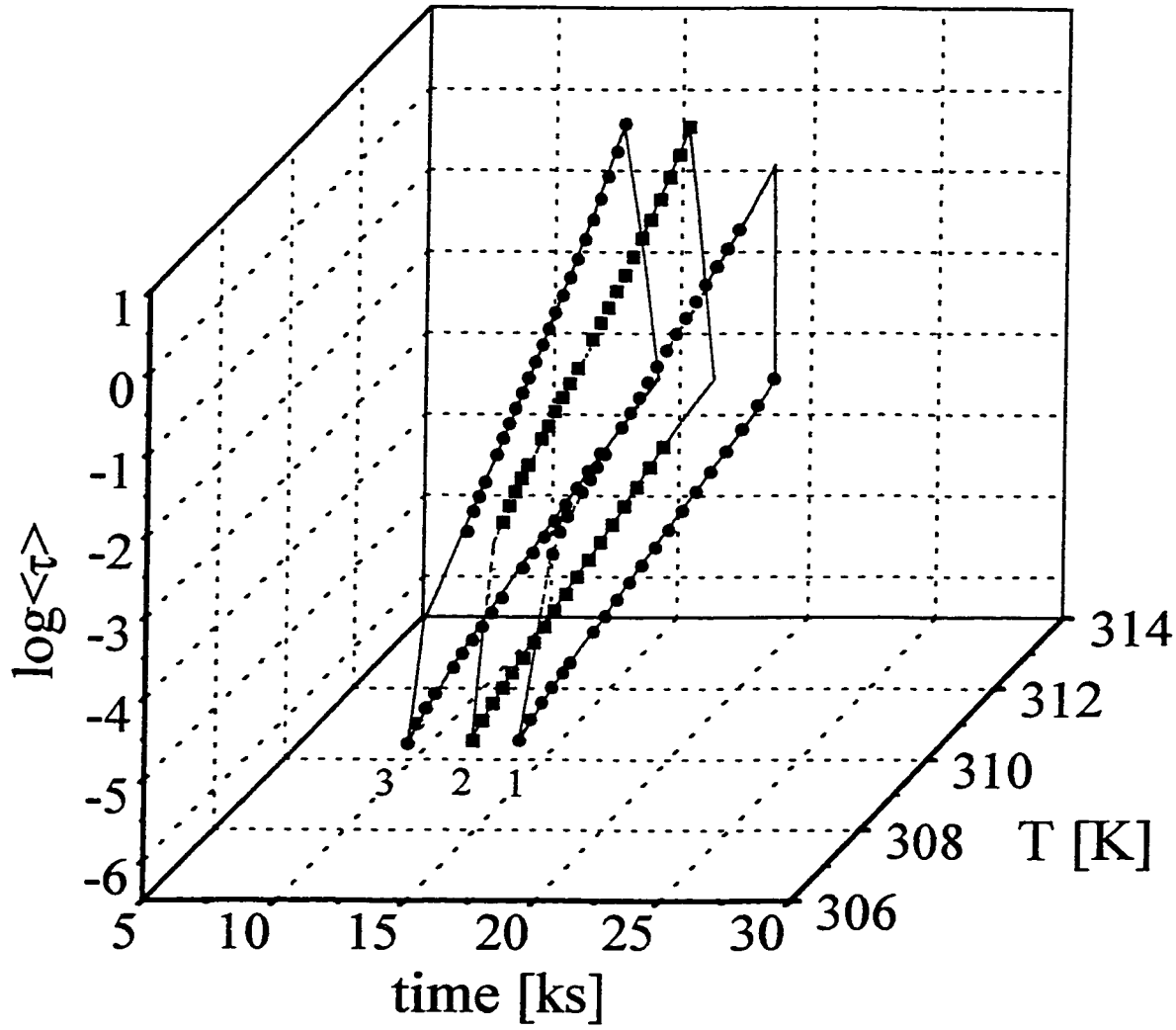

Figure 6.8: The <τ>, temperature, and polymerization time surfaces for the polymerization of DGEBA-CHA at pressures of 1, 103, and 206 bar. Note that the data for 300.2 K has been omitted for clarity.

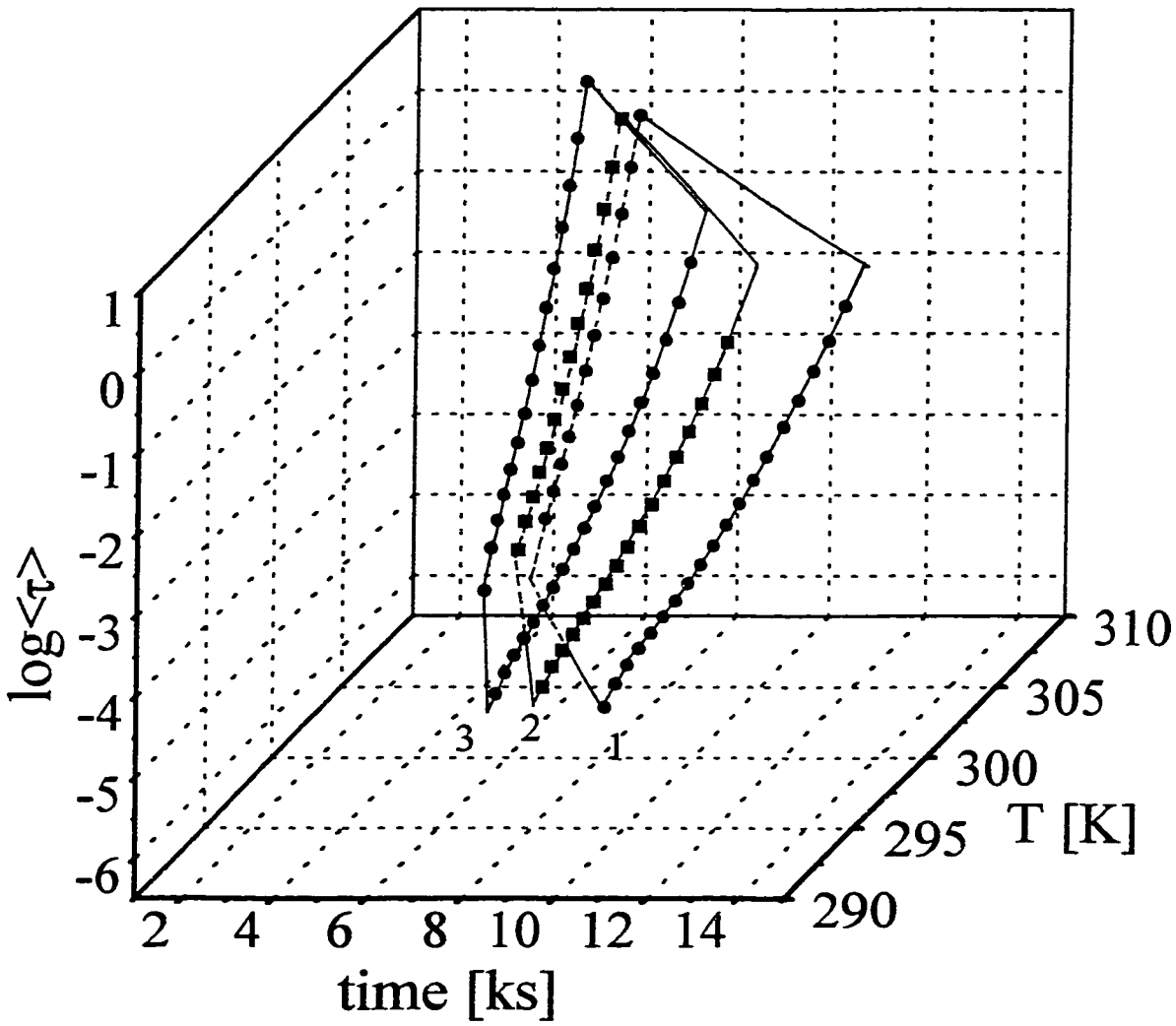

Figure 6.9: The <τ>, temperature, and polymerization time surfaces for the polymerization of DGEBA-EDA at pressures of 1, 103, and 206 bar. Note that the data for 314.0 K has been omitted for clarity.

It should be noted that the values of $(\partial P/\partial T)_{t,<\tau>}$ listed in Table 6.3 contain contributions from both a chemical effect through a change in the reaction rate and a physical effect. The latter comes from the coefficients, $(\partial \ln<\tau>/\partial P)_T$ and $(\partial \ln<\tau>/\partial T)_P$ for a time-invariant or structurally stable state of a fixed number of covalent bonds, at time t, according to,

$$\left(\frac{\partial P}{\partial T}\right)_{<\tau>} = - \left(\frac{\partial P}{\partial \ln\langle\tau\rangle}\right)_T \left(\frac{\partial \ln\langle\tau\rangle}{\partial T}\right)_P \qquad (6.11)$$

for which $(\partial P/\partial T)_{<\tau>}$ is known to be positive [Johari and Dannhauser (1969a), Johari and Whalley (1972)]. This means that the values of $(\partial P/\partial T)_{<\tau>}$, obtained from the cross-plots of the data in Figures 6.3 and 6.4 give an underestimate of the true effect of pressure on the time required for the polymerized structure to reach a given value of $<\tau>$. Further experiments over a greater pressure range as well as high-pressure calorimetry may better resolve the relative contributions of the physical and chemical effects.

6.1.3 The Effects of Pressure on Configurational Entropy

The change in $<\tau>$ with the polymerization time can be examined in terms of configurational entropy theory [Adam and Gibbs (1965)], discussed in Section 6.2.3. For the purposes of discussion, Equation (5.7) is re-expressed here as,

$$\ln\langle\tau\rangle = \ln\langle\tau\rangle^{(\infty)} + c/T S_{conf} \qquad (6.12)$$

with the definitions of the terms being the same as with Equation (5.7), namely, $c = \Delta\mu s_c^*/k_B$ and $\Delta\mu$ is the potential energy hindering the cooperative rearrangement per monomer

segment of the molecule and s_c^* is the critical entropy of the smallest volume of relaxing molecules. Here, $\langle\tau\rangle^{(\infty)}$ represents the average relaxation time at $T \to \infty$, *i.e.* $\langle\tau(T \to \infty)\rangle$. It is useful to consider the change in $\langle\tau\rangle$ with respect to both T and P. However, as written, Equation (6.12) describes the change in $\langle\tau\rangle$ with respect to T alone. In deriving this equation, it was assumed that, to a good approximation, the dependence of $\Delta\mu$ on T and z can be neglected [Adam and Gibbs (1965)]. Here z is the number of molecules in a cooperatively rearranging region, although studies of the viscosity of several liquids over a wide temperature range [Laughlin and Uhlman (1972)] has demonstrated that z calculated from Equation (6.12) is unrealistically small, even less than the size of a single molecule. Following Adam and Gibbs [(1965)], the dependence of $\Delta\mu$ on P may be neglected, and so the three isobaric surfaces corresponding to 1 bar, 103 bar and 206 bar in the plots of $\log\langle\tau\rangle$, t and T shown in Figures 6.8 and 6.9 correspond also to the surfaces of $(\log\langle\tau\rangle^{(\infty)} + c/TS_{conf})$ or equivalently the variable $(1/TS_{conf})$ for different polymerization times at different pressures because $\langle\tau\rangle^{(\infty)}$ corresponds to the vibrational time of the molecules in the structure. Therefore, like a particular value of $\langle\tau\rangle$, S_{conf} may also be reached by following different paths along any one of the three variables, polymerization time, temperature and pressure, as well as any of the multiplicity of different combinations of them.

Equation (6.12) may be differentiated with respect to the polymerization time at a constant temperature and pressure to obtain,

$$\left(\frac{\partial \ln\langle\tau\rangle}{\partial t}\right)_{P,T} = -\frac{c}{TS_{conf}^2}\left(\frac{\partial S_{conf}}{\partial t}\right)_{P,T} \qquad \textbf{(6.13)}$$

where c is taken as a constant. By combining Equations (6.2) and (6.13), the chemical process whose occurrence increases α becomes directly related to the physical process of the change in the configurational entropy by the relation,

$$\left(\frac{\partial \alpha}{\partial t}\right)_{P,T} = -\frac{c}{SpT\alpha^{p-1}S_{conf}^{2}}\left(\frac{\partial S_{conf}}{\partial t}\right)_{P,T} \tag{6.14}$$

Now, as α increases, or the macromolecule grows, S_{conf} decreases. But since α can reach at most the value of unity and S_{conf} decreases from a much larger magnitude of $k_B \ln\Omega$ (where Ω is the number of available configurations) to nearly zero, it follows that the term ($1/\alpha^{p-1} S^2_{conf}$) should increase rapidly as a macromolecule grows isothermally.

The consequence of Equation (6.14) is that $(\partial\alpha/\partial t)_{P,T}$, a property determined by calorimetry and reserved for describing rates of reactions, can be directly related to S_{conf}, a property obtained through dielectrics (in this case) to describe the physical state of the polymerizing mixture. This makes it is possible to examine the effects of pressure (and temperature) not only in terms of the rate constants obtained from reaction rate laws, but also in terms of an equilibrium and determinable thermodynamic property such as configurational entropy. Equation (6.2), used in the absence of a fundamental relation between $<\tau>$ and α for convenience, does not change the relationship between the polymerization kinetics and the configurational thermodynamics described above.

Equation (6.14) can be used to consider how changes in α and S_{conf} determine the shape of the α against t plot during the polymerization process. Generally, the shape of such plots is a stretched sigmoid in shape, as seen in Figure 4.3, *i.e.* $(\partial\alpha/\partial t)_{T,P}$ reaches a peak

value at a certain time corresponding to the point of inflection of the α against t curve. According to Equation (6.14), initially from $t = 0$, an increase in the $\alpha^{p-1}S^2_{conf}$ term dominates over the decrease in the $(\partial S_{conf}/\partial t)$ term as polymerization occurs, and after a certain polymerization time the decrease in the $(\partial S_{conf}/\partial t)$ becomes predominant, and $(\partial\alpha/\partial t)$ reaches a peak value. Thereafter, $(\partial\alpha/\partial t)$ decreases. Thus the rate of polymerization $(\partial\alpha/\partial t)$ can yield information on the rate at which S_{conf} decreases on polymerization once p is known.

The difference between the dielectric consequences of the developing structures of each of the polymerizing mixtures shown in Figures 6.3 to 6.6 can be examined also in terms of the configurational entropy theory. The plots of $<\tau>$ at a constant pressure and temperature of polymerization as seen in Figures 6.3 to 6.6 also represent the plots of c/S_{conf} for the two different polymerizations. The cross-plots of the data given in these figures can be used to obtain S_{conf} for a fixed polymerization time, where the value of S_{conf} obtained corresponds to different molecular structural states for the polymers.

It may also be noted that the slope of the plots increases in Figures 6.3 to 6.6, indicating that c/S_{conf} increases as t increases, or that S_{conf} decreases progressively more rapidly, implying that it may approach zero. But the magnitude of S_{conf} as determined from Equation (6.12) will not become zero as $t \rightarrow \infty$ because that occurrence implies that $d\ln<\tau>/dt$ will approach infinity at longer polymerization times (or, $\alpha \rightarrow 1$), which it does not when the temperature of polymerization is close to, or above, the glass transition temperature of the ultimately formed structure. This is consistent with the view that

configurational contributions to the entropy due to the orientational freedom of the polymer chains upon complete polymerization remains finite. This also indicates that the S_{conf} frozen-in at 0 K on cooling the reacted states to vitrification will decrease as the extent of reaction increases, therefore being the lowest for the fully reacted polymer.

6.1.4 The Effects of Pressure on the Static Permittivity

As a molecular liquid polymerizes, its density increases, dipoles associated with the NH_2 and epoxide groups vanish and those associated with -C-OH, and -C-N(R)- groups are produced, and the dipolar correlation between different molecules and molecular segments changes. Subsequently, its refractive index and infrared spectrum changes, which changes the magnitude of the limiting high frequency permittivity, ε_∞. The net effect as observed by drawing extensions to the lines as shown in the plots of ε' in Figures 4.12 to 4.21 is a decrease in ε_s of the mixture, although densification is expected to increase it, provided no other quantities in the Onsager-Kirkwood-Fröhlich equation [Onsager (1936), Kirkwood (1939), Fröhlich (1958)],

$$\varepsilon_s - \varepsilon_\infty = \left(\frac{\varepsilon_\infty + 2}{3}\right)^2 \left(\frac{3\varepsilon_s}{2\varepsilon_s + \varepsilon_\infty}\right) \left(\frac{4\pi N_d}{3k_B T}\right) g\,\mu_o^2 \qquad \textbf{(6.15)}$$

changed. In Equation (6.15), N_d is the number density of the dipoles, k_B the Boltzmann constant, g the dipolar orientational correlation factor, and μ_0 is the vapour phase dipole moment. This equation is used to describe the behaviour of polymers containing a variety of dipole moments, distribution of molecular weight and unreacted components and

plasticizers, and it is used here to approximately describe the complex systems used in this study. It should be noted that "...the application of the Fröhlich theory to a particular model for a liquid polymer gives a relation very similar to that obtained for associating small molecules in the liquid state" [McCrum, *et al.* (1967)].

The increase in the density on polymerization of a diepoxide with a diamine has been found to be ~10% [Choy and Plazek (1986)]. So, N_d increases by 10% and on this basis alone ε_s is expected to increase by about 10% according to Equation (6.15). But since ε_s is found to *decrease* in Figures 4.12 to 4.21, $g\mu_o^2$ must decrease on polymerization with increase in pressure at all temperatures studied, according to Equation (6.15). The relative merits of g and μ_o^2 can be examined by considering that when a covalent bond is formed on chemical reaction, one OH group is produced, one cyclic ether group is removed and the dipolar contributions from rotational diffusion of the amine molecule decreases when the molecule becomes bonded to the growing polymeric structure by the N atom and the NH_2 group is removed. The net effect is likely to be a combination of both a decrease in g and μ_o, *i.e.*, a lowering of the dipolar orientational correlation and the net dipole moment in the fully polymerized structure.

We now examine the effects of pressure on ε_s during the polymerization process. The data in Tables 6.1 and 6.2 show that ε_s of the molecular liquid mixture, which is nearly equal to $\varepsilon'(t \rightarrow 0)$ for $\omega = 2\pi$ krads/s, increases marginally on the application of pressure, in all cases except for the DGEBA-CHA mixture at 313.8 K and the DGEBA-EDA mixture at 314.0 K. This increase is 5±3% for 206 bar at 307.5 K for DGEBA-CHA and less than 1%

at 206 bar at 306.1 K for DGEBA-EDA. This is attributable to the increase in N_d and $g\mu_o^2$ on compression of the unreacted mixture, and is consistent with other studies that showed that the temperature dependent $(\partial\varepsilon_s/\partial P)$ for most liquids is 2%-10% per kbar [Johari and Dannhauser (1969a), Chen *et al.* (1969), Johari and Whalley (1972)]. This observation has been made more difficult by the shift of the ε' step-decrease in Figures 4.12 to 4.17 to shorter times on increasing the pressure. The plots in these figures do show that ε_s at a given pressure decreases on increasing the temperature and $(\partial\varepsilon_s/\partial t)_{P,T}$ increases as evident from a greater slope of the extension lines at higher temperatures. These are entirely a consequence of a decrease in viscosity and diffusion rate on increasing the temperature [Johari and Dannhauser (1969a), Chen *et al.* (1969)].

6.2 THE TRANSITION FROM MASS-CONTROLLED TO DIFFUSION-CONTROLLED KINETICS DURING POLYMERIZATION

6.2.1 General Effects of Pressure on Polymerization Kinetics

As described in the last section, an increase in pressure has two principal effects on the dielectric properties: (i) an increase in the number density of the dipoles, which raises the static permittivity, ε_s, and the average relaxation time, $\langle\tau\rangle$, and (ii) a change in the chemical reaction rate, which alters the rate at which a measured property changes irreversibly with time. The first is a physical effect that is reversible and observable for all chemically stable materials, the second is a chemical effect, irreversible and absent from chemically stable materials. When changes in the distribution of τ (the angular brackets are excluded for convenience) with increase in the extent of polymerization, α,

after the main or α-relaxation has sufficiently emerged are neglected [Wasylyshyn and Johari (1997b), Deng and Martin (1994a), Parthun and Johari (1995b), Wasylyshyn and Johari (1996)], the magnitude of ε' from the two effects may be written in terms of α, up to a certain extent of polymerization, α_i,

$$\begin{aligned}\varepsilon'(\alpha_i) = [\varepsilon'(\alpha=0)]_{P_1} &+ \int_0^{\alpha_1}\left[\left(\frac{\partial\varepsilon'}{\partial\varepsilon_s}\right)\left(\frac{\partial\varepsilon_s}{\partial\alpha}\right)+\left(\frac{\partial\varepsilon'}{\partial\tau}\right)\left(\frac{\partial\tau}{\partial\alpha}\right)\right]_{P_1} d\alpha \\ &+\int_{P_1}^{P_2}\left[\left(\frac{\partial\varepsilon'}{\partial\varepsilon_s}\right)\left(\frac{\partial\varepsilon_s}{\partial P}\right)+\left(\frac{\partial\varepsilon'}{\partial\tau}\right)\left(\frac{\partial\tau}{\partial P}\right)\right]_{\alpha_1} dP + \int_{\alpha_1}^{\alpha_i}\left[\left(\frac{\partial\varepsilon'}{\partial\varepsilon_s}\right)\left(\frac{\partial\varepsilon_s}{\partial\alpha}\right)+\left(\frac{\partial\varepsilon'}{\partial\tau}\right)\left(\frac{\partial\tau}{\partial\alpha}\right)\right]_{P_2} d\alpha\end{aligned} \tag{6.16}$$

and, in terms of the polymerization time, t, up to t_i

$$\begin{aligned}\varepsilon'(t_i) = [\varepsilon'(t=0)]_{P_1} &+ \int_0^{t_1}\left[\left(\left(\frac{\partial\varepsilon'}{\partial\varepsilon_s}\right)\left(\frac{\partial\varepsilon_s}{\partial\alpha}\right)+\left(\frac{\partial\varepsilon'}{\partial\tau}\right)\left(\frac{\partial\tau}{\partial\alpha}\right)\right)\left(\frac{\partial\alpha}{\partial t}\right)\right]_{P_1} dt \\ &+\int_{P_1}^{P_2}\left[\left(\frac{\partial\varepsilon'}{\partial\varepsilon_s}\right)\left(\frac{\partial\varepsilon_s}{\partial P}\right)+\left(\frac{\partial\varepsilon'}{\partial\tau}\right)\left(\frac{\partial\tau}{\partial P}\right)\right]_{t_1} dP + \int_{t_1}^{t_i}\left[\left(\left(\frac{\partial\varepsilon'}{\partial\varepsilon_s}\right)\left(\frac{\partial\varepsilon_s}{\partial\alpha}\right)+\left(\frac{\partial\varepsilon'}{\partial\tau}\right)\left(\frac{\partial\tau}{\partial\alpha}\right)\right)\left(\frac{\partial\alpha}{\partial t}\right)\right]_{P_2} dt\end{aligned} \tag{6.17}$$

where P is the pressure. Correspondingly, ε'' can be expressed as,

$$\begin{aligned}\varepsilon''(\alpha_i) = [\varepsilon''(\alpha=0)]_{P_1} &+ \int_0^{\alpha_1}\left[\left(\frac{\partial\varepsilon''}{\partial\varepsilon_s}\right)\left(\frac{\partial\varepsilon_s}{\partial\alpha}\right)+\left(\frac{\partial\varepsilon''}{\partial\tau}\right)\left(\frac{\partial\tau}{\partial\alpha}\right)+\frac{1}{\omega\varepsilon_o}\left(\frac{\partial\sigma}{\partial\alpha}\right)\right]_{P_1} d\alpha \\ &+\int_{P_1}^{P_2}\left[\left(\frac{\partial\varepsilon''}{\partial\varepsilon_s}\right)\left(\frac{\partial\varepsilon_s}{\partial P}\right)+\left(\frac{\partial\varepsilon''}{\partial\tau}\right)\left(\frac{\partial\tau}{\partial P}\right)+\frac{1}{\omega\varepsilon_o}\left(\frac{\partial\sigma}{\partial P}\right)\right]_{\alpha_1} dP \\ &+\int_{\alpha_1}^{\alpha_i}\left[\left(\frac{\partial\varepsilon''}{\partial\varepsilon_s}\right)\left(\frac{\partial\varepsilon_s}{\partial\alpha}\right)+\left(\frac{\partial\varepsilon''}{\partial\tau}\right)\left(\frac{\partial\tau}{\partial\alpha}\right)+\frac{1}{\omega\varepsilon_o}\left(\frac{\partial\sigma}{\partial\alpha}\right)\right]_{P_2} d\alpha\end{aligned} \tag{6.18}$$

or, in terms of t,

$$\varepsilon''(t_i) = \left[\varepsilon''(t=0)\right]_{P_1} + \int_0^{t_i}\left[\left(\left(\frac{\partial\varepsilon''}{\partial\varepsilon_s}\right)\left(\frac{\partial\varepsilon_s}{\partial\alpha}\right)+\left(\frac{\partial\varepsilon''}{\partial\tau}\right)\left(\frac{\partial\tau}{\partial\alpha}\right)+\frac{1}{\omega\varepsilon_o}\left(\frac{\partial\sigma}{\partial\alpha}\right)\right)\left(\frac{\partial\alpha}{\partial t}\right)\right]_{P_1} dt$$
$$+\int_{P_1}^{P_2}\left[\left(\frac{\partial\varepsilon''}{\partial\varepsilon_s}\right)\left(\frac{\partial\varepsilon_s}{\partial P}\right)+\left(\frac{\partial\varepsilon''}{\partial\tau}\right)\left(\frac{\partial\tau}{\partial P}\right)+\frac{1}{\omega\varepsilon_o}\left(\frac{\partial\sigma}{\partial P}\right)\right]_{t_1} dP \qquad (6.19)$$
$$+\int_{t_1}^{t_i}\left[\left(\left(\frac{\partial\varepsilon''}{\partial\varepsilon_s}\right)\left(\frac{\partial\varepsilon_s}{\partial\alpha}\right)+\left(\frac{\partial\varepsilon''}{\partial\tau}\right)\left(\frac{\partial\tau}{\partial\alpha}\right)+\frac{1}{\omega\varepsilon_o}\left(\frac{\partial\sigma}{\partial\alpha}\right)\right)\left(\frac{\partial\alpha}{\partial t}\right)\right]_{P_2} dt$$

In Equations (6.16) - (6.19), σ is the dc conductivity, and the other quantities are as described before. The limits of integration here are P_1 (1 bar) to P_2 (200 bar) and t_i and α_i, the polymerization time and the extent of polymerization under consideration. The second integral in Equations (6.16) - (6.19) represents the net physical effect of pressure, and the first and third integrals represent the net chemical effect. The physical effect, which is instantaneous, alters the static and dynamic properties of the liquid, and the chemical effect, which is time-dependent, alters the polymerization kinetics depending qualitatively upon whether the kinetics are mass-controlled or diffusion-controlled.

Referring to Section 4.3.1, the first and second sets of experiments on polymerization were performed at P = 1 bar and 200 bar, and therefore the second and third integral terms make no contribution to the ε' and ε'' data. In the third and fourth sets of experiments, all integral terms contribute to ε' and ε'', but as the $(\partial\varepsilon'/\partial\varepsilon_s)(\partial\varepsilon_s/\partial P)$ term is negligible in comparison with the $(\partial\varepsilon'/\partial\tau)(\partial\tau/\partial P)$ [Johari and Dannhauser (1969a), Chen *et al.* (1969)] all terms involving $\partial\varepsilon_s$ may be neglected in comparison with those involving $\partial\tau$. This leads to:

$$\varepsilon'(t) = \left[\varepsilon'(t=0)\right]_{P_1} + \int_0^{t_1}\left[\left(\frac{\partial\varepsilon'}{\partial\tau}\right)\left(\frac{\partial\tau}{\partial\alpha}\right)\left(\frac{\partial\alpha}{\partial t}\right)\right]_{P_1} dt + \int_{P_1}^{P_2}\left[\left(\frac{\partial\varepsilon'}{\partial\tau}\right)\left(\frac{\partial\tau}{\partial P}\right)\right]_{t_1} dP + \int_{t_1}^{t_f}\left[\left(\frac{\partial\varepsilon'}{\partial\tau}\right)\left(\frac{\partial\tau}{\partial\alpha}\right)\left(\frac{\partial\alpha}{\partial t}\right)\right]_{P_2} dt \tag{6.20}$$

At times longer than the critical gel time, t_{gel}, during polymerization, σ is found to be negligible [Wasylyshyn and Johari (1997b)], as is its change with P. Thus, for the fourth set of experiments in Section 4.3.1,

$$\varepsilon''(t) = \left[\varepsilon''(t=0)\right]_{P_1} + \int_0^{t_1}\left[\left(\frac{\partial\varepsilon''}{\partial\tau}\right)\left(\frac{\partial\tau}{\partial\alpha}\right)\left(\frac{\partial\alpha}{\partial t}\right)\right]_{P_1} dt + \int_{P_1}^{P_2}\left[\left(\frac{\partial\varepsilon''}{\partial\tau}\right)\left(\frac{\partial\tau}{\partial P}\right)\right]_{t_1} dP + \int_{t_1}^{t_f}\left[\left(\frac{\partial\varepsilon''}{\partial\tau}\right)\left(\frac{\partial\tau}{\partial\alpha}\right)\left(\frac{\partial\alpha}{\partial t}\right)\right]_{P_2} dt \tag{6.21}$$

Equations (6.16) - (6.21) thus provide us a framework for separating the physical and chemical effects of pressure on the dielectric properties of a liquid undergoing polymerization.

6.2.2 The Physical Effects of Pressure through Instantaneous Densification

Analogous to a decrease in temperature, hydrostatic pressure affects the dielectric behaviour of a chemically invariant material in six ways:

(i) a decrease in σ_{dc}, the dc conductivity,

(ii) a change in ε_s, the limiting low-frequency permittivity,

(iii) an increase in $\langle\tau\rangle$, the average relaxation time,

(iv) a change in the distribution of relaxation times,

(v) evolution of a second relaxation process, and

(vi) a change in ε_∞, the limiting high-frequency permittivity.

When μ_o and g in Equation (6.16) do not change on increasing the pressure, and the change in ε_∞ due to the optical and vibrational polarization is negligible,

$$(\partial\varepsilon_s/\partial P)= (\partial N_d/\partial P) \tag{6.22}$$

or,

$$\varepsilon_s(P_2) = \varepsilon_s(P_1)\left[\frac{N_d(P_2)}{N_d(P_1)}\right] \tag{6.22a}$$

where $N_d(P_1)$ refers to the number density of the dipoles at pressure P_1 and $N_d(P_2)$ that at P_2.

In terms of the transition state theory applied to dielectric relaxation and viscous flow, the pressure dependence of the relaxation time is expressed as [Kauzmann (1942)],

$$(\partial \ln\tau/\partial P)_T = \Delta V_\tau^{\neq}/RT \tag{6.23}$$

where $\Delta V_\tau^{\neq}$ is the activation volume for dielectric relaxation and R the gas constant. Since the changes in ε_s, ε_∞, and the distribution of relaxation times on increase in P are usually much smaller than the increase in τ, and a second relaxation process has not evolved sufficiently to contribute at the low frequency of 1 kHz, the magnitude of ε' and ε'' are affected by P mainly due to an increase in τ. The magnitude of the latter effect depends upon the magnitude of $\Delta V_\tau^{\neq}$, which itself has been found to increase with P, and the plots of τ against P found to ultimately curve upwards on raising P [Johari and Dannhauser (1969a), Johari and Whalley (1972), Scaife (1986)].

6.2.3 The Chemical Effect of Pressure through Reaction Kinetics

As the pressure is raised, the shear (and volume) viscosity, η, of the chemically-invariant liquid increases according to the relation [Kauzmann (1942)],

$$(\partial \ln\eta/\partial P)_T = \Delta V_\eta^{\neq}/RT \qquad \textbf{(6.24)}$$

where $\Delta V_\eta^{\neq}$ is the activation volume for the viscosity. Its value has been found to change with P nonlinearly as the plots of $\log\eta$ curve upwards with increase in P [Johari and Dannhauser (1969b)]. If τ was directly proportional to η then $\Delta V_\tau^{\neq}$ will be equal to $\Delta V_\eta^{\neq}$ according to the Maxwell equation, $\tau \propto \eta_M$.

We first consider how the increase in η on increasing P in a reversible manner may be combined with the spontaneous (irreversible) increase in η during isothermal polymerization and then relate the combined effect to the chemical rate constant. The pressure dependence of the reaction rate constant k, may be written in general terms,

$$\left(\frac{\partial \ln k}{\partial P}\right)_T = \left(\frac{\partial \ln k}{\partial \ln V}\right)_T \left(\frac{\partial \ln V}{\partial P}\right)_T + \left(\frac{\partial \ln k}{\partial \ln \eta}\right)_T \left(\frac{\partial \ln \eta}{\partial P}\right)_T \qquad \textbf{(6.25)}$$

since , $\beta_K = -(\partial \ln V/\partial P)_T$ is the isothermal compressibility, Equation (6.25) becomes,

$$\left(\frac{\partial \ln k}{\partial P}\right)_T = -\beta_K \left(\frac{\partial \ln k}{\partial \ln V}\right)_T + \left(\frac{\partial \ln k}{\partial \ln \eta}\right)_T \left(\frac{\partial \ln \eta}{\partial P}\right)_T \qquad \textbf{(6.26)}$$

Since $(\partial \ln k/\partial \ln V)_T$ in Equation (6.26) is negative, the first term on the right-hand-side is positive. Furthermore, as $(\partial \ln k/\partial \ln \eta)_T$ is negative and $(\partial \ln \eta/\partial P)_T$ positive, the second term on RHS is negative.

For a mass-controlled chemical reaction, η is already low, and a further increase in η at a constant T and P has no effect on the reaction rate constant, k. But if η is

increased isothermally by raising P, the liquid densifies, which in turn raises the probability of chemical reaction. Since changes in viscosity do not affect the kinetics of reactions in the mass-controlled regime [Hamman (1957)], the term $(\partial \ln k/\partial \ln \eta)_T$ on the RHS of Equation (6.26) is negligible or zero, and $(\partial \ln k/\partial P)_T$ is positive. Thus an increase in P *increases* the reaction rate.

When η has increased as a result of polymerization to a value high enough such that the reaction kinetics become diffusion-controlled, a further increase in η by an increase in P would make the second term on the RHS of Equation (6.26) significant because $(\partial \ln k/\partial \ln \eta)_T$ is finite and $(\partial \ln \eta/\partial P)_T$ is large, as found earlier [Johari and Dannhauser (1969b)]. In this case $(\partial \ln k/\partial P)_T$ is negative and an increase in P *decreases* the reaction rate.

It is worth considering how the effect of pressure itself changes when the polymerization kinetics of a liquid have changed from the mass-controlled to the diffusion-controlled regime. In the early stages of polymerization, when the polymerization rate is mass-controlled and the liquid's viscosity is low, only the first term on the RHS in Equation (6.26) is significant and k increases with increase in P, as discussed above. Also, as the liquid's density increases on polymerization at a constant T and P, β_K in Equation (6.26) decreases typically from ~10^{-4} bar^{-1} for the liquid state towards ~10^{-6} bar^{-1} for the vitrified state. This means that the first term on the RHS of Equation (6.26) decrease as β_K decreases with t, thereby increasing the relative significance of the second term on the RHS of Equation (6.26). In the latter stage of

polymerization, when η is high and the kinetics approach the diffusion-controlled regime, the second term on the RHS in Equation (6.26) becomes significance relative to the first term. This second term increases further as η continues to increase during polymerization. This increase depends on the magnitudes of: (a) the physical effect through the term $(\partial \ln\eta/\partial P)_T$ of Equation (6.24), and (b) the chemical effect through the term $(\partial \ln k/\partial \ln\eta)_T$ of Equation (6.26). Taken together, this means that the measured $(\partial \ln k/\partial P)_T$ will be positive in the beginning of polymerization, will become zero when the increase in k caused by densification alone on raising P is compensated by the decrease in k caused by an increase in η on raising P, and ultimately will become negative. It will remain negative until α has reached the value of 1.

The pressure dependence of k is described by the transition state theory [Evans and Polanyi (1935)]. In the early stages of polymerization, when the reaction is mass-controlled, the pressure dependence of the reaction rate is given by [Hamman (1957)],

$$(\partial \ln k/\partial P)_T = -\Delta V_k^{\neq}/RT \qquad \textbf{(6.27)}$$

where $\Delta V_k^{\neq}$ is the volume of activation for the reaction, which itself depends upon the pressure. Dividing Equation (6.27) by Equation (6.24),

$$(\partial \ln k/\partial \ln\eta)_T = -\Delta V_k^{\neq}/\Delta V_\eta^{\neq} \qquad \textbf{(6.28)}$$

In the mass-controlled regime, when $(\partial \ln k/\partial \ln\eta)_T$ or $-\Delta V_k^{\neq}/\Delta V\eta^{\neq} \approx 0$, it would imply that $-\Delta V_k^{\neq} << \Delta V\eta^{\neq}$, and in the diffusion-controlled regime, when $(\partial \ln k/\partial \ln\eta)_T$ or $-\Delta V_k^{\neq}/\Delta V\eta^{\neq} < 0$, it would imply that at the onset of diffusion-control, the sign of $\Delta V_k^{\neq}$ should change from negative to positive. It follows that the plots of $-\ln k$ versus P would cross the plots

of $\ln\eta$ at a certain P when $\Delta V_k^{\neq}$ becomes positive. Below that pressure, the reaction is mass-controlled, and above it, it is diffusion-controlled. This has been given by Isaacs (1981), where a plot of $\ln k$ against P shows first an increase followed by a maximum, then a decrease. The pressure at which the slope of the $\ln k$ - P plot changes sign would thus be the onset point of diffusion-controlled kinetics.

6.2.4 Diffusion-Controlled Polymerization Kinetics

As discussed thus far, diffusion-control becomes significant as the liquid's viscosity increases for reactions in the liquid state. Waite (1957) has provided a mathematical treatment of the transition of mass- to diffusion-control in terms of simple Brownian diffusion of particles as they coalesce into larger particles. He discussed that the transition from mass- to diffusion-controlled kinetics occurs when E_D^*, the activation energy for the diffusion of the relevant molecules, A and B, exceeds E_R^*, the activation energy of the chemical reaction. The absolute magnitudes of the two quantities was seen as irrelevant; the only requirement being that the quantity $(E_D^* - E_R^*)$ change from negative to positive at a certain value of α, or t.

Waite (1957) defined the condition for the transition from mass- to diffusion-controlled kinetics in terms of a parameter, $s \approx \exp[(E_D^* - E_R^*)/RT]$, which makes the concept of diffusion-control occurring at a particular value of τ or α irrelevant. Briefly, any A molecule has a definite probability of reaction with any B molecule (and *vice versa*) when the two approach to within the capture radius, r_o, as a result of their random

diffusion. When $s << 1$, the reaction rate is determined solely by the probability that an A molecule and a B molecule will react upon collision, i.e., an A and B separated by a capture radius, r_o, have a high probability of diffusing apart without reacting, because the barrier to reaction is higher than the barrier to diffusion. Alternatively, when $s >> 1$, the reaction rate is determined by the diffusion time required for A and B to approach a separation distance of r_o because the barrier to diffusion is higher than the barrier to reaction. The reaction may become diffusion-controlled either at a low or a high viscosity depending upon the rate at which the diffusion coefficient of the reacting groups decreases with increase in α, and the chemical reaction rate decreases.

There are a number of theories and models [Chandrasekhar (1943), Doi (1975), de Gennes (1982), Calef and Deutch (1983), Plonka, (1986)] beginning with Smoluchowski's (1916), (1917) treatment of the agglomeration of colloidal particles to the growth of a macromolecule. All of these conclude that for a bimolecular reaction, A + B $\rightarrow$ AB, such as that under consideration here, the reaction occurs according to pseudo first-order kinetics with a time dependent rate constant, k. Since the extent of reaction, α, also changes with time, it may be interpreted as an α-dependent k.

Smoluchowski (1916), (1917) showed that the rate constant for a diffusion-controlled reaction of spherical solute molecules of radius R and diffusivity D, undergoing Brownian motion in a viscous liquid is given by,

$$k = 4\pi (D_A + D_B)(R_A + R_B) \qquad \textbf{(6.29)}$$

Calef and Deutch (1983) have reviewed the development of Smoluchowki's equation and replacing the D by the viscosity of the solvent, η_s, according to the Stokes-Einstein equation, they rewrote Equation (6.29),

$$k = \frac{2RT}{3\eta_s}\left[\frac{(R_A + R_B)^2}{R_A R_B}\right] \tag{6.30}$$

Since $(R_A + R_B)^2$ generally increases more rapidly than $R_A R_B$ (the square bracketed term in Equation (6.30) is ~4 when $R_A \approx R_B$), a decrease in k with t requires that η_s increases more rapidly with t than the remainder of the term.

A connection between D and k is difficult to formulate when the reacting site is enveloped by the non-reacting part of the remaining molecule, although it has been done for rigid spherical molecules and small molecules with reacting sites on the surface. There is also a fundamental difficulty in relating the onset of diffusion-control to the dielectric relaxation rate, because the dipolar relaxation rate refers to the average reorientation rate of all dipoles, and not necessarily the diffusion rate of the reacting group that is attached to the rest of the molecule. Specifically, the reaction is possible only when the structure has opened enough to allow the two groups, A and B, to approach each other, thus making the dipolar reorientation rate of the remaining part of the cluster irrelevant. This is mainly because the dipolar relaxation is a measure of the dipoles associated with the -OH groups and the $-CH_2-N(R)-CH_2-$ linkages that form upon reaction. Therefore, the theoretical conditions for the onset of diffusion-control from the relaxation data are not directly obtainable [Wasylyshyn and Johari (1998)].

For consecutive reaction rate kinetics, the overall reaction rate is determined by the slower of the two processes, particularly, the molecular motions of that part of the macromolecule that must first unshield the active site from reaction. Although several approaches that deal with the molecular motions have been considered in recent years [Smoluchowski (1916), (1917), Chandrasekhar (1943), Doi (1975), de Gennes (1982), Calef and Deutch (1983), Plonka, (1986)], all involve cases in which the reaction itself does not alter the diffusion coefficient of the reacting sites. Instead, it alters only the probability that a given molecule will reach a reacting site when many other non-reacting sites are available. A connection between k and t is even more difficult with the dielectric relaxation studies, since a dipolar group does not necessarily act as the reacting sites nor does it's re-orientation necessarily facilitate the reaction. Thus, in the absence of adequate theoretical descriptions, relations between k, D, and t had to be obtained directly from the measured data, as described below.

The rate at which an equilibrium property such as volume, refractive index, relaxation time, *etc.*, changes with the polymerization time is a direct indication of the rate of polymerization. Any change in ε' and ε'' with the polymerization time in these cases results from the six effects described in Section 6.2.2. During the polymerizing period when the change in τ with t becomes dominant (contribution (iii)), the rates of change of ε' and ε'' with t correspond to the rate of polymerization. This condition is satisfied only by the data obtained at t longer than t_{peak} in the plots of ε'' in Figures 4.12 to 4.21. For fixed frequency measurements of a process in which τ increases irreversibly,

$\omega\tau$ for 1 kHz frequency increases from a value as low as 10^{-6} to as high as 10^{6}. The peak in ε'' appears at t when $\omega\tau = 1$. At t much longer than this time, $\omega\tau >> 1$, and for that condition both $(\partial\varepsilon'/\partial t)$ and $(\partial\varepsilon''/\partial t)$ become negative, ultimately approaching zero on complete polymerization. Hence, for all sets of experiments shown in Figures 4.12 to 4.21, the sum of the first three terms in Equations (6.20) and (6.21) becomes equal to $\left[\varepsilon'(t_1 > t_{\omega\tau>>1})\right]_{P_2}$ and $\left[\varepsilon''(t_1 > t_{\omega\tau>>1})\right]_{P_2}$,respectively. Therefore,

$$\varepsilon'(t > t_{\omega\tau>>1}) = \left[\varepsilon'(t_1 > t_{\omega\tau>>1})\right]_{P_2} + \int_{t_1}^{t_f}\left[\left(\frac{\partial\varepsilon'}{\partial\tau}\right)\left(\frac{\partial\tau}{\partial\alpha}\right)\left(\frac{\partial\alpha}{\partial t}\right)\right]_{P_2} dt \qquad (6.31)$$

$$\varepsilon''(t > t_{\omega\tau>>1}) = \left[\varepsilon''(t_1 > t_{\omega\tau>>1})\right]_{P_2} + \int_{t_1}^{t_f}\left[\left(\frac{\partial\varepsilon''}{\partial\tau}\right)\left(\frac{\partial\tau}{\partial\alpha}\right)\left(\frac{\partial\alpha}{\partial t}\right)\right]_{P_2} dt \qquad (6.32)$$

When the small change in ε_s, ε_∞ and the relaxation time distribution parameter with t is ignored, ε' and ε'' become a function of τ^{-2} and τ^{-1}, respectively, for a single relaxation process. (For a distribution of τ this power changes to include the distribution parameter.) Thus, the inverse of the slope of the ε'' plot against t for these conditions becomes related to the rate of change of τ with t,

$$\left(\frac{\partial\ln(\varepsilon'-\varepsilon_\infty)}{\partial t}\right)_{P,T,\omega\tau>>1} = -2\left(\frac{\partial\ln\tau}{\partial t}\right)_{P,T,\omega\tau>>1} \qquad (6.33)$$

and

$$\left(\frac{\partial\ln\varepsilon''}{\partial t}\right)_{P,T,\omega\tau>>1} = -\left(\frac{\partial\ln\tau}{\partial t}\right)_{P,T,\omega\tau>>1} \qquad (6.34)$$

As ε'' for $\omega\tau >>1$ is inversely related to τ, which is an equilibrium property representing the structure of the liquid, the plots of $(\partial \ln\varepsilon''/\partial t)_{P,T,\omega\tau>>1}$ against ε'' would reveal how the polymerization rate changes with the structure. These plots are shown in Figures 6.10 to 6.13 for the data from Figures 4.12 to 4.21. Figure 6.10(a,b) is for the polymerization of DGEBA-AN and DGEBA-HA at 351.5 K and 304.0 K, respectively, and Figure 6.11(a,b) is that for DGEBA-EDA and DGEBA-HDA at 307.2 K and 303.4 K. Figure 6.12 is for the polymerization of DGEBA-CHA at 300.2, 307.5, and 313.8 K, and Figure 6.13 is that for DGEBA-EDA at 296.6, 306.1, and 314.0 K.

A vertical cut of the plots in Figures 6.10 to 6.13 corresponds to a fixed ε'', or equivalently, τ^{-1}. Thus, $[\Delta(\partial\varepsilon''/\partial t)_{\omega\tau>>1}/\Delta P]_{\tau,T}$ becomes a property of the liquid independent of its chemical reaction history. This ratio is negative when τ is short or ε'' is large (due to σ_{dc}), or when the polymerization is mass-controlled. $[\Delta(\partial\varepsilon''/\partial t)_{\omega\tau>>1}/\Delta P]_{\tau}$, becomes zero at τ when the curves cross, and positive when the curves have crossed over. In each case the plots seem to converge and, in some cases, cross-over as ε'' decreases or equivalently τ (and ε'') increases (the progress of polymerization is from right to left). The magnitude of τ at which the curves cross-over corresponds to the diffusion coefficient of the reacting sites at the onset of diffusion-control. It should be noted that as $t \rightarrow \infty$, $(\partial \ln\varepsilon''/\partial t)_{P,T,\omega\tau>>1}$ approaches zero while ε'' remains finite.

The measured dielectric data for the polymerization of the DGEBA-CHA mixture plotted in Figure 4.13 show that the value of ε'' as $t \rightarrow \infty$ is higher for 307.5 K and 206 bar than that at 1 and 103 bar for the same temperature. This is also the case in Figure

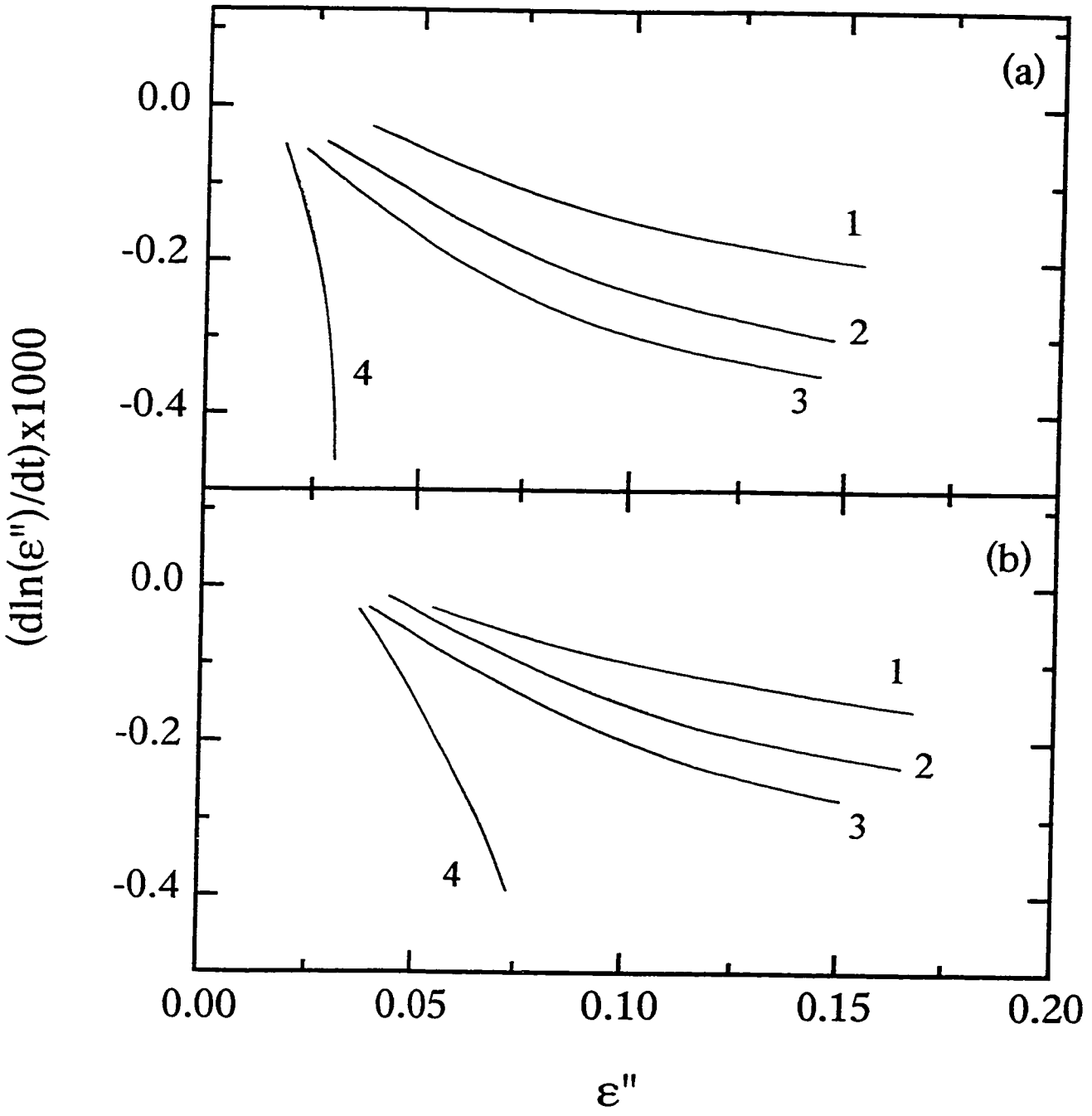

Figure 6.10: $(\partial\varepsilon''/\partial t)$ is plotted against ε'' for the linear-chain polymerization of; **(a)** the DGEBA-AN mixture at 351.5 K, and **(b)** the DGEBA-HA mixture at 304.0 K. Curves 1 and 2 correspond to the experiments at 1 bar and 200 bar, curves 3 and 4 correspond to the experiments in which pressure was applied when the liquid's viscosity was low (curve 3) and high (curve 4). The data correspond to those in Figures 4.18 and 4.19.

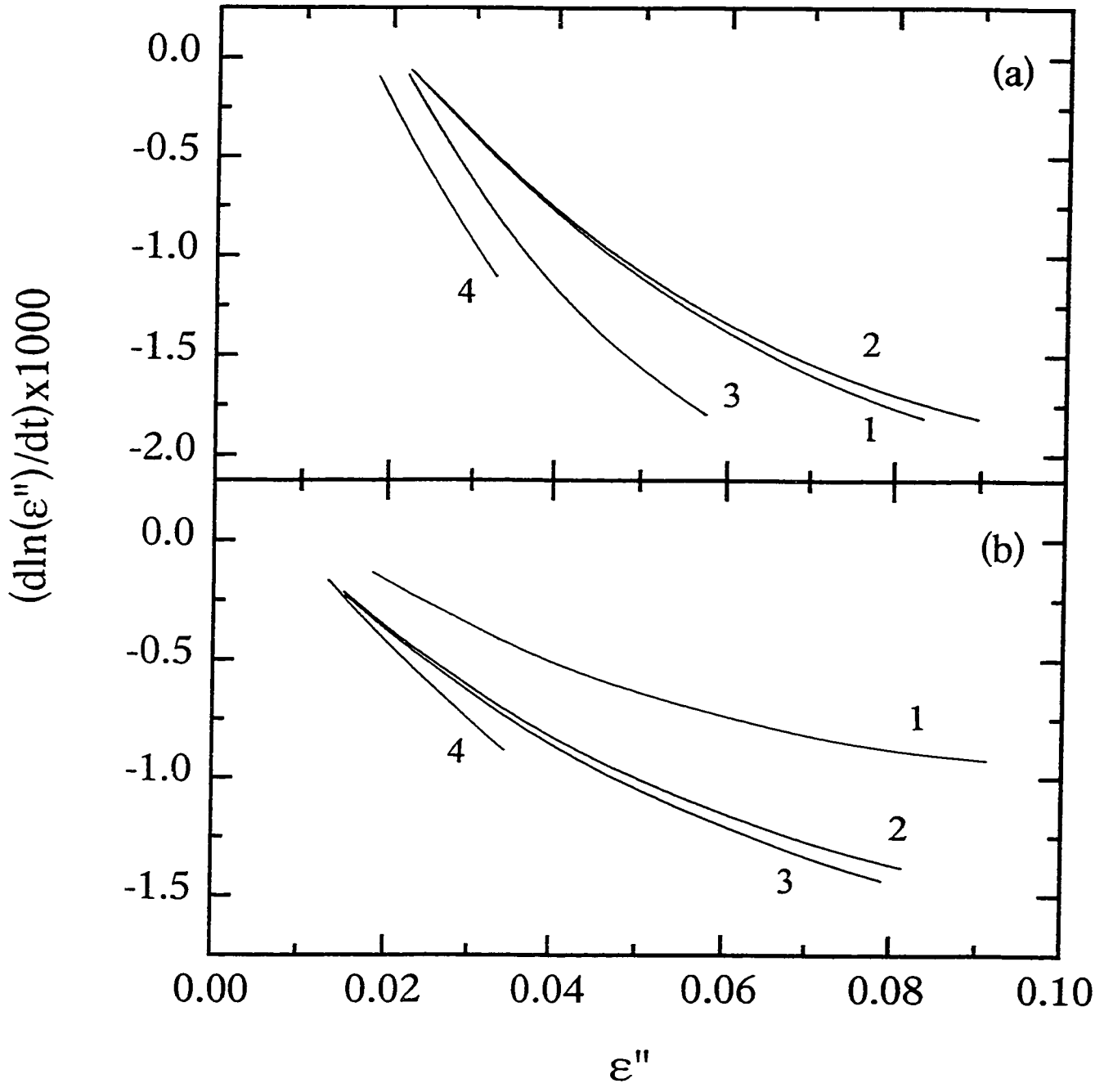

Figure 6.11: $(\partial\varepsilon''/\partial t)$ is plotted against ε'' for the network polymerization of; **(a)** the DGEBA-EDA mixture at 307.2 K, and **(b)** the DGEBA-HDA mixture at 303.4 K. Curves 1 and 2 correspond to the experiments at 1 bar and 200 bar, curves 3 and 4 correspond to the experiments in which pressure was applied when the liquid's viscosity was low (curve 3) and high (curve 4). The data correspond to those in Figures 4.20 and 4.21.

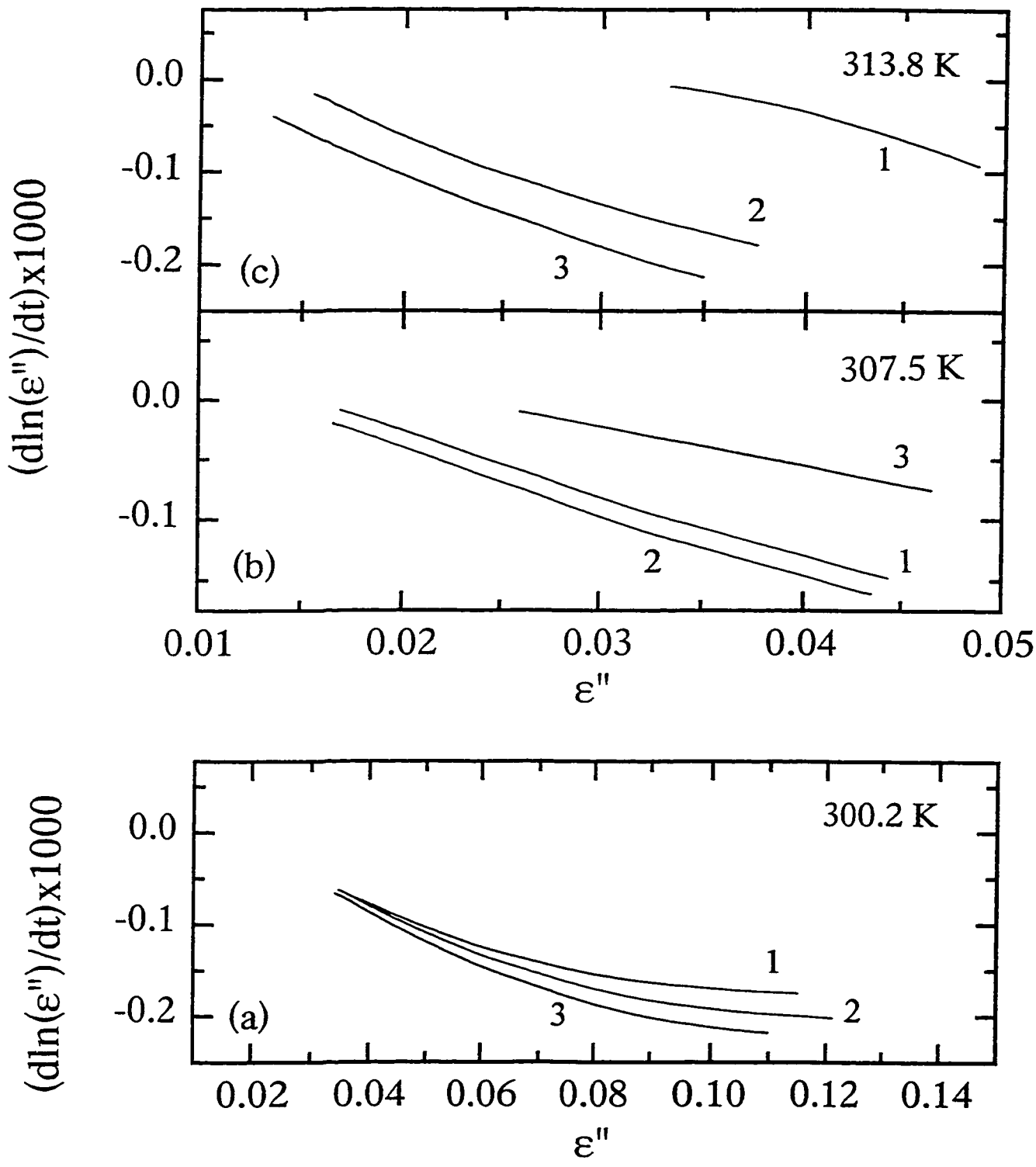

Figure 6.12: The $(\partial\varepsilon''/\partial t)$ is plotted against ε'' for the linear-chain polymerization of the DGEBA-CHA mixture at **(a)** 300.2 K, **(b)** 307.5 K, and **(c)** 313.8 K. Curves 1, 2, and 3 correspond to measurements at 1, 103, and 206 bar, respectively.

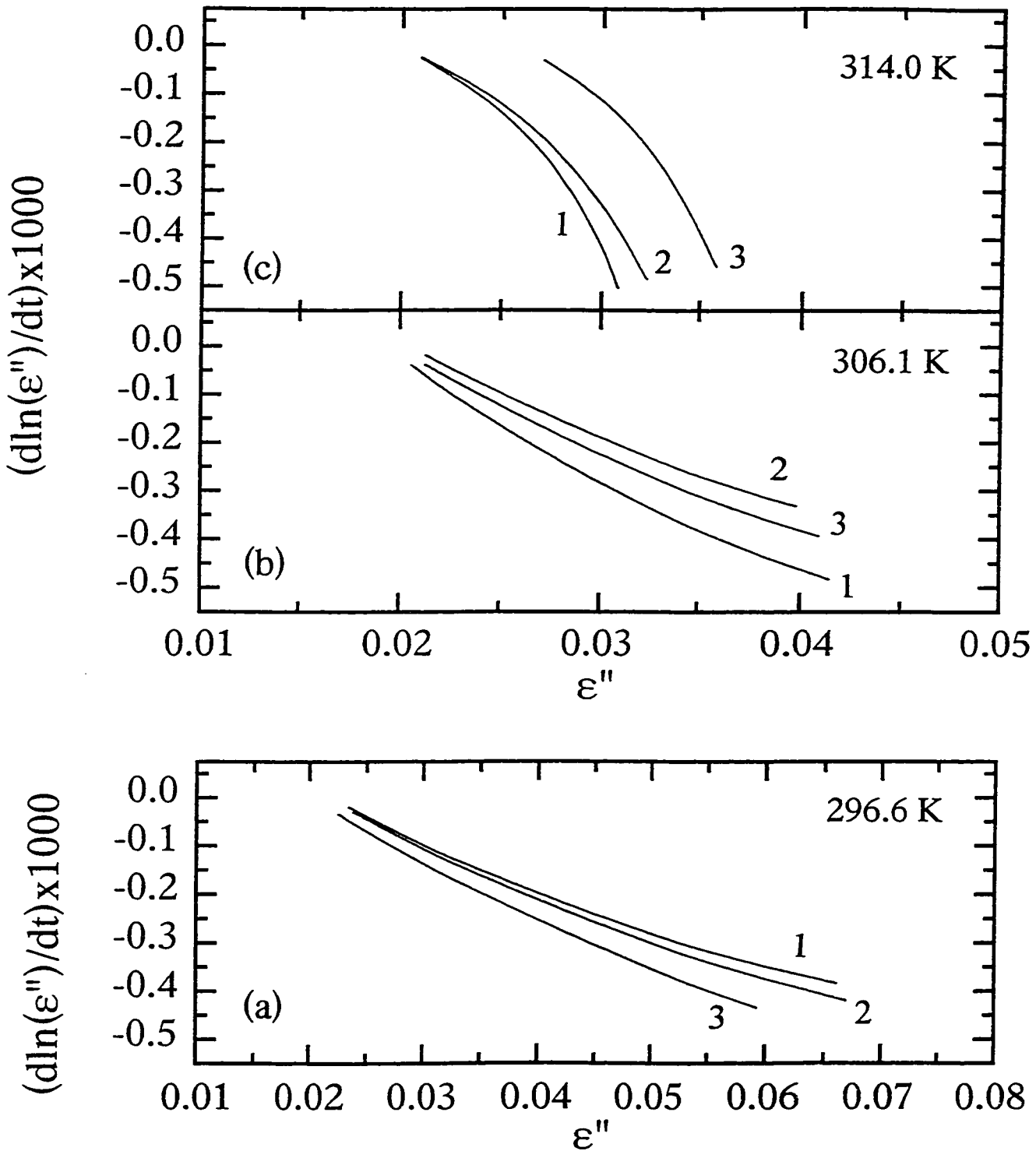

Figure 6.13: The $(\partial\varepsilon''/\partial t)$ is plotted against ε'' for the network polymerization of the DGEBA-EDA mixture at **(a)** 296.6 K, **(b)** 306.1 K, and **(c)** 314.0 K. Curves 1, 2, and 3 correspond to measurements at 1, 103, and 206 bar, respectively.

4.14 for the same mixture at 313.8 K and 1 bar. This is expected for the former case, since the evolution of the secondary-, or β- relaxation is expected to cause ε″ to increase towards a maximum as $t \rightarrow \infty$ [Wasylyshyn and Johari (1997b)]. Additionally, the increase in the rate of polymerization due to the effect of pressure should cause the β-relaxation peak in ε″ to evolve at shorter times. For the plot in Figure 4.14 at 313.8 K and 1 bar, a β-relaxation peak in ε″ is not expected to evolve more rapidly than at higher pressures for similar reasons. Without being able to provide a clear explanation for these discrepancies, the corresponding curve 3 in Figures 6.12(b) and curve 1 in Figure 6.12(c) will be excluded from the following discussions. The plots for the high-pressure curves lie both above and below those for 1 bar in Figures 6.10 to 6.13, and this behaviour is possibly due to an error in the empty cell capacitance. Although the expected cross-over of the low-pressure and high-pressure plots is not observed for all cases, there is an indication that the two plots would cross-over for lower values of ε″ in all cases. Experimental limitations prevented accurate, low value ε″ measurements.

It should be noted that if the decrease in ε″ resulting from a pressure-induced increase in τ as part of the physical effect according to Equation (6.21) is taken into account, all the higher pressure plots in Figures 6.10 to 6.13 will shift to the RHS along the ε″ axis. The shift of each data point would differ since it is more when ε″ is low (or τ is high), and less when ε″ is high (or τ is low), because $\Delta V_{\tau}^{\neq}$ of Equation (6.23) has generally been found to increase with τ [Johari and Dannhauser(1969a), Johari and Whalley (1972)]. This correction could make the cross-over of the pressure plots in

Figures 6.10 to 6.13 observable at a higher value of ε'' or lower τ, but in a process that is itself time dependent, $\Delta V_{\tau}^{\neq}$ is not readily determined directly. The effect of pressure-induced increase in τ on such plots may be useful for future investigations of the transition from mass- to diffusion-controlled polymerization kinetics.

The conclusions drawn from Sections 6.1 and 6.2 are that hydrostatic pressure generally increases the rate of a macromolecule's growth up to substantially long reaction periods and high extents of polymerization. There is little qualitative distinction between the linear-chain and network structure's growth. The effect of pressure on the rate of change of dielectric relaxation time with the polymerization time is positive when the polymerization kinetics are mass-controlled and negative when it is diffusion-controlled. The changes in the dielectric behaviour of a polymerizing liquid can be used for revealing the changes in the reaction kinetics with increase in the extent of polymerization. This may be used as a criterion for determining the onset of diffusion-control and the state of the liquid in terms of the relaxation time at which this onset occurs.

6.3 MATHEMATICAL SIMULATION OF THE EFFECTS OF STEP-INCREASED AND STEP-DECREASED PRESSURE

In the previous sections, the response of the polymerizing mixtures subjected to a constant pressure and step-increase in pressure was used to develop criteria for the transition from the mass-controlled to the diffusion-controlled regimes of polymerization kinetics. It was found that pressure has both a chemical effect and a physical effect on the polymerizing mixtures. The former occurred as an increased rate of polymerization,

causing the dielectric properties to change more rapidly with time. The latter manifested itself as a reversible change in an equilibrium property, such as density, relaxation time, static permittivity, *etc*. In the following, the qualitative effect of pressure on each stage of the changing dielectric relaxation properties will be considered in terms of existing formalisms.

6.3.1 The Chemical and Physical Effects of Pressure on Polymerization

An increase of pressure to a liquid mixture of reacting species alters the equilibrium of a reaction and thus the amount of the reaction product according to Le Chatelier's Principle [Isaacs (1981)]. Pressure favours the denser polymeric product, thus a greater extent of reaction is obtained at equilibrium when polymerization occurs at elevated pressures. The rate at which the polymerization proceeds towards the ultimate extent of reaction at equilibrium, however, depends upon whether the polymerization is in the mass- or diffusion-controlled regime [Hamman (1957), Isaacs (1981)].

In terms of the transition state theory [Evans and Polanyi (1935)], the pressure dependence of the rate constant for the formation of the product, $k^{\neq}$, was expressed as,

$$\frac{\partial \ln k^{\neq}}{\partial P} = -\frac{\Delta V^{\neq}}{RT} \tag{6.35}$$

where $\Delta V^{\neq}$ is the volume of activation. From Equation (6.35), it is seen that the sign of $\Delta V^{\neq}$ determines whether a reaction is accelerated or retarded when pressure is applied. For the case of multimolecular associations (multiple reactants forming a single product) [Hamman (1957)], longer Van der Waals' interactions are replaced by shorter covalent

bonds, thus, $\Delta V^{\neq} < 0$ [Hamman (1957)]. This is confirmed in Figures 4.12 to 4.21 and Figures 6.3 to 6.6 where an increase in pressure caused the dielectric properties to evolve at a faster rate with an increase in pressure from 1 bar to 200 bar.

To describe the increase in α with polymerization time, t, the following empirical equation is used [Parthun *et al.* (1996)],

$$\alpha = 1 - \exp\left(-k' t^{m}\right) \tag{6.36}$$

where m and k' are empirical parameters that determine α at a given t. Note that for m = 1, $k' = k$, the reaction rate constant described earlier. Since an increase in pressure increases $k^{\neq}$ of Equation (6.35) for polymerization generally, it is expected that k will similarly increase with an increase in P. The increase in α on increase in k from k_i at pressure P_i to k_{ii} at pressure P_{ii} was calculated from Equation (6.30) by assuming $m = 1$ and independent of pressure, $k_i = 10\ \mu s^{-1}$ and $k_{ii} = 14\ \mu s^{-1}$. The calculation was done for the change in P corresponding qualitatively to the experimental conditions in Figures 4.26 to 4.29 and is shown in Figure 6.14(a) when the step-change was made at ~5 ks intervals. The calculated plots of α for a fixed k_i and k_{ii} are shown by the dotted and dashed curves in Figure 6.14(b). These two curves correspond to conditions when pressures P_i or P_{ii} were maintained constant from the beginning to the end of polymerization, provided the reaction remained mass-controlled. As every step-increase in P causes the polymerization rate to increase according to the increase in k from k_i to k_{ii} for the period of the increased pressure, the corresponding curve continuously shifts towards the dashed-line curve but does not reach it because the extent of polymerization

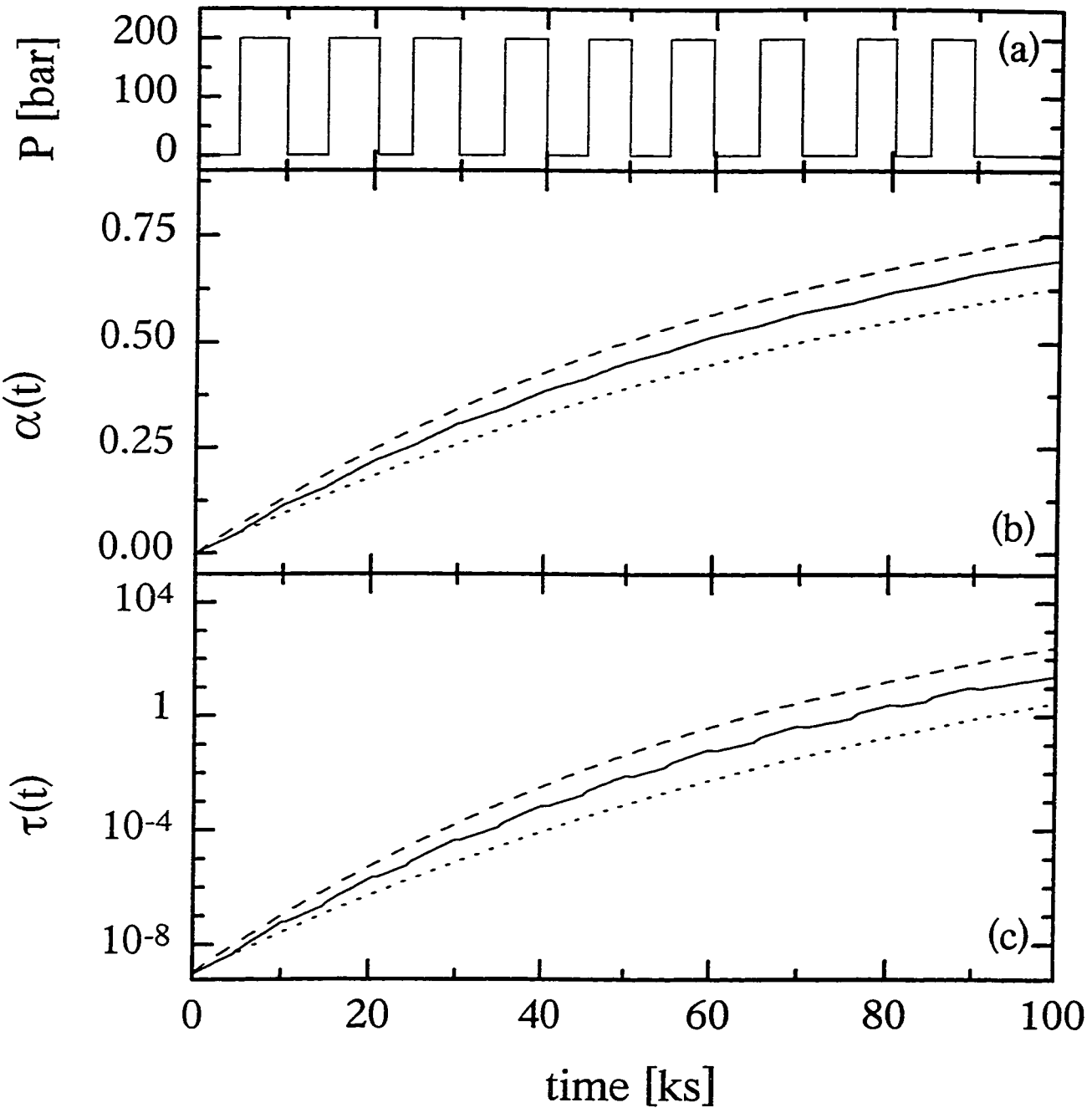

Figure 6.14: **(a)** The stepped-pressure profile used for the simulation of; **(b)** the extent of reaction, α, calculated from Equation (6.36), plotted against the polymerization time, t, and, **(c)** the relaxation time, $\langle\tau\rangle$, calculated from Equation (6.2) plotted against t. For α and $\langle\tau\rangle$, the dotted lines correspond to polymerization at a low pressure, and the dashed lines that at a high pressure. The continuous lines represent the result of applying the stepped-pressure profile as indicated in (a). Parameters for the simulation are given in the text.

at equilibrium at P_i is greater than at P_{ii} according to Le Chatelier's principle. This new curve, corresponding to the pressure-steps in Figure 6.14(a), is calculated using the general equation,

$$\alpha(t) = \int_0^{t_1} \left(\frac{\partial \alpha}{\partial t}\right)_{P_i} dt + \int_{t_1}^{t_N} \left(\frac{\partial \alpha}{\partial t}\right)_{P_{ii}} dt \qquad (6.37)$$

and is shown in Figure 6.14(b). To elaborate, α increases at a rate corresponding to $k = k_i$ up to t_1 (and a value of α_1), at $P = P_i$. At t_1, P is increased from P_i to P_{ii} and the polymerization proceeds from α_1 at a rate corresponding to k_{ii}. Thus, $(d\alpha/dt)_T$ at $t < t_1$ is less than $(d\alpha/dt)_T$ at $t > t_1$. From here, α increases to α_2 (at t_2), when P is decreased from P_{ii} to P_i. From α_2 (at t_2), α increases at a rate corresponding to k_i, as initially. This increase in α with t will be combined with other physical parameters to describe the net changes.

The Effect on the Relaxation Time

Amongst the physical processes the most sensitive one is the molecular diffusion represented as the dielectric relaxation time, $\langle\tau\rangle$, which increases with α or t as already discussed. $\langle\tau\rangle$ also increases with pressure according to Equation (6.23). Thus, the limiting values, $\langle\tau\rangle_o$ and $\langle\tau\rangle_\infty$ of Equation (6.2) should increase upon increase in P, but not by the same factors, as described in Section 6.1.1, since $\Delta V_\tau^{\neq}$ itself increases with α. Such a response of the liquid is due to the physical effects of pressure on the relaxation processes. For simplicity of treatment, p in Equation (6.2) is taken as unity and independent of P, which makes the plot of $\ln\langle\tau\rangle$ against α linear with a slope of S =

$\ln(<\tau>_\infty/<\tau>_o)$ and endpoints of $<\tau>_o$ and $<\tau>_\infty$. Therefore, for a pressure, P_i, $<\tau>_o = \tau_{o,i}$, $<\tau>_\infty = \tau_{\infty,i}$, and $S = S_i$, and for P_{ii}, the corresponding values are $\tau_{o,ii}$, $\tau_{\infty,ii}$, and S_{ii}.

The rate of change of $\log<\tau>$ with t is related to the rate of change of α according to Equation (6.36), and this relation must be examined first. In Equation (6.2), $<\tau>$ depends upon the rate parameter, k of Equation (6.36), as well as $<\tau>_o$ and $<\tau>_\infty$. As an increase in P increases k and through it the rate of increase of $<\tau>$ as well as the limiting values of $<\tau>$, the values of $<\tau>$ can be calculated for the given values of k_i and k_{ii}, and Equations (6.2), (6.23) and (6.36). By using $<\tau>_o = \tau_{o,i} = 1$ ns, and $<\tau>_\infty = \tau_{\infty,i} = 1$ Ms in Equation (6.2), the same k_i as for the calculation of α from Equation (6.36), and $\Delta V^{\neq}_{\tau_o} =$ 12 ml/mol and $\Delta V^{\neq}_{\tau_\infty} = 42$ ml/mol in Equation (6.23) $<\tau>_i$ and $<\tau>_{ii}$ are plotted against t in Figure 6.14(c). The 10% increase in $<\tau>_o$ and 40% increase in $<\tau>_\infty$ were chosen in qualitative similarity to experimental studies [Johari and Dannhauser (1969a), Chen *et al.* (1969), Johari and Whalley (1972)].

The full line curve in Figure 6.14(c) was calculated for the step-increase and step-decrease profile in Figure 6.14(a) using the general equation,

$$<\tau(t)>=\tau_{o,i}+\int_0^{t_1}\left[\left(\frac{\partial<\tau>}{\partial\alpha}\right)\left(\frac{\partial\alpha}{\partial t}\right)\right]_{P_i}dt+\int_{P_i}^{P_{ii}}\left[\left(\frac{\partial<\tau>}{\partial P}\right)\right]_{t_1}dP + \int_{t_1}^{t_N}\left[\left(\frac{\partial<\tau>}{\partial\alpha}\right)\left(\frac{\partial\alpha}{\partial t}\right)\right]_{P_{ii}}dt \tag{6.38}$$

To elaborate, during polymerization from $t = 0$ to t_1 at $P = P_i$, $\log\tau$ increases according to Equation (6.2) with $<\tau>_o = \tau_{o,i}$, and $<\tau>_\infty = \tau_{\infty,i}$, and Equation (6.36) with $k = k_i$. At t_1 (at

α_1), P is increased from P_i to P_{ii}. The instantaneous change in $<\tau>$ at α_1 is due to the physical changes in $<\tau>_o$ and $<\tau>_\infty$, which increase to $\tau_{o,ii}$ and $\tau_{\infty,ii}$, respectively. From t_1 (α_1), logτ changes at an increased rate according to Equation (6.2) with $<\tau>_o = \tau_{o,ii}$, $<\tau>_\infty = \tau_{\infty,ii}$, and Equation (6.36) with $k = k_{ii}$. At t_2 (α_2) when P is decreased from P_{ii} to P_i, the instantaneous decrease $<\tau>$ is due to the decrease of $<\tau>_o$ and $<\tau>_\infty$ to values of $\tau_{o,i}$, and $\tau_{\infty,i}$, respectively. From t_2 (α_2) to time, t_N, $<\tau>$ increases with time according to Equation (6.2) with $<\tau>_o = \tau_{o,i}$, and $<\tau>_\infty = \tau_{\infty,i}$, and Equation (6.2) with $k = k_i$. Thus, the instantaneous change in $<\tau>$ with P, $(\Delta \log <\tau>/\Delta P)_{t_N}$ is positive for $\Delta P > 0$ and negative for $\Delta P < 0$. Thus, like α, the $<\tau>$ curve continuously shifts towards the dashed line curve but does not reach it because $<\tau>$ at equilibrium at P_{ii} is greater than at P_i because α is greater.

The Effect on the Volume During Polymerization

As a diepoxide-diamine liquid mixture polymerizes, its volume decreases by ~10% [Choy and Plazek (1986)] as covalent bonds form. Therefore, the decrease in volume becomes directly related to α by an empirical relation,

$$V(\alpha) = V_o + (V_f - V_o)\alpha \qquad \textbf{(6.39)}$$

where V_o is the volume of the unpolymerized liquid ($\alpha = 0$), and V_f is that of the polymer ($\alpha = 1$). V increases linearly with a slope (V_f - V_o).

The physical effect of pressure on the volume is expressed as the isothermal compressibility, β_K, which decreases as the liquid polymerizes and $\alpha \rightarrow 1$. To a first

approximation, β_K is proportional to V, and therefore, α. This dependency upon α can be qualitatively expressed as,

$$\beta_K(\alpha) = \beta_{K,f} + (\beta_{K,f} - \beta_{K,o})\alpha \qquad \textbf{(6.40)}$$

where $\beta_K(\alpha)$ is the compressibility at the extent of reaction, α and β_{Ko} and β_{Kf} are the values of β_K at $\alpha = 0$ and $\alpha = 1$, respectively. Combining Equations (6.39) and (6.40),

$$V_{ii}(\alpha) = V_i(\alpha)\left[1 - \Delta P \beta_K(\alpha)\right] \qquad \textbf{(6.41)}$$

where $V_i(\alpha)$ is the volume at α and pressure, P_i. $V_{ii}(\alpha)$ is that at P_{ii}, and $\Delta P = P_{ii} - P_i$.

A plot of volume, V, against the polymerization time, t, is excluded, although the important features of such a plot can be described in order to examine the chemical effects of pressure on V through the rate of change of α as follows. When the molecular relaxation time is shorter than the time for a significant increase in α, $V_{ii}(\alpha)$ decreases towards its new value more rapidly than $V_i(\alpha)$ does because $k_{ii} > k_i$. For step increased-pressure, at $P = P_i$, $V_i(\alpha)$ would decrease at a rate corresponding to $k = k_i$. For an increase in pressure at $t = t_1$ from P_i to P_{ii}, $V_i(\alpha)$ would show an immediate decrease to $V_{ii}(\alpha)$, corresponding to Equation (6.41). From t_1, $V_{ii}(\alpha)$ would decrease at a rate corresponding to $k = k_{ii}$. The parameters used here are $\beta_{Ko} = 10^{-5}$ bar^{-1}, $\beta_{Kf} = 10^{-6}$ bar^{-1}, and $\Delta P = 200$ bar. The description of the physical change of the volume upon an increase in pressure is discussed here in order to proceed with the following section on the effect of pressure on the equilibrium property ε_s.

The Effect on ε_s, ε_∞ and σ_{dc}

We first consider the effects of pressure on ε_s. From Equation (6.15), a pressure increase alters the magnitudes of ε_∞, N_d, g, μ_o, and correspondingly, ε_s, as discussed in Section 6.1.4. The effect of pressure on ε_∞ of a liquid has been found to be negligible [Chen *et al.* (1969), Johari and Whalley (1972), Johari *et al.* (1996), Wasylyshyn and Johari (1997a)] such that the pressure effects on g, μ_o, and N_d contribute mostly to the change of ε_s. Chen *et al.* (1969) found $g\mu_o^2$ to vary by ~10% for a pressure change of 4 kbar. Since the maximum pressure used here was 206 bar, $(dg\mu_o^2/dP)$ is negligible compared to (dN_d/dP). Hence, $(d\varepsilon_s/dP)_\alpha \propto (dN_d/dP)_\alpha \propto -(dV/dP)_\alpha$. $(dV/dP)_\alpha$ has been discussed already in terms of β_K as the liquid polymerizes. Thus, it is concluded that as in Equation (6.22), when $\alpha = \alpha_i$, $\varepsilon_{s,ii} = \varepsilon_{s,i}(N_{d,ii}/N_{d,i})$.

As discussed in Section 6.1.4, the limiting low-frequency permittivity, ε_s, of a molecular liquid decreases as the number density of dipoles, N_d, the orientational correlation factor, g, and the vapour-phase dipole moment, μ_o, from Equation (6.15) vary as α increases during polymerization [Parthun and Johari (1995a), Tombari and Johari (1992), Johari and Pascheto (1995), Wasylyshyn and Johari (1997b)].

The rate of change of ε_s has been expressed as [Parthun *et al.* (1996)], $\varepsilon_s = \exp(-A_1 t'^n)(\varepsilon_{s,o} - \varepsilon_{s,f}) + \varepsilon_{s,f}$, where $\varepsilon_{s,o}$ is ε_s at t = 0 and $\varepsilon_{s,f}$ is that at $t \rightarrow \infty$. For describing the qualitative decrease in ε_s with t, this can be re-expressed with $A_1 = k$ and $n' = m$ from Equation (6.36) such that,

$$\varepsilon_s = \varepsilon_{s,o} + (\varepsilon_{s,f} - \varepsilon_{s,o})\alpha \qquad \textbf{(6.42)}$$

As the rate of change of α with t depends upon P through k of Equation (6.36), so is the rate of change of ε_s.

The second dielectric term, ε_∞, is now considered. The decrease in volume on a step-increase by ΔP is at most ~0.01%, causing less than 0.01% increase in the refractive index according to the Lorentz-Lorenz equation and contributions from vibrational polarization to ε_s. As the liquid polymerizes, ε_∞ of the α-process decreases according to the kinetics of that process. Since the change in the latter is more, ε_∞ decreases upon polymerization. The net 3-5% decrease in ε_∞ during polymerization is considered insignificant and the effect of its change with t (hence the chemical effects), will not be considered.

In summary, ε_s and ε_∞ decrease with the polymerization time, t, during polymerization corresponding to a rate constant, k, which itself depends upon the pressure, P. When P is increased from P_i to P_{ii} at a time, t_1 (α_1), the instantaneous increase in ε_s from $\varepsilon_{s,i}$ to $\varepsilon_{s,ii}$ is mainly due to the increase in N_d from $N_{d,i}$ to $N_{d,ii}$. Both the chemical effect and the physical effects of pressure on ε_∞ are considered negligible, and therefore excluded.

The dc conductivity of a material contributes to the measured values of both ε' and ε''. To include the effects due to changes in σ_{dc}, the physical effect of pressure are considered first. As pressure increases the viscosity of a liquid, the mobility of its ionic impurities is decreased. Since the contribution from the ionic mobility is highest in the early stages of polymerization and there are more proton translocating H-bonds [Johari

(1994a), Wasylyshyn and Johari (1997b)], pressure decreases σ_{dc} much more when α is low than when it is high.

The effect of reduced ionic mobility is clearly observed in the plots of ε'' against t in Figures 4.26 to 4.29 for the first step-increase of pressure to 200 bar. In this time range, the dipolar contribution, ε''_{dip}, to ε'' is negligible compared to the contribution from ε''_{dc} ($= \sigma_{dc}/\omega\varepsilon_o$) such that the measured value of ε'' is mostly due to σ_{dc}. Thus, the decrease in ε''_{dc} in this time range immediately on increasing P is due to the decrease in σ_{dc}. This decrease is 5 – 10% for ΔP= 199 bar, which is approximately equal to the decrease in σ_{dc}.

The dc conductivity, σ_{dc}, decreases also on polymerization from an initial value, σ_o at $t = 0$ ($\alpha = 0$) as the diffusivity of the impurity ions decreases, the population of zwitter ions is reduced and the proton transfer along the inter-monomer H-bond becomes less frequent as covalent bonds form [Johari (1994a)]. The latter has been considered in terms of known percolation theories [Flory (1941) and (1953), Stockmayer (1943), de Gennes (1979) and (1982)] that attempted to describe a critical extent of polymerization, α_{gel}, at which an infinitely connected covalent bonded cluster forms, or the material loses its conduction paths to become an electrical insulator. In Johari's theory (1994a), when a gel acquires a mechanical stability, proton transfer along the H-bonded network is no longer possible, and σ_{dc} tends towards zero. Limited vibrational motions of ions within the polymerizing mixture, however, persist and σ_{dc} does not become zero. Thus, σ_{dc}

persists even in a fully polymerized state in which ionic diffusion and proton translocation completely cease to occur [Johari (1994a), Wasylyshyn and Johari (1997b)].

The chemical effect of pressure upon σ_{dc} can be discussed in a similar manner as for ε_s and ε_∞, *i.e.*, in terms of its effect upon the polymerization rate constant of Equation (6.36). When k is high, as at higher P, α_{gel} is reached more quickly than when k is low at a low P. Thus, as k increases on increase of P in the mass-controlled regime, the time taken to reach α_{gel}, t_{gel}, decreases. To conclude, during polymerization σ_{dc} would decrease with t towards a limiting, lower limit at a faster rate when P is high than when it is low.

The decrease in σ_{dc} with polymerization time is expressed as [Johari (1994a)],

$$\sigma_{dc} = \sigma_o \left[\frac{t_{gel} - t}{t_{gel}} \right]^x \tag{6.43}$$

which follows from the scaling concepts in gelation phenomena, where x is the critical exponent of the scaling equation used as a generalized property function [de Gennes (1979), Djabourov (1988)]. Equation (6.43) has been found to describe the decrease in σ_{dc} with t during polymerization for a variety of cross-linking epoxide-amine mixtures [Johari (1994a) and references therein], but not that for linear-chain polymerization of epoxide-amines. The reason is that the latter does not form a gel. Regardless of the structure formed, however, the qualitative decrease in σ_{dc} with t is similar for both cross-linking and linear-chain polymerizations [Johari (1994a) and references therein, Wasylyshyn *et al.* (1996)].

Since it is derived from statistical considerations [Flory (1941) and (1953)], α_{gel} should be independent of the rate of reaction. However, Stockmayer (1943) showed that looped structures can form due to the differing reaction rates among the reacting species, and these structures do not contribute to the growth of the macromolecule. Experiments have however shown that t_{gel} can be determined from σ_{dc} data and Equation (6.36) to obtain α_{gel}, once k and m are known. For $k = k_i$ at pressure P_i, $t_{gel,i}$ can be calculated for a given α_{gel}. For the same α_{gel} but for $k = k_{ii}$, at P_{ii}, $t_{gel,ii}$ may be calculated. From Equation (6.43) with $\sigma_{o,i}$ (σ_o at P_i) and $\sigma_{o,ii}$ (σ_o at P_{ii}), the decrease in σ_{dc} with t may be determined for both pressures P_i and P_{ii}. For mathematical simulation, the parameters here were; α_{gel} = 0.5, $\varepsilon_{s,o}$ = 10, $\varepsilon_{s,f}$ = 8, $\sigma_{o,i}$ = 50 nS/m, $\sigma_{o,ii}$ = 45 nS/m, and ε_∞ = 4.

It is worth summarizing the net effects of pressure on the dielectric consequences of polymerization in the mass-controlled regime. The physical effects on a chemically invariant state are such that V and σ_{dc} decrease and τ, ε_s, and ε_∞ increase. In terms of the chemical effects, the decrease in V, σ_{dc}, ε_s and ε_∞, and increase in τ is determined by the increase in α. The changes in each of these properties are related by a set of equations.

Each of the effects described above contributes to the dielectric permittivity, ε' and/or dielectric loss, ε'', measured for a constant frequency during the polymerization of a liquid mixture at a pressure, P. ε' and ε'' are related to τ, ε_s and ε_∞ in the single relaxation time model (Debye model) described in Section 2.5,

$$\varepsilon' = \varepsilon_\infty + \frac{\Delta\varepsilon}{1+\omega^2\tau^2} \qquad \textbf{(6.44)}$$

and,

$$\varepsilon'' = \frac{\Delta\varepsilon\omega\tau}{1+\omega^2\tau^2} + \frac{\sigma_{dc}}{\omega\varepsilon_o} \qquad (6.45)$$

where $\Delta\varepsilon = \varepsilon_s - \varepsilon_\infty$ and ω is the angular frequency in rad/s. The first term on the RHS of Equation (6.45) represents the dipolar contribution to ε'' and the second term the dc conductivity contribution. These equations are thus used to determine the physical and chemical effects of pressure on ε' and ε'' from changes in the equilibrium properties ε_s, ε_∞ and τ through the rate constant, k, of Equation (6.36). $\varepsilon'(t)$ and $\varepsilon''(t)$ calculated from Equations (6.43) and (6.44) are plotted against the polymerization time, t, for a constant angular frequency, ω = 1000 rads/s in Figure 6.15(b,c). The bar chart in the figure is for the pressure-step profile. The dotted line was calculated for ε' and ε'' with $k = k_i$ (= 10 μs^{-1}) in Equation (6.36) for 1 bar, and the dashed line with $k = k_{ii}$ (= 14 μs^{-1}) in Equation (6.36) for 200 bar. Because $k_{ii} > k_i$, the dielectric features of the plots of ε' and ε'' evolve more rapidly for the calculated curves corresponding to 200 bar (P_{ii}) than for that at 1 bar (P_i). The filled circles are for the calculated ε' and ε'' when the pressure is raised to 200 bar and then released at intervals of ~5 ks. The discontinuities in ε' and ε'' at each of the pressure steps at time, t_N, arise from the instantaneous physical changes in ε_s, τ and σ_{dc}, through the relationships described from Equations (6.39) to (6.43). After the discontinuity, the slower change in ε' and ε'' in Figure 6.15 is calculated from Equations (6.44) and (6.45) using the time-dependent (therefore, α-dependent) values of τ, σ_{dc}, and ε_s at the relevant pressures. High pressure causes ε' and ε'' to evolve more quickly than for lower pressures.

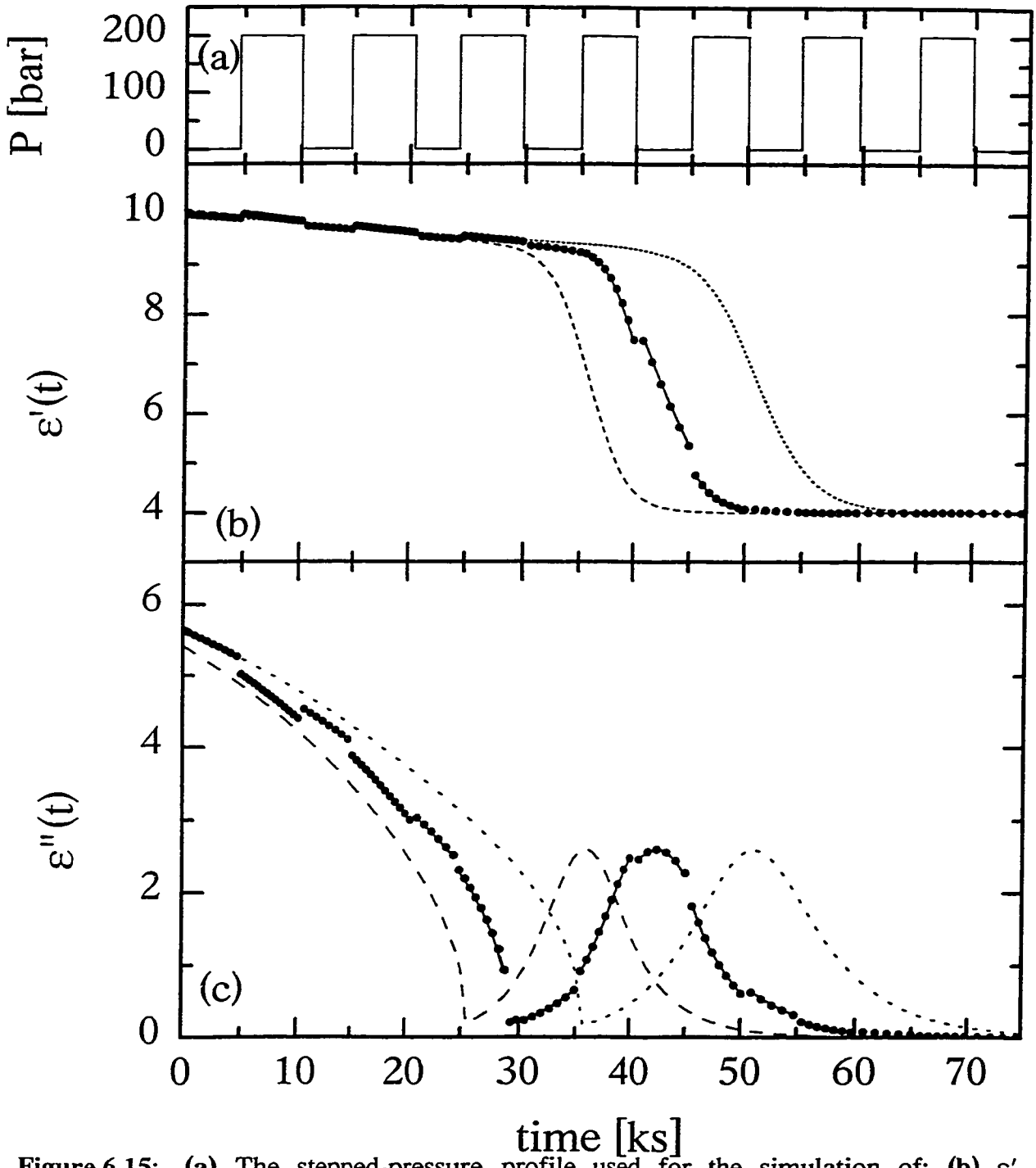

Figure 6.15: **(a)** The stepped-pressure profile used for the simulation of; **(b)** ε', calculated from Equation (6.44), plotted against the polymerization time, t, and, **(c)** ε'' calculated from Equation (6.45) plotted against t. For ε' and ε'', the dotted lines correspond to polymerization at a low pressure, and the dashed lines that at a high pressure. The filled circles represent the result of applying the stepped-pressure profile as indicated in (a). Parameters for the simulation are given in the text.

The combined physical and chemical effects of pressure on the evolution of the dielectric properties simulated in Figure 6.15 qualitatively agree with the behaviour observed in Figures 4.26 to 4.29. For the plot of the simulated ε' against t in Figure 6.15(b), the instantaneous response of ε' to pressure is a result of $(\Delta\varepsilon_s/\Delta P)_t$, through $(\Delta N_d/\Delta P)_t$ from Equation (6.41) $(V_i(\alpha)/V_{ii}(\alpha) = N_{d,ii}/N_{d,i})$, and $(\Delta\tau/\Delta P)_t$ from Equation (6.2). Similarly, from Figure 6.15(c), the instantaneous response of the simulated ε'' to pressure during polymerization is a result of $(\Delta\varepsilon_s/\Delta P)_t$, through $(\Delta N_d/\Delta P)_t$ from Equation (6.41), $(\Delta\tau/\Delta P)_t$ from Equation (6.2), and $(\Delta\sigma_{dc}/\Delta P)_t$ from Equation (6.43).

Thus, the overall changes in both ε' and ε'' observed experimentally can be formulated in terms of the concepts developed here. Although simplifying assumptions were made in order to more easily calculate and simulate the observed behaviour, the general response of ε' and ε'' to pressure still remains as;

i) a chemical response, *i.e.*, an increase in the rate of polymerization for higher pressures compared to lower pressures, and,

ii) a physical response, *i.e.*, an instantaneous increase in N_d and τ, and a decrease in σ_{dc} upon a step-pressure application, causing ε' and ε'' to respond accordingly.

CHAPTER VII

CONCLUSIONS

Epoxy resins were reacted with different amine curing agents in order to study the changes in the relaxation properties as the polymerization progressed towards completion. The structure of the polymeric solid formed was either a linear-chain or network structure, depending upon the number of reactive sites per monomer molecule. The polymerization process was investigated using calorimetry, dielectric spectroscopy, and time domain reflectometry (TDR). Differential scanning calorimetry (DSC) was used on order to determine the number of covalent bonds formed at any instant during the polymerization, thus enabling the other time-dependent properties measured to be associated to a specific structure of the liquid mixture.

The effect of the number of covalent bonds formed on the secondary relaxations was investigated using fixed-frequency temperature scans at 1 kHz as well as isothermal spectra in the gigahertz frequency range. It was found that the sub-T_g relaxation associated with the initial monomeric mixture decreased in strength as the liquid polymerized. Concomitantly, the sub-T_g relaxation associated with the polymeric product increased in strength during polymerization.

The position of the ε″ peaks did not change in the temperature plane of the fixed-frequency measurements, nor did they change position in the spectra measured using TDR. This was examined in terms of configurational entropy theory, for which it was determined that the evolution of the sub-T_g relaxation processes proceeds in a manner independent of the change of configurational entropy.

The origin of the secondary relaxations was considered in terms of localized, high-energy sites present in the overall topography of the monomeric liquid [Johari (1994a)]. The collapse of the monomeric high-energy sites manifested itself as an extinction of the corresponding sub-T_g ε″ peak. The creation of similar sites in the resulting polymeric product caused the growth of the corresponding polymeric sub-T_g ε″ peak.

By using the analogy to the fictive temperature, T_f, associated with the theories of structural relaxation of glasses, the concept of 'chemical fictive temperature', $T_{f,chem}$, was introduced. In this manner, by considering covalent bonds as a general type of intermolecular interactions, the loss of chemical metastability upon polymerization and the ultimate approach to a chemically stable state is phenomenologically similar to the loss of kinetic metastability and the approach to a physically stable state.

Pressure was applied to the polymerizing mixtures in order to establish its chemical and physical effects on the rate kinetics and molecular dynamics. Pressure was found to increase the rate of polymerization of all the mixtures, even though the resulting increase in the viscosity was expected to slow the kinetics. This was justified in terms of

mass-controlled and diffusion-controlled reaction kinetics using the concept of 'negative feed-back' during polymerization.

In the mass-controlled regime of polymerization, when the viscosity of the mixture is relatively low, an increase pressure increases the viscosity and thus, the density of the liquid. The increase in the viscosity is negligible, but the density increases such that average distance between the reacting species decreases, which increases the probability of reaction, therefore the reaction rate increases. In the diffusion-controlled regime, when the viscosity is already high, an increase in the pressure further increases the viscosity. In this case, the increase in the density of the reactant species is insufficient to counter the corresponding decrease in their diffusivity, thus the rate of polymerization is decreased.

The onset of diffusion-controlled kinetics was examined using transition state theory as well as theories based on Brownian motions. The dielectric data measured during the polymerization of the mixtures under pressure was plotted as $(\partial\varepsilon''/\partial t)_{T,P}$ against ε'' at times corresponding to $\omega\tau >> 1$ in order to reveal for which value of ε'', and therefore τ, the pressure increase caused the onset of diffusion control. With sufficiently accurate data, this method may be used as a criterion for determining the transition from one regime to the other as well as the state of the mixture in terms of the molecular dynamics at which it occurs.

The chemical and physical effects of pressure on the dielectric properties during polymerization was simulated under three conditions, i) a constant, relatively low

pressure, ii) a constant, relatively higher pressure, and iii) a stepped-pressure that was increased and decreased at regular intervals during polymerization. The chemical effects of pressure were seen to affect the rate at which the extent of polymerization, α, changes with time. This change in α manifested itself in the change of the dielectric properties with time. The physical effects of pressure on the equilibrium properties of the liquid mixture, *i.e.*, volume, relaxation time, low- and high- limiting permittivities, and conductivity, were simulated using established formalisms and concepts that previously did not explicitly account for changes in the pressure applied to a polymerizing mixture.

REFERENCES

Adam, G., and Gibbs, J.H. (1965), *J. Chem. Phys.*, **43**, 139.

Alig, I., and Johari, G.P. (1993), *J. Polym. Sci. B, Polym. Phys.*, **104**, 5683.

Alig, I., Lellinger, D., and Johari, G.P. (1992), *J. Polym. Sci. B, Polym. Phys.*, **30**, 791.

Angel, C.A. (1995), *Science*, **267**, 1924.

Aronhime, M.T., and Gillham, J.K. (1987), *Adv. Polym. Sci.*, **78**, 85.

Aukward, J.A., Warfield, R.W., and Petree, M.C. (1958), *J. Polym. Sci.*, **27**, 199.

Barton, J.M. (1985), *Adv. Polym. Sci.*, **11**, 1617.

Bertolini, D., Cassettari, M., Salvetti, G., Tombari, E., and Veronesi, S. (1990), *Rev. Sci. Instrum.*, **61**, 450.

Boltzmann, L. (1876), *Pogg. Ann. Physik*, 7, 108.

Calef, D.F., and Deutch, J.M. (1983), *Ann. Rev. Phys. Chem.*, **34**, 493.

Carrozzino, S., Levita, G., Rolla, P., and Tombari, E. (1990), *Polym. Eng. Sci.*, **20**, 366.

Cassettari, M., Salvetti, G., Tombari, E., Veronesi, S., and Johari, G.P. (1993a), *Physica A*, **201**, 95;

Cassettari, M., Salvetti, G., Tombari, E., Veronesi, S., and Johari, G.P. (1993b), *J. Polym. Sci. B, Polym. Phys.*, **31**, 199.

Cassettari, M., Salvetti, G., Tombari, E. Veronesi, S., and Johari, G.P. (1994), *J. Non-cryst. Solids*, **172-174**, 554.

Cavaille, J.Y., Perez, J., and Johari, G.P. (1989), *Phys. Rev. B*, **39**, 4411.

Chandrasekhar, S., (1943), *Rev. Mod. Phys.*, **15**, 1.

Charlesworth, J.M. (1988a), *Polym. Eng. Sci.*, **28**, 214; (1988b), *ibid*, **28**, 221.

Chen, T., Dannhauser, W., and Johari, G.P. (1969), *J. Chem. Phys.*, **50**, 2046.

Choy, I.-C., and Plazek, D.J. (1986), *J. Polym. Sci. B, Polym. Phys.*, **24**, 1303.

Cole, K.S., and Cole, R.H. (1941), *J. Chem. Phys.*, **19**, 1484.

Cole, R.H. (1983), *IEEE Trans. Instrum. Meas.*, **IM-32**, 42.

Cole, R.H., Berberian, J.G., Mashimo, S., Chryssikos, G., Burns, A., and Tombari, E. (1989), *J. Appl. Phys.*, **66**, 793.

Cole, R.H., Mashimo, S., and Winsor, P. (1980), *J. Phys. Chem.*, **84**, 786.

Curie, P.J. (1888), *Ann. Chim. Phys.*, **17**, 385.

Davidson, D.W. (1961), *Canadian Journal of Chemistry*, **39**, 571.

Davidson, D.W., and Cole, R.H. (1950), *J. Chem. Phys.*, **18**, 1417.

Davidson, D.W., and Cole, R.H. (1951), *J. Chem. Phys.*, **19**, 1484.

Debye, P. (1929), Polar Molecules, Chem. Catalog., New York.

de Gennes, P.G. (1979), Scaling Concepts in Polymer Physics, Cornell University Press, New York.

de Gennes, P.G. (1982), *J. Chem. Phys.*, **76**, 3316, 3322.

Delmonte, J. (1959), *J. Appl. Polym. Sci.*, **2**, 108.

Deng, Y., and Martin, G.C. (1994a), *J. Polym. Sci. B, Polym. Phys.*, **32**, 2115.

Deng, Y., and Martin, G.C. (1994b), *Macromolecules,* **27**, 5147.

DiMarzio, E.A. (1964), *J. Res. N.B.S.*, **68A**, 611.

Dishon, M., Weiss, G.H., and Bendler, J.T. (1985), *J. Res. N.B.S.*, **90**, 27.

Djabourov, M. (1988), *Contempt. Phys.*, **29**, 273.

Doi, M., (1975), *Chem. Phys.*, **9**, 455, and references therein.

Douglas, R.W. (1963), *Proc. 4th Int. Conf. on Rheology*, Providence, R.I., Part I, Eds. E.H. Lee and A.L. Copley, Wiley, New York.

Douglas, R.W. (1966), *Br. J. Appl. Phys.*, **17**, 435.

Dušek, K. (1985), *Adv. Polym. Sci.*, **78**, 1.

Ellis, B. (ed.) (1993), Chemistry and Technology of Epoxy Resins, Chapman and Hall, London.

Enns, J.B., and Gillham, J.K. (1983), *J. Appl. Polym. Sci.*, **28**, 2567.

Evans, M.G., and Polanyi, M. (1935), *Trans. Faraday Soc.*, **31**, 875.

Fedtke, M., Sorokin, V., and Taenzer, W. (1987), *Vysokomol. Soed.* **A29**, 1275.

Ferrari, C., Salvetti, G., Tombari, E., and Johari, G.P. (1996), *Phys. Rev. E*, **54**, R1058.

Flory, P.J. (1941), *J. Amer. Chem. Soc.*, **63**, 3083, 3091, 3096.

Flory, P.J. (1953), Principles of Polymer Chemistry, Cornell University Press, New York.

Fournier, J., Williams, G., Duch, C., and Aldridge, G.A. (1996), *Macromolecules*, **29**, 7097.

Fox, T.G., and Loshaek, S. (1955), *J. Polym. Sci.*, **15**, 371.

Fröhlich, H. (1958), Theory of Dielectrics, 2nd Ed., Oxford University Press, Oxford.

Frick, B., and Richter, D. (1995), *Science*, **267**, 1939.

Fuoss, R.M., and Kirkwood, J.G. (1941), *J. Amer. Chem. Soc.*, **63**, 369.

Gilchrist, A., Earley, J.E., and Cole, R.H. (1957), *J. Chem. Phys.*, **26**, 196.

Glasstone, A.S., Laidler, K.J., and Eyring, H. (1941), Theory of Rate Processes, McGraw Hill, New York.

Grenier-Loustalot, M.F., Grenier, P., Horny, P., and Chenard, J.Y. (1988), *Br. Polym. J.*, **20**, 463.

Hamman, S.D. (1957), Physico-Chemical Effects of Pressure, Butterworths, London.

Hamon, G.V. (1952), *Proc. Inst. Elec. Engrs.*, **99**, Pt.IV, 27.

Havriliak S., and Negami, S. (1966), *J. Polym. Sci. C, Polym. Symp.*, **14**, 99.

Hofer, K., Hallbrucker, A., Mayer, E., and Johari, G.P. (1989), *J. Phys. Chem.*, **93**, 4674.

Hofmann, A., Kremer, F., Fischer, E.W., and Schönhals, A. (1994), In, Disorder Effects in Relaxational Processes, Eds. R. Richter and A. Blumen, Springer-Verlag, Berlin, p.310

Hopkinson, J. (1877), *Phil. Trans. Roy. Soc.*, **167**, 599.

Horie, K., Hiura, H., Sawada, M., Mita, I., and Kambe, H. (1970), *J. Polym. Sci. A-1*, **8**, 1357.

Isaacs, N.S. (1981), Liquid Phase High Pressure Chemistry, John Wiley & Sons Ltd., New York.

Johari, G.P. (1973), *J. Chem. Phys.*, **58**, 1766.

Johari, G.P. (1976), *Ann. New York Acad. Sci.*, **279**, 117.

Johari, G.P. (1982), *J. Chem. Phys.*, **77**, 4619.

Johari, G.P. (1993a), *J. Chem. Phys.*, **98**, 7324.

Johari, G.P. (1993b), In, Chemistry and Technology of Epoxy Resins, ed. B. Ellis, Chapman and Hall, London, Chapter 4.

Johari, G.P. (1994a), In, Disorder Effects in Relaxational Processes, Eds. R. Richter and A. Blumen, Springer-Verlag, Berlin, p.627.

Johari, G.P. (1994b), *J. Chem. Soc., Faraday Trans.*, **90**, 883.

Johari, G.P., and Dannhauser, W. (1969a), *J. Chem. Phys.*, **50**, 1862.

Johari, G.P., and Dannhauser, W. (1969b), *J. Chem. Phys.*, **51**, 1626.

Johari, G.P., and Goldstein, M. (1970), *J. Chem. Phys.*, **53**, 2372.

Johari, G.P., and Mangion, M.B.M. (1991), *J. Non-Cryst. Solids*, **131-133**, 921.

Johari, G.P., and Pascheto, W. (1994), *J. Chem. Soc., Faraday, Trans.*, **91**, 343.

Johari, G.P., and Pathmanathan, K. (1986), *J. Chem. Phys.*, **85**, 6811.

Johari, G.P., and Perez, J. (1994), *J. Mol. Phys.*, **83**, 235.

Johari, G.P., and Whalley, E. (1972), *J. Chem. Soc. II, Faraday Symp.*, **6**, 23.

Johari, G.P., Hallbrucker, A., and Mayer, E (1987), *Nature*, **330**, 522.

Johari, G.P., Hallbrucker, A., and Mayer, E (1990), *J. Chem. Phys.*, **92**, 6742.

Johari, G.P., McAnanama, J.G., and Wasylyshyn, D.A. (1996), *J. Chem. Phys.*, **105**, 10621.

Johnson, W.C. (1950), Transmission Lines and Networks, McGraw-Hill, New York.

Karasz, F.E. (ed.) (1972), Dielectric Properties of Polymers, Plenum Press, New York.

Katz, D., and Tobolsky, V. (1962), *Polymer*, **4**, 417.

Kienle, R.H., and Race, H.H. (1934), *Trans. Electrochem. Soc.*, **65**, 87.

Kim, D.H., and Kim, S.H. (1987), *Polym. Bull.*, **18**, 533.

Kirkwood, J.G. (1939), *J. Chem. Phys.*, **7**, 911.

Kohlrausch, R. (1847), *Ann. Phys. (Leipzig)*, **91**, 179.

Laughlin, W.T., and Uhlman, D.R. (1972), *J. Phys. Chem.*, **76**, 2317.

Lindsey, C.P., and Patterson, G.D. (1980), *J. Chem. Phys.*, **73**, 3348.

Malkin, A.Y., and Kulichikhin, S.G. (1991), *Adv. Polym. Sci.*, **101**, 217.

Mangion, M.B.M., and Johari, G.P. (1990), *J. Polym. Sci. B, Polym. Phys.*, **28**, 1621.

Mangion, M.B.M., and Johari, G.P. (1991a), *J. Polym. Phys. B, Polym. Phys.*, **29**, 437.

Mangion, M.B.M., and Johari, G.P. (1991b), *J. Polym. Sci. B, Polym. Phys.*, **29**, 1127.

Mangion, M.B.M., Vanderwal, J.J., Walton, D., and Johari, G.P. (1991), *J. Polym. Sci. B, Polym. Phys.*, **29**, 723.

Mashimo, S., Umehara, T., Ota, T., Kuwabara, S., Shinyashiki, N., and Yagihara, S. (1987), *J. Mol. Liq.* **36**, 135.

Matsuoka, S., Fredrickson, G.H., and Johnson, G.E. (1987), In, Molecular Dynamics and Relaxation Phenomena in Glasses, Eds. Th. Dorfmüller and G. Williams, Lecture Notes in Physics, Springer, Berlin, p.188.

McCrum, N.G., Read, B.E., and Williams, G. (1967), Anelastic and Dielectric Effects in Polymeric Solids, John Wiley, New York.

Mijovic, J., Kim, J., and Slaby, J. (1984), *J. Appl. Polym. Sci.*, **29**, 1449.

Mijovic, J. (1986), *J. Appl. Polym. Sci.*, **31**, 1177.

Moynihan, C.T., Boesch, L.P., and Labarge, N.L. (1973), *Phys. Chem. Glasses*, **14**, 122.

Muzeau, E., Cavaille, J.Y., Vassoille, R., Perez, J., and Johari, G.P. (1992), *Macromolecules*, **25**, 5108.

Muzeau, E., Vigier, G., and Vassoille, R. (1994), *J. Non-Cryst. Solids*, **172-174**, 575.

Narayanaswamy, O.S. (1971), *J. Am. Chem. Soc.*, **54**, 491.

Narracott, E.S. (1953), *Br. Plast.*, **26**, 120.

Onsager, L. (1936), *J. Amer. Ceram. Soc.*, **58**, 1486.

Parthun, M.G., and Johari, G.P. (1992a), *Macromolecules*, **25**, 3254.

Parthun, M.G., and Johari, G.P. (1992b), *J. Polym. Sci. B, Polym. Phys.*, **30**, 655.

Parthun, M.G., and Johari, G.P. (1995a), *J. Chem. Phys.*, **102**, 6301.

Parthun, M.G., and Johari, G.P. (1995b), *J. Chem. Phys.*, **103**, 7611.

Parthun, M.G., and Johari, G.P. (1995c), *J. Chem. Phys.*, **103**, 440.

Parthun, M.G., Wasylyshyn, D.A., and Johari, G.P. (1996), *J. Mol. Liq.*, **69**, 219.

Perez, J. (1992), Physique et Mechanique des Polymeres Amorphes, Lavoisier, Tech. & Doc.

Plazek, D.J., and Frund Jr., Z.N. (1990), *J. Polym. Sci. B, Polym. Phys.*, **28**, 431.

Plonka, A. (1986), Time-Dependent Reactivities of Species in Condensed Media, Lecture Notes in Chemistry, Springer, Berlin.

Riccardi, C.C., Adabbo, H.E., and Williams, R.J.J. (1984), *J. Appl. Polym. Sci.*, **29**, 2481.

Riccardi, C.C., and Williams, R.J.J. (1986), *J. Appl. Polym. Sci.*, **32**, 3445.

Ryan, C.M., and Dutta, A. (1979), *Polymer*, **20**, 203.

Sartor, G., Mayer, E., and Johari, G.P. (1994), *Biophys. J.*, **66**, 249.

Sentura, S.D., and Sheppard Jr., N.F. (1986), *Adv. Polym. Sci.*, **80**, 1.

Sidebottom, D., and Johari, G.P. (1990), *Chem. Phys.*, **147**, 205.

Smoluchowski, M.V. (1916), *Physik*, **17**, 557, 585; (1917), *Physik. Chem.*, **92**, 192.

Somlo, P.I. (1967), *Proc. IREE*, **28**, 7.

Stockmayer, W.H. (1943), *J. Chem. Phys.*, **11**, 45.

Tanaka, Y., Tomoi, M., and Kakiuchi, H. (1967), *J. Macromol. Sci. Chem.*, **1**, 477.

Tombari, E., and Johari, G.P. (1992), *J. Chem. Phys.*, **97**, 6677.

Tombari, E., Ferrari, C., Salvetti, G., and Johari, G.P. (1997), *J. Phys.:Condens. Matter*, **9**, 7017.

Tool, A.Q. (1946), *J. Am. Ceram. Soc.*, **29**, 240.

Wagner, K.W. (1913), *Ann. der Physik*, **40**, 817.

Waite, T.R. (1957), *Phys. Rev.* **107**, 463; (1958) *J. Chem. Phys.* **28** 103; (1960) *ibid*, **32**, 21.

Waite, T.R. (1957), *Phys. Rev.* **107**, 463; (1958) *J. Chem. Phys.* **28** 103; (1960) *ibid*, **32**, 21.

Wasserman, S., and Johari, G.P. (1993), *J. Appl. Polym. Sci.*, **48**, 905.

Wasserman, S., and Johari, G.P. (1994), *J. Appl. Polym. Sci.*, **53**, 331.

Wasylyshyn, D.A., and Johari, G.P. (1996), *J. Chem.Phys.*, **104**, 5683.

Wasylyshyn, D.A., Parthun, G.P., and Johari, G.P. (1996), *J. Mol. Liq.*, **69**, 283.

Wasylyshyn, D.A., and Johari, G.P. (1997a), *J. Chem. Soc., Faraday Trans.*, **93**, 4025.

Wasylyshyn, D.A., and Johari, G.P. (1997b), *J. Polym. Sci. B, Polym. Phys.*, **35**, 437.

Wasylyshyn, D.A., Johari, G.P., Salvetti, G., and Tombari, E. (1997a), *J. Phys.:Condens. Matter*, **9**, 10521.

Wasylyshyn, D.A., Johari, G.P., Tombari, E., and Salvetti, G. (1997b), *Chem. Phys.*, **223**, 313.

Wasylyshyn, D.A., and Johari, G.P. (1998), Submitted to *J. Chem. Phys.*

Whitehead, J.B., and Banos, A. (1931), *Trans. AIEEE*, **51**, 392.

Williams, G., and Watts, D.C. (1970), *Trans. Faraday Soc.*, **66**, 80.

Williams, G., Duch, C., Fournier, J., Andrews, S., and Smith, I. (1995), Dielectric Relaxation Spectroscopy of Polymerizing Systems, Abstract from the conference, "Impedance Spectroscopy at Electrodes and Interfaces", held at the University of Kent, U.K., April 10-12, 1995.

Wisanrakkit, G., and Gillham, J.K. (1990), *J. Appl. Polym. Sci.*, **41**, 2885.

Wisanrakkit, G., Gillham, J.K., and Enns, J.B. (1987), *Polym. Mater. Sci. Eng.*, **57**, 87.

Yeager, W.A. (1936), *Physica*, **7**, 434.

Younes, M., Wartewig, S., Lellinger, D., Strehmel, B., and Strehmel, V. (1994), *Polymer*, **35**, 5269.